Novel Schiff-base and Benzamide *N,O*-Donor Ligands for Development as Fluorionophores and Selective Metal Ion Binders

A thesis submitted to the National University of Ireland in fulfilment of the requirements for the degree of

Doctor of Philosophy

By

John Michael Denis Walsh B.Sc. (Hons.)

NUI MAYNOOTH
Ollscoil na hÉireann Má Nuad

Department of Chemistry,
Faculty of Science and Engineering,
National University of Ireland, Maynooth,
Maynooth,
Co. Kildare,
Éire.

October 2010

Research Supervisor: Dr. John McGinley

Head of Department: Professor John P. Lowry

Declaration

This is to certify that the material presented within this thesis has not been submitted previously for a Degree to this or any other University. All material presented, except where acknowledged and cited, is the original work of the author.

John Michael Denis Walsh

_____

National University of Ireland, Maynooth   October 2010

ii

acknowledge the vast improvements in culinary standards in the department. To the downstairs postgrads (Paul, Foxy, Emer and Eimear, Orla, Anita, Ursula, Conor and Lynn, Keeley, Ken, Saidhbhe and Rachel) who toil away in what only can be described as sweatboxes I wish you all the very best. Apologies if I forgot anyone, the place has grown considerably in five years.

To the postdocs, past and present whose knowledge and advice were greatly appreciated, in particular Martin, Fiachra, Finno and Ishwar- thank you.

Away from the lab there are also a few people I wish to thank, specifically my family both immediate and extended. To Mam and Dad, you have always offered unquestioning and unfailing support and love in everything I have ever done and words alone cannot describe how much you have done for me. I am dedicating this thesis to you. To my brothers, Conor and Ronan, who always offered encouraging words and have resisted the temptation to slag off their older (and shorter) brother for not entering the real world and getting a proper job. To my grandaunt, Martha and also to my aunt Shiela, who always offered support and encouragement, thank you so much.

To the Sinnotts (Anne, Eddie, Paul, Ger and Oliver), who have always treated me as one of their own and have always made me feel at home, a heartfelt thank you.

Last but by no means least I would like to thank Mary for your unfailing love, support, encouragement and advice.

It's been emotional.

Dedication

To my parents, John and Anne, with love.

Thank you for everything.

Abstract

A new family of Schiff-base ligands using *meta*-hydroxybenzaldehyde and a variety of di- and triamines as precursors were prepared and fully characterised. These ligands were reacted with various MX_2 salts (M = Cu, Ni and Zn and X = perchlorate, acetate and chloride). In every case except one (where a coordination polymer was formed), hydrolysis of the ligand occurred to give the liberated amine and aldehyde. The amine bound to the metal ion to give the appropriate metal-amine complex. In two cases these by-products were characterised by X-ray crystallography. One showed the entrapment of a two-coordinate copper(II)chloride molecule within the lattice, along with the inclusion of a monochloro-bridged dinuclear copper species.

A novel class of benzazines were prepared, some of them macromolecular derivatives, using a tetra *tert*-butylcalix[4]arene difunctionalised at the lower rim as a molecular scaffold. X-ray crystal structures for these calix[4]arene derivatives were obtained in four cases. Zn(II) complexes of this family of compounds were prepared in several cases. Both the ligands and their Zn(II) complexes were examined for fluorescent character. An increase in emission upon complexation of the Zn(II) ion was obtained.

A new benzamide derivative was synthesised and characterised by X-ray crystallography. The HCl salt of the ligand was also prepared and its X-ray structure obtained. The free ligand displayed ambidentate character and complexes with the various metal salts mentioned above, were prepared. In the case of its reaction with Cu(II) perchlorate, two complexes, one with an octahedral geometry and the other with a square planar geometry were obtained, both of whom were solved by X-ray crystallography.

The above ligand was also bound to the calix[4]arene. Two derivatives were prepared, one with a methyl protecting group on the terminal phenol (X-ray crystal structure solved), the other possessed the free phenol. Both were examined for metal binding traits using Na(I), Ag(I) and Zn(II) salts. Only the deprotected ligand was found to bind metals and was selective for acetate salts. An explanation for its selectivity was given using pK_a values.

List of abbreviations

Ac	Acetyl
AcOH	Acetic acid
Anal. Calc.	Analytical calculation
Å	Ångstrom
Ar	Aryl
B.M.	Böhr Magneton
br	Broad
t-Bu	*tert*-Butyl
Boc	*tert*-Butyloxycarbonyl
$CDCl_3$	Deuterated chloroform
cm	Centimetre
cm^{-1}	Wavenumbers
d	Doublet
dap	1,3-Diaminopropane
decomp	Decomposition
°C	Degrees Celsius
dd	Doublet of doublets
d.e.	Diastereomeric excess
Δ	Reflux temperature
δ	Chemical shift
dmda	3,3'-Diamino-N-methyldipropylamine
DMF	*N,N*-Dimethylformamide
d_6-DMSO	Deuterated dimethyl sulphoxide
dt	Doublet of triplets
e.e.	Enantiomeric excess
en	Ethylenediamine
ESI	Electrospray ionisation
EtOH	Ethanol
FTIR	Fourier Transform Infrared
h	Hour
HCl	Hydrochloric acid
HOMO	Highest occupied molecular orbital
Hz	Hertz
IR	Infrared
J	Coupling constant
KBr	Potassium bromide
KOH	Potassium hydroxide
λ	Wavelength (nm)

LC	Liquid chromatogram
LC/TOF-MS	Liquid chromatography time-of-flight mass spectrometer
L/min	Litres per minute
lit	Literature value
LUMO	Lowest unoccupied molecular orbital
M	Molar
m	Multiplet
Me	Methyl
MeOH	Methanol
Me_4Si	Tetramethylsilane
MHz	Megahertz
min	Minute
mL	Millilitre
mmol	Millimole
m.p.	Melting point
μ_{eff}	Effective magnetic moment
μL	Microlitre
μM	Micromolar
N_2	Dinitrogen
NaCl	Sodium chloride
NaOH	Sodium hydroxide
NMR	Nuclear magnetic resonance
nm	Nanometre
OEt	Ethoxide anion
O_2	Molecular oxygen
pH	Logarithmic scale of concentration of hydronium ions ($-\log[H_3O^+]$)
PhMe	Toluene
pK_a	Minus log of association constant K_a of a given solution ($-\log K_a$)
ppm	Parts per million
PSIG	Pounds per square inch gauge
py	Pyridine
q	Quartet
s	Singlet
sp.	Species
t	Triplet
τ	Addison parameter
TFA	Trifluoroacetic acid
UV/vis	Ultraviolet/visible
V	Volts
ν	Wavenumbers

Table of Contents

xiii

1. Introduction

1.1   Schiff-bases and metal complexation

1.1.1   Overview

The rich vein of literature publications regarding Schiff-base ligands reveals the scope of using these ligand molecules to complex metal ions. Schiff-base ligand formation requires conditions that are not very stringent, necessitating only a dry solvent or a method of removing the water produced in the condensation reaction between an aldehyde/ketone and an amine. The lone pair on the nitrogen atom of the imine moiety provides a suitable donor atom for metal ion complexation. These ligands are particularly adept at binding transition metal ions, with the range of uses for these complexes varying from catalysts to biological mimics.[1,2] The work described in this thesis attempts to extend the range of novel Schiff-base ligands and also to prepare their copper(II), nickel(II) and zinc(II) metal complexes.

1.1.2   Syntheses of Schiff-base ligands

Named after Hugo Schiff, a Schiff-base is a molecule that contains an imine moiety with an alkyl or aryl substituent attached to the imine nitrogen atom. The Schiff-base reaction is a reversible acid-catalysed condensation between a primary amine (not ammonia) and either an aldehyde or a ketone. Typical conditions for imine formation require a protic solvent that is sufficiently dry to prevent subsequent hydrolysis of the newly formed imine bond. Generally these condensation reactions proceed smoothly, although some reactants (usually as a result of electronic effects) can require forcing conditions such as heating to reflux in a high boiling solvent and may include the use of a Dean-Stark apparatus or molecular sieves to remove the by-product, water.[3] The general consensus of the mechanism of formation of the imine, as shown in Scheme 1.1, is that it requires protonation, or the use of a Lewis acid on the carbonyl oxygen atom to enhance the electrophilicity of the carbonyl carbon. This protonation step precedes (and facilitates) nucleophilic attack of the primary amine on the carbonyl carbon. A 1,3-H shift follows, which facilitates the elimination of water to give the protonated imine, with subsequent disassociation of this species to give the imine product.

Scheme 1.1: Mechanism of imine formation.
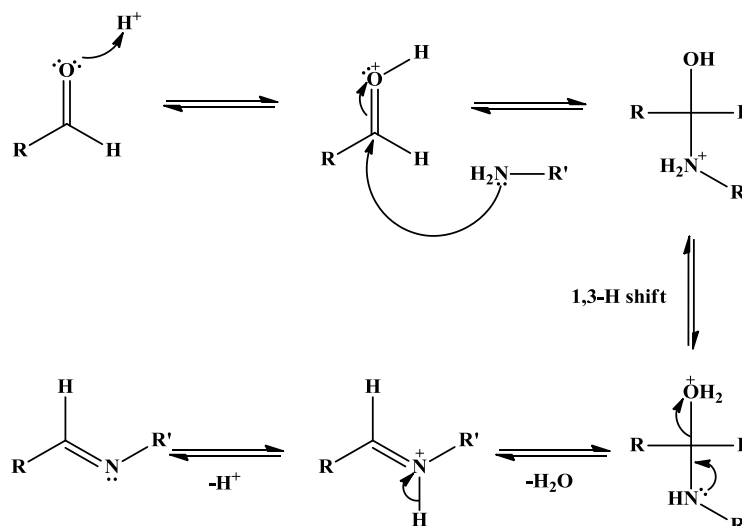
The geometry of the imine double bond generally adopts a *trans* orientation, which limits the steric interactions of the bulkier R groups, with R being either aryl or alkyl substituents.

The synthesis of tripodal Schiff-base ligands such as that in Figure 1.1, is generally difficult, mainly due to the problematic task of purifying the ligand as the molecule can undergo hydrolysis when exposed to chromatographic methods. Ways to obviate these problems involve the use of zinc(II) perchlorate to form a template with the reactant triamine.
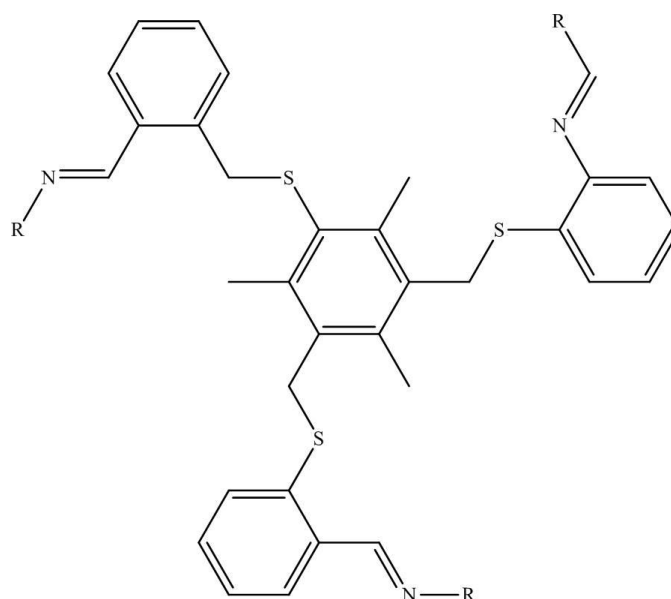
Figure 1.1: Tripodal ligand (where R = various aromatic moieties) synthesised using a zinc template method.[4]

According to the proposed mechanism by Hundal *et al.*, coordination of the zinc(II) ion to the aldehyde results in an enhancement in the electrophilicity of the aldehyde.[4] The zinc(II) ion is also suggested to localise the electron density of the aromatic amine on the nitrogen, thereby making it a stronger nucleophile and allowing the Schiff-base reaction to occur. Finally, the zinc(II) ion is labile enough to liberate the newly formed tripodal ligand (whose structure is shown in Figure 1.1) in high yield and purity, something which does not occur in the absence of the zinc salt.

1.1.3   Schiff-base derivatives

Schiff-base compounds prepared using salicylaldehyde (sal) or its derivatives, are extremely common in the literature. Their successful use in the preparation of mono-, di- and multinuclear complexes along with the sheer scope of ligands prepared is emphasised by several extensive reviews.[5]

Salicylaldehyde or 2-hydroxybenzaldehyde or sal is an important framework around which some well known reagents have been based. Salicylaldehyde is a suitable building block due to the substitution pattern of the ring. Once the imine forms a situation arises where the imine is *ortho* to the hydroxyl functional group. This orientation means that if complexation takes place at this N_2O_2 binding site, it forms a six-member chelate ring with the bound metal ion, thus increasing the stability of the complex. This strategy has proved to be broad in scope, with various *d*- and *f*-block metals being bound at this site.[6,7] Jacobsen's catalyst (shown in Figure 1.2), which has *tert*-butyl substituents *ortho* and *para* to the phenolic oxygen is one such example. This manganese(III) coordination complex stereoselectively converts unfunctionalised alkenes to epoxides, with the largest enantiomeric excess (e.e.) reported at 97 %.[8]
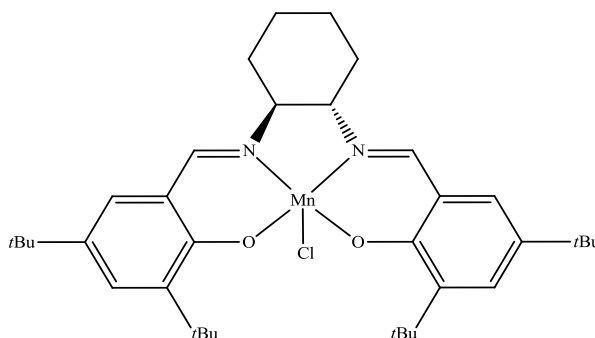
Figure 1.2: Jacobsen's catalyst.

The central diamine is the key to the wide variation of binding characteristics of these compounds. The linkage bridging the two nitrogens may be aliphatic or aromatic with the limitations of the functional groups attached only kept in check by their chemical compatibility with the amines.

The most commonly used diamine is 1,2-diaminoethane or ethylene diamine (en). This diamine provides a two carbon chain between the two imine nitrogens, and upon complexation with a metal through the imine nitrogens it participates in forming a relatively stable five-member ring, as shown in the N-Mn-N fraction of Jacobsen's catalyst. The carbon chain itself may be functionalised to prepare asymmetric centres on the chain. Groups such as naphthyl, phenyl or isooctyl moieties have been added to the chain to prepare a wide range of derivatives. These ligands have been employed in the synthesis of catalysts,[9] spin crossover complexes[6] and fluorescence sensors.[10]

Increasing the length of the aliphatic chain does not seem to diminish the ability of the imine nitrogen to bind, as can be seen from complexes bearing a ligand with a three- or four-carbon chain, but it can however promote the formation of dimers when the chain is four or five carbons in length.[11] The flexible behaviour of the unfunctionalised alkyl chain, and consequently, the formation of a dimer, may be curtailed by the use of cyclic diamines, with both saturated and unsaturated ring derivatives having been employed to this effect. Indeed, it is the saturated ring diamines, with their inherently chiral nature, which are employed to prepare optically pure ligand precursors for such catalysts as those mentioned previously. Generally the ligands do not function as an organocatalyst and require a metal to be present to effect the transformation.

More recent literature work has seen a simple method developed to provide access to asymmetric varieties of the sal (ligands based on the use salicylaldehyde and an alkyl or aryl primary diamine) Schiff-base derivative. It involves monoprotection of the diamine with hydrochloric acid to give the ammonium intermediate with a single free amine group, as outlined in Scheme 1.2. This allows formation of the imine on only one end of the diamine molecule. Deprotection is easily accomplished with triethylamine to give the free amine which can subsequently react with a different aldehyde to give the asymmetric derivative.[12]

Besides increasing the length of the alkyl chain, it is possible to introduce one or more additional S-[13], N-[14] or O-donor[15] atoms into the imine-imine bridge. This would have the effect of providing additional potential binding modes to the metal ion.
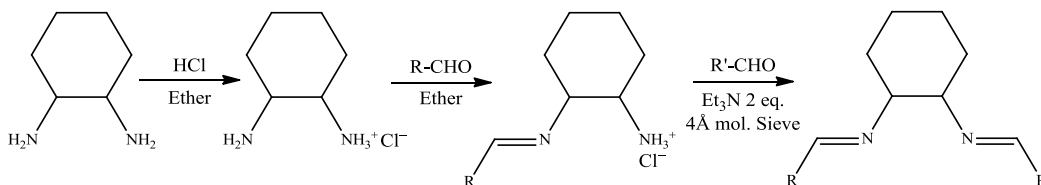
Scheme 1.2: Synthesis of asymmetric Schiff-base using mono-protected diamine.

The benzaldehyde moiety can be functionalised on the aromatic ring with the usual candidates e.g. alkyl groups, halides, nitro groups, methoxy and hydroxy groups to alter the electronics of the aromatic ring. Their effect is seen in the varying degree of activities in respective catalysts. In addition to functionalising the benzaldehyde ring, the ring itself can be substituted for a heterocyclic analogue, preferably with donor atoms in proximity to the imine nitrogen to facilitate metal ion complexation. Examples of these used include pyridine, furan and thiophene moieties.[16,17] The possibility of dimerisation is more likely to occur in these heterocyclic derivatives as both the bound and the free ligand are charge neutral.

Schiff-base derivatives are, by and large, very hydrophobic but this feature can be overcome by the addition of sulfonate functional groups to the corresponding aldehyde precursor.[18]

1.1.4   Schiff-base metal complexation

1.1.4.1   Overview

Schiff-bases are generally regarded as good ligands. The orientation of the lone pair on the nitrogen atom means that it can participate in donation into the appropriate metal ion. This donation, in conjunction with the adjacent oxygen atom that is present in sal Schiff-base derivatives or the heteroatom in pyridine and thiophene derivatives means that a large array of transition metal coordination complexes can be prepared. Their excellent metal binding characteristics have resulted in the preparation of a vast number of complexes of which a large amount have found use as transition metal catalysts, as outlined in a recent review by Gupta *et al.*[9] For the purposes of the

material in this thesis, an overview will be provided on only the copper(II), nickel(II) and zinc(II) coordination chemistry of these ligands.

1.1.4.2   Copper Schiff-base complexes

Copper is a late first row transition metal with an electronic configuration of $[Ar]3d^{10}4s^1$. Copper coordination complexes generally have the copper ion in the +1 or, more commonly, in +2 oxidation state, which is the most stable. Copper(III) and copper(IV) are also known but are rare in comparison.[19] This introduction will concentrate on the coordination chemistry of the copper ion in the +2 oxidation state.

The copper(II) ion has a d^9 configuration and is paramagnetic due to its single unpaired electron, unlike the copper(I) ion which is always diamagnetic. This d^9 configuration means that the coordination of the copper(II) ion is subject to Jahn-Teller distortion when in an octahedral or a tetrahedral geometry. This means that it 'requires molecules to adopt geometries that do not lead to a degeneracy in valence level orbitals'[19] i.e. distortion occurs from the true octahedral or tetrahedral geometry. Copper(II) coordination complexes are generally coloured blue or green and in some cases, brown, with the coordination sphere of the copper(II) ion influencing the resultant colour of the complex.

Copper(II) coordination complexes using Schiff-bases modelled on the sal ligand are numerous in the literature. These compounds have found use as catalysts,[20] antimicrobial agents[21] and metal chelate inhibitors[2] amongst others. The ligand generally binds through the nitrogen and oxygen donors in an equatorial fashion to the metal with the axial sites occupied by the appropriate counterion or a donor solvent, as shown in Figure 1.3, as befitting of copper(II) complexes which generally adopt five- or six-coordinate environments.

Outside of the sal template there is also an array of Schiff-base ligands that use heterocyclic functional groups to provide the donor atoms. Chief among these are the ligands using the heterocyclic pyridine moiety to effect complexation. These pyridine derivatives are a suitable substitute for the phenol, with the additional nitrogen atom in the same role as the *ortho* oxygen atom in the sal derivatives.
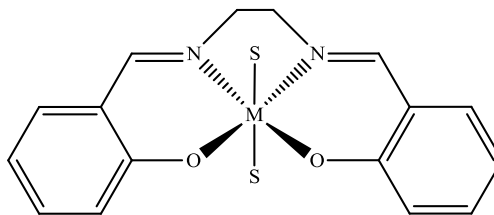
Figure 1.3: General N_2O_2 binding mode of salen Schiff-base derivatives with S denoting a donor molecule.

1.1.4.3   Nickel Schiff-base complexes

Nickel is a late first row transition metal with an electronic configuration of [Ar]$3d^8 4s^2$. The most common oxidation state of the metal, and the only one that will be introduced here is the +2 oxidation state.

Nickel(II) complexes can adopt a wide variety of coordination geometries and vary from octahedral to square planar, but may also include five-coordinate and tetrahedral coordination modes. The most common geometry is the six-coordinate octahedral orientation. Aqua and ammine nickel(II) complexes always adopt this geometry, with their colouring ranging from blue to bright green, which is a result of the spectrochemical series. The d^8 configuration of octahedral complexes result in paramagnetic complexes formed. This can be explained by the splitting of the d-orbitals in crystal field theory.

Five-coordinate nickel(II) complexes are reasonably common. They adopt either the square pyramidal or the trigonal bipyramidal geometry and both high- and low-spin derivatives are known.

Four-coordinate nickel(II) complexes can be either tetrahedral or square planar. Enforcement of the tetrahedral geometry is achieved by the use of bulky substituents on the ligands which sterically hinder the formation of the square planar derivative. The term tetrahedral is used loosely as they are often highly distorted. They are, however, paramagnetic and this trait is useful in distinguishing them from square planar complexes, which are predominantly diamagnetic. This is because the configuration causes one of the d-orbitals ($d_{x^2-y^2}$) to be high in energy, with the eight d-electrons occupying the four remaining d-orbitals.[19]

The use of sal Schiff-base ligands in the preparation of nickel(II) complexes generally leads to the formation of square planar nickel(II) complexes.[22] From these nickel(II) complexes tin(IV) adducts have been prepared.[23] These have found uses as potential catalysts. There are several exceptions where the nickel(II) ion adopts an octahedral geometry. Its coordination sphere is completed by coordination of a donor solvent, in this case water.[24] In the case of neutral ligands, if the metal occupies the octahedral geometry the axial groups may be either solvent or a coordinating counter anion. Complexes with coordinating anions such as azides and thiocyanates have been prepared.[25] The difference in the counterion of the nickel(II) salt used influences the coordination sphere adopted by the metal.

Nickel(II) Schiff-base complexes have found use in the asymmetric synthesis of α-amino acids[26,27] and in alkylation reactions of these amino acids by alkyl halides as well as in Michael addition reactions.[28] An example of some of the catalysts used is shown in Figure 1.4. These reactions have been reported to yield diastereomeric excesses (d.e.) greater than 98 % and e.e.s of up to 97 %. These nickel(II) complexes function by exploiting the coordination chemistry of the nickel(II) ion and its preference for adopting a square planar geometry and result in the stereoselectivity mentioned.
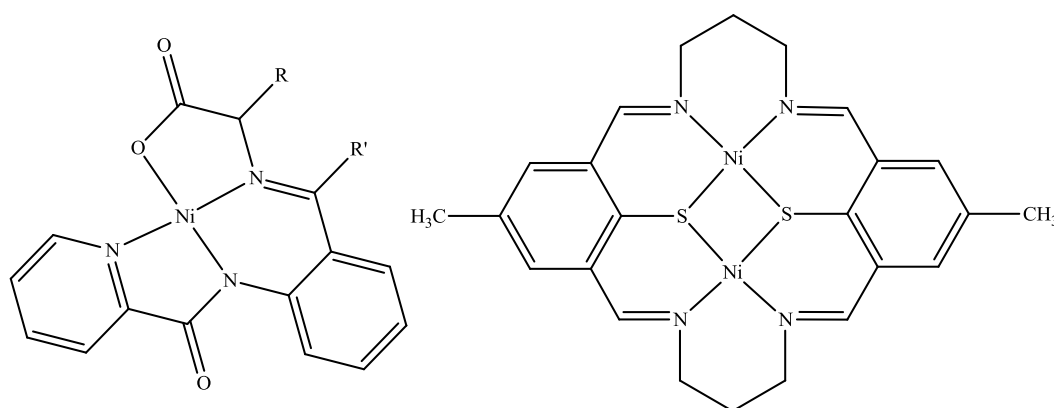
Figure 1.4: Nickel(II) catalyst (left), used in synthesis of α-amino acids, where R = CH$_3$, H and R' = Ph, H.[27] Enzyme mimic (right) developed by Brooker *et al.* with counterions either perchlorate, triflate or thiocyanate not shown.

Another use for nickel(II) Schiff-base complexes is the preparation of enzyme models, specifically metalloenzymes. One example of this is the work carried out by Brooker *et al.*, where the use of macrocyclic ligands are employed.[29] These macrocyclic ligands

afford additional stability to the nickel(II) thiocyanate complexes, some of whom are problematic.[30]

1.1.4.4   Zinc Schiff-base complexes

Zinc is a late first row transition metal (Group 12) with an electronic configuration of $[Ar]3d^{10}4s^2$. It contrasts with other first row metals in that, whereas copper may lose one of its *d*-orbital electrons along with its *s*-orbital electron to give the copper(II) ion, this does not happen with zinc. Zinc forms the zinc(II) ion exclusively by the loss of the two *s* electrons. Its full *d*-orbitals mean that zinc(II) complexes are diamagnetic. It also means that there is no ligand field stabilisation effect in its coordination complexes. The stereochemistries of these species are determined by considerations of electrostatic forces, covalent bonding forces and the size of the metal ion.[19]

Historically, organozinc compounds are important as they were the first organometallic species to be prepared in 1849 by Edward Frankland. His preparation of diethylzinc led to an explosion in the use of organometallic reagents, many of whom are still indispensible today, namely the organolithium and Grignard reagents. Organometallic zinc compounds can exist as organozinc halides or as diorganozinc and are synthetically important in strategies that require chemical compatibility with functional groups such as esters. Examples of the use of organozinc reagents include the Reformatsky[31] and Simmons-Smith[32] reactions. Further work on the addition of these organozinc compounds to aldehydes has given rise to asymmetric derivatives.[33]

Zinc neurochemistry has enjoyed a lot of attention as it is the second most abundant *d*-block metal, after iron, in the brain. Work on determining the function of zinc in the brain has been carried out by Lippard and co-workers, using selective fluorescent sensors for the zinc(II) ion.[34] It is now known to regulate a variety of ion channels, is involved in neurodegenerative disorders and may be vital to neurotransmission.[35]

Zinc(II) Schiff-base coordination complexes are well known, although not in the same abundance as that reported for the copper and nickel derivatives. The zinc(II) ion is known to occupy either a four-, five- or six-coordinate geometry, with the four- and five-coordinate complexes being the most common.[19] An exception to this trend is a communication by Ma *et al.* who have designed a pentadentate Schiff-base ligand, as shown in Figure 1.5, that yields a heptacoordinate zinc(II) complex when reacted with

zinc(II) chloride, with the two remaining coordination sites occupied by donor solvent molecules.[36]
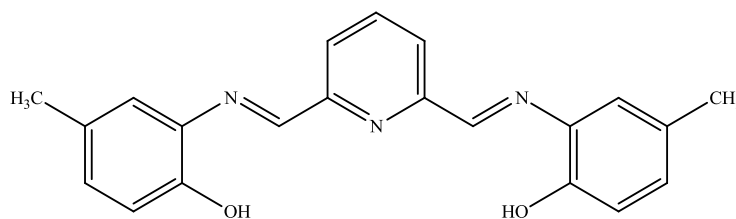
Figure 1.5: Pentadentate Schiff-base ligand by Ma *et al.*[36]

On complexation to sal Schiff-base derivatives, the zinc(II) ion tends to occupy a four-coordinate square planar N_2O_2 coordination sphere. The planar binding of the ligand is not exclusive to the zinc(II) ion. This has also been observed for both the copper(II) and nickel(II) derivatives. For the zinc(II) salphen complex (where the diimines are linked *via* an *ortho* substituted benzene ring) a five-coordinate complex is prepared by the addition of various functionalised pyridine derivatives. These yield a distorted square pyramidal zinc(II) complex, shown in Figure 1.6, with the pyridine donor occupying the apex of the coordination sphere. A feature of note in the work by Kleij *et al.* is that when the pyridine donors have substituents at the *ortho* positions, their ability to coordinate to the zinc is sterically impeded. Even small methyl groups are enough to cause this effect.[37]
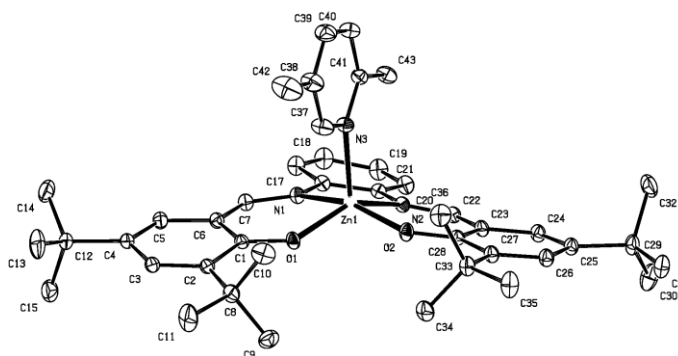
Figure 1.6: Five-coordinate Zinc(II) salphen complex.[37]

According to a wide ranging review on the properties of Schiff-base transition metal catalysts by Gupta *et al.*, the catalytic activity of a zinc(II) Schiff-base complex on the decomposition of hydrogen peroxide has been explored and yielded unexceptional results.[9] This is not surprising since the zinc(II) ion is not a redox metal. Interest in

these zinc complexes because of their luminescent characteristics has led to research in their use as potential organic light emitting diodes.[38]

1.2   Calix[4]arene chemistry

1.2.1   Overview

Because of their ease of preparation and subsequent functionalisation, parent calix[4]arenes and their derivatives are very popular and versatile macromolecules in the realm of supramolecular chemistry. Uses for these derivatives have ranged from heavy metal extraction to capsules for drug delivery. The upper and lower rims have been subjected to a variety of transformations with metals bound at both. The aim of this Section is to give an overview of the synthesis of the parent macrocycles, the methods employed in functionalising them (material will concentrate solely on lower rim functionalisation) and a flavour of the wide scope of tasks these molecules have been employed in.

1.2.2   Synthesis of calix[4]arenes

The calixarene is a macrocycle that is formed *via* a base-catalysed condensation between a *para*-substituted phenol and formaldehyde. Depending on the base used, derivatives such as the calix[4]arene, calix[5]arene, calix[6]arene or calix[8]arene can be prepared. Calixarenes originated from work on phenol and formaldehyde chemistry, specifically from work reported by von Baeyer in 1872, although the analytical tools at the time resulted in incomplete characterisation of the macrocycles.[39] Work by Zinke in 1942 reported the first crystalline product from a condensation reaction between 4-*tert*-butyl phenol and formaldehyde. He determined its empirical formula to be $C_{11}H_{14}O$, and assigned it a tetrameric structure mainly because the substituted phenol could only have reacted at the *ortho* position.[39]

Work by Cornforth in 1955 built on the previous studies by Zinke.[40] He repeated Zinke's work and was able to isolate two similar products that possessed different melting points. Cornforth, like Zinke, assigned tetrameric structures to both of his products. He proposed that the two compounds were due to the presence of two

isomers, isomers which are known to exist today as a result of the restriction in the rotation about the aromatic-methylene C-C single bond. These isomers, which were later comprehensively characterised, are the commonly known diastereoisomers: cone, partial cone, 1,2-alternate and 1,3-alternate conformers and are displayed in Figure 1.7. The cone conformation is the most stable conformer due to the participation of the hydroxyl functional groups in intramolecular hydrogen bonding and that this has the effect of stabilising the configuration.
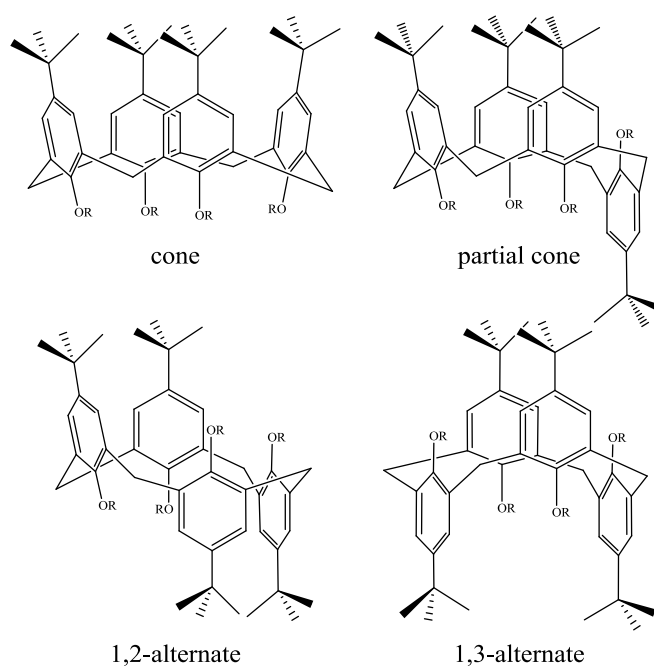
Figure 1.7: Four conformers of calix[4]arene.

Definitive assignment of the calix[4]arene structure was provided in 1979 in a communication by Andreetti *et al.* who solved the X-ray crystal structure of the *p-tert*-butylcalix[4]arene.[41] The group grew the calix[4]arene crystal from a toluene solution, which formed an inclusion complex with the solvent situated in the cavity of the macrocycle. This breakthrough followed the comprehensive keystone work carried out by C. David Gutsche. Gutsche's group were exploring the possible use of these calixarenes as a source of cavities to mimic the active sites of enzymes. It was Gutsche that first suggested that this family of macrocycles be known as 'calixarenes' because of their resemblance to a chalice (*calix* is Latin for chalice). Meshing this word with another representing the presence of an aryl moiety- 'arene' gives the familiar term that is well used today.

Gutsche's group used a method of preparing these macrocycles developed by Munch who used a slurry of *p-tert*-butyl phenol and paraformaldehyde in xylenes. This was heated to reflux in the presence of a catalytic amount of 50 % potassium hydroxide solution in an apparatus equipped with a Dean-Stark trap. Much of Gutsche's work lay in determining the optimum conditions for Munch's preparation and involved varying the catalyst, ratio of reactants and solvents used.[42] They subjected the Munch product to examination by mass spectrometry, and with a trimethylsilyl derivative discovered that it was in fact an octameric structure: calix[8]arene, a derivative that is now known colloquially as octamer. Conclusive proof of the existence of the calix[8]arene came in 1985 when Gutsche published its X-ray crystal structure.[43]

Whilst the Munch method provides for a convenient route to the calix[8]arene precursor, previous to this a far more laborious route was taken. An example of this was the step-wise route published by Hayes and Hunter,[39] of which is seen in Scheme 1.3. This involved the protection of one of the reactive sites with bromine. After a base promoted hydroxymethylation to provide the necessary methyl linker, steps (i) and (ii) were repeated as necessary to give the appropriate number of repeat units for the linear oligomer. Finally, the bromine was removed by palladium hydrogenolysis and the linear oligomer self condensed under high dilution conditions in the presence of acid to give the final product.

Munch's method, while high yielding and convenient to carry out, only yields the calix[8]arene, hence requiring conversion to the smaller tetrameric form. Gutsche published a method that involved heating to reflux in diphenyl ether in the presence of a catalytic amount of sodium hydroxide. Precipitation of the product was achieved by the addition of ethyl acetate to the warm phenyl ether solution. The exact mechanism of conversion is unknown. It is thought to involve the calix[8]arene 'pinching' in the middle and this is swiftly followed by cleavage of the molecule to give two equivalents of calix[4]arene. Gutsche dubbed this 'molecular mitosis'. His group published work on the mechanism of the tetramer formation and concluded that, although molecular mitosis is seen to occur, it is one of several different formation pathways that proceed concurrently.[44]

Given that both the octamer and tetramer are highly symmetric it is surprisingly easy to distinguish between the two. As both are highly symmetric, they have relatively

simple NMR spectra. It is possible to distinguish between them by the shift of the signal of the phenolic proton in the ^{1}H NMR spectra of the two compounds. Because of the size of the octamer, the lower rim has a larger circumference and so the phenolic groups have weaker hydrogen bonding interactions than the smaller calix[4]arene, who because of the smaller size of the lower rim, have stronger hydrogen bonding interactions occurring. As a result, the peak of the OH protons in the ^{1}H NMR spectrum of the calix[8]arene is 9.63 ppm and the corresponding signal for the calix[4]arene resonates at 10.34 ppm.

(i): HCHO, NaOH; (ii): **I**, HCl.
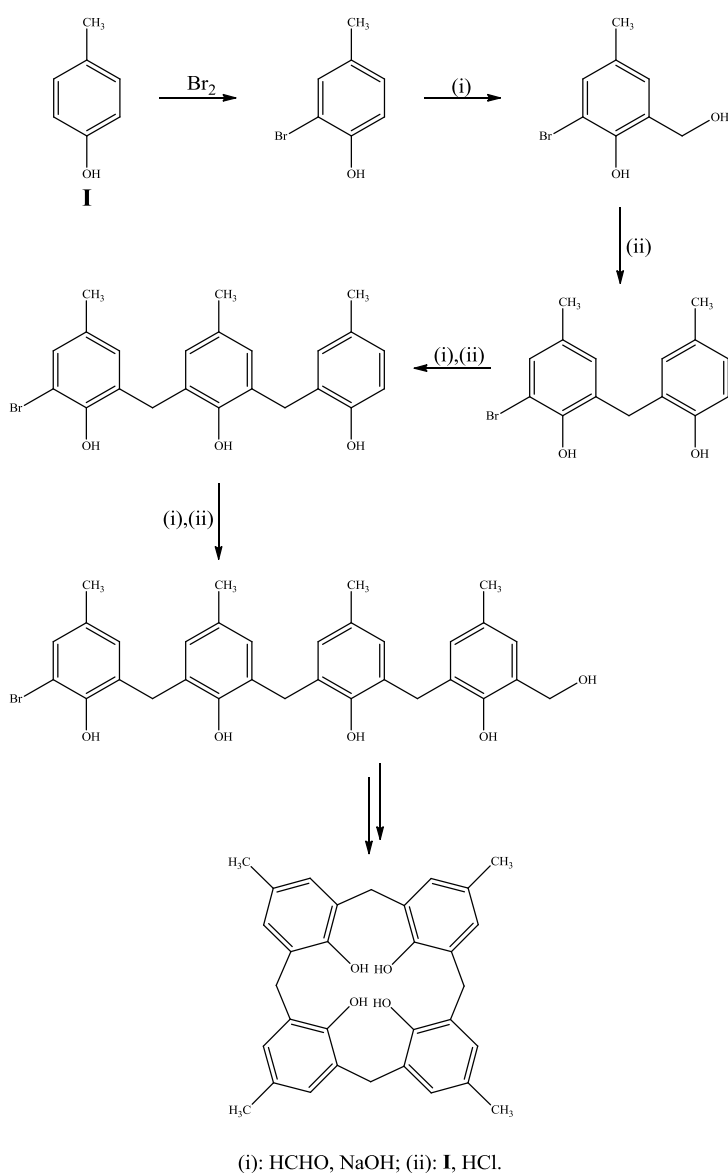
Scheme 1.3: Stepwise synthesis of cyclic macromolecule by Hayes and Hunter.[39]

1.2.3   Lower rim functionalisation of calix[4]arenes

As mentioned in the previous Section, the calix[4]arene has four conformers with the cone orientation being the only one that will be covered in this thesis. In the cone conformation, the hydroxyl groups are aligned on the same side of the cavity. Similar to the way a vase stands on its narrow end, so does the convention in the way calix[4]arenes are drawn, the narrower rim with the hydroxyl groups drawn below the wider rim that possesses the *tert*-butyl groups. As a result, the wider rim is denoted the upper rim and the narrower rim is denoted the lower rim as outlined by the representation in Figure 1.8.
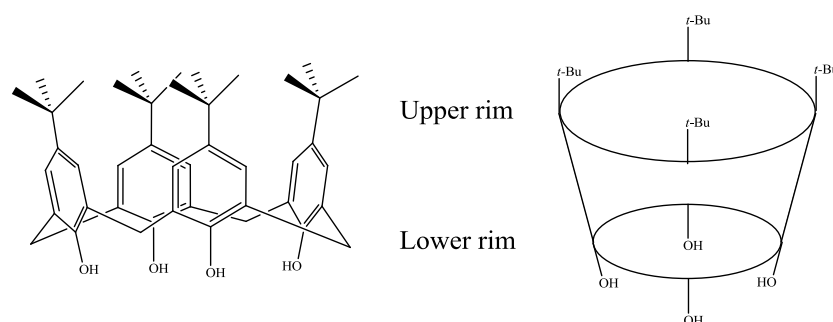
Figure 1.8: Calix[4]arene showing locations of the upper and lower rim.

Functionalisation of both the upper[45] and lower rim[46,47] has been achieved with great success and there are several reviews detailing the scope of modifications carried out. The calix[4]arene derivatives in this thesis are all achieved *via* the attachment of fragments to the lower rim of the macrocycle and as such, the material covered in this introduction will extend only to transformations on the lower rim of the calix[4]arene, specifically fragments containing Schiff-base or amide functional groups suitable for metal ion binding.

Functionalisation of the lower rim is relatively easy to achieve by way of well-established acid-base and nucleophilic reactions. Modifications generally entail the use of base, typically potassium carbonate, to give the calix[4]arene alkali salt. This reacts *in situ* with the appropriate alkyl halide to give the phenoxy-ether product. Halide derivatives used are of the chloro, bromo, and iodo varieties.[48,49] *p*-Toluenesulphonate containing electrophiles have also been employed to the same effect.[50] Phosphorus(V) ligand-containing calix[4]arene derivatives one of which is shown in Figure 1.9, have also been prepared. This is achieved through the use of

various derivatives of phosphorus(III) halides. They have been mainly used as ligands for transition metal ions to prepare novel catalysts.[51] All of the above have calix[4]arene-oxygen-substituent bonds. Prior to this, Georghiou *et al.*[52] used Sonogashira coupling to effect the formation of an aryl-allyl carbon-carbon bond on the lower rim, as displayed in Figure 1.9, an impressive achievement considering that similar work had been done using Suzuki-Miyaura[53] coupling to little or no effect. The hydroxyl group was converted to a triflate (in place of the usual halide) to provide a labile group to enable the palladium-catalysed reaction to proceed.
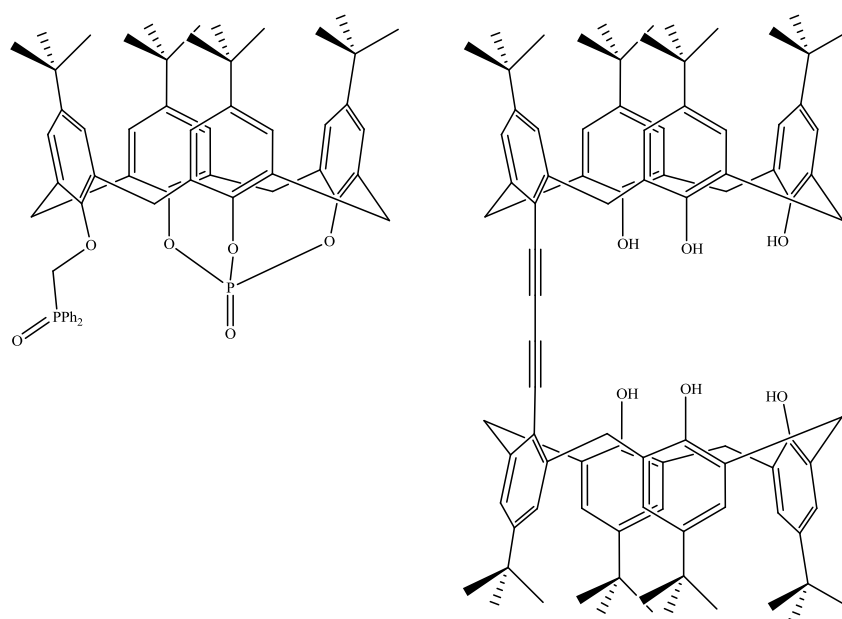
Figure 1.9: Phosphorus(V) containing calix[4]arene (left) and Sonogashira coupled calix[4]arene dimer (right).

Regioselectivity is an issue with difunctionalised calix[4]arenes. Products prepared can be either 1,2-proximal or 1,3-distal substituted, as shown in Figure 1.10. Hydrogen bonding interactions in the stability of the alkoxide intermediate dictate the formation of the 1,3-distal disubstituted regioisomer to be the major product. As the first equivalent of base proceeds to deprotonate the first phenoxy proton, the two proximal phenoxide moieties function as hydrogen bond donors to stabilise the intermediate, as shown in Figure 1.11. A nucleophilic substitution with the first equivalent of alkyl halide takes place to give the monosubstituted derivative. This can be isolated, however it usually requires purification by chromatography as it is often contaminated with unreacted calix[4]arene and some disubstituted product. The monosubstituted calix[4]arene is selectively deprotonated at the distal phenoxide as in this situation the

two proximal hydroxyl moieties are able to act as stabilising hydrogen bond donors. Contrast this with the case if deprotonation were to occur at a proximal hydroxy group. The alkoxide would be stabilised by only one hydrogen bond donor as the distance between two distal orientated phenolic oxygens on the macrocycle is in the range of 3.1-3.6 Å, (range taken from the X-ray data of calix[4]arene structures presented in this thesis) a distance too great for hydrogen bonding to occur. As in the previous situation, nucleophilic substitution occurs with a second equivalent of the alkyl halide to give the 1,3-distal disubstituted product.

1,2-Proximal   1,3-Distal
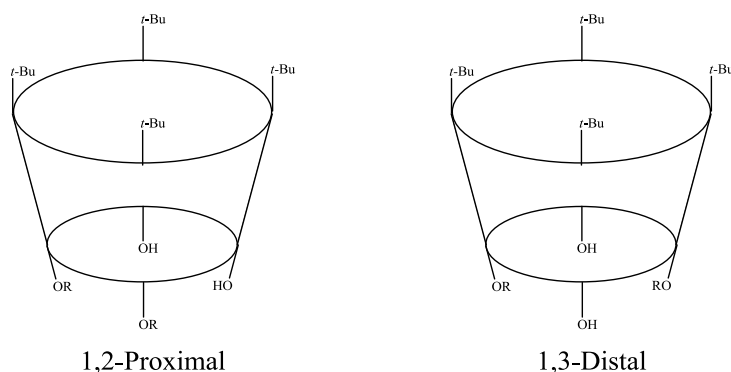
Figure 1.10: Regioisomers of disubstituted calix[4]arenes.

Evidence that hydrogen bonding interactions occur at the lower rim are when efforts are made to functionalise the remaining two phenoxy groups. The strength of the base required to deprotonate the residual alcohol groups is significantly greater than the relatively mild base (potassium carbonate) used for the initial phenoxy moieties. The use of sodium hydride or barium oxide has been employed for this purpose.[49,54] This is because there are no longer any hydroxyl protons present that can participate in stabilising the alkoxide ion formed, which renders the deprotonated alcohol fairly reactive (more basic in nature).
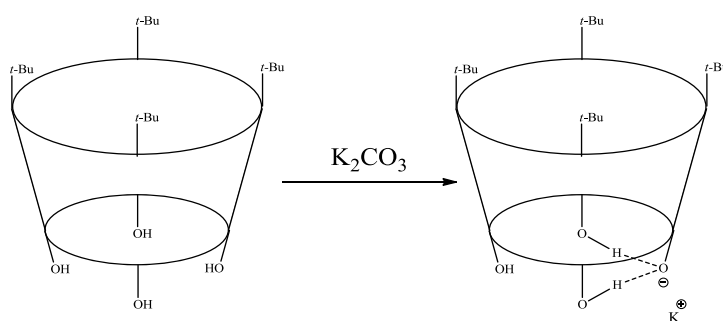
Figure 1.11: Deprotonation of lower rim hydroxyl showing H-bonding interactions.

1.2.4   Calix[4]arene Schiff-bases and amides

Functionalised calix[4]arenes containing Schiff-base and amide moieties are abundant in the literature. They are used as easily prepared linkages to ionophoric and/or fluorophoric fragments. Schiff-base linkages are often introduced *via* reaction with the benzaldehyde moiety or as an amine appendage precursor on the calix[4]arene. As mentioned previously, the aldehyde moiety participates as a reactant in imine formation. Both upper[55] and lower rim derivatives with Schiff-base moieties have been prepared. Calix[4]arene difunctionalised with the 2-aminoethyl moiety (whose structure, **II**, is shown in Scheme 1.4) provides a suitable point for imine formation to occur. One case of this is that by Liu *et al.* who attached *ortho*-vanillin to the diamine derivative, **II**, to prepare a lanthanoid ion binder that was selective for Eu(III) ions.[56]
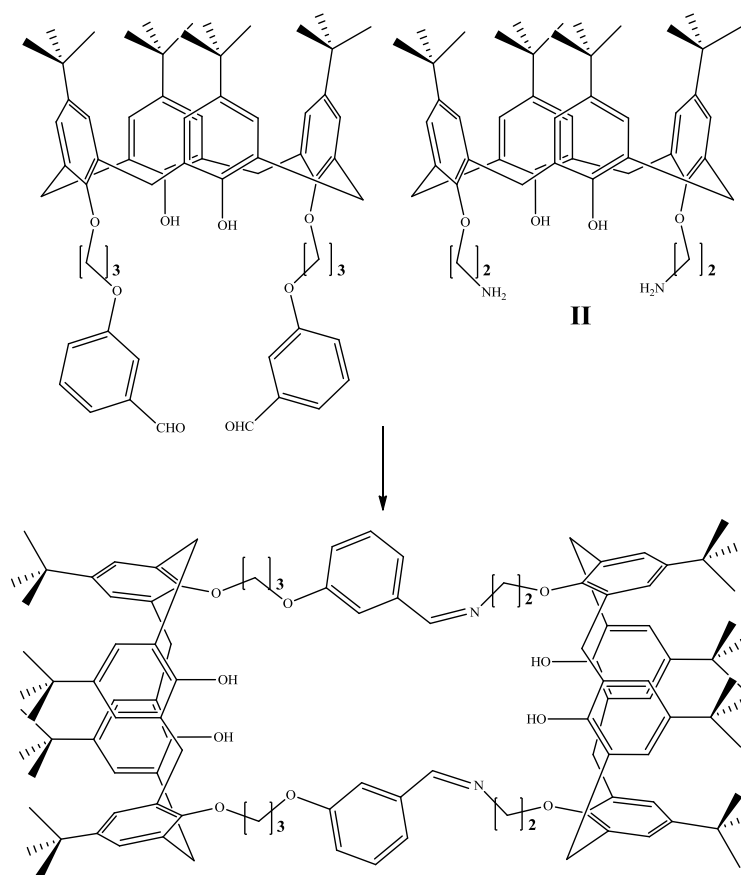
Scheme 1.4: Synthesis of calix[4]arene 'tube' by Murray *et al.*[57]

Some of these lower rim functionalised macromolecules have been used to prepare calix[4]arene 'tubes', where two calix[4]arenes are joined by their lower rims (tail-to-tail) *via* a Schiff-base linkage or in conjunction with another functional group, such as

a hydrazide. An example of this is the work of Murray and co-workers who prepared a calix[4]arene tube, as shown in Scheme 1.4, using an imine linkage to join the aldehyde and amine functionalised calix[4]arene precursors together.[57] This tube was subjected to binding studies using silver(I) salts and found that it does indeed bind to the silver(I) ion. It is not known how selective the calix[4]arene tube is as competitive binding studies were not reported.

Derivatives involving the use of the salicylaldehyde moiety as a linker have also been prepared. This involves the attachment of a linker to the *o*-hydroxy moiety of salicylaldehyde thus providing a tether to the macrocycle. Reaction of this calix[4]arene dialdehyde with a diamine (such as ethylene diamine) to prepare a bridged lower rim calix[4]arene derivative in the hope that binding to metal ions in a similar fashion to salen ligands would occur, i.e. through an N_2O_2 coordination sphere. Preliminary metal extraction studies by Vicens *et al.* resulted in a moderate affinity for copper(II) ions.[58] Further work on this ligand by the same group and the preparation of derivatives, shown in Figure 1.12, improved the metal ion extraction properties slightly.[59]

= $(CH_2)_n$, (n = 2-4), *o*- and *m*-C_6H_4
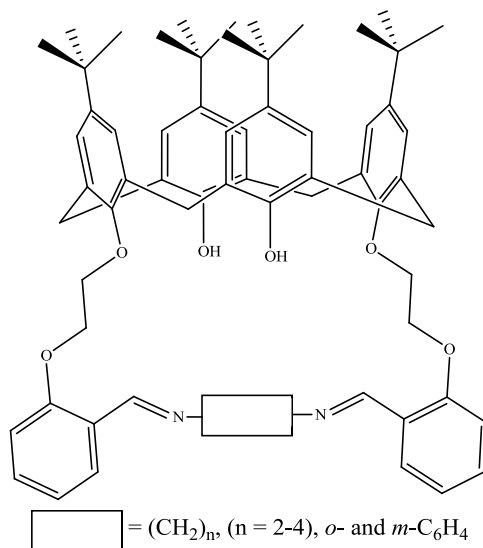
Figure 1.12: Selection of Schiff-base ligands prepared by Vicens *et al.*[58]

Aside from functioning as a precursor in the preparation of metal ion sequesters, the dialdehyde calix[4]arene has been used to prepare a fluororeceptor for the detection of dicarboxylates,[60] and involved the synthesis of a sodium borohydride-reduced Schiff-base derivative using an aminobenzimidazole moiety. The sensor showed good

selectivity toward pimelate (heptanedioic acid) over other dicarboxylates. An important point to note was that the calix[4]arene itself augmented the binding of the pendant arms as the phenolic hydroxyl groups participated in cooperative hydrogen bonding interactions with the carboxylate.

Apart from Schiff-base linkages, one of the most common ways to attach various functional groups is through the use of an amide or ester linkage. This literature survey will deal only with amide derivatives. These are often prepared by the synthesis of a calix[4]arene diester precursor, published by McKervey *et al.* through the use of an α-halo ester electrophile to give the 1,3-distally disubstituted product.[48] This group continued this work and extended the array of diamides prepared some of which are shown in Scheme 1.5. Some of the diamides were prepared by conversion of the ester to its more reactive acetyl chloride equivalent. The ester itself can, in some cases, be subsequently reacted with the appropriate amine to prepare a bridged diamide species on the lower rim. In fact, it is the overwhelmingly dominant product formed. 10-fold equivalent of the diamine still result in the capped structure with yields of up to 90 %.[61] Metal ion recognition studies have been carried out on the alkyl derivatives of these diamides.[62]

The introduction of additional heteroatoms improved the binding properties of the above diamides, specifically nitrogen donor atoms. Copper(II) complexes of these azacrown calix[4]arenes have been prepared by McGinley *et al.*, specifically a derivative synthesised using diethylenetriamine and the diester analogue shown in Scheme 1.5.[63] Whereas the binding ability of the alkyl diamide was limited in neutral conditions, the addition of a third donor atom allowed the calix[4]arene to bind to the copper(II) ion through the central nitrogen donor and also through the oxygen of one of the amide moieties: an N,O ligand. Reaction temperature and time was deemed to be crucial when using copper(II) chloride in complexation reactions with the azacrown calix[4]arene. Prolonged heating of the mixture results in cleavage of the amide bond to give the liberated amine which subsequently forms a coordination complex with the copper salt. A sketch of the calix[4]arene ligand and isolated by-product is shown in Figure 1.13.
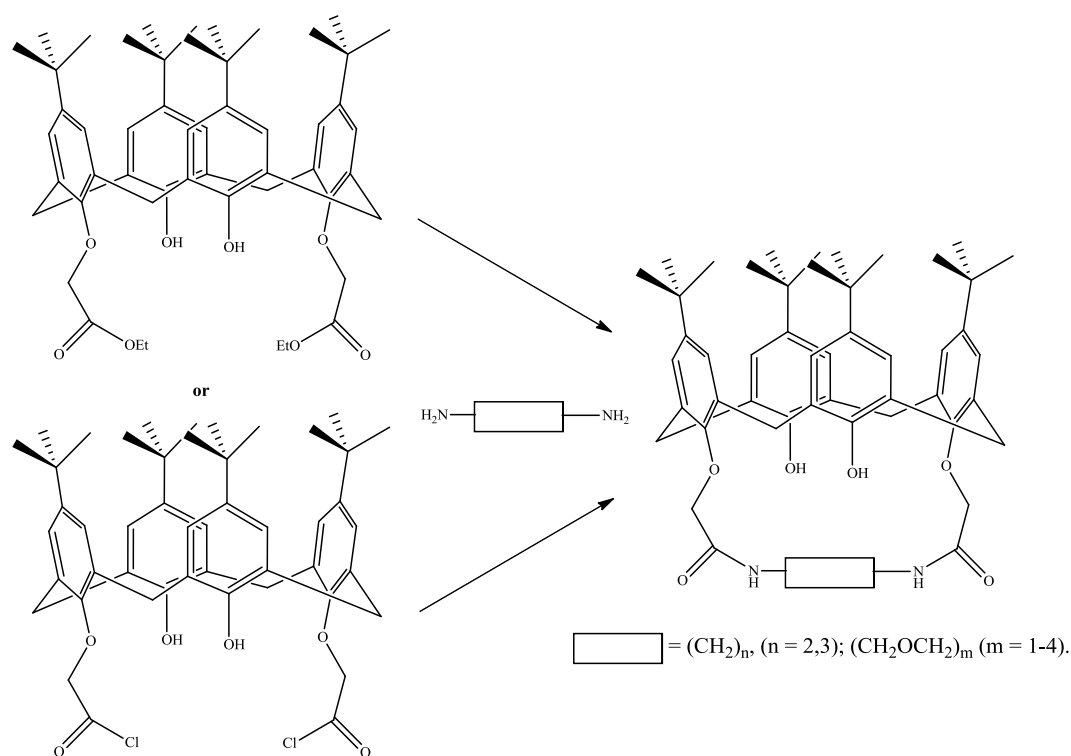
Scheme 1.5: Selection of diamide calix[4]arenes prepared using ester and acyl chloride derivatives by McKervey *et al.*[61]
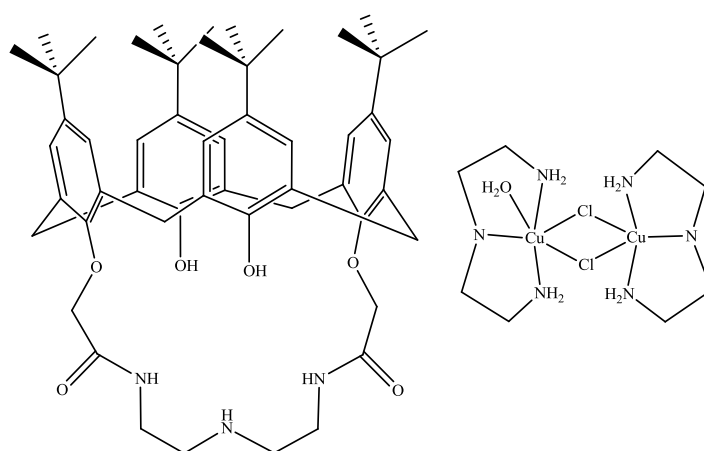
Figure 1.13: Calix[4]arene azacrown and amide cleavage by-product as a result of the addition of copper(II) chloride, isolated by McGinley *et al.*[63]

Amide derivatives have also been used in the preparation of enantioselective catalysts. Through the use of optically active amino acids and a derivative containing an optically pure binaphthyl derivative, Gaeta *et al*. were only able to achieve moderate to poor e.e. results, up to a maximum of 28 % in a titanium(IV) catalysed aldol reaction.[64] Amides have also found use as linkers to introduce fluorophoric moieties but these will be introduced in Section 1.3.2 in this thesis.

1.3   Fluorescence

1.3.1   Overview

The material covered in this thesis details preliminary investigations of the fluorescent properties of molecules containing the azine moiety. Fluorescence spectroscopy, its uses and the techniques employed are a whole realm of chemistry onto itself and as such will only be covered here in fundamental detail.
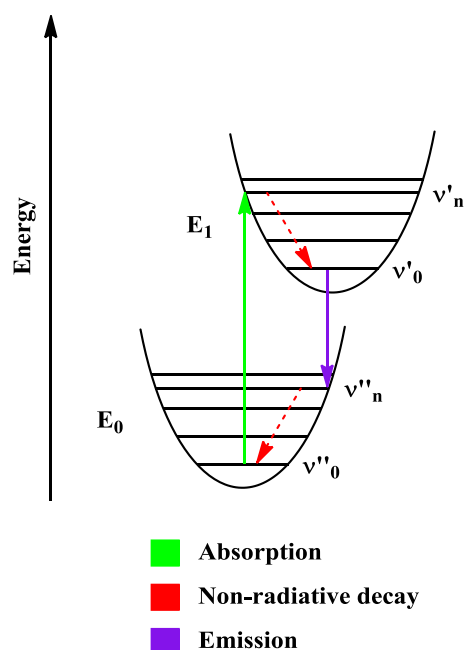
Figure 1.14: Effects of surrounding environment (solvent shell) showing how short range repulsive interactions of the molecule's excited state shift the excited state's potential causing a difference in energy between absorption and emission in solution.

Fluorescence is a natural phenomenon whereby the emission of a photon from an electronic excited state of a molecule occurs at a lower energy (longer wavelength) than the wavelength at which the photon was absorbed.[65] The difference in energy is known as the Stokes shift and can be explained by the Franck-Condon principle. The Frank-Condon principle states that 'an electronic transition is most likely to occur without changes in the positions of the nuclei in the molecular entity and its environment (e.g. its solvation sphere)'.[66] The transition is known as a vertical transition. As a result of the higher potential of the excited state, as seen in Figure 1.14, the vertical transition from the lowest vibrational energy level of the ground state, ν''_0, intersects the excited state at the ν'_n energy level. The excited electron loses energy

through non-radiative decay to the lowest vibrational energy level in the excited state: ν'_0. The emitted photon originates from a transition, ν'_0 to ν''_n, a point where its vertical transition intersects the ground state potential energy curve. As before, non-radiative decay returns the electron to the lowest vibronic energy level: ν''_0. The above transitions are summarised by the drawing in Figure 1.14, the difference in energy between absorption ($\nu''_0 \rightarrow \nu'_n$) and emission ($\nu'_0 \rightarrow \nu''_n$) is the reason why a Stokes shift occurs.

Fluorescence has short lifetimes (the time between its excitation and its return to ground state), typically in the order of less than 10 nanoseconds. This differentiates it from the other luminescent phenomenon which is phosphorescence. Phosphorescence can have extended lifetimes in excess of one millisecond.[66]

In the case of fluorescence, a photon (thermal energy is not enough to effect an electronic transition) is absorbed by the molecule. A single electron absorbs this energy and undergoes an electronic transition from the singlet ground state S_0 to the singlet excited state, S_1. This excited electron, arbitrarily denoted a, ($S_a = +\frac{1}{2}$) is spin paired with the corresponding electron, denoted a^*, in the ground state orbital ($S_{a*} = -\frac{1}{2}$) and is known as a singlet-singlet transition which is spin allowed ($\Delta S = 0$). The notation of the singlet state originating from the multiplicity formula M $= 2S + 1$, where M is the multiplicity of the state and S the number of unpaired electrons. The excited electron must lose energy to return to the more stable ground state and it does this by a number of possible pathways including emission of light (luminescence) and non-radiative transitions (where energy is transferred to the surrounding solvent, vibrations, rotations etc.). The excited electron must lose energy to return to the ground state and if it does this by emitting a photon then fluorescence occurs.[67]

Phosphorescence, in comparison involves a spin forbidden transition ($\Delta S \neq 0$). Absorption occurs in the same manner as with the fluorescence absorption transition. In phosphorescence however the electron undergoes a change of spin ($S_a = +\frac{1}{2}$ to $-\frac{1}{2}$) to the T_1 triplet state. This triplet state is slightly lower in energy than the corresponding S_1 state (due to Hund's Rule). Conversion from S_1 state to the T_1 state (intersystem crossing) becomes possible due to spin-orbit coupling. The result of this is that the wavefunction of the singlet state always contains a small but not negligible fraction of a triplet wavefunction.

24

Fluorescence is more common in fluid solutions, where many deactivation processes may take place that compete with emission such as non-radiative decay (energy loss through the solvent).[66] A summary of the radiative and non-radiative processes are shown in the Jablonski diagram in Figure 1.15.[66]
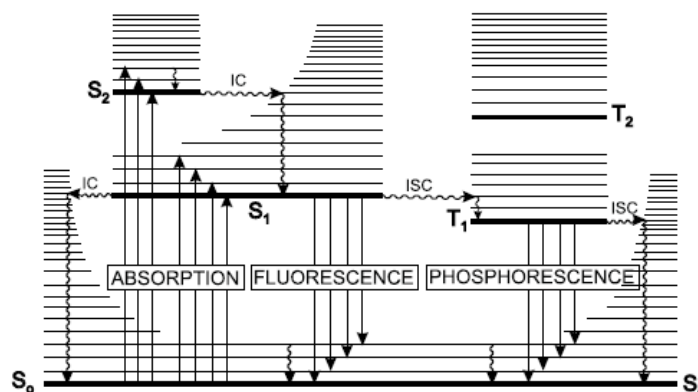
Figure 1.15: Jablonski diagram showing possible processes between electronic states with abbreviations denoting S-singlet state, T-triplet state, IC-internal conversion and ISC-intersystem crossing.[66]

1.3.2   Fluorescent ionophores

Fluorescence is commonly observed in aromatic molecules. This is because of the extensive electron delocalisation of the π electrons. This extensive π system lowers the energy required for a $\pi \rightarrow \pi^*$ transition (the lowest energy transition) and as a result yields a larger wavelength emission band than the corresponding absorption band. In cases where a heteroatom is present, the lowest absorption may be the $n \rightarrow \pi^*$ transition.

Fluorophores (fluorescent sensors) can be separated into three classes, those that a) undergo quenching on collision with an analyte, b) reversibly bind to an analyte, and c) a fluorophoric moiety linked to a receptor (with the option of using a spacer). Class a) involves a fluorescence-on fluorophore that collides with an analyte and results in quenching of the fluorophore. Quenching by O_2 is well known.[66]

Class b) has the fluorophore acting as a ligand. In essence, the sensor has a dual role in that it binds the substrate and acts as an indicator with changes in its fluorescence intensity upon complexation or dissociation. This class of fluorophore can also function as a pH indicator. If a metal ion is bound the term fluorescent chelating agent can be used. If a proton is the analyte, the term fluorescent pH indicator is appropriate.

If fluorescent enhancement occurs upon analyte binding the compound is said to be fluorogenic. This class of sensor has two possible modes of action. It can be either a Chelation Enhancement of Fluorescence (CEF) or Chelation Enhancement of Quenching (CEQ) indicator.[66]

Class c) contains two separate functioning moieties, a receptor for the analyte and a fluorophore as an indicator. This class is commonly used in supramolecular chemistry. These sensors are designed with selectivity and affinity in mind to function as selective ion sensors and are known as ionophores. The entire system with both the fluorophore and the ionophore is, appropriately enough, known as a fluorionophore. These can function either by CEF or CEQ. A schematic representing the three sensing modes is shown in Figure 1.16.
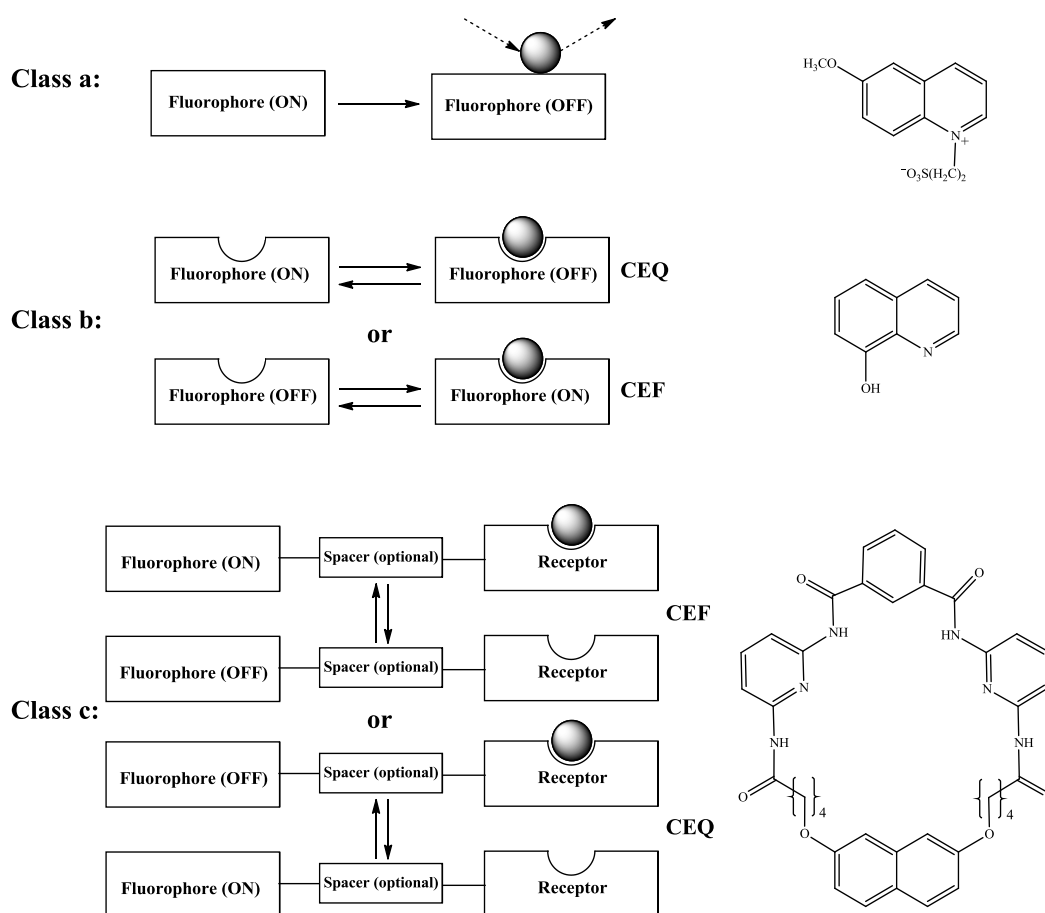
Figure 1.16: Three classes of fluorophores with examples of each: a) quenching by collision; b) Chelation Enhancement of Quenching (CEQ) or Chelation Enhancement of Fluorescence (CEF) by ion complexation; c) CEQ or CEF fluorophores linked to receptor.

Fluorophores such as coumarins and fluorescein have found use as pH indicators because of large variation in their fluorescence intensity versus pH and have been used

to determine intracellular pH.[68] A derivative of fluorescein, BCECF (2',7'-bis(carboxyethyl)-5(or 6)-carboxyfluorescein (the structure of which is shown in Figure 1.17) has become the most widely used fluorescent pH indicator because it possesses a pK_a of approximately 7.[69]
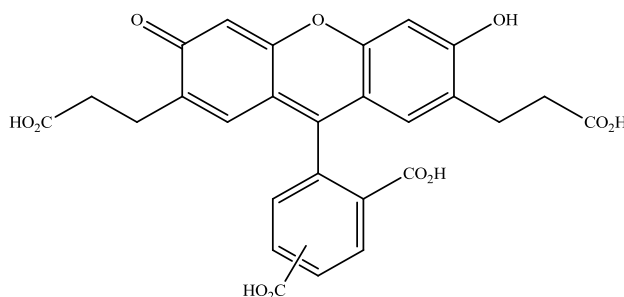
Figure 1.17: Fluorophore BCECF.

The properties of ionophores are dependent on several conditions. Considerations must be made about the nature of the cation and the environment (e.g. solvent employed and pH). To design a successful ionophore, the required properties of the ligand should complement the characteristics of the cation. Factors such as ionic size, coordination number and the hard or soft nature of the cation are considered. The number and nature of donor atoms involved in complexation should complement the nature of the cation. For example, oxygen donors generally prefer binding to hard metal cations such as sodium, potassium or magnesium ions. Soft donor atoms such as nitrogen, sulfur and phosphorus prefer softer metal cations such as transition metal ions. Solvent effects can have a bearing on whether complexation with the cation occurs or not. The solvating power of the ligand must exceed that of the solvent.

One of the most common characteristics of fluorescent detectors is that they employ the use of Photoinduced Electron Transfer (PET). Most fluorescent PET molecular sensors consist of a fluorophore linked to an amine moiety (an electron donor) *via* a spacer. PET takes place from the amine groups to the aromatic hydrocarbon (fluorophore) causing fluorescence quenching of the latter. When the amine (donor) group binds to a cation, electron transfer is hindered and an enhancement of fluorescence is observed.[67] The schematic in Figure 1.18 represents the processes involved.[66] Upon excitation of the fluorophore, an electron is promoted from the Highest Occupied Molecular Orbital (HOMO) to the Lowest Unoccupied Molecular Orbital (LUMO). This is followed by PET from the HOMO of the donor to the HOMO

of the fluorophore, causing quenching of fluorescence. Electron transfer is disrupted when the lone pair of the donor becomes unavailable because it is occupied in binding to the metal ion. This results in a rising of the redox potential of the donor and a consequential lowering of the HOMO energy of the donor which prohibits PET from occurring.[66]
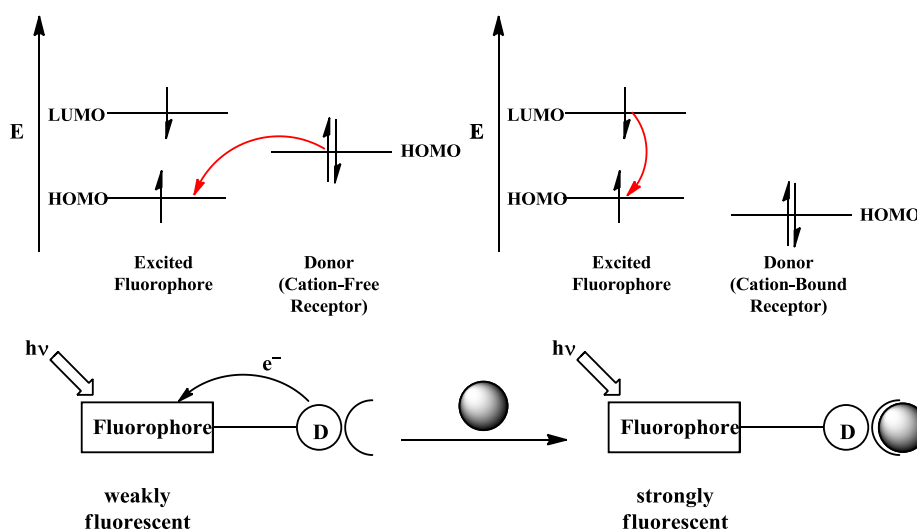
Figure 1.18: Representation of the PET process.[66]

Fluorionophores are generally based on the PET mode of action with crown-ethers and cryptands forming the ionophoric moiety for a majority of designs. Their hard donor nature means they are designed for sensing Group I and II metal ions with potassium and sodium being the most common.[70] Carboxylate groups are also good binders that are suitable for the binding of these hard cations, particularly divalent cations such as calcium(II) and magnesium(II).[67] Ionophores with softer donor atoms (nitrogen, sulfur or phosphorus) show selectivity in binding softer metal ions such as zinc(II), nickel(II) or copper(II). One such family of compounds are the polyamines who possess multiple nitrogen donors for metal binding.[71]

The PET phenomenon can also be applied to excimer- or exciplex-based sensors. Excimer is an abbreviation of 'excited dimer' where two identical fluorophores (one in the excited state) are brought in close proximity to each other whereas exciplexes are analogues of excimers (excited complex) where two different molecules are brought close to each other.[66] The formation of both are generally diffusion controlled but, relating to excimers, if the two fluorophores are on the same molecule excimer formation can be induced by the presence of a metal cation which brings the

fluorophores nearer to each other, thus allowing excimer formation to occur.[66] An example of an excimer-based sensor is shown in Figure 1.19.[72] On addition of copper(II), the monomer-excimer ratio was seen to change. The binding site is described as having a *pseudo*-crown ether character. The copper(II) ion induces a conformational change in the chelator, thus bringing the two naphthyl moieties together to form the excimer complex, and consequent quenching of fluorescence.
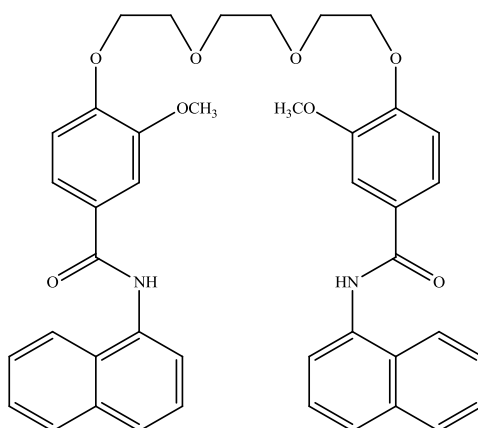
Figure 1.19: Sensor for copper(II) using excimer formation.[72]

Transition metals, especially the ones with redox properties, can participate in electron transfer from the fluorophore to the bound metal ion, or vice versa.[66] In some cases with the *d*-block metals, electron exchange takes place which results in quenching of the fluorophore by non-radiative energy transfer.[73] One such case is the fluorescent sensor developed by De Santis *et al.*,[74] which consists of a crown-thioether ionophore and an anthracene fluorophore, as shown in Figure 1.20. Quenching occurs on the copper(II) ion binding to the sulfur atoms. Quenching arises *via* a photoinduced electron transfer (PET) from the fluorophore to the metal centre and involves the copper(II)/copper(I) couple. Evidence for the presence of a PET effect is when the ligand binds silver(I) ions, a change in the fluorescence intensity is not observed because of the poor redox activity of the cation. This means it is unable to participate in any potential electron transfer process. The binding mode of this ionophore for the zinc(II) ion, and its lack of redox traits would most likely be unable to curb PET from occurring, similar to that observed of the silver(I) ion.

Calix[4]arene fluorophores have also been developed because of the ionophoric properties of the macrocycle and there are several reviews in the literature covering this class of ion binder.[47,75] Usually modification of the calix[4]arene takes place with

the addition of a known fluorophore such as pyrene or dansyl derivatives.[76,77] Many of these sensors are difunctionalised calix[4]arenes and as such, are suited to form excimers upon metal ion binding. A recent example in the literature that goes against this trend is a novel sensor synthesised by Matthews *et al.*, who incorporated triazoles into their design to facilitate metal binding.[76] The fluorescence of the free ligand is restrained due to the formation of excimers with the pendant pyrene units. The triazole functional groups, as shown in Figure 1.21, can selectively bind cadmium(II) and zinc(II) ions, and results in an enhancement of fluorescence as excimer formation is discouraged by the presence of the bound metal ion.
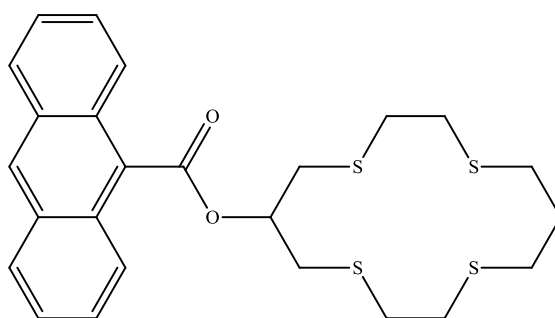
Figure 1.20: Copper(II) sensor resulting in quenching from PET.[74]
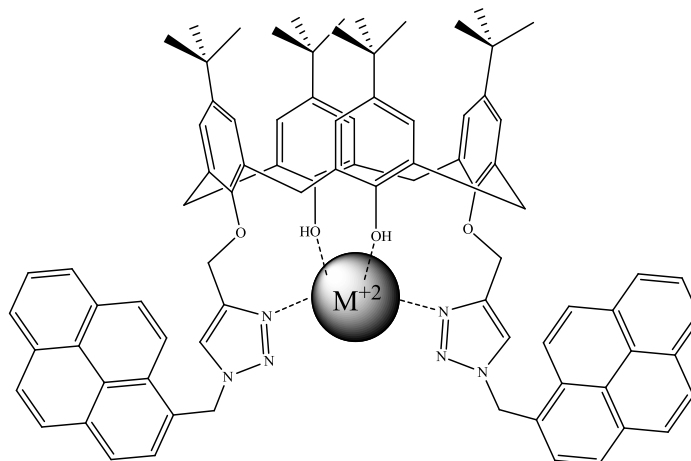
Figure 1.21: Cadmium(II) and zinc(II) fluorionophore prepared by Matthews *et al.*[76]

1.3.3   Zinc(II) fluorionophores

As mentioned previously, the zinc(II) ion does not possess redox properties and so cannot participate in electron transfer, like other 3*d* metals.[19] It is however,

biologically important and so there are abundant cases in the literature that report developments of biologically suitable fluorescent zinc(II) ionophores.[34,78]

Zinc neurochemistry has enjoyed a lot of attention as it is the second most abundant *d*-block metal, after iron, in the brain. Much of the pioneering work on developing these biocompatible sensors has been carried out by Lippard and co-workers, using selective fluorescent sensors for the zinc(II) ion.[34] Zinc is now known to regulate a variety of ion channels, is involved in neurodegenerative disorders and may be vital to neurotransmission.[35] In addition to these processes it is known to be present in some metalloenzymes where it functions as a Lewis acid. The most well known of these enzymes, carboxy peptidase A and carbonic anhydrase, have been intensively studied and their modes of action are well known.[19]

The main requirements of an effective zinc fluorophore are that it must provide enough donor atoms to fill the common coordination sphere of the zinc(II) ion with the metal ion having common coordination modes varying from numbers four to six. The zinc(II) ion is not a very hard cation and so the use of softer donor atoms would be prudent, nitrogen being the donor atom of choice, though oxygen donor atoms are also adequate for this function. If the sensor is to be used in a biological environment it should be excitable with visible light, as the use of UV light can result in cell damage and so should be avoided.[79]

Using Schiff-bases to construct fluorionophores has become a convenient way of preparing novel zinc(II) sensors. One recent example of this is the sensor developed by Wu and co-workers, who have developed a water soluble ligand that selectively exhibits enhanced fluorescence upon binding to zinc(II) in competition with other metal ions (sodium(I), potassium(I), calcium(II), and magnesium(II)).[10] The ligand (shown in Figure 1.22) contains a carboxylic acid functional group that facilitates its dissolution in water.

Another class of fluorophores that are facile to synthesise are those based on the azine moiety. Azines have an integrated degree of conjugation from the two imine bonds which are separated by a single bond between the two imine nitrogen atoms so the addition of a fluorophore is unnecessary. The conjugation is extended to include the aromatic rings. Examples of benzazines are those prepared by Görner *et al.* (shown in Figure 1.23), who used standard Schiff-base reaction conditions to form the product

from the reactant hydrazine and aldehyde.[80] These ligands were subsequently reacted with zinc(II) acetate to form the corresponding zinc azine coordination complex. The group studied the photochemistry of both the free ligands and the metal complexes. The hydroxyl group *ortho* to the imine participates in a photo-induced intramolecular proton transfer to the imine nitrogen, leading to the formation of several transient species that exist in a tautomeric keto-enol relationship.
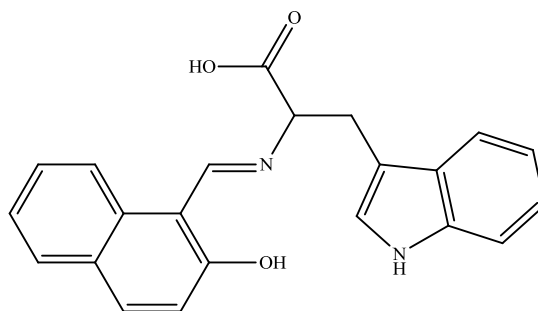
Figure 1.22: Water soluble zinc(II) selective fluorophore prepared by Wu and co-workers.[10]
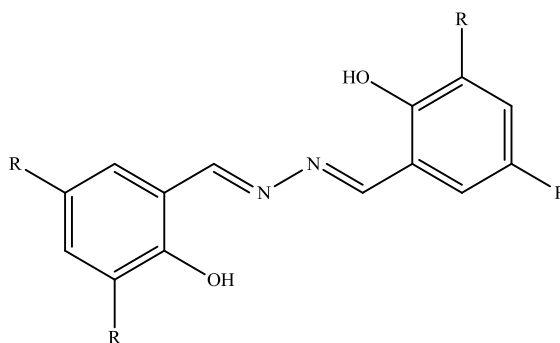
Figure 1.23: Azine ligands (where R = H or *tert*-butyl) prepared by Görner *et al.*[80]

More recently, work has been carried out on expanding the array of benzazines that are subjected to examination of their photochemical characteristics. A study by Tong and co-workers suggested that fluorescence by the molecules can be enhanced by aggregation.[81] This is unusual since most fluorescent molecules show quenching in their aggregate or solid states because of excimer formation which causes enhanced non-radiative emission of the excited state. The N-N single bond of the azine allows for free intramolecular rotation (known to be effective for fluorescence quenching) in the single molecule state but in an aggregate state this rotation is inhibited. Rotation exclusively about the N-N only is ensured by the formation of intramolecular hydrogen bonds between the *ortho* hydroxyl moiety and the imine nitrogen. The group explored the possibility of using the azines as hydrazine sensors.[81]

1.4   Benzamides and metal complexation

1.4.1   Binding modes and synthesis of amides

Benzamides, while not as straightforward to prepare as imines, are still one of the most common functional groups employed in the preparation of an aromatic ligand. The amide functional group by its nature can give rise to the formation of regioisomers when forming a metal complex as it is possible to coordinate through either the nitrogen or the oxygen atoms, i.e. it is a ligand with ambidentate character. An example of the anionic binding mode of the amide is the work by Fry *et al.* who used a diamide with adjacent S, O and P donors, whose structures are shown in Figure 1.24, to prepare a ruthenium coordination complex.[82] The parent amide required deprotonation of the amide hydrogen by a strong base, in this case sodium hydride, to enable the ligand to bind to the ruthenium ion.
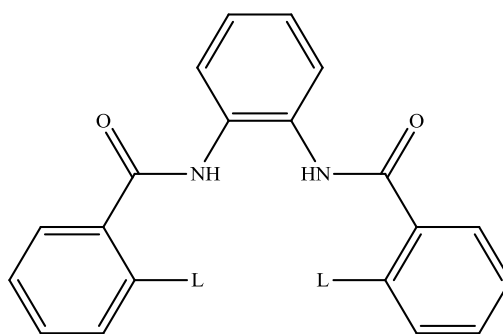
Figure 1.24: Selection of benzamide ligands (where L = SH, OH, P(Ph)$_2$) used by Fry *et al.*[82]

Efforts have been made to prepare chiral ligands based on the diamide template for the preparation of asymmetric catalysts. Schafer *et al.* developed a chiral catalyst using amide functional groups to prepare the ligand.[83] The group used resolved biphenyl diamines to induce chirality in the catalyst. This strategy was developed by Zi and co-workers, who developed a variety of titanium and zirconium coordination compounds for use as hydroamination/cyclisation catalysts.[84] Chirality of the catalyst is ensured by the use of a binaphthyl diamine to prepare the ligand. This strategy has been reasonably effective with a maximum e.e. of 93 % reported. In this case the amide groups are binding through both the N and O atoms, as shown in Figure 1.25. This binding mode is similar to the behaviour of acetate anions. The X-ray crystal

structure of the complex was obtained, thus confirming the bidentate binding mode of the amide.
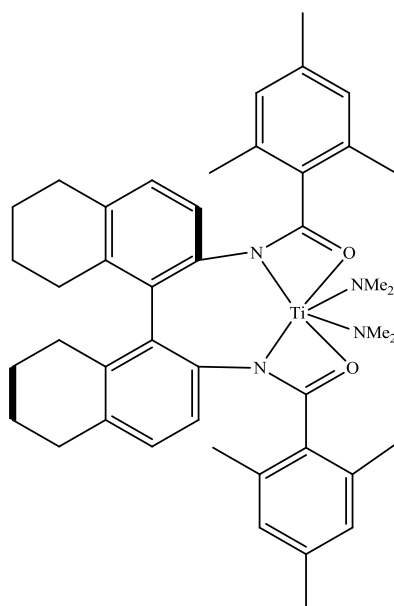
Figure 1.25: Catalyst developed by Zi *et al.* showing amide N,O binding mode.[84]

Another example of the variation of the binding modes of amides is donation exclusively through the carbonyl oxygen with the amide nitrogen playing no part in ligation of the metal. This is observed in two iron and manganese complexes prepared by Costes and co-workers.[85] Donation by the carbonyl oxygen is facilitated by the presence of a hydroxyl moiety on the aromatic ring *ortho* to the amide. Deprotonation of this hydroxyl with an alkali hydroxide or alkoxide base facilitates binding of the metal ion and the carbonyl oxygen stabilises this interaction by its involvement in the formation of a six-member chelate ring, thus forming a relatively stable coordination compound. Evidence of the carbonyl binding was provided by the group obtaining X-ray crystal structures of the manganese(III) complex (shown in Figure 1.26) and its iron(III) complex analogue.

Methods of preparing amides are broad in both scope and versatility,[86] but only the main synthetic reactions will be discussed here. One of the main advantages of the amide functional group over the imine is that it is far less susceptible to hydrolysis. Whereas upon protonation of the imine nitrogen rendered the imine carbon susceptible to attack from water, the amide has a reduced tendency for this to happen because of the influence of the adjacent nitrogen atom. The nitrogen atom can donate its lone pair

to reduce the electrophilicity of the amide carbonyl carbon, thus rendering it less susceptible to nucleophilic attack.[87]
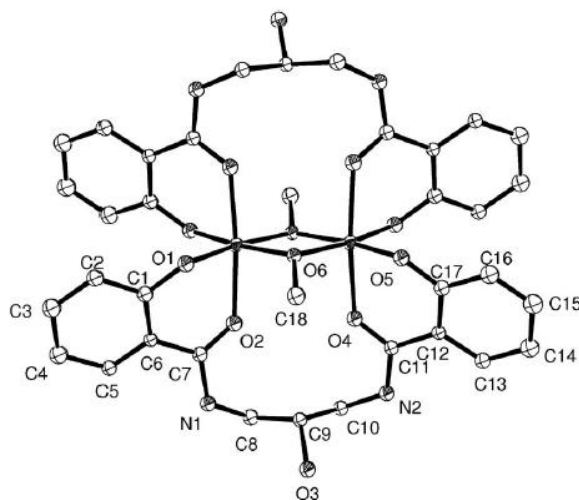
Figure 1.26: Manganese(III) complex prepared by Costes and co-workers.[85]

The formation of peptide (amide) bonds between amino acids requires a condensation reaction between a carboxylic acid group and either a primary or secondary amine.[87] The problem with this reaction however, is that the carboxylic acid and the basic amine will react in an acid-base titration to give an ammonium carboxylate salt. To circumnavigate this problem, the hydroxyl moiety of the carboxylic acid functional group, which is a poor leaving group, must be converted into a superior one. This is normally achieved through the use of carbodiimides, of which dicyclohexylcarbodiimide (DCC), shown in Figure 1.27, is the most well known. The mechanism of using these coupling reagents will not be discussed here as it is irrelevant to the work done in this thesis but results in the formation of a urea by-product and the resultant amide formed.

Aside from the carbodiimide derivatives, another coupling reagent that is rapidly gaining popularity in its use is 4-(4,6-dimethoxy-1,3,5-triazin-2-yl)-4-methyl-morpholinium chloride, or DMT-MM. This coupling reagent, whose structure is shown in Figure 1.27, is unlike the carbodiimides in that it does not require the use of an inert atmosphere or dry solvents for the reaction to proceed. Moreover, it also has the added advantage of an easy workup to isolate the coupled amide product, namely a straightforward filtration to remove the co-product formed.[88]
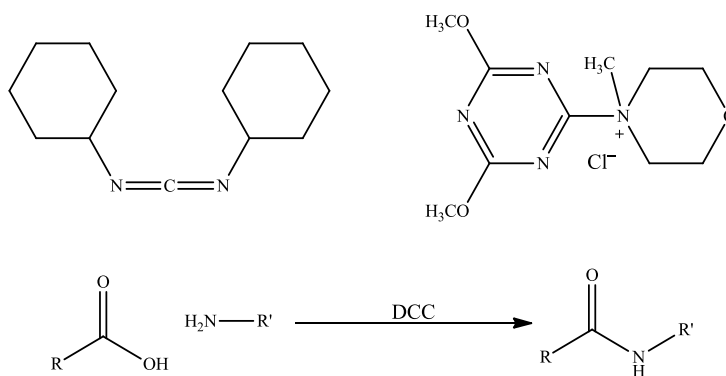
Figure 1.27: Coupling reagents DCC (top left) and DMT-MM (top right) with general representation of coupling reaction with DCC in the preparation of an amide (bottom).

Another way of preparing amides is through the method of converting the acid to an ester, thereby providing a superior leaving group (i.e. swapping OH for OR). This method has been employed to prepare the bridged calix[4]arene diamides previously mentioned. An example of this is the procedure by McGinley et al.[63] The diamine is heated to reflux in a toluene-methanol solvent mix with the diethyl ester calix[4]arene precursor. A transesterification reaction takes place that converts the ethyl ester to the methyl derivative which then reacts with the amine to give the amide. One disadvantage of this method is the length of time for the reaction to complete. Reaction times measured in days are not uncommon. To increase the rate of reaction, a more reactive variation of the ester is prepared. To this end, an acid chloride derivative is employed.

Acid chlorides are highly reactive carbonyl derivatives that are prepared by conversion of the parent carboxylic acid by the use of a chlorinating agent. The most commonly used reagents are phosphorus pentachloride, thionyl chloride and oxalyl chloride.[87] The phosphorus halide was the most commonly used until its use was superseded by the development of thionyl chloride. Usually catalysed by a drop of DMF, it is considered superior to the pentavalent phosphorus reagent as the by-products of the chlorination reaction are gaseous sulfur dioxide and hydrogen chloride. In addition, excess thionyl chloride is easily removed under reduced pressure to give the isolated product.

The acid chloride derivatives are more reactive and their reasons are twofold.[87] The chlorine withdraws electron density, the result of its electronegative nature, thus rendering the adjacent carbonyl with reduced electron density and as a consequence a

higher partial positive charge (δ^+). This situation is augmented by the ability of the chlorine to function as a decent leaving group, which facilitates the nucleophilic substitution attempted. A drawback of the use of acid chlorides is that, by their very reactive nature, they can hydrolyse under ambient conditions to give the carboxylic acid reactant, unless protected by a guard tube. As a consequence, the use of acid chlorides must include the use of dry aprotic solvents. Usually an amine base, such as triethylamine or pyridine, is added to neutralise the acid produced upon formation of the amide.[89]

1.4.2   Copper(II), nickel(II) and zinc(II) amide complexes

As mentioned previously, amides are very robust and versatile ambidentate donor ligands for the preparation of coordination complexes. Their resistance to hydrolysis means that by-products resulting from ligand cleavage are less likely to occur. That does not mean that ligand break up does not occur, as mentioned *vide supra*.

As well as symmetric diamides, a significant amount of asymmetric amide derivatives have been developed. A considerable number of these have included the Schiff-base moiety.[90] They are most commonly used in the preparation of compartmental ligands.[91] Outside of these criteria the number of benzamide complexes drops enormously. Asymmetric benzamides without an imine moiety attached are relatively uncommon but they do exist and copper(II) and nickel(II) complexes of these ligands have been prepared.

The copper(II) complexes of these ligands have formed heterometal multinuclear adducts with sodium and magnesium salts.[92] These copper amide complexes have been the subject of study into their magnetic properties. They are often used in conjunction with lanthanide salts to prepare these magnetic materials. One recent example of this strategy are the compounds prepared by Costes and co-workers, who prepared the copper(II) benzamide complex shown in Figure 1.28, and then exposed the complex to either gadolinium(III) or terbium(III) chloride with tetramethylheptanedione added as a ligand, to prepare the heterometal dinuclear derivative.[93]

Asymmetric nickel(II) Schiff-base amide complexes have been developed and studied in electron transfer and radical forming investigations and in the process form the

nickel(III) derivative. The choice of solvent is influential in whether electron transfer takes place from the metal to the ligand. An example of one of the complexes prepared by Jarjayes *et al.*[94] is shown in Figure 1.29. One point of note is the influence of the amido moiety when compared to the imine functional group. The more powerful effect of the amido results in the metal ion adopting a square planar geometry. This is because the deprotonated amide is a stronger donor than the corresponding imine, and donor ligands such as pyridine are less likely to bind in the axial position to give a square pyramidal geometry.
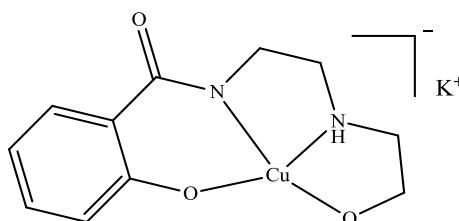
Figure 1.28: Copper(II) benzamide precursor prepared by Costes and co-workers.[93]
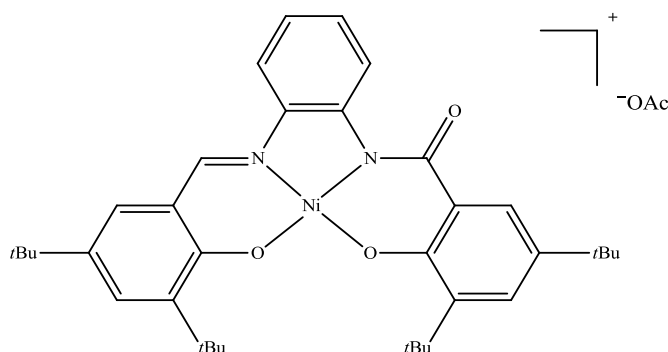
Figure 1.29: Nickel asymmetric amide complex prepared by Jarjayes *et al.*[94]

As outlined in a previous Section, amide bonds feature extensively in nature, otherwise known as peptide bonds when linking amino acid residues. With this knowledge, amide functional groups were employed to construct a model of an active site of a bifunctional metalloenzyme, an acetyl synthase/carbon monoxide dehydrogenase which was prepared by Olmstead *et al.*[95] Using the nickel(II) amido thiol precursor, shown in Figure 1.30, they prepared a variety of trinuclear bimetallic complexes (using copper(I) phenanthroline derivatives) and examined their redox and carbon monoxide binding properties.

Copper(II) and nickel(II) complexes have found themselves as subjects in studies varying from catalysis to biological mimics to molecular magnets, as has been

previously mentioned in this Section because of their redox properties. It is to the dearth of zinc that it does not possess any of these properties, and, as a result, incidences in the literature regarding the use of zinc amide complexes are restricted. Where zinc is used, it is in conjunction with other metals. It is employed, for example, as a control in the work of Matsumoto *et al.* who developed heterometal cyclic tetranuclear complexes.[96] Using an asymmetric Schiff-base amide to prepare a copper(II)   coordination   compound,   this   was   reacted   with   zinc(II) hexafluoroacetylacetone to prepare the dimeric structure shown in Figure 1.31. Evidence supporting the proposed structure is from X-ray crystal structures obtained from the cobalt(II), copper(II) and manganese(II) analogues of the structure shown in Figure 1.31.
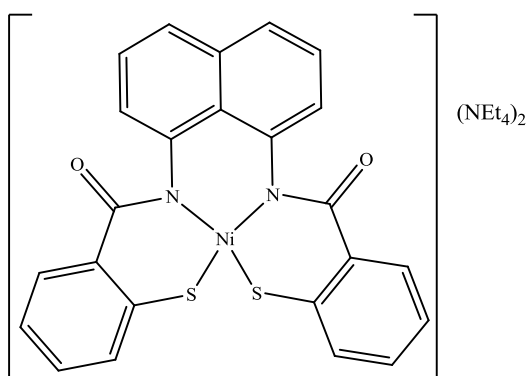
Figure 1.30: Enzyme precursor prepared by Olmstead *et al.*[95]

Zinc(II) amide complexes have also been used in antimicrobial testing. Nishat and co-workers have prepared a variety of dinuclear metal complexes with a ligand possessing a potential hexadentate N_4O_2 coordination site.[97] The compound prepared, shown in Figure 1.32, exhibited reasonable antibacterial (*Pseudomonas aeruginosa* and *Bacillus subtilis*) and antifungal (*Mucor* sp., *Trichophyton* sp. and *Fusarium* sp.) activity. The complexes in all cases showed enhanced activities when compared to the free ligand.

Overall, metal amide complexes offer some advantages over their Schiff-base equivalents. Chief among these is the superior stability of the ligands under aqueous conditions. When the amide proton is removed the anionic character of the ligand affords strong binding to the appropriate metal ion, notwithstanding the usual metal ion and ligand required characteristics (nature of both ions: hard, soft etc.). Changing reaction conditions can also afford complexes that are regioisomers because of the

ambidentate nature of the amide functional group. Using the trends observed in the literature, it should be possible to synthesise a ligand with the desired binding properties to selectively bind one metal ion over another.
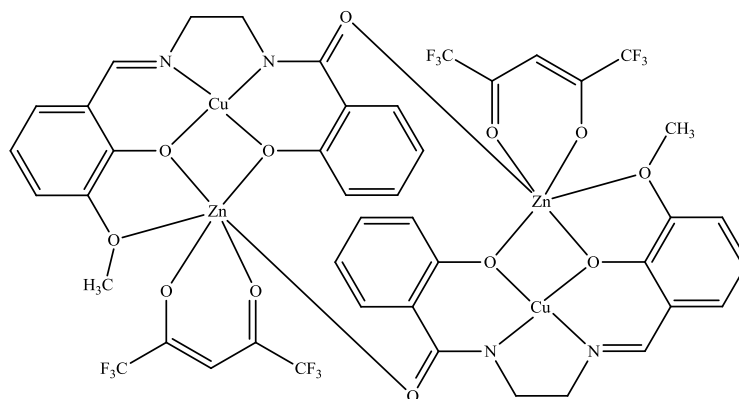
Figure 1.31: Tetranuclear zinc(II)-copper(II) complex prepared by Matsumoto *et al.*[96]
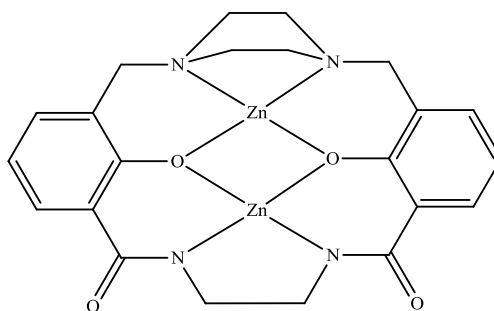
Figure 1.32: Zinc(II) amide complex prepared by Nishat and co-workers.[97]

1.5   Aims of thesis

Overall, the project was to expand the amide and Schiff-base ligand and coordination complex libraries in a three-pronged approach. In the first part the object was to explore the binding characteristics of two novel 3-hydroxy Schiff-base derivatives with copper(II), nickel(II) and zinc(II) salts and to compare and contrast these novel complexes with the more abundant 2-hydroxy Schiff-base metal analogues.

To continue this theme, but as an independent investigation running in tandem with the above, a new family of potential fluorophores, using the calix[4]arene macrocycle as a scaffold were proposed to be based on the azine moiety. These novel compounds would be subjected to preliminary fluorescence studies and also examined for their metal binding properties. Any metal complexes prepared were to be subsequently subjected to scrutiny for any potential fluorescent activity.

The third approach was to use the findings of the two previous investigations to design a novel calix[4]arene metal ionophore employing the amide functional group in its synthesis. As a prequel to this work, a ligand with an amide moiety (a benzamide) with the potential to be coupled to the calix[4]arene would be developed. This precursor would be screened for any metal binding characteristics, and if so, would be used to prepare an array of novel copper(II), nickel(II) and zinc(II) complexes. This benzamide ligand, with ambidentate potential, would be attached to the calix[4]arene and then the two families of compounds compared and contrasted for their metal ion binding properties.

2. Experimental

2.1   Instrumentation

Reagents and reactants were supplied by either Alfa Aesar, Fluorochem or Sigma-Aldrich and were used as received without further purification. Solvents were distilled before use and purified according to standard procedures. Products were characterised by NMR and IR spectroscopy unless otherwise indicated. ^{1}H and ^{13}C NMR (δ ppm; J Hz) spectra were recorded on a Bruker Avance 300 MHz spectrometer at a probe temperature of 25 °C using saturated $CDCl_3$ solutions with Me_4Si reference, and resolutions of 0.18 Hz and 0.01 ppm respectively unless otherwise indicated. ^{1}H NMR and ^{13}C NMR spectra were run at 300 MHz and 75 MHz respectively. Infrared spectra (cm^{-1}) were recorded as KBr discs or liquid films between NaCl plates using a Perkin Elmer system 2000 FT-IR spectrophotometer. UV-vis spectra were recorded using a Unicam UV 540 spectrometer. Excitation and emission spectra were recorded on a JASCO FP-6300 spectrofluorometer. Melting point analyses were carried out using a Stewart Scientific SMP 1 melting point apparatus and are uncorrected. Mass spectrometry was carried out on an Agilent LC/TOF-MS model 6210 Time-Of-Flight LC/MS with an electrospray source positive and negative (ESI+/−), capillary 3500 V, nebuliser spray 30 psig, drying gas 5 L/min and source temperature 325 °C. The fragmentor was used at 175 V. The LC was run on an Agilent 1200 series model and injection volumes were typically 10 μL. Column used was an Agilent Eclipse XBD-C18 with a diameter of 4.6 mm and length of 150 mm. A particle size of 5-micron was employed. The mobile phase constituted A (acetonitrile with 0.1 % formic acid) and B (0.1 % aqueous formic acid) with a gradient of 5 % A to 100 % at a flow rate of 0.5 mL/min over 15 minutes. Microanalyses were carried out at either the Microanalytical Laboratory of University College, Dublin, the National University of Ireland, Cork or the National University of Ireland, Maynooth.

2.2 Synthesis of *m*-hydroxybenzaldehyde Schiff-bases and their metal complexations

2.2.1 Synthesis of 3,3'-((1*E*,1'*E*)-(ethane-1,2-diylbis(azanylylidene))-bis(methanylylidene))diphenol (*3-hydroxysal*): (1)
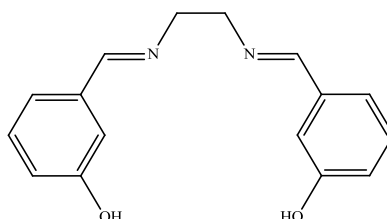
A solution of 3-hydroxybenzaldehyde (2.0 g, 16.4 mmol) in acetonitrile (25 mL) and ethylene diamine (0.49 g, 8.1 mmol) in acetonitrile (50 mL) were placed in a round-bottomed flask, and the resulting yellow solution stirred at room temperature. After 5 minutes, a white solid started to precipitate and stirring was continued for a further 45 minutes. The suspension was filtered, washed with acetonitrile and the resulting white solid was dried in an oven at 75 °C overnight.

Yield: 93 % (2.03 g, 7.6 mmol). m.p.: 186-190 °C (lit: 189-191 °C).[16] δ_H (d_6-DMSO): 3.84 (4H, s, NCH_2), 6.83 (2H, m, ArH), 7.16 (6H, m, ArH), 8.24 (2H, s, HC=N), 9.03 (2H, br s, OH). δ_C (d_6-DMSO): 60.8, 113.6, 117.8, 119.3, 129.6, 137.4, 157.5, 161.9. v_{max} (KBr): 3051, 2929, 1647, 1595, 1456, 1275, 1082, 779, 685 cm^{-1}.

2.2.2 Synthesis of 3,3'-((1*E*,1'*E*)-(propane-1,3-diylbis(azanylylidene))-bis(methanylylidene))diphenol (*3-hydroxysalpropane*): (2)
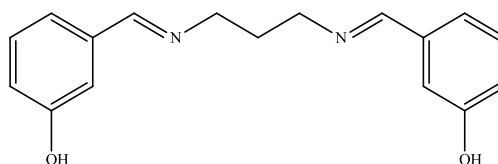
A solution of 3-hydroxybenzaldehyde (4.0 g, 32.7 mmol) in acetonitrile (25 mL) and 1,3-diaminopropane (1.21 g, 16.3 mmol) in acetonitrile (25 mL) were placed in a round-bottomed flask, and the resulting yellow solution stirred at room temperature. After 5 minutes, a white solid started to precipitate and stirring was continued for a

further 45 minutes. The suspension was filtered, washed with acetonitrile and the resulting white solid was dried in an oven at 75 °C overnight.

Yield: 93 % (4.29 g, 15.2 mmol). m.p.: 146-148 °C. Anal. Calc. for $(C_{17}H_{18}N_2O_2)_4 \cdot H_2O$: C, 71.18; H, 6.50; N, 9.77 %; found: C, 71.53; H, 6.36; N, 9.83 %. δ_H (d_6-DMSO): 2.01 (2H, m, NCH$_2$CH_2), 3.68 (4H, t, NCH_2CH$_2$, J = 7.0 Hz), 6.92 (2H, m, ArH), 7.24 (6H, m, ArH), 8.33 (2H, s, HC=N), 9.64 (2H, br s, OH). δ_C (d_6-DMSO): 32.3, 58.6, 114.0, 118.1, 119.6, 130.0, 137.9, 159.9, 161.3. ν_{max} (KBr): 3056, 2852, 1650, 1596, 1456, 1395, 1275, 1096, 785, 690 cm^{-1}.

2.2.3 Synthesis of 3,3'-((1*E*,1'*E*)-(((methylazanediyl)bis(propane-3,1-diyl))bis(azanylylidene))bis(methanylylidene))diphenol (*3-hydroxysalpropyl methylamine*): (3)
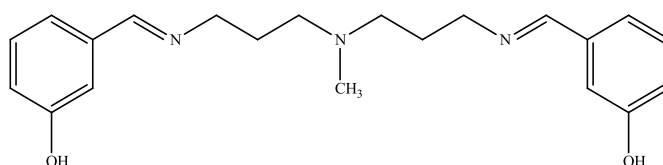
A solution of 3-hydroxybenzaldehyde (5.0 g, 40.9 mmol) in methanol (100 mL) and 3,3'-diamino-N-methyldipropylamine (2.97 g, 20.4 mmol) in methanol (50 mL) were placed in a round-bottomed flask. The yellow solution was stirred for 3 h at room temperature. The solvent was removed under reduced pressure to leave a yellow viscous oil.

Yield: 95 % (6.89 g, 19.5 mmol). Anal. Calc. for $(C_{21}H_{27}N_3O_2)_2 \cdot CH_3OH$: C, 69.89; H, 7.91; N, 11.37 %; found: C, 69.99; H, 7.55; N, 11.33 %. δ_H (d_6-DMSO): 1.71 (4H, m, CH$_2$CH_2CH$_2$), 2.13 (3H, s, NCH_3), 2.32 (4H, t, CH$_3$NCH_2CH$_2$, J = 7.0 Hz), 3.53 (4H, t, NCH_2CH$_2$CH$_2$, J = 7.0 Hz), 6.83 (2H, m, ArH), 7.16 (6H, m, ArH), 8.21 (2H, s, HC=N), 9.55 (2H, br s, OH). δ_C (d_6-DMSO): 28.2, 41.5, 54.9, 58.5, 117.6, 113.5, 119.2, 129.6, 137.5, 157.6, 160.6. ν_{max} (KBr): 2946, 1645, 1582, 1456, 1375, 1274, 1031, 785, 690 cm^{-1}.

2.2.4 General procedure for the metal complexation reactions of Schiff-base ligands 1, 2 and 3

The ligand (1.0 mmol) was dissolved in the appropriate solvent (10 mL) in an Erlenmeyer flask. To this was added the metal salt (1.0 mmol) in the same solvent (10 mL). The resulting solution was stirred for 45 minutes at room temperature. The solution was allowed to stand and the solvent was allowed to evaporate. On almost complete reduction, acetonitrile (10 mL) was added and a brown solid precipitated from the mixture. The brown suspension was filtered and the filtrate allowed to evaporate slowly. After a few days crystals started to form. The crystals were removed by filtration, washed with cold acetonitrile and dried in a vacuum oven at 56 °C. The reactions are summarised in Table 2.1.

Table 2.1 Summary of complexation reactions.

Entry No.	Ligand	Metal salt	Solvent	Result
4	1	$CuCl_2 \cdot 2H_2O$	MeOH	Metal-amine complex
5	1	$Cu(ClO_4)_2 \cdot 6H_2O$	EtOH	Metal-amine complex
6	1	$Cu(O_2CCH_3)_2 \cdot H_2O$	EtOH	Ligand hydrolysis
7	1	$NiCl_2 \cdot 6H_2O$	MeOH	Ligand hydrolysis
8	1	$Ni(ClO_4)_2 \cdot 6H_2O$	MeOH	Ligand hydrolysis
9	1	$Ni(O_2CCH_3)_2 \cdot 4H_2O$	EtOH	Metal-amine complex
10	1	$ZnCl_2$	MeOH	Metal complex formation
11	1	$Zn(O_2CCH_3)_2 \cdot 2H_2O$	MeOH	Ligand hydrolysis
12	1	$Cu(O_2CCH_3)_2 \cdot py$	Pyridine	Ligand hydrolysis
13	2	$CuCl_2 \cdot 2H_2O$	MeOH	Metal-amine complex
14	2	$Cu(ClO_4)_2 \cdot 6H_2O$	MeOH	Ligand hydrolysis
15	2	$Cu(O_2CCH_3)_2 \cdot H_2O$	MeOH	Metal-amine complex
16	2	$NiCl_2 \cdot 6H_2O$	MeOH	Ligand hydrolysis
17	2	$Ni(ClO_4)_2 \cdot 6H_2O$	EtOH	Metal-amine complex
18	2	$Ni(O_2CCH_3)_2 \cdot 4H_2O$	EtOH	Metal-amine complex
19	2	$ZnCl_2$	MeOH	Complex decomposed
20	2	$Zn(O_2CCH_3)_2 \cdot 2H_2O$	MeOH	Ligand hydrolysis
21	3	$CuCl_2 \cdot 2H_2O$	MeOH	Metal-amine complex
22	3	$Cu(ClO_4)_2 \cdot 6H_2O$	MeOH	Ligand hydrolysis
23	3	$Cu(O_2CCH_3)_2 \cdot H_2O$	MeOH	Ligand hydrolysis
24	3	$NiCl_2 \cdot 6H_2O$	MeOH	Ligand hydrolysis
25	3	$Ni(ClO_4)_2 \cdot 6H_2O$	EtOH	Ligand hydrolysis
26	3	$Ni(O_2CCH_3)_2 \cdot 4H_2O$	EtOH	Ligand hydrolysis

| 27 | 3 | ZnCl$_2$ | MeOH | Complex decomposed |
| 28 | 3 | Zn(O$_2$CCH$_3$)$_2$·2H$_2$O | MeOH | Ligand hydrolysis |

Successful complexation reaction products were analysed by IR. For failed reactions, recovery of starting material was confirmed by ^{1}H NMR spectroscopy. The summary of IR absorption bands are given in Table 2.2.

Table 2.2 Infrared spectral data for metal-amine complexes.

Table 1 no.	Complex colour	v_{max} (KBr)/ cm^{-1}	Ref.
4	Light blue	3446, 3299, 2968, 1570, 1270, 1043, 681.	98
5	Purple	3348, 2906, 1583, 1470, 1145, 1087, 1042, 626.	98
9	Light green	3358, 2924, 1759, 1740, 1551, 1428, 1222, 1024, 680.	99
13	Dark green	3435, 3275, 2874, 1572, 1402, 1275, 1164, 1027, 664.	100
15	Blue/purple	3410, 3259, 2971, 1613, 1571, 1420, 1331, 1188, 1041, 674.	100
17	Light green	3423, 2923, 1682, 1282, 1080, 625.	101
18	Light green	3345, 2942, 1558, 1420, 1141, 912, 671.	99
21	Dark blue	3288, 3200, 2256, 1592, 1585, 1155, 767.	

2.2.5   Synthesis of a complex from the reaction of 1 and zinc(II) chloride: (10)
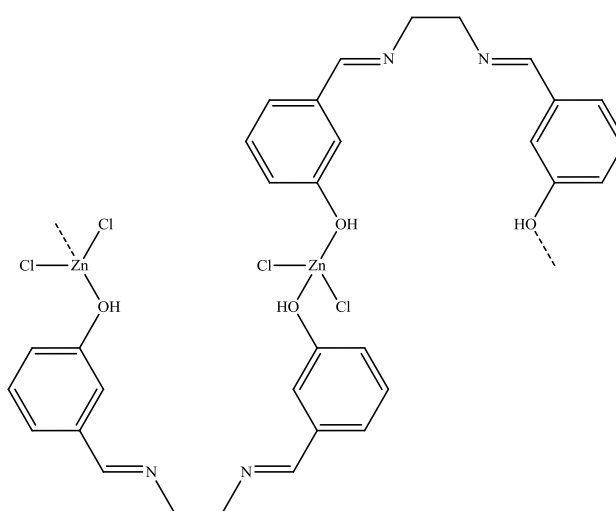
To a solution of **1** (0.15 g, 0.59 mmol) in ethanol (5 mL) was added with stirring a solution of zinc(II) chloride (0.08 g, 0.59 mmol) in ethanol (5 mL) in an Erlenmeyer

flask which resulted in the immediate formation of a white precipitate. Stirring was continued for a further 30 minutes whereupon the white solid was isolated by suction filtration, washed with cold ethanol and dried in a vacuum oven at 56 °C.

Yield: 74 % (0.17 g, 0.43 mmol). Anal. Calc. for $C_{16}H_{14}N_2Cl_2O_2Zn$: C, 47.71; H, 3.51; N, 6.96 %; found: C, 47.22; H, 4.03; N, 6.82 %. δ_H (d_6-DMSO): 3.83 (4H, s, NCH_2), 6.82 (2H, m, ArH), 7.24-7.08 (6H, m, ArH), 8.24 (2H, s, HC=N), 9.55 (2H, br s, OH). ν_{max} (KBr): 3336, 2949, 1641, 1584, 1475, 924, 795 cm^{-1}.

2.2.6 Synthesis of a complex from the reaction of 2 and copper(II) acetate monohydrate: (15)
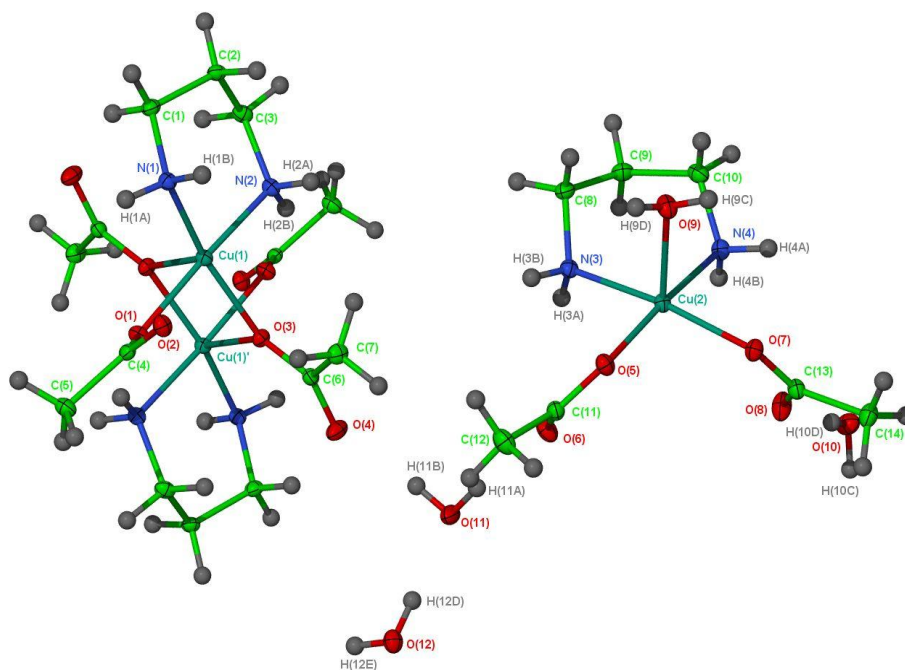
Copper(II) acetate monohydrate (0.34 g, 1.7 mmol) was dissolved in methanol (10 mL) and added to a solution of **2** (0.48 g, 1.7 mmol) dissolved in methanol (10 mL). The solvent was reduced and replenished with acetonitrile which resulted in a dark green/blue solution. The solvent was allowed to reduce over several days resulting in the formation of blue/purple crystals. The crystals were removed by filtration, washed with acetonitrile and dried in a vacuum oven. Single crystals suitable for X-ray crystallographic analysis were grown by slow evaporation from acetonitrile.

Yield: 0.21 g. Anal. Calc. for $C_{21}H_{50}N_6Cu_3O_{13}$: C, 32.12; H, 6.42; N, 10.70 %; found: C, 32.37; H, 6.15; N, 10.70 %. ν_{max} (KBr): 3410, 3259, 2971, 1613, 1571, 1420, 1331, 1188, 1041, 674 cm^{-1}. μ_{eff}: 1.88 B.M.

2.2.7   Synthesis of a complex from the reaction of 3 and copper(II) chloride dihydrate: (21)
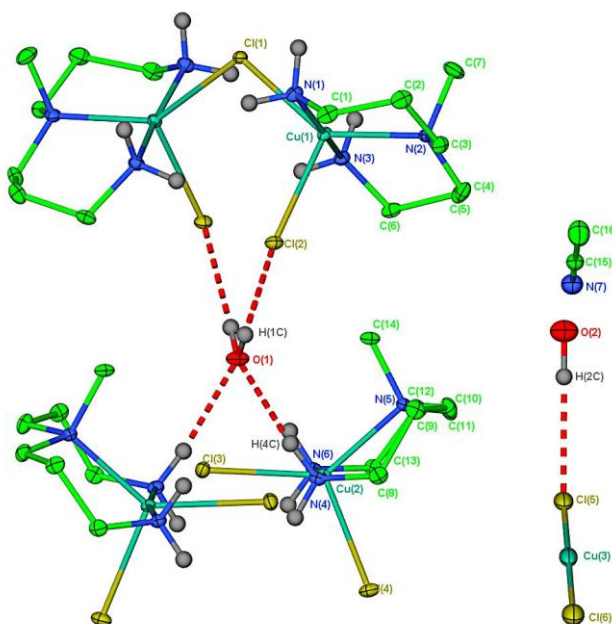
Copper(II) chloride dihydrate (0.28 g, 1.62 mmol) was dissolved in methanol (10 mL) and added to a solution of **3** (0.57 g, 1.62 mmol) dissolved in methanol (10 mL). The blue solution was allowed to reduce slowly over several days. Acetonitrile was added to the flask which resulted in a green suspension. The suspension was filtered and resulted in the removal of a brown solid. The filtrate was allowed to reduce slowly and after several days resulted in the formation of dark green crystals. The crystals were removed by filtration, washed with cold acetonitrile and dried in a vacuum oven at 56 °C. Single crystals suitable for X-ray crystallographic analysis were grown by slow evaporation from acetonitrile.

Yield: 0.086 g. Anal. Calc. for $C_{29}H_{79}N_{12}Cl_9Cu_5O_2$: C, 27.54; H, 6.30; N, 13.29 %; found: C, 27.34; H, 5.98; N, 12.85 %. ν_{max} (KBr): 3288, 3200, 2256, 1592, 1585, 1155, 767 cm^{-1}. μ_{eff}: 1.67 B.M.

2.3   Syntheses of calix[4]arene derivatives for fluorescence studies

2.3.1   Synthesis of 5,11,17,23,29,35,41,47-octa-*tert*-butyl-49,50,51,52,53,54,55,56-octa-hydroxycalix[8]arene (*octamer*): (26)[102]
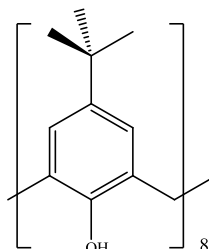
A slurry of *p-tert*-butylphenol (112 g, 720 mmol), paraformaldehyde (36 g, 1200 mmol) and 10 M potassium hydroxide (1.7 mL) in xylenes (600 mL) was heated with stirring to reflux for 4 h in a flask equipped with a Dean-Stark trap. After cooling the precipitate was filtered and the solid washed in succession with toluene, diethyl ether, acetone and water (4* 200 mL) and dried in an oven at 75 °C overnight to give a white solid.

Yield: 72 % (84.00 g, 64.7 mmol). m.p.: >300 °C (lit: 411-412 °C).[102] δ_H (CDCl$_3$): 1.28 (72H, s, *t*-Bu), 3.48 (8H, br d, CH_2, J = 13.0 Hz), 4.39 (8H, br d, CH_2, J = 13.0 Hz), 7.17 (16H, s, ArH), 9.63 ppm(8H, s, OH). δ_C (CDCl$_3$): 31.4, 32.3, 34.0, 125.5, 128.7, 144.7, 146.6. ν_{max} (KBr): 3409, 3235, 2956, 1487, 1451, 1393, 1362, 1291, 1249, 1204, 1117, 875, 816, 784, 728 cm^{-1}.

2.3.2   Synthesis of 5,11,17,23-tetra-*tert*-butyl-25,26,27,28-tetrahydroxy-calix[4]arene (*tetramer*): (27)[102]
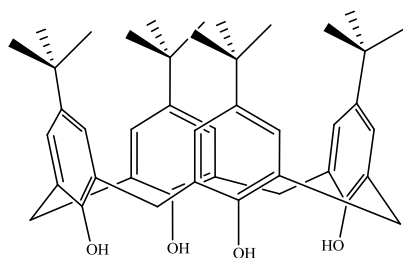
A slurry containing **26** (44 g, 30 mmol) and 10 M sodium hydroxide (1.5 mL) in diphenyl ether (400 mL) was heated to reflux with vigorous stirring for 1.5 h in a 2000

mL flask equipped with a Dean-Stark trap. The reaction was allowed to cool (~100 °C) and then treated with ethyl acetate (400 mL). The precipitate was washed in succession with toluene, diethyl ether, acetone and water (4* 200 mL) and then dried in an oven at 75 °C overnight to give a white solid.

Yield: 48 % (21 g, 14.4 mmol). m.p.: >300 °C (lit: 344-346 °C).[102] δ_H (CDCl$_3$): 1.21 (36H, s, t-Bu), 3.50 (4H, br d, CH_2, J = 12.4 Hz), 4.26 (4H, br d, CH_2, J = 12.4 Hz), 7.04 (8H, s, ArH), 10.34 ppm(8H, s, OH). δ_C (CDCl$_3$): 31.4, 32.6, 34.0, 125.9, 127.7, 144.4, 146.7. ν_{max} (KBr): 3167, 2960, 2905, 2868, 1482, 1392, 1362, 1201, 871, 818, 782, 710, 675, 592 cm^{-1}.

2.3.3   Synthesis of 5,11,17,23-tetra-*tert*-butyl-25,27–dihydroxy-26,28-bis(2-bromoethoxy)calix[4]arene (*bromoethoxy calixarene*): (28)[103]
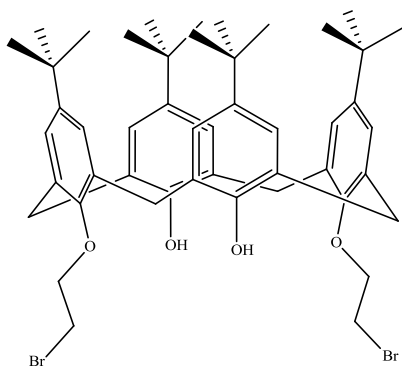
A mixture of **27** (5 g, 7.7 mmol), potassium carbonate (2.12 g, 15.4 mmol) and 1,2-dibromoethane (30 g, 154 mmol) were heated to reflux in acetonitrile (200 mL) under N$_2$ for 48 h. The mixture was cooled, filtered and the filtrate concentrated under reduced pressure. This was added with vigorous stirring to ice cold water (250 mL). The yellow viscous 'gum' was filtered off and dried in an oven at 75 °C for 48 h to give an off-white solid.

Yield: 81 % (5.37 g, 6.22 mmol). m.p.: 290-294 °C (lit: 278-280 °C).[103] δ_H (CDCl$_3$): 0.95 (18H, s, t-Bu), 1.29 (18H, s, t-Bu), 3.33 (4H, d, ArCH_2Ar, J = 13.0 Hz), 3.84 (4H, t, OCH$_2$CH_2Br, J = 6.5 Hz), 4.30 (4H, d, ArCH_2Ar, J = 13.0 Hz), 4.31 (4H, t, OCH_2-CH$_2$Br, J = 6.5 Hz), 6.78 (4H, s, ArH), 6.92 (2H, s, OH), 7.06 (4H, s, ArH). δ_C (CDCl$_3$): 29.3, 31.0, 31.7, 33.8, 33.9, 75.4, 77.2, 125.2, 125.7, 127.7, 132.4, 141.6,

147.2, 149.4, 150.5. ν_{max} (KBr): 3447, 2959, 2905, 2865, 1485, 1459, 1362, 1270, 1239, 1195, 1176, 1124, 1101, 1068, 1007, 759, 565 cm^{-1}.

2.3.4 **Synthesis of 5,11,17,23-tetra-*tert*-butyl-25,27-dihydroxy-26,28-[bis(2-formylphenoxyethoxy)]calix[4]arene (*o-ethoxybenzaldehyde calixarene*): (29)**[58]
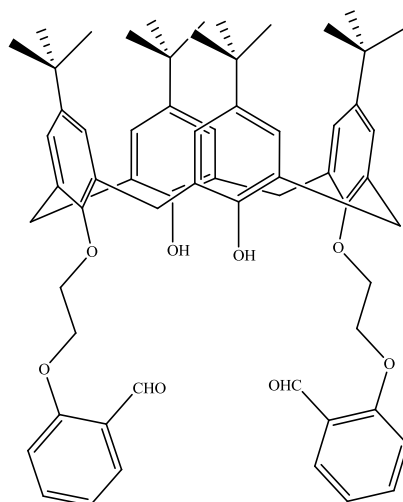
A mixture of **28** (5.0 g, 5.8 mmol), salicylaldehyde (1.46 g, 12.0 mmol) and potassium carbonate (1.65 g, 11.7 mmol) was heated to reflux in acetonitrile (400 mL) under N$_2$ for 18 h. The suspension was cooled, filtered and the solvent removed under reduced pressure. The residue was taken up in chloroform and the solution was gravity filtered. The filtrate was taken and the solvent removed under reduced pressure. The residue was taken up in diethyl ether (20 mL) and the white precipitate was filtered, washed with diethyl ether and dried in an oven at 75 °C overnight.

Yield: 31 % (1.69 g, 1.78 mmol). m.p.: 188-192 °C (lit: 201-202 °C).[58] δ_H (CDCl$_3$): 1.02 (18H, s, *t*-Bu), 1.25 (18H, s, *t*-Bu), 3.31 (4H, d, ArC*H*$_2$Ar, *J* = 12.9 Hz), 4.30 (4H, d, ArC*H*$_2$Ar, *J* = 12.9 Hz), 4.43-4.37 (8H, m, OC*H*$_2$C*H*$_2$O), 6.88 (4H, s, Ar*H*), 7.02 (4H, s, Ar*H*), 6.96-7.04 (4H, m, Ar*H*), 7.49 (2H, s, O*H*), 7.47-7.53 (2H, m, Ar*H*), 7.83 (2H, dd, Ar*H*, *J* = 1.8 Hz), 10.50 (2H, s, C*H*O). δ_C (CDCl$_3$): 31.1, 31.7, 31.8, 33.8, 34.0, 67.5, 73.7, 112.4, 121.0, 125.2, 125.8, 127.8, 128.3, 132.7, 135.8, 141.8, 147.4, 149.8, 150.3, 160.8, 190.2. ν_{max} (KBr): 3366, 2961, 2904, 2868, 1682, 1599, 1485, 1459, 1394, 1363, 1290, 1247, 1193, 1162, 1056, 923, 871, 833, 756 cm^{-1}.

2.3.5 Synthesis of 5,11,17,23-tetra-*tert*-butyl-25,27-dihydroxy-26,28-[bis[*o*-(*E*)-(2-oxyethoxy)benzylidene)hydrazine]]calix[4]arene (*calix hydrazone*): (30)
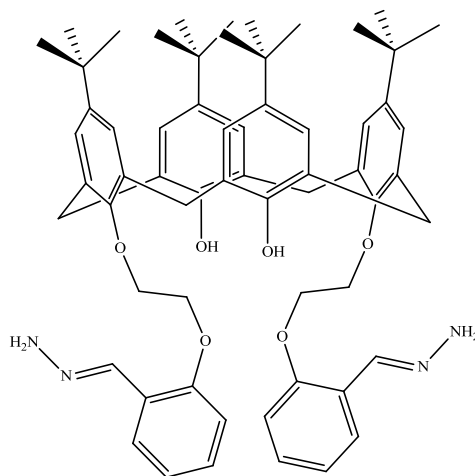
A solution of **29** (0.5 g, 0.5 mmol) in acetonitrile (50 mL) was added dropwise, over 20 minutes, to hydrazine hydrate (0.53 g, 10.6 mmol). The resulting yellow solution was stirred for 12 h. The solvent was removed under reduced pressure and the residue was treated with ethanol (20 mL) to yield a white precipitate. The white solid was filtered, washed with ethanol and dried in an oven at 75 °C overnight.

Yield: 76 % (0.40 g, 0.41 mmol). m.p.: 218-220 °C. Anal. Calc. for $C_{62}H_{76}N_4O_6$: C, 76.50; H, 7.88; N, 5.76 %; found: C, 76.52; H, 7.87; N, 5.94 %. δ_H (CDCl$_3$): 1.00 (18H, s, *t*-Bu), 1.27 (18H, s, *t*-Bu), 3.33 (4H, d, ArC*H*$_2$Ar, *J* = 13.0 Hz), 4.24 (8H, m, OC*H*$_2$C*H*$_2$O), 4.39 (4H, d, ArC*H*$_2$Ar, *J* = 13.0 Hz), 4.95 (4H, br s, N*H*$_2$), 6.72 (2H, m, Ar*H*), 6.85 (4H, s, Ar*H*), 6.93 (2H, m, Ar*H*), 7.06 (4H, s, Ar*H*), 7.17 (2H, m, Ar*H*), 7.75 (2H, d, Ar*H*), 7.77 (2H, s, O*H*), 8.21 (2H, s, *H*C=N). δ_C (CDCl$_3$): 31.1, 31.7, 33.9, 34.0, 66.8, 74.2, 111.7, 121.1, 124.2, 125.3, 125.6, 125.7, 127.6, 129.6, 132.6, 139.7, 141.7, 147.2, 149.6, 150.7, 155.8. ν_{max} (KBr): 3534, 3378, 2961, 1687, 1600, 1485, 1289, 1058, 924, 756 cm^{-1}.

2.3.6   Synthesis of 5,11,17,23-tetra-*tert*-butyl-25,27-dihydroxy-26,28-(1*E*,2*E*)-1,2-bis(2-(2-oxyethoxy)benzylidene)hydrazinecalix[4]arene (*calixazine intra clip*): (31)
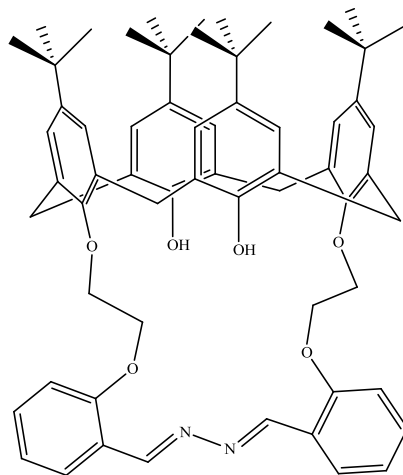
Salicylaldehyde hydrazone (0.6 g, 4.43 mmol) and **29** (1.0 g, 1.06 mmol) were heated to reflux in ethanol (60 mL) for 3 h. During the reflux, a yellow precipitate formed and, on cooling, was removed by filtration. The yellow solid was washed with ethanol and dried in a vacuum oven at 56 °C.

Yield: 46 % (0.45 g, 0.49 mmol). m.p.: 210-212 °C. Anal. Calc. for $C_{62}H_{72}N_2O_6 \cdot H_2O$: C, 77.63; H, 7.78; N, 2.92 %; found: C, 77.67; H, 7.59; N, 2.69 %. δ_H (CDCl$_3$): 0.92 (18H, s, *t*-Bu), 1.23 (18H, s, *t*-Bu), 3.11 (4H, d, ArC*H$_2$*Ar, *J* = 12.9 Hz), 4.31 (4H, d, ArC*H$_2$*Ar, *J* = 12.9 Hz), 4.45 (8H, m, OC*H$_2$*C*H$_2$*O), 6.78 (4H, s, Ar*H*), 6.88 (2H, m, Ar*H*), 6.94 (4H, s, Ar*H*), 7.01 (2H, m, Ar*H*), 7.28 (2H, s, O*H*), 7.36 (2H, m, Ar*H*), 7.82 (2H, m, Ar*H*), 9.02 (2H, s, *H*C=N). δ_C (CDCl$_3$): 31.0, 31.1, 31.7, 33.7, 33.9, 65.7, 73.6, 111.6, 120.9, 123.7, 124.8, 125.5, 127.7, 130.9, 131.5, 133.0, 141.0, 146.9, 149.0, 150.6, 157.2, 157.3. ν_{max} (KBr): 3435, 2960, 2905, 1621, 1601, 1485, 1458, 1392, 1253, 1052, 924, 872, 751, 553 cm^{-1}.

2.3.7 Synthesis of 5,11,17,23-tetra-*tert*-butyl-25,27-dihydroxy-26,28-[bis[2-((*E*)-((*E*)-(2-(2-oxyethoxy)benzylidene)hydrazono)methyl)phenol]]calix[4]arene (*calix[4]arene salazine*): (32)
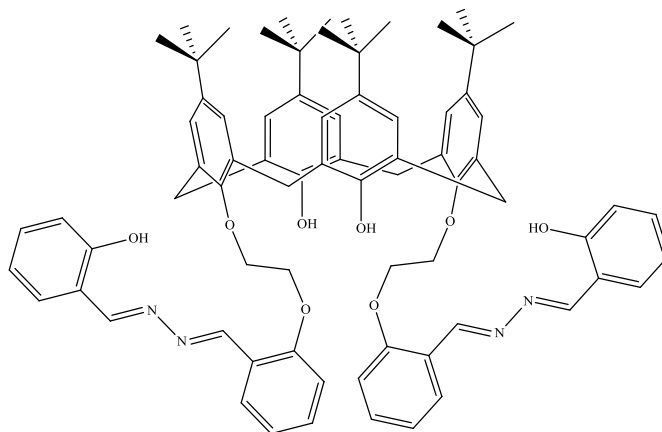
A suspension of **29** (2.0 g, 2.1 mmol), salicylaldehyde hydrazone (0.69 g, 5.1 mmol) and acetic acid (2 mL) were stirred in absolute ethanol (150 mL) for 24 h. The yellow solid was filtered, washed with ethanol and dried in an oven at 75 °C overnight.

Yield: 87 % (2.2 g, 1.84 mmol). m.p.: 166-168 °C. Anal. Calc. for $(C_{76}H_{84}N_4O_8)_2 \cdot H_2O$ (2381.08): C, 76.67; H, 7.20; N, 4.71 %; found: C, 76.80; H, 6.94; N, 4.66 %. δ_H (CDCl$_3$): 1.11 (18H, s, *t*-Bu), 1.17 (18H, s, *t*-Bu), 3.27 (4H, d, ArC*H*$_2$Ar, *J* = 13.0 Hz), 4.33 (4H, d, ArC*H*$_2$Ar, *J* = 13.0 Hz), 4.40 (8H, m, OC*H*$_2$C*H*$_2$O), 6.85 (4H, s, Ar*H*), 6.91 (2H, t, Ar*H*), 6.96 (4H, s, Ar*H*), 7.02 (6H, m, Ar*H*), 7.27 (2H, m, Ar*H*), 7.33 (2H, t, Ar*H*), 7.42 (2H, t, Ar*H*), 7.46 (2H, s, O*H*), 8.08 (2H, d, Ar*H*), 8.64 (2H, s, *H*C=N), 9.12 (2H, s, *H*C=N), 11.71 (2H, s, O*H*). δ_C (CDCl$_3$): 31.0, 31.6, 31.7, 33.7, 34.0, 67.2, 73.6, 112.0, 116.9, 117.8, 119.2, 121.1, 122.6, 125.1, 125.7, 127.5, 127.7, 132.2, 132.6, 132.8, 132.9, 141.5, 147.2, 149.6, 150.3, 158.2, 158.4, 159.9, 164.1. ν_{max} (KBr): 3457, 2958, 1624, 1603, 1486, 1275, 1249, 1194, 924, 870, 750 cm^{-1}.

2.3.8 Synthesis of 3-methoxysalicylaldehyde hydrazone: (33)[104]
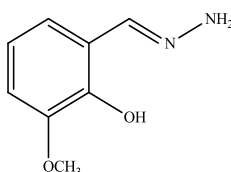
33 was prepared using a variation on a literature method.[104] To a stirring solution of hydrazine hydrate (1.64 g, 32.86 mmol) in ethanol (10 mL) was added dropwise, over 20 minutes, a solution of 3-methoxysalicylaldehyde (1.0 g, 6.57 mmol) in ethanol (40 mL). The yellow solution was stirred for 1 h, after which time the solvent was removed under reduced pressure to leave a yellow oil which on standing, crystallised to yield a yellow solid.

Yield: 88 % (1.07 g, 6.45 mmol). m.p.: 168-170 °C. δ_H (CDCl$_3$): 3.90 (3H, s, OCH_3), 5.46 (2H, s, NH_2), 6.87–6.72 (3H, m, ArH), 7.86 (1H, s, HC=N), 11.20 (1H, s, OH). δ_C (CDCl$_3$): 56.1, 112.3, 118.6, 118.8, 121.2, 146.6, 147.3, 148.1. ν_{max} (KBr): 3380, 1620, 1576, 1468, 1320, 1246, 1090, 964, 838, 776, 625 cm^{-1}.

2.3.9   Synthesis of 5,11,17,23-tetra-*tert*-butyl-25,27-dihydroxy-26,28-[bis[2-((*E*)-((*E*)-(2-(2-oxyethoxy)benzylidene)hydrazono)methyl)3-methoxy-phenol]]calix[4]arene (*calix o-vanillin azine*): (34)
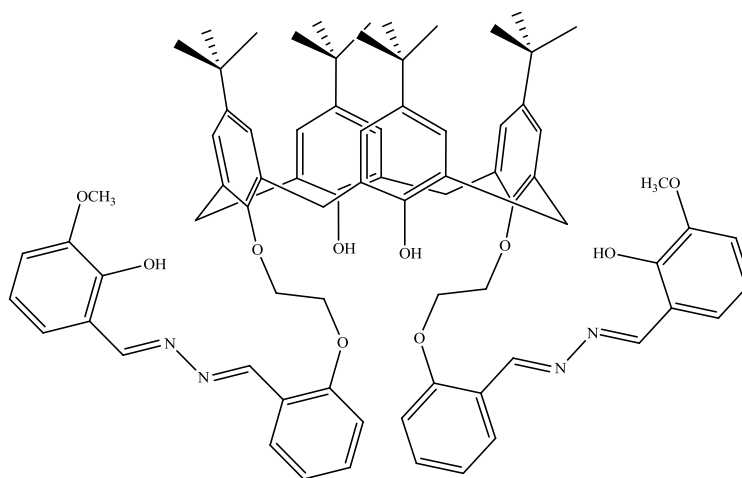
A solution of **29** (0.36 g, 0.38 mmol) and 3-methoxysalicylaldehyde hydrazone (**33**, 0.18 g, 0.98 mmol) in ethanol (20 mL) was heated to reflux under N$_2$ for 1 h. On cooling, a yellow precipitate formed which was removed by filtration. The pale yellow solid was washed with ethanol and dried in an oven at 75 °C.

Yield: 64 % (0.31 g, 0.24 mmol). m.p.: 226-228 °C. Anal. Calc. for C$_{78}$H$_{88}$N$_4$O$_{10}$·2H$_2$O: C, 73.32; H, 7.26; N, 4.39 %; found: C, 73.45; H, 7.03; N, 4.71 %. δ_H (CDCl$_3$): 0.93 (18H, s, *t*-Bu), 1.23 (18H, s, *t*-Bu), 3.12 (4H, d, ArCH_2Ar, *J* = 12.8 Hz), 3.94 (6H, s, OCH_3), 4.31 (4H, d, ArCH_2Ar, *J* = 12.8 Hz), 4.44 (8H, m,

OC*H₂*C*H₂*O), 6.78 (4H, s, Ar*H*), 6.91 (4H, m, Ar*H*), 6.93 (4H, s, Ar*H*), 7.03 (4H, m, Ar*H*), 7.35 (2H, s, O*H*), 7.37 (2H, m, Ar*H*), 7.83 (2H, m, Ar*H*), 8.71 (2H, s, *H*C=N), 9.03 (2H, s, *H*C=N), 11.57 (2H, s, O*H*). δ_C (CDCl₃): 31.0, 31.1, 31.7, 33.7, 33.9, 56.2, 65.7, 73.6, 111.6, 115.1, 117.3, 119.4, 120.9, 123.7, 124.0, 124.8, 125.5, 127.6, 131.0, 131.5, 133.0, 140.9, 146.9, 148.3, 149.0, 150.6, 157.2, 157.3, 164.8. ν_{max} (KBr): 3376, 2961, 1682, 1560, 1459, 1394, 1248, 1075, 923, 756 cm⁻¹.

2.3.10 Synthesis of 2-pyridinecarboxaldehyde hydrazone: (35)[105]
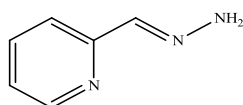
To a stirring solution of hydrazine hydrate (0.7 g, 14.0 mmol) in ethanol (10 mL) was added dropwise, over 20 minutes, a solution of 2-pyridinecarboxaldehyde (0.5 g, 4.67 mmol) in ethanol (30 mL). The yellow solution was stirred for 12 h after which the solvent was removed under reduced pressure to leave a yellow/brown oil.

Yield: 91 % (0.58 g, 4.78 mmol). δ_H (CDCl₃): 5.83 (2H, br s, N*H2*), 7.17 (1H, m, Ar*H*), 7.65 (1H, m, Ar*H*), 7.77 (1H, m, Ar*H*), 7.83 (1H, s, *H*C=N), 8.54 (1H, m, Ar–*H*). δ_C (CDCl₃): 119.7, 122.8, 136.3, 142.6, 149.2, 154.3. ν_{max} (neat): 3368, 3181, 1583, 1565, 1473, 1389, 1150, 993, 776, 622 cm⁻¹.

2.3.11 Synthesis of 5,11,17,23-tetra-*tert*-butyl-25,27-dihydroxy-26,28-[bis[2-((*E*)-((*E*)-(2-(2-oxyethoxy)benzylidene)hydrazono)methyl)pyridine]]-calix[4]arene (*calix 2-pyridine azine*): (36)
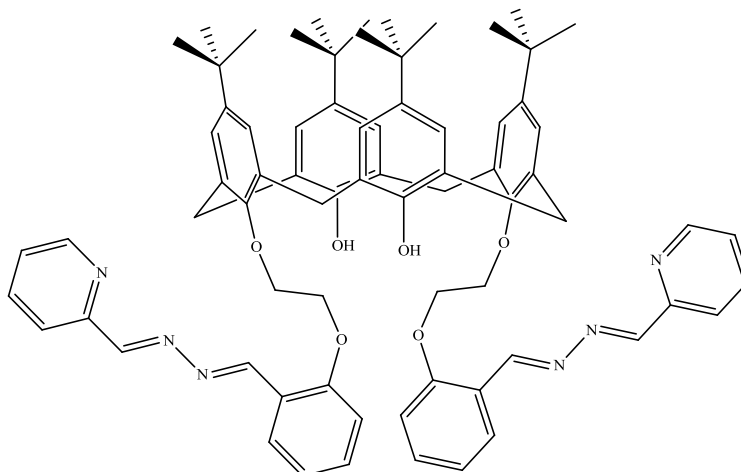
A suspension of **29** (0.5 g, 0.53 mmol) and 2-pyridinecarboxaldehyde hydrazone (**35**, 0.74 g, 5.29 mmol) in acetonitrile (40 mL) was stirred at room temperature for 24 h. The yellow suspension was filtered and the pale yellow solid was washed with acetonitrile and dried in an oven at 75 °C.

Yield: 72 % (0.44 g, 0.38 mmol). m.p.: 166-168 °C. Anal. Calc. for $C_{74}H_{82}N_6O_6$: C, 77.17; H, 7.18; N, 7.30 %; found: C, 76.78; H, 7.09; N, 6.99 %. δ_H (CDCl$_3$): 1.01 (18H, s, *t*-Bu), 1.21 (18H, s, *t*-Bu), 3.28 (4H, d, ArC*H*$_2$Ar, *J* = 12.9 Hz), 4.36 (4H, d, ArC*H*$_2$Ar, *J* = 12.9 Hz), 4.37 (8H, m, OC*H*$_2$C*H*$_2$O), 6.87 (4H, s, Ar*H*), 6.92 (2H, m, Ar*H*), 6.97 (4H, s, Ar*H*), 7.03 (2H, m, Ar*H*), 7.29 (2H, m, Ar*H*), 7.29 (2H, dt, Ar*H*, *J* = 7.7 & 1.7 Hz), 7.66 (2H, m, Ar*H*), 7.67 (2H, s, O*H*), 7.93 (2H, m, Ar*H*), 8.14 (2H, dd, Ar*H*, *J* = 7.7 & 1.7 Hz), 8.62 (2H, s, *H*C=N), 8.66 (2H, m, Ar*H*), 9.24 (2H, s, *H*C=N). δ_C (CDCl$_3$): 31.1, 31.6, 32.0, 33.8, 34.0, 67.2, 73.7, 112.1, 121.2, 122.0, 124.6, 125.1, 125.7, 127.7, 127.8, 132.8, 132.9, 136.3, 141.4, 149.7, 149.8, 150.5, 153.5, 158.2, 159.0, 160.9. ν_{max} (KBr): 3348, 2959, 2868, 1690, 1619, 1602, 1485, 1450, 1250, 1058, 752 cm^{-1}.

2.3.12 Synthesis of 5,11,17,23-tetra-*tert*-butyl-25,27-dihydroxy-26,28-[bis[2-amino-3-((*E*)-(2-(2-oxyethoxy)benzylidene)amino)maleonitrile]]-calix[4]arene (*calix[4]arenesalmaleonitrile*): (37)
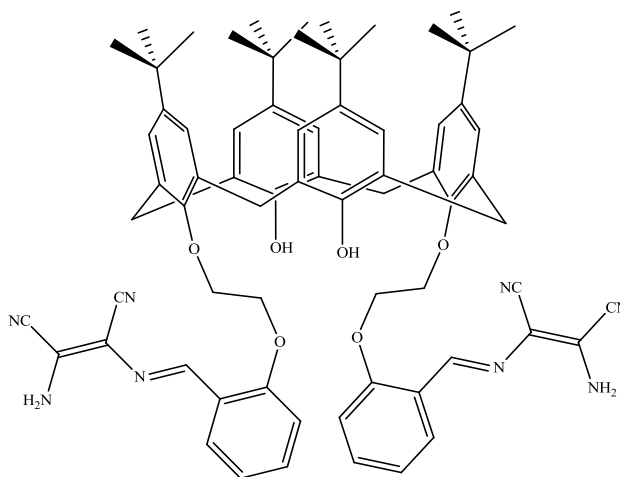
A solution of **29** (1.0 g, 1.05 mmol), diaminomaleonitrile (0.27 g, 2.55 mmol) and acetic acid (1 mL) were stirred together in absolute ethanol (80 mL) for 24 h. The resulting pale yellow precipitate was removed by filtration, washed with ethanol and dried in an oven at 75 °C. A second crop of the product was obtained by concentrating

the filtrate under reduced pressure and taking up the residue in methanol. The insoluble yellow material was removed by filtration.

Yield: 97 % (1.15 g, 1.01 mmol). m.p.: 290-292 °C (decomp). Anal. Calc. for $C_{70}H_{76}N_8O_6 \cdot 1.5(CH_3CO_2H)$: C, 72.13; H, 6.80; N, 9.22 %; found: C, 71.88; H, 6.49; N, 9.43 %. δ_H (d_6-DMSO): 1.15 (18H, s, t-Bu), 1.22 (18H, s, t-Bu), 3.38 (4H, d, ArCH_2Ar, J = 12.7 Hz), 4.25 (4H, d, ArCH_2Ar, J = 12.7 Hz), 4.36 (8H, m, OCH_2CH_2O), 7.08 (4H, s, ArH), 7.12 (2H, m, ArH), 7.13 (4H, s, ArH), 7.20 (2H, m, ArH), 7.61 (2H, m, ArH), 7.74 (4H, s, NH_2), 8.30 (2H, m, ArH), 8.33 (2H, s, OH), 8.76 (2H, s, HC=N). δ_C (d_6-DMSO): 30.8, 31.3, 31.5, 33.5, 33.9, 67.2, 73.4, 103.7, 112.4, 113.5, 114.4, 120.8, 123.9, 125.0, 125.6, 126.2, 127.3, 128.0, 133.1, 133.2, 140.9, 146.9, 149.4, 150.0, 150.8, 158.0. ν_{max} (KBr): 3455, 3337, 2956, 2233, 2205, 1603, 1485, 1364, 1162, 924, 755 cm^{-1}.

2.3.13 Synthesis of 2-((E)-((E)-(2-methoxybenzylidene)hydrazono)methyl)phenol: (38)
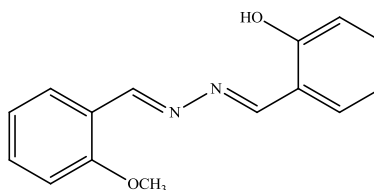
A solution of salicylaldehyde hydrazone (1.0 g, 7.34 mmol) dissolved in absolute ethanol (15 mL) was added to a solution of 2-methoxybenzaldehyde (1.0 g, 7.34 mmol) in absolute ethanol (15 mL) in a round-bottomed flask. A yellow precipitate formed within 5 minutes. Stirring was continued for a further 10 minutes and the suspension was filtered. The light yellow solid was removed by filtration, washed with ethanol and dried in an oven at 75 °C.

Yield: 73 % (1.36 g, 5.36 mmol). m.p.: 138-140 °C. Anal. Calc. for $C_{15}H_{14}N_2O_2$: C, 70.84; H, 5.55; N, 11.02 %; found: C, 70.77; H, 5.53; N, 10.93 %. δ_H (CDCl$_3$): 3.91 (3H, s, OCH_3), 7.05-6.92 (4H, m, ArH), 7.36 (2H, m, ArH, J = 7.9 Hz), 7.44 (1H, t, ArH, J = 7.9 Hz), 8.09 (1H, m, ArH), 8.76 (1H, s, HC=N), 9.05 (1H, s, HC=N), 11.87 (1H, s, OH). δ_C (CDCl$_3$): 55.6, 111.2, 117.0, 117.8, 119.4, 120.9, 122.1, 127.4, 132.3,

132.7, 133.1, 158.5, 159.3, 159.9, 164.4. ν_{max} (KBr): 3454, 1622, 1488, 1463, 1273, 1251, 1022, 958, 753, 676 cm^{-1}.

2.3.14 Synthesis of 2-methoxysalicylaldehyde hydrazone: (39)[106]
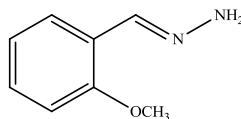
39 was prepared using a similar method published previously.[106] A solution of 2-methoxybenzaldehyde (2.0 g, 14.7 mmol) in ethanol (60 mL) was added dropwise over 1 h to a stirring solution of neat hydrazine hydrate (2.2 g, 44.1 mmol) in a round-bottom flask. The yellow solution was stirred for a further hour before the volatiles were removed under reduced pressure to leave a yellow oil.

Yield: quantitative. δ_H (CDCl$_3$): 3.83 (3H, s, OCH_3), 5.22 (2H, br s, NH_2), 6.87 (1H, d, ArH, J = 8.3 Hz), 6.94 (1H, t, ArH, J = 7.3 Hz), 7.30-7.21 (1H, m, ArH, J = 7.3 & 8.3 Hz), 7.77 (1H, m, ArH), 8.15 (1H, s, HC=N). δ_C (CDCl$_3$): 55.5, 110.9, 120.9, 123.7, 125.8, 129.6, 139.2, 156.9. ν_{max} (neat): 3390, 2936, 1601, 1574, 1489, 1464, 1437, 1249, 1048, 1026, 755 cm^{-1}.

2.3.15 Synthesis of 2-methoxy-6-((*E*)-((*E*)-(2-methoxybenzylidene)hydrazono) methyl)phenol: (40)
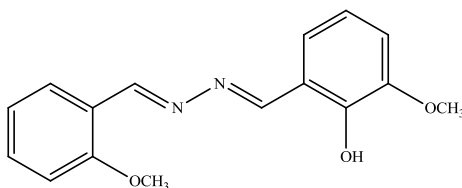
A solution of *o*-vanillin (0.51 g, 3.33 mmol) in ethanol (10 mL) was added to a round-bottom flask containing a stirring solution of **39** (0.50 g, 3.33 mmol). Formation of a yellow precipitate occurred within 5 minutes. Stirring of the suspension was continued overnight after which the yellow solid was removed by filtration, washed with ethanol and dried in an oven at 75 °C.

Yield: 76 % (0.72 g, 2.53 mmol). m.p.: 152-154 °C. Anal. Calc. for C$_{16}$H$_{16}$N$_2$O$_3$: C, 67.58; H, 5.68; N, 9.86 %; found: C, 67.40; H, 5.56; N, 9.83 %. δ_H (CDCl$_3$): 3.90 (3H,

s, OCH_3), 3.93 (3H, s, OCH_3), 7.05-6.86 (5H, m, ArH, J = 7.7 Hz), 7.47-7.41 (1H, m, ArH, J = 1.7 Hz), 8.08 (1H, dd, ArH, J = 7.7 & 1.7 Hz), 8.75 (1H, s, HC=N), 9.02 (1H, s, HC=N), 12.08 (1H, s, OH). δ_C (CDCl$_3$): 55.6, 56.3, 111.2, 114.7, 117.9, 119.1, 120.9, 122.1, 123.9, 127.4, 133.1, 148.3, 149.8, 158.4, 159.3, 164.4. ν_{max} (KBr): 3439, 3071, 3004, 1621, 1601, 1466, 1319, 1298, 1257, 959, 759, 736 cm^{-1}.

2.3.16 Synthesis of a complex from the reaction of 32 and zinc(II) perchlorate hexahydrate: (41)
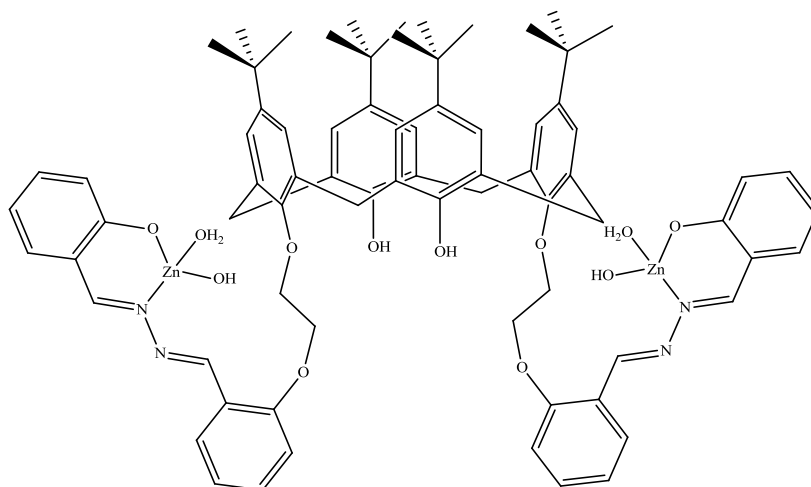
A round-bottom flask was charged with **32** (0.1 g, 0.08 mmol) and absolute ethanol (10 mL). To this yellow suspension was added 1 M sodium hydroxide solution (0.2 mL), giving a yellow solution. Zinc(II) perchlorate hexahydrate (0.13 g, 0.34 mmol) dissolved in absolute ethanol (10 mL) was added to the flask and the mixture stirred for 16 h after which a yellow precipitate had formed. This was filtered off and the neon yellow solid washed with ethanol and dried in a vacuum oven at 56 °C.

Yield: 17 % (0.020 g, 0.01 mmol). Anal. Calc. for C$_{76}$H$_{88}$N$_4$O$_{12}$Zn$_2$: C, 66.11; H, 6.43; N, 4.06 %; found: C, 66.99; H, 6.11; N, 3.91 %. δ_H (d_6-DMSO): 1.06 (18H, s, t-Bu), 1.17 (18H, s, t-Bu), 3.03 (4H, d, ArCH_2Ar, J = 12.9 Hz), 4.05 (4H, d, ArCH_2Ar, J = 12.9 Hz), 4.26-4.04 (8H, m, OCH_2CH_2O), 6.53 (2H, t, ArH, J = 7.6 Hz), 6.63 (2H, d, ArH, J = 8.4 Hz), 6.96 (4H, s, ArH), 6.97 (4H, s, ArH), 7.11-7.00 (6H, m, ArH), 7.23 (2H, d, ArH, J = 8.4 Hz), 7.50 (2H, m, ArH, J = 7.6, 7.3 & 1.5 Hz), 7.79 (2H, dd, ArH, J = 7.3 & 1.5 Hz), 7.98 (2H, s, OH), 8.11 (2H, s, HC=N), 9.03 (2H, s, HC=N). ν_{max} (KBr): 3432, 2960, 1618, 1603, 1530, 1485, 1463, 1190, 754 cm^{-1}.

2.3.17 Synthesis of a complex from the reaction of 32 and zinc(II) chloride: (42)
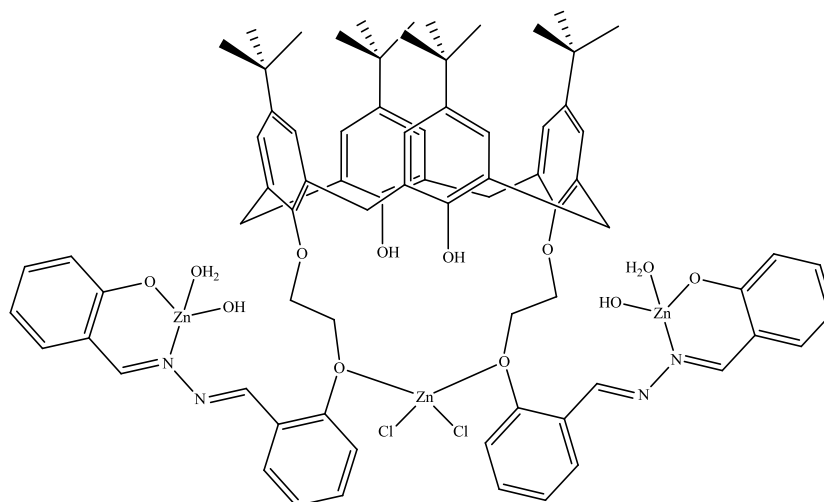
A round-bottom flask was charged with **32** (0.1 g, 0.08 mmol) and absolute ethanol (10 mL). To this yellow suspension was added 1 M sodium hydroxide solution (0.3 mL), giving a yellow solution. Zinc(II) chloride (0.03 g, 0.19 mmol) dissolved in absolute ethanol (5 mL) was added to the flask and the mixture stirred for 75 minutes after which a yellow precipitate had formed. The neon yellow solid was removed by filtration, washed with ethanol and dried in a vacuum oven at 56 °C.

Yield: quantitative (0.094 g, 0.06 mmol). Anal. Calc. for $C_{76}H_{88}N_4O_{12}Cl_2Zn_3$: C, 60.17; H, 5.85; N, 3.70 %; found: C, 60.85; H, 5.78; N, 3.57 %. δ_H (d_6-DMSO): 1.09 (18H, s, t-Bu), 1.20 (18H, s, t-Bu), 3.31 (4H, d, ArCH_2Ar, J = 12.5 Hz), 4.16 (4H, m, OCH_2CH$_2$Ocalix), 4.25 (4H, d, ArCH_2Ar, J = 12.5 Hz), 4.50 (4H, m, OCH$_2$CH_2Ocalix), 6.46 (2H, t, ArH, J = 7.4 Hz), 6.68 (2H, d, ArH, J = 8.4 Hz), 6.98 (4H, m, ArH, J = 7.6 & 7.4 Hz), 7.06 (4H, s, ArH), 7.10 (4H, s, ArH), 7.18 (2H, m, ArH), 7.40 (4H, m, ArH, J = 8.4 Hz), 8.82 (2H, d, ArH, J = 7.6 Hz), 8.21 (2H, s, HC=N), 8.79 (2H, s, OH), 9.30 (2H, s, HC=N). ν_{max} (KBr): 3426, 2959, 1619, 1531, 1485, 1463, 1190, 754 cm^{-1}.

2.3.18 Synthesis of a complex from the reaction of 38 and zinc(II) chloride: (43)
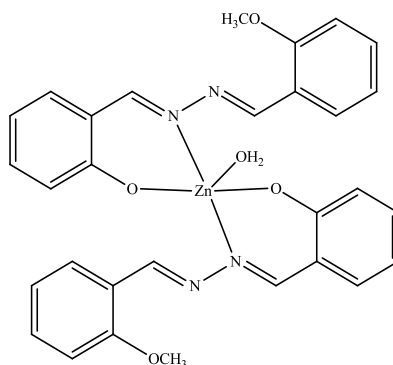
A suspension of **38** (0.2 g, 0.78 mmol) in ethanol (8 mL) was treated with 1 M sodium hydroxide (0.8 mL) to give a yellow solution. To this mixture was added a solution of zinc(II) chloride (0.12 g, 0.79 mmol) in ethanol (8 mL). A yellow precipitate formed within 2 minutes. Stirring was continued for a further 10 minutes at which point the yellow precipitate was removed by filtration, washed with ethanol and dried.

Yield: 63 % (0.145 g, 0.24 mmol) Anal. Calc. for $C_{30}H_{28}N_4O_5Zn \cdot 1.5H_2O$: C, 58.40; H, 5.06; N, 9.08 %; found: C, 58.32; H, 4.38; N, 9.32 %. δ_H (d_6-DMSO): 3.50 (6H, s, OCH_3), 6.61 (2H, m, ArH), 6.76 (2H, m, ArH), 7.04-6.97 (4H, m, ArH, J = 7.6 & 7.2 Hz), 7.30 (2H, m, ArH), 7.52-7.43 (4H, m, ArH, J = 7.6 Hz), 8.87 (2H, d, ArH, J = 7.2 Hz), 8.96 (2H, s, HC=N), 9.04 (2H, s, HC=N). ν_{max} (KBr): 3433, 1615, 1602, 1582, 1528, 1464, 1441, 1342, 1150, 1024, 752 cm^{-1}.

2.3.19 Synthesis of a complex from the reaction of 40 and zinc(II) acetate: (44)
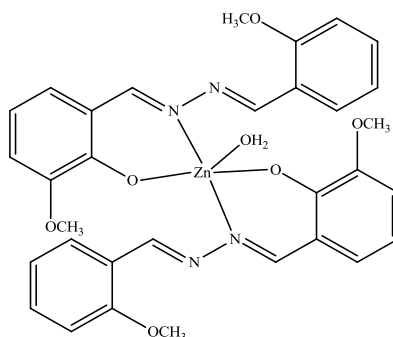
To a stirring suspension of **40** (0.1 g, 0.35 mmol) in ethanol (5 mL) was added a solution of zinc(II) acetate dihydrate (0.085 g, 0.39 mmol) in ethanol (10 mL). Stirring

of the suspension was continued for 72 h, after which the yellow precipitate was removed by filtration, washed with ethanol and dried in a vacuum oven at 56 °C.

Yield: 35 % (0.040 g, 0.06 mmol). Anal. Calc. for $C_{32}H_{32}N_4O_7Zn$: C, 59.13; H, 4.96; N, 8.62 %; found: C, 59.31; H, 4.77; N, 8.33 %. δ_H (d_6-DMSO): 3.46 (6H, s, OCH_3), 3.74 (6H, s, OCH_3), 6.58 (2H, t, ArH J = 7.7 Hz), 7.02-6.98 (6H, m, ArH), 7.16 (2H, d, ArH, J = 7.7 Hz), 7.46 (2H, t, ArH, J = 7.1 Hz), 7.85 (2H, d, ArH, J = 7.1 Hz), 8.60 (2H, s, HC=N), 9.04 (2H, s, HC=N). ν_{max} (KBr): 3460, 1615, 1602, 1583, 1542, 1464, 1445, 1345, 1247, 1209, 1028, 756 cm^{-1}.

2.3.20 *In situ* synthesis of 2-((*E*)-((*E*)-(2-methoxybenzylidene)hydrazono) methyl)pyridine and subsequent complexation with zinc(II) chloride: (45)
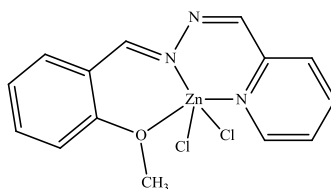
35 (0.1 g, 0.73 mmol) was added dropwise to neat 2-methoxybenzaldehyde (0.1 g, 0.73 mmol). The yellow oil was stirred for 5 minutes after which a solution of zinc(II) chloride (0.2 g, 14.7 mmol) in absolute ethanol (5 mL) was added to the oil. Immediate precipitation of an orange/yellow solid occurred. The suspension was stirred for 2 minutes after which the yellow solid was removed by filtration, washed with several drops of absolute ethanol and dried in a vacuum oven at 56 °C.

Yield: 72 % (0.20 g, 0.53 mmol). Anal. Calc. for $C_{14}H_{13}N_3Cl_2OZn$: C, 44.75; H, 3.49; N, 11.19 %; found: C, 44.39; H, 3.56; N, 11.61 %. δ_H (d_6-DMSO): 3.90 (3H, s, OCH_3), 7.07 (1H, t, ArH J = 7.5 Hz), 7.17 (1H, d, ArH, J = 8.2 Hz), 7.57-7.51 (2H, m, ArH), 8.01-7.94 (2H, m, ArH), 8.11 (1H, m, ArH, J = 7.9 Hz), 8.60 (1H, s, HC=N), 8.73 (1H, m, ArH, J = 4.1 Hz), 8.97 (1H, s, HC=N). ν_{max} (KBr): 3430, 1623, 1594, 1543, 1488, 1474, 1251, 1161, 1151, 1019, 758 cm^{-1}.

2.4 Fluorescence spectroscopy of calix[4]arene azine derivatives in Section 2.3

2.4.1 Overview and parameters

Samples of the azine derivatives and their zinc complexes were prepared as DMSO solutions. Solubility issues resulted in the exclusive use of DMSO to prepare solutions. Samples were run at room temperature as 10 μM solutions based on their proposed structures. UV-vis spectra were obtained to determine absorption maxima. Calix[4]arene has an absorption max at 280 nm.[39]

2.4.2 Fluorescence data

Table 2.3: Absorption maximum of UV absorption spectrum (λ_{abs}) was used as an excitation parameter to generate emission spectrum with maximum (λ_f^{em}). Emission maximum was used as an emission parameter to generate excitation spectrum with maximum (λ_f^{ex}). Data were obtained for calix[4]arene azine derivatives and their zinc(II) complexes, along with free benzazine derived ligands and their corresponding zinc(II) complexes. In a single case, No Fluorescence was Observed (NFO).

Sample No.	λ_{abs} (nm)	λ_f^{em} (nm)	λ_f^{ex} (nm)
32	352	544	351, 289
34	324	415	301
36		NFO	
38	356	433	293, 340
40	340	437	340, 274
41	365	505	470
42	418	504	411
43	409	493	409
44	336	431	317
45	366	418	358

2.5 Synthesis of 5-nitrobenzamide derivatives and their metal complexes

2.5.1 Synthesis of *N*-(2-aminoethyl)-2-hydroxy-5-nitrobenzamide: (46)
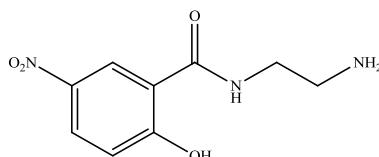
Methyl 2-hydroxy-5-nitrobenzoate (2 g, 10.14 mmol) and ethylene diamine (1.82 g, 30.42 mmol) were heated to reflux in a toluene and methanol mixture (1:1, 80 mL) for 4 h. A yellow precipitate formed upon reaching reflux. The suspension was allowed to cool to room temperature. The yellow precipitate was removed by filtration and dried in an oven at 75 °C overnight.

Yield: 91 % (2.06 g, 9.22 mmol). m.p.: 230-234 °C (decomp). Anal. Calc. for $C_9H_{11}N_3O_4$: C, 47.98; H, 4.93; N, 18.66 %; found: C, 47.89; H, 4.93; N, 18.53 %. δ_H (d_6-DMSO): 2.96 (2H, t, C*H*$_2$NH$_2$, *J* = 7.5 Hz), 3.50 (2H, m, NHC*H*$_2$), 6.27 (1H, d, Ar*H*, *J* = 9.5 Hz), 7.71 (2H, br s, N*H*$_2$), 7.80 (1H, dd, Ar*H*, *J* = 9.5 & 3.3 Hz), 8.65 (1H, d, Ar*H*, *J* = 3.3 Hz), 11.43 (1H, t, CON*H*, *J* = 5.7 Hz). δ_C (d_6-DMSO): 36.5, 39.5, 117.5, 122.6, 127.3, 128.4, 129.8, 167.8, 178.2. ν_{max} (KBr): 3441, 3193, 2914, 1626, 1590, 1557, 1430, 1341, 1298, 1201, 1151, 1131, 842, 755, 678 cm^{-1}.

2.5.2 Synthesis of *N*-(2-aminoethyl)-2-hydroxy-5-nitrobenzamide hydrochloride: (47)
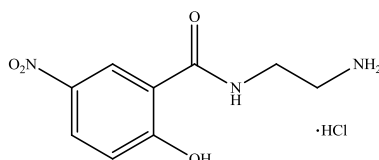
A stirred suspension of **46** (0.15 g, 0.67 mmol) in water (5 mL) was treated with the dropwise addition of 1 M hydrochloric acid (7 mL) until the yellow solid dissolved and the solution turned clear. Stirring was continued for 1 h. The solvent was reduced until a white solid precipitated. The white solid was removed by filtration, washed with cold water and dried in the air.

Yield: 82 % (0.14 g, 0.55 mmol). m.p.: 268-270 °C (decomp). Anal. Calc. for $C_9H_{12}N_3ClO_4$: C, 41.29; H, 4.62; N, 16.06 %; found: C, 41.19; H, 4.61; N, 15.79 %. δ_H (d_6-DMSO): 3.02 (2H, m, NHCH_2), 3.61 (2H, m, CH_2NH$_3$), 7.22 (1H, d, ArH, $J = 9.2$ Hz), 8.17 (3H, br s, NH_3), 8.27 (1H, dd, ArH, $J = 9.2$ & 2.7 Hz), 8.86 (1H, d, ArH, $J = 2.9$ Hz), 9.28 (1H, t, CONH, $J = 4.8$ Hz) 13.45 (1H, br s, OH). δ_C (d_6-DMSO): 37.0, 38.2, 116.6, 118.2, 125.5, 128.5, 139.1, 164.6, 166.9. ν_{max} (KBr): 3383, 2969, 1641, 1605, 1557, 1497, 1329, 1207, 1172, 1159, 844, 749 cm^{-1}.

2.5.3   Synthesis of bis-*O,O'*-(*N*-(2-aminoethyl)-2-hydroxy-5-nitrobenzamide)-copper(II) perchlorate dihydrate: (48)
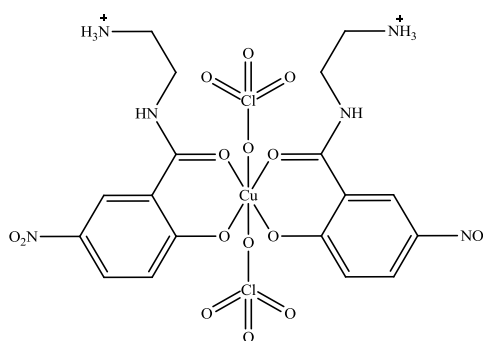
Copper(II) perchlorate hexahydrate (0.34 g, 0.88 mmol) was dissolved in water (5 mL) and added to an Erlenmeyer flask containing a stirring solution of **46** (0.1 g, 0.44 mmol) in water (10 mL). This solution was stirred for 5 minutes and then allowed to stand for several days after which dark green crystals had formed. The crystals were removed by filtration, washed sparingly with water and dried in a vacuum oven at 56 °C.

Yield: 59 % (0.08 g, 0.13 mmol) Anal. Calc. for $C_{18}H_{24}N_6Cl_2CuO_{17}$: C, 29.58; H, 3.31; N, 11.50 %; found: C, 29.40; H, 3.01; N, 11.20 %. ν_{max} (KBr): 3391, 3083, 1608, 1545, 1483, 1471, 1436, 1307, 1141, 1120, 1110, 1086, 834, 749 cm^{-1}.

2.5.4 Synthesis of *N*-(2-aminoethyl)-2-oxo-5-nitro-benzamidatocopper(II) hydrate: (49)
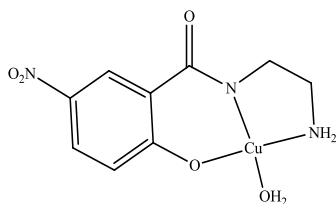
Copper(II) perchlorate hexahydrate (0.08 g, 0.22 mmol) was dissolved in water (5 mL) and added to an Erlenmeyer flask containing a solution of **46** (0.1 g, 0.44 mmol) in water (20 mL). This solution was stirred for 5 minutes and then allowed to stand. Some of the amide starting material crystallised within the first hour. The solution was decanted off the crystals and allowed to stand. The solution reduced over several days to yield a mixture of brown crystals and amide starting material. The crystals were removed by filtration, washed sparingly with water and dried in a vacuum oven at 56 °C.

Yield: 31 % (0.02 g 0.07 mmol). Anal. Calc. for $C_9H_{11}N_3CuO_5$: C, 35.47; H, 3.64; N, 13.79 %; found: C, 35.45; H, 3.58; N, 13.45 %. v_{max} (KBr): 3438, 3225, 1611, 1569, 1525, 1435, 1317, 1283, 1231, 1142, 1131, 834, 696 cm^{-1}.

2.5.5 Reaction of 46 with copper(II) perchlorate hexahydrate in acetonitrile

To **46** (0.1 g, 0.44 mmol) in acetonitrile (5 mL) was added a solution of copper (II) perchlorate hexahydrate (0.18 g, 0.45 mmol) in acetonitrile (15 mL) and the resulting moss green solution was stirred for 10 h. No precipitate resulted and the solvent was allowed to reduce in the fumehood. The green precipitate was removed by filtration and dried in air. Product gave similar analytical results to **48**.

Yield: 78 % (0.08 g, 0.17 mmol); Anal. Calc. for $C_{18}H_{24}N_6Cl_2CuO_{17}$: C, 29.57; H, 3.31; N, 11.50 %; found: C, 29.29; H, 3.29; N, 11.95 %. v_{max} (KBr): 3398, 1610, 1550, 1467, 1439, 1308, 1231, 1141, 1122, 834, 783, 755, 696 cm^{-1}.

2.5.6   Synthesis   of   bis-*O,O'*-(*N*-(2-aminoethyl)-2-hydroxy-5-nitrobenzamide) copper(II) chloride: (50)
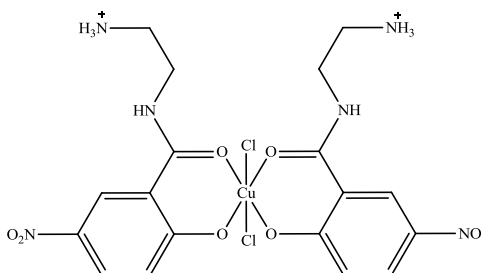
To a solution of **46** (0.1 g, 0.44 mmol) in water (15 mL) was added a solution of copper(II) chloride dihydrate (0.15 g, 0.88 mmol) in water (5 mL) and the resulting green solution was stirred for 1 h. A green solid precipitated from solution. The solid was removed by filtration and dried in air.

Yield: 51 % (0.07 g, 0.11 mmol). Anal. Calc. for $C_{18}H_{22}N_6Cl_2CuO_8$: C, 36.96; H, 3.79; N, 14.37 %; found: C, 36.95; H, 3.79; N, 14.24 %. ν_{max} (KBr): 3378, 3006, 1604, 1579, 1558, 1466, 1307, 1271, 1161, 839, 750 cm^{-1}.

2.5.7   Reaction of copper(II) chloride dihydrate and 46 in acetonitrile

To a suspension of **46** (0.1 g, 0.44 mmol) in acetonitrile (5 mL) was added copper(II) chloride dihydrate (0.08 g, 0.48 mmol) in acetonitrile (15 mL) and the resulting orange solution was stirred for 10 h. After 5 h, a yellow/green solid precipitated from solution. The solid was removed by filtration and dried in air. The product gave similar analytical results to **50**.

Yield: 84 % (0.11 g, 0.18 mmol). Anal. Calc. for $C_{18}H_{22}N_6Cl_2CuO_8$: C, 37.04; H, 4.15; N, 14.41 %; found: C, 36.38; H, 4.21; N, 14.45 %. ν_{max} (KBr): 3375, 1610, 1556, 1465, 1358, 1321, 1273, 1163, 839, 777, 752 cm^{-1}.

2.5.8   Reaction of copper(II) acetate and 46 in water

To a solution of **46** (0.1 g, 0.44 mmol) in water (15 mL) was added a solution of copper(II) acetate monohydrate (0.18 g, 0.89 mmol) in water (5 mL) and the resulting purple/brown solution was stirred for 1 h. A pale purple solid precipitated from

solution within 2 minutes. The purple solid was removed by filtration and dried in air. Similar results to **49**.

Yield: 79 % (0.11 g, 0.35 mmol). Anal. Calc. for $C_9H_{11}N_3CuO_5$: C, 35.47; H, 3.64; N, 13.79 %; found: C, 35.45; H, 3.58; N, 13.45 %. ν_{max} (KBr): 3515, 3227, 3147, 1609, 1570, 1528, 1449, 1435, 1315, 1232, 1142, 1131, 834, 706 cm^{-1}.

2.5.9 Synthesis of a complex from the reaction of 46 and copper(II) acetate in acetonitrile: (51)
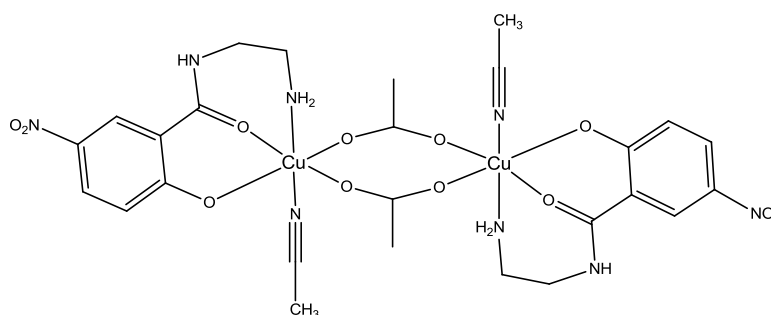
To **46** (0.1 g, 0.44 mmol) in acetonitrile (5 mL) was added copper(II) acetate monohydrate (0.1 g, 0.49 mmol) in acetonitrile (15 mL) and the resulting green suspension was stirred for 10 h. The green solid was removed by filtration and dried in air.

Yield: 78 % (0.12 g, 17 mmol). Anal. Calc. for $C_{26}H_{34}N_8Cu_2O_{12} \cdot 2H_2O$: C, 38.38; H, 4.71; N, 13.77 %; found: C, 38.24; H, 4.03; N, 13.48 %. ν_{max} (KBr): 3433, 3324, 3260, 1600, 1574, 1533, 1471, 1427, 1310, 1146, 1131, 1084, 859, 755, 706, 678 cm^{-1}.

2.5.10 Synthesis of a complex from the reaction of 46 and nickel(II) perchlorate in water: (52)
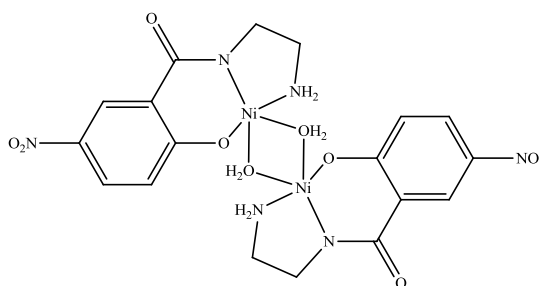
A 1 M sodium hydroxide solution (0.49 mL) was added to a suspension of **46** (0.1 g, 0.44 mmol) in water (5 mL). To this yellow suspension was added a solution of nickel(II) perchlorate hexahydrate (0.325 g, 0.89 mmol) in water (10 mL) which resulted in the immediate precipitation of a light green solid. The suspension was stirred at room temperature overnight. The solid was removed by filtration, washed with water and dried in an oven at 75 °C.

Yield: 96 % (0.128 g, 0.21 mmol). Anal. Calc. for $C_{18}H_{22}N_6Ni_2O_{10}$: C, 36.04; H, 3.70; N, 14.01 %; found: C, 36.08; H, 3.68; N, 13.59 %. ν_{max} (KBr): 3400, 3317, 3153, 1611, 1546, 1468, 1318, 1275, 1152, 836, 587 cm^{-1}. μ_{eff}: 2.79 B.M.

2.5.11 Synthesis of a complex from the reaction of 46 and nickel(II) chloride in water: (53)
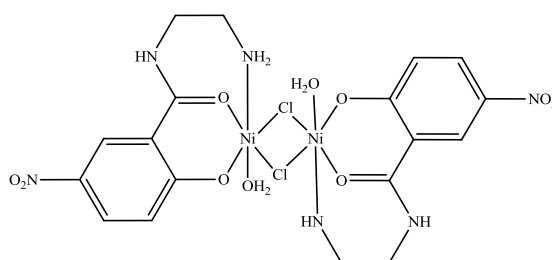
A 1 M sodium hydroxide solution (0.49 mL) was added to a suspension of **46** (0.1 g, 0.44 mmol) in water (5 mL). To this yellow suspension was added a solution of nickel(II) chloride hexahydrate (0.211 g, 0.89 mmol) in water (5 mL) which resulted in the immediate precipitation of a yellow/brown solid. The suspension was stirred at room temperature for thirty minutes. The solid was removed by filtration, washed with water and dried in an oven at 75 °C.

Yield: 42 % (0.062 g, 0.09 mmol). Anal. Calc. for $C_{18}H_{24}N_6Cl_2Ni_2O_{10}$: C, 33.02; H, 3.39; N, 12.84 %; found: C, 32.95; H, 3.57; N, 12.19 %. ν_{max} (KBr): 3414, 1615, 1545, 1475, 1435, 1311, 1147, 1080, 838, 639 cm^{-1}. μ_{eff}: 3.45 B.M.

2.5.12 Synthesis of a complex from the reaction of 46 and nickel(II) acetate in water: (54)
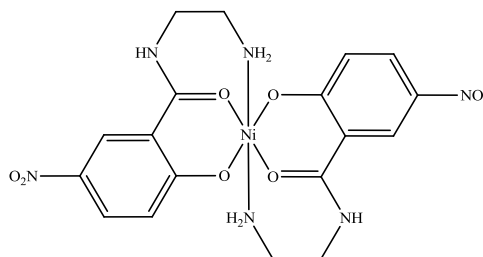
To a hot solution of **46** (0.1 g, 0.44 mmol) in water (10 mL) was added a solution of nickel(II) acetate tetrahydrate (0.22 g, 0.89 mmol) in water (5 mL) and the mixture was stirred for 10 minutes. Within 2 minutes a yellow/green precipitate had formed. The mixture was allowed to cool and the yellow/green solid was removed by filtration and dried in air.

Yield: 75 % (0.084 g, 0.17 mmol). Anal. Calc. for $C_{18}H_{20}N_6NiO_8$: C, 42.63; H, 3.98; N, 16.57 %; found: C, 42.56; H, 4.23; N, 15.95 %. ν_{max} (KBr): 3399, 3155, 1614, 1547, 1467, 1440, 1423, 1320, 1275, 1152, 1010, 1002, 838, 589 cm^{-1}. μ_{eff}: 3.03 B.M.

2.5.13 Synthesis of *N*-(2-aminoethyl)-2-oxo-5-nitro-benzamidatozinc(II) hydrate: (55)
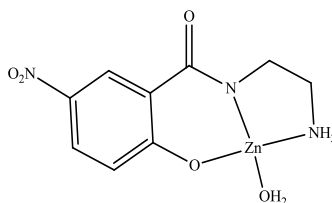
A solution of zinc(II) perchlorate hexahydrate (0.17 g, 0.44 mmol) in water (5 mL) was added dropwise to a solution of **46** (0.1 g, 0.44 mmol) and sodium hydroxide (0.018 g, 0.44 mmol) in water (5 mL). An immediate yellow precipitate resulted and the resulting suspension was stirred for 1 h. The yellow solid was removed by filtration, washed with water and dried in air.

Yield: 78 % (0.11 g, 0.34 mmol). Anal. Calc. for $C_9H_{11}N_3ZnO_5$: C, 35.26; H, 3.62; N, 13.71 %; found: C, 35.45; H, 3.58; N, 13.45 %. δ_H (*d$_6$*-DMSO): 2.83 (2H, br s, C*H$_2$*NH$_2$),3.43 (2H, br s, NHC*H$_2$*), 6.56 (1H, d, Ar*H*, *J* = 9.3 Hz), 7.88 (1H, dd, Ar*H*,

J = 9.3 & 2.9 Hz), 8.65 ppm(1H, d, ArH, J = 2.9 Hz). ν_{max} (KBr): 3443, 2915, 1613, 1590, 1448, 1431, 1341, 1301, 1131, 843, 678 cm^{-1}.

2.5.14 Reaction of 46 with zinc(II) acetate dihydrate in water

Similar procedure to that of zinc complex **55**, except that zinc(II) acetate dihydrate (0.096 g, 0.44 mmol) was used, resulting in the formation of a yellow solid that analysed as for **55**.

Yield: 85 % (0.12 g, 0.37 mmol). Anal. Calc. for $C_9H_{11}N_3ZnO_5$: C, 35.26; H, 3.62; N, 13.71 %; found: C, 35.54; H, 3.84; N, 13.95 %. ν_{max} (KBr): 3515, 3227, 3147, 1609, 1570, 1528, 1449, 1435, 1315, 1232, 1142, 1131, 834, 706 cm^{-1}.

2.5.15 Synthesis of 5,11,17,23-tetra-*tert*-butyl-25,27-diethoxycarbonylmethoxy-calix[4]arene (*Diester*): (56)[107]
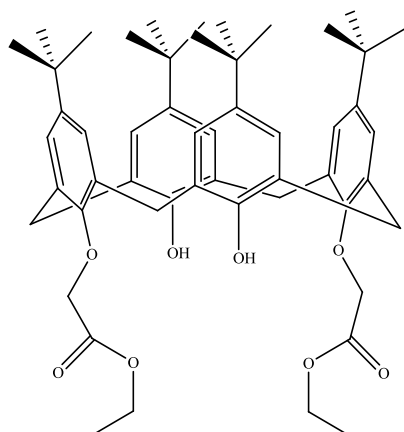
A stirred suspension of **27** (10.00 g, 15.4 mmol), potassium carbonate (2.34 g, 16.94 mmol) and ethyl bromoacetate (5.2 g, 31.0 mmol) was heated to reflux in acetonitrile (160 mL) for 18 h under a flow of nitrogen. After cooling, the mixture was filtered and the volatiles removed under reduced pressure. The residue was dissolved in hot ethanol and the insolubles were removed by hot filtration. The filtrate was allowed to cool after which time a while solid had precipitated. The solid was removed by filtration, washed with ethanol and dried in an oven at 75 °C.

Yield: 57 % (7.10 g, 8.78 mmol). m.p.: 178-180 °C (lit: 182-184 °C).[107] δ_H (CDCl$_3$): 0.97 (18H, s, *t*-Bu), 1.26 (18H, s, *t*-Bu), 1.32 (6H, t, OCH_2CH$_3$, J = 7.1 Hz), 3.31 (4H,

d, ArCH_2Ar, J = 13.1 Hz), 4.29 (4H, q, OCH_2CH$_3$, J = 7.1 Hz), 4.44 (4H, d, ArCH_2Ar, J = 13.1 Hz), 4.72 (4H, s, OCH_2CO), 6.81 (4H, s, ArH), 7.02 (4H, s, ArH) 7.05 (2H, s, OH). δ_C (CDCl$_3$): 14.2, 31.0, 31.7, 31.9, 33.8, 33.9, 61.3, 72.4, 125.1, 125.8, 128.0, 132.5, 141.5, 147.1, 150.3, 150.7, 169.3. ν_{max} (KBr): 3421, 2962, 1759, 1485, 1394, 1382, 1362, 1298, 1209, 1189, 1128, 870, 750, 555 cm^{-1}.

2.5.16 Synthesis of 5,11,17,23-tetra-*tert*-butyl-25,27-dihydroxycarbonylmethoxy-calix[4]arene (*Diacid*): (57)[48]
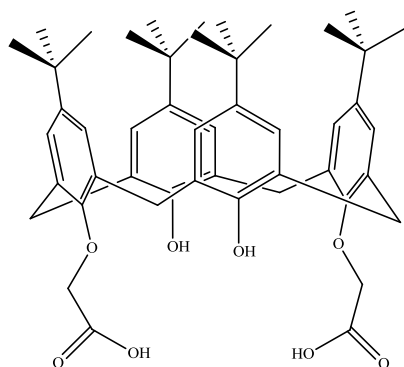
A suspension of **56** (2.0 g, 2.42 mmol) in ethanol (100 mL) was treated with a 10 M sodium hydroxide solution (5 mL) and the solution was heated to reflux for 24 h. The solution was cooled and the solvent was removed under reduced pressure. The residue was poured into a 6 M hydrochloric acid solution (200 mL) which produced a white precipitate. The white solid was removed by filtration, washed with water and dried in an oven at 75 °C.

Yield: 89 % (1.64 g, 2.15 mmol). m.p.: 220-240 °C (decomp) (lit: >200 °C (decomp)).[48] δ_H (CDCl$_3$): 1.07 (18H, s, *t*-Bu), 1.26 (18H, s, *t*-Bu), 3.44 (4H, d, ArCH_2Ar, J = 13.4 Hz), 4.44 (4H, d, ArCH_2Ar, J = 13.4 Hz), 4.69 (4H, s, OCH_2CO), 6.96 (4H, s, ArH), 7.06 (4H, s, ArH). δ_C (CDCl$_3$): 31.0, 31.6, 32.4, 33.9, 34.2, 72.3, 125.7, 126.3, 127.3, 132.5, 143.2, 148.5, 149.0, 149.1, 170.1. ν_{max} (KBr): 3435, 2961, 1747, 1484, 1362, 1195, 1125, 1058, 979, 948, 908, 872, 817 cm^{-1}.

2.5.17 Synthesis of 5,11,17,23-tetra-*tert*-butyl-25,27-dichlorocarbonylmethoxy-calix[4]arene: (58)[48]
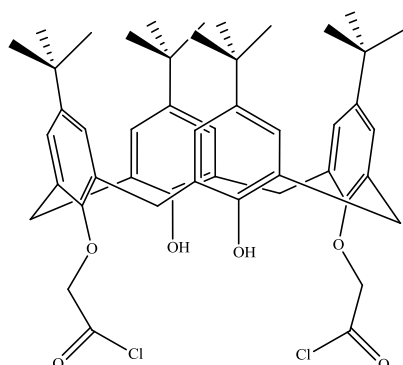
58 was prepared similar to literature methods.[48] **57** (1.0 g, 1.30 mmol) was heated to reflux in thionyl chloride (15 mL) under a guard tube for 3 h. The solution was allowed to cool and the volatiles were removed under reduced pressure to leave an off-white solid. The analysis of the off-white solid corresponds to literature data.

Yield: quantitative. δ_H (CDCl$_3$): 0.90 (18H, s, *t*-Bu), 1.31 (18H, s, *t*-Bu), 3.31 (4H, d, ArC*H*$_2$Ar, *J* = 13.8 Hz), 4.29 (4H, d, ArC*H*$_2$Ar, *J* = 13.8 Hz), 4.97 (4H, s, OC*H*$_2$CO), 6.70 (4H, s, Ar*H*), 7.01 (4H, s, Ar*H*), 7.16 (2H, s, O*H*). ν_{max} (KBr): 3419, 2964, 1813, 1481, 1364, 1230, 1119, 837 cm^{-1}.

2.5.18 Synthesis of *N*-Boc(2-aminoethyl)amine: (59)[108]
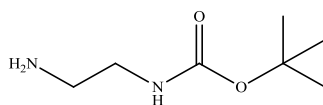
The protected amine was prepared according to literature method.[108] A solution of Boc anhydride (2.0 g, 9.16 mmol) in chloroform (100 mL) was added dropwise over 3 h to a solution of ethylene diamine (5.49 g, 91.6 mmol) at 0 °C. Upon addition the solution was allowed to warm to room temperature. Stirring was continued overnight after which a white precipitate had formed. The suspension was washed with a saturated brine solution (4*50 mL) and water (50 mL). The clear solution was dried over magnesium sulphate, gravity filtered and the solvent removed under reduced pressure to yield a yellow/green oil. Spectral analysis of the yellow/green viscous oil corresponds to literature data.

Yield: quantitative. δ_H (CDCl$_3$): 1.21 (2H, br s, NH_2), 1.45 (9H, s, t-Bu), 2.79 (2H, m, CH$_2$CH_2NH$_2$, J = 5.8 Hz), 3.16 (2H, m, CH_2CH$_2$NH$_2$, J = 5.8 Hz), 5.13 (1H, s, br s, NH). δ_C (CDCl$_3$): 28.4, 41.9, 43.5, 79.2, 156.2. ν_{max} (neat): 3362, 2976, 1707, 1687, 1520, 1365, 1245, 1162 cm^{-1}.

2.5.19 Synthesis of 5,11,17,23-tetra-*tert*-butyl-25,27-di(N-Boc(2-aminoethyl))-carbonylmethoxycalix[4]arene: (60)[89]
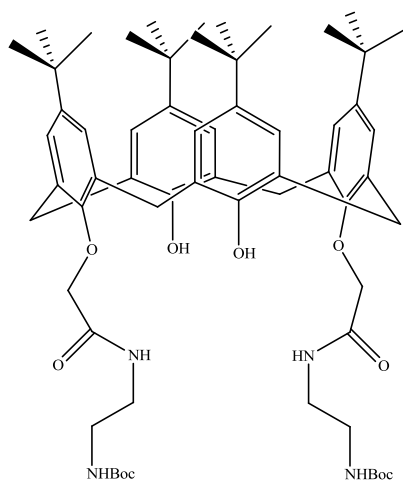
60 was prepared using a literature method.[89] A solution of **58** (1.05 g, 1.31 mmol) in dry dichloromethane (15 mL) was added dropwise to a solution of **59** (0.84 g, 5.24 mmol) and triethylamine (3 mL) in dry dichloromethane (30 mL) at 0 °C. The solution was allowed to stir at room temperature for 13 h. The volatiles were removed under reduced pressure and the residue was taken up in methanol to precipitate a white solid. Spectral analysis of the off-white solid corresponds to literature values.

Yield: 60 % (0.82 g, 0.79 mmol). m.p.: 180-186 ^{o}C (lit: 184-186 °C).[89] δ_H (CDCl$_3$): 1.07 (18H, s, t-Bu), 1.25 (18H, s, t-Bu), 1.34 (18H, s, Ot-Bu), 3.34 (4H, m, NHCH$_2$CH_2NHBoc), 3.44 (4H, d, ArCH_2Ar, J = 13.3 Hz), 3.53 (4H, m, NHCH_2CH$_2$NHBoc), 4.16 (4H, d, ArCH_2Ar, J = 13.3 Hz), 4.61 (4H, s, OCH_2CO), 5.09 (2H, m, NHCH$_2$CH$_2$NHBoc), 6.97 (4H, s, ArH), 7.07 (4H, s, ArH), 8.03 (2H, s, OH), 8.98 (2H, m, NHCH$_2$CH$_2$NHBoc). δ_C (CDCl$_3$): 28.3, 31.0, 31.6, 32.2, 33.9, 34.2, 39.3, 40.8, 74.8, 79.2, 125.8, 126.4, 127.3, 132.6, 143.5, 148.7, 148.8, 149.1, 155.9, 168.7. ν_{max} (KBr): 3346, 2962, 1708, 1694, 1667, 1551, 1485, 1439, 1364, 1299, 1249, 1193, 1175, 1035, 590, 575 cm^{-1}.

2.5.20 Synthesis of 5,11,17,23-tetra-*tert*-butyl-25,27-di((2-aminoethyl))carbonyl-methoxycalix[4]arene trifluoroacetic acid salt: (61)[89]
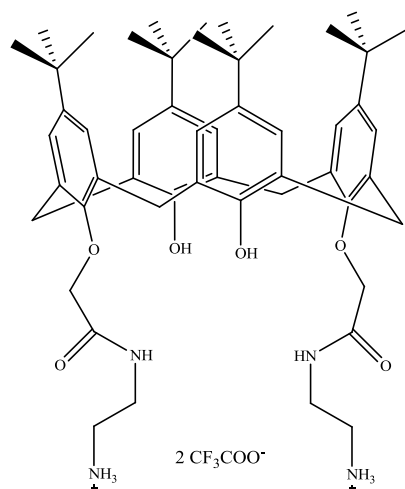
The deprotected amine was prepared according to a literature procedure.[89] Trifluoroacetic acid was added dropwise to a solution of **60** (1.0 g, 0.95 mmol) in dichloromethane (30 mL) at 0 °C. The mixture was stirred for 2 h and the volatiles were removed under reduced pressure to leave an off-white solid.

Yield: quantitative. m.p.: 192-196 °C (lit: 197-198 °C).[89] δ_H (CDCl$_3$): 0.96 (18H, s, *t*-Bu), 1.26 (18H, s, *t*-Bu), 3.26 (4H, m, NHC*H*$_2$CH$_2$NH$_3$), 3.35 (4H, d, ArC*H*$_2$Ar, J = 12.3 Hz), 3.73 (4H, m, NH CH$_2$C*H*$_2$NH$_3$), 4.07 (4H, d, ArC*H*$_2$Ar, J = 12.3 Hz), 4.53 (4H, s, OC*H*$_2$CO), 6.81 (4H, s, Ar*H*), 7.05 (4H, s, Ar*H*), 7.34 (2H, s, O*H*), 7.34 (6H, m, NHCH$_2$CH$_2$N*H*$_3$), 9.11 (2H, m, N*H*CH$_2$CH$_2$NH$_3$). δ_C (CDCl$_3$): 28.7, 29.9, 30.0, 30.5, 32.9, 33.0, 36.2, 38.9, 73.0, 124.6, 125.1, 126.6, 131.1, 142.3, 147.3, 147.7, 148.1, 169.0. δ_F (CDCl$_3$): −75.5 (3F, s, C*F*$_3$). ν_{max} (KBr): 3432, 2963, 1677, 1546, 1485, 1445, 1364, 1204, 1138, 1047, 800, 723 cm^{-1}.

2.5.21 Synthesis of 2-methoxy-5-nitrobenzoic acid: (62)[109]
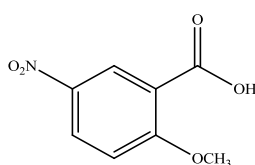
Methyl-2-methoxy-5-nitrobenzoate (2.0 g, 9.48 mmol) was heated to reflux in methanol (100 mL) and 10 M sodium hydroxide solution (1 mL) for 5 h. The solution

was allowed to cool to room temperature and the solvent was removed under reduced pressure. The residue was taken up in water (70 mL) and added to a 6 M hydrochloric acid solution (200 mL) to afford a white crystalline precipitate. The suspension was filtered and the white solid washed with water and dried in an oven at 75 °C.

Yield: 70 % (1.30 g, 1.31 mmol). m.p.: 144-146 °C (lit: 163-164 °C).[109] δ_H (d_6-DMSO): 3.97 (3H, s, OCH_3), 7.36 (1H, d, ArH, J = 9.2 Hz), 8.39 (1H, dd, ArH, J = 9.2 & 2.9 Hz), 8.45 (1H, d, ArH, J = 2.9 Hz), 13.30 (1H, s, COOH). δ_C (d_6-DMSO): 56.9, 113.3, 121.6, 126.3, 128.5, 139.9, 163.0, 165.3. ν_{max} (KBr): 2847, 1705, 1670, 1615, 1489, 1342, 1294, 1271, 1151, 1013, 928, 532 cm^{-1}.

2.5.22 Synthesis of 2-methoxy-5-nitrobenzoyl chloride: (63)[109]
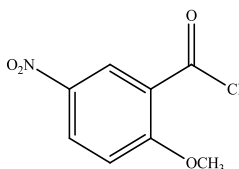
62 (1.0 g, 5.1 mmol) was heated to reflux under a guard tube in thionyl chloride (16 mL) for 4 h. The solution was allowed to cool and the volatiles were removed under reduced pressure to leave an off-white solid.

Yield: quantitative. m.p.: 84-88 °C (lit: 82-83 °C).[109] δ_H (CDCl$_3$): 4.07 (3H, s, OCH_3), 7.14 (1H, d, ArH, J = 9.2 Hz), 8.47 (1H, dd, ArH, J = 9.2 & 2.6 Hz), 9.56 (1H, d, ArH, J = 2.6 Hz). δ_C (CDCl$_3$): 57.2, 112.5, 123.1, 129.9, 130.9, 140.6, 162.7, 163.4. ν_{max} (KBr): 3115, 3076, 1776, 1755, 1609, 1490, 1287, 1261, 1103, 1002, 750 cm^{-1}.

2.5.23 Synthesis of 5,11,17,23-tetra-*tert*-butyl-25,27-di((2-amido(2'-methoxy-5'-nitrobenzyl)ethyl))amidomethoxycalix[4]arene: (64)
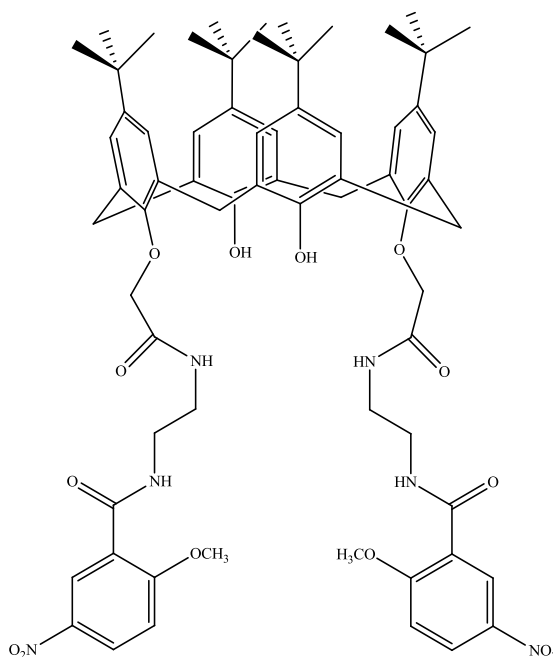
A suspension of **61** (0.84 g, 0.78 mmol) and dry triethylamine (4 mL) in dry dichloromethane (30 mL) were cooled to 0 °C under an argon atmosphere. A solution of **63** (0.84 g, 3.90 mmol) in dry dichloromethane (10 mL) was added dropwise through the septum whilst maintaining cooling. After addition the solution was allowed to rise to room temperature and the stirring was continued for 11 h. The volatiles were removed under reduced pressure. The residue was taken up in methanol (30 mL) and the insolubles were isolated by filtration. The off-white solid was dissolved in chloroform (80 mL) and washed with 1 M sodium hydroxide solution (2*40 mL), 1 M hydrochloric acid solution (2*40 mL) and saturated brine solution (3*40 mL). The organic layer was dried over magnesium sulphate, the inorganic salts removed by filtration and the solvent removed under reduced pressure. The residue was treated with acetone (15 mL) to precipitate a white solid. The solid was removed by filtration, washed with acetone and dried in an oven at 75 °C. A second crop was obtained from the mother liquor by cooling in a freezer at −20 °C overnight.

Yield: 46 % (0.43 g, 0.36 mmol). m.p.: 160-164 °C. Anal. Calc. for $C_{68}H_{82}N_6O_{14}$: C, 67.63; H, 6.85; N, 6.96 %; found: C, 67.81; H, 6.64; N, 6.83 %. δ_H (CDCl$_3$): 1.03 (18H, s, *t*-Bu), 1.20 (18H, s, *t*-Bu), 3.24 (4H, d, ArC*H$_2$*Ar, J = 13.2 Hz), 3.70 (4H, m, NHCH$_2$C*H$_2$*NHOCPh), 3.78 (4H, m, NHC*H$_2$*CH$_2$NHOCPh), 3.98 (6H, s, OC*H$_3$*) 4.05

(4H, d, ArCH_2Ar, $J = 13.2$ Hz), 4.66 (4H, s, OCH_2CO), 6.78 (2H, d, ArH, $J = 9.1$ Hz), 6.85 (4H, s, ArH), 6.88 (4H, s, ArH), 7.92 (2H, s, OH), 8.08 (2H, m, NHCH$_2$CH$_2$NHOCPh), 8.14 (2H, dd, ArH, $J = 9.1$ & 2.8 Hz), 9.00 (2H, d, ArH, $J = 2.8$ Hz), 9.12 (2H, m, NHCH$_2$CH$_2$NHOCPh). δ_C (CDCl$_3$): 29.9, 30.5, 30.9, 32.8, 33.1, 37.0, 39.8, 55.6, 73.7, 110.4, 120.9, 124.3, 125.2, 125.9, 126.8, 127.0, 131.4, 140.5, 141.9, 147.6, 147.7, 148.0, 160.5, 162.4, 168.3. ν_{max} (KBr): 2958, 1655, 1615, 1522, 1485, 1343, 1282, 1192, 1125, 1088, 1016, 874, 823, 749 cm^{-1}.

2.5.23.1 Metal complexation studies for 64 using NMR

Metal complexation reactions were performed in either d_6-DMSO or a d_6-DMSO/H$_2$O mixture using stoichiometric equivalents of metal salt solutions. In all cases no shift of the ligand peaks were observed. The reactions performed are summarised in Table 2.4.

Table 2.4: Summary of metal complexation reactions of **64**.

Metal Salt	Metal Equivalents	Solvent
NaClO$_4$·6H$_2$O	5.0	d_6-DMSO
NaO$_2$CCH$_3$·3H$_2$O	5.0	d_6-DMSO
Zn(O$_2$CCH$_3$)$_2$·2H$_2$O	5.0	d_6-DMSO
ZnCl$_2$	5.0	d_6-DMSO
Zn(ClO$_4$)$_2$·H$_2$O	6.0	d_6-DMSO
AgClO$_4$	6.0	d_6-DMSO
Ag O$_2$CCH$_3$	2.0	d_6-DMSO/H$_2$O

2.5.24 Synthesis of 5,11,17,23-tetra-*tert*-butyl-25,27-di((2-amido(2'-hydroxy-5'-nitrobenzyl)ethyl))amidomethoxycalix[4]arene: (65)
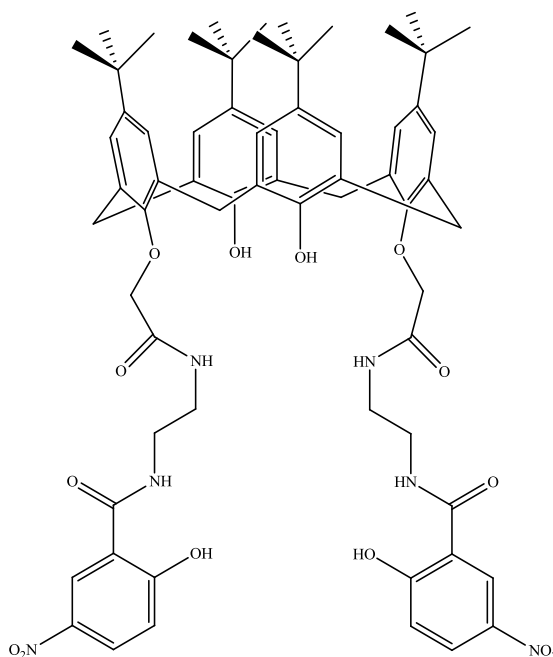
64 (0.050 g, 0.041 mmol) was dissolved in dry dichloromethane (10 mL) and the solution was cooled to 0 °C under a flow of nitrogen. A 1 M solution of boron tribromide in dichloromethane (0.065 mL) was added dropwise to the cooled flask. The solution was allowed to rise to room temperature and stirring was continued for a further 12 h. The solution was cooled to 0 °C and water (2 mL) was added dropwise. The solution was stirred for a further 30 minutes after which the biphasic solution was transferred to a separating funnel. The aqueous layer was removed and the organic layer was washed with 1M hydrochloric acid solution (2 mL) and saturated brine solution (2 mL). The organic layer was dried over sodium sulphate, filtered and the solvent removed under reduced pressure. The residue was dissolved in methanol (3 mL) and resulted in the immediate precipitation of a white solid. The solid was removed by filtration, washed with methanol and dried in an oven at 75 °C.

Yield: 33 % (0.016 g, 0.013 mmol). m.p.: >250 °C. LC/TCOF-MS: $(M + Na)^+$ requires: 1201.5468 g, found: 1201.5526 g, difference 4.82 ppm. δ_H (CDCl$_3$): 1.08 (18H, s, *t*-Bu), 1.14 (18H, s, *t*-Bu), 3.36 (4H, d, ArC*H*$_2$Ar, J = 13.2 Hz), 3.78 (8H, m, NHC*H*$_2$C*H*$_2$NH), 4.09 (4H, d, ArC*H*$_2$Ar, J = 13.2 Hz), 4.65 (4H, s, OC*H*$_2$CO), 6.79 (2H, d, Ar*H*, J = 9.3 Hz), 6.84 (4H, s, Ar*H*), 6.94 (4H, s, Ar*H*), 8.02 (2H, dd, Ar*H*, J = 9.3 & 2.3 Hz), 8.22 (2H, s, O*H*), 8.55 (2H, br s, N*H*OCPh), 8.64 (2H, d, Ar*H*,

J = 2.3 Hz), 9.61 (2H, br s, NHOCCH$_2$), 13.48 (2H, s, OH). δ_C (CDCl$_3$): 30.0, 30.5, 31.0, 32.8, 33.2, 37.6, 38.2, 73.5, 112.3, 117.7, 122.4, 124.5, 125.4, 125.8, 128.0, 131.7, 137.7, 142.1, 147.5, 147.5, 147.9, 166.0, 168.2, 169.0. ν_{max} (KBr): 3362, 2960, 1667, 1651, 1607, 1524, 1484, 1341, 1300, 1205, 1126, 1039, 872, 839 cm^{-1}.

2.5.24.1 Metal complexation studies for 65 using NMR

Metal complexation titrations were performed in d_6-DMSO (except in the case of silver(I) acetate which was performed in a d_6-DMSO/H$_2$O solvent mixture because of solubility issues) using stoichiometric equivalents of metal salt solutions. The reactions performed are summarised in Table 2.5.

Table 2.5: Summary of metal complexation reactions of **65**.

Metal Salt	Metal Equivalents (up to)	Solvent
NaClO$_4$·6H$_2$O	5.0	d_6-DMSO
NaO$_2$CCH$_3$·3H$_2$O	5.0	d_6-DMSO
Zn(O$_2$CCH$_3$)$_2$·2H$_2$O	5.0	d_6-DMSO
ZnCl$_2$	5.0	d_6-DMSO
Zn(ClO$_4$)$_2$·H$_2$O	5.0	d_6-DMSO
AgClO$_4$	5.0	d_6-DMSO
AgO$_2$CCH$_3$	1.6	d_6-DMSO/H$_2$O

From the metal titrations carried out it was found that the only case where interaction (or possible metal complexation) occurs with the ligand is when metal acetate salts are used. The ^{1}H NMR spectra suggest that the sodium(I) acetate interacts with **65** in a 2:1 metal-to-ligand ratio. The zinc(II) and silver(I) acetate salts both appear to interact in a 1:1 metal-to-ligand ratio. A summary of the ^{1}H NMR spectral data of the metal acetate titrations is presented in Table 2.6.

Table 2.6: Summary of ^{1}H NMR spectral data of ligand **65** in d_6-DMSO[a] or d_6-DMSO/H$_2$O[b] and corresponding chemical shift of the ligand's signals on addition of various equivalents of metal acetates.

65	65 & 2 eq. NaO$_2$CCH$_3$[a]	65 & 1 eq. Zn(O$_2$CCH$_3$)$_2$[a]	65 & 1 eq. AgO$_2$CCH$_3$[b]
13.94 (2H, s, ArOH)	—	—	—
9.38 (2H, br s, NHOCCH2)	11.27	10.29	10.89
9.02 (2H, br s, NHOCPh)	8.79	8.76	8.92

8.67 (2H, d, Ar*H*, *J* = 2.5 Hz)	8.58	8.61	8.51
8.33 (2H, s, O*H*)	8.47	8.38	8.28
7.97 (2H, dd, Ar*H*, *J* = 9.2 & 2.5 Hz)	7.72	7.85	7.69
7.10 (4H, s, Ar*H*)	7.13	7.12	7.03
6.87 (2H, d, Ar*H*, *J* = 9.2 Hz)	6.19	6.58	6.28
6.79 (4H, s, Ar*H*)	7.08	7.04	6.88

2.6 Crystallographic Parameters

2.6.1 Overview

X-ray crystallographic work was carried out at either (a) Department of Chemistry, University of Bath by Dr. Mary Mahon with data collected using a Bruker SMART diffractometer, structures solved using SHELXS-97 and refined using full-matrix least squares in HELXL-97,[110] or (b) Department of Chemistry, Loughborough University by Prof. Vickie McKee using a Bruker APEXII CCD diffractometer and solved by direct methods and refined on F^2 using all the reflections.[110]

2.6.2 Crystallographic data for 15

Table 2.7: Crystal data and structure refinement for **15**.

Empirical formula	$C_{14}H_{40}Cu_2N_4O_{12}$
Formula weight	583.58
Temperature	150(2) K
Wavelength	0.71073 Å
Crystal system	Monoclinic
Space group	$P2_1/c$
Unit cell dimensions	a = 16.8610(3) Å; α = 90°
	b = 9.2650(2) Å; β = 108.354(1)°
	c = 16.8760(3) Å; γ = 90°
Volume	2502.21(8) $Å^3$
Z	4
Density (calculated)	1.549 Mg/m^3
Absorption coefficient	1.761 mm^{-1}
F(000)	1224
Crystal size	0.13 x 0.13 x 0.10 mm
Theta range for data collection	4.13 to 27.52°
Index ranges	$-21 \leq h \leq 21$; $-12 \leq k \leq 12$; $-21 \leq l \leq 21$
Reflections collected	34719

Independent reflections	34728 [R(int) = 0.0000]
Reflections observed (>2σ)	28188
Data Completeness	0.988
Absorption correction	Semi-empirical from equivalents
Max. and min. transmission	0.21 and 0.18
Refinement method	Full-matrix least-squares on F^2
Data / restraints / parameters	34728 / 8 / 327
Goodness-of-fit on F^2	1.046
Final R indices [I>2σ(I)]	$R_1 = 0.0462$ $wR_2 = 0.1035$
R indices (all data)	$R_1 = 0.0643$ $wR_2 = 0.1149$
Largest diff. peak and hole	0.463 and −0.485 e$Å^{-3}$

Successful refinement was only achieved after accounting for a small amount of non-merohedral twinning about the (1,0,0) reciprocal axis.

2.6.3   Crystallographic data for 21

Table 2.8: Crystal data and structure refinement for **21**.

Empirical formula	$C_{15}H_{41}Cl_{4.50}Cu_{2.50}N_{6.50}O$
Formula weight	646.92
Temperature	150(2) K
Wavelength	0.71073 Å
Crystal system	Orthorhombic
Space group	Pbcm
Unit cell dimensions	a = 11.4150(1) Å; α = 90°
	b = 18.1840(2) Å; β = 90°
	c = 25.8210(2) Å; γ = 90°
Volume	5359.67(9) $Å^3$
Z	8
Density (calculated)	1.603 Mg/m^3
Absorption coefficient	2.442 mm^{-1}
F(000)	2668
Crystal size	0.50 x 0.40 x 0.40 mm
Theta range for data collection	3.57 to 29.99°
Index ranges	−16<=h<=16; −25<=k<=25; −36<=l<=36
Reflections collected	81648
Independent reflections	7926 [R(int) = 0.0789]
Reflections observed (>2σ)	5823
Data Completeness	0.994
Absorption correction	Semi-empirical from equivalents
Max. and min. transmission	0.62 and 0.58
Refinement method	Full-matrix least-squares on F^2
Data / restraints / parameters	7926 / 2 / 288
Goodness-of-fit on F^2	1.025
Final R indices [I>2σ(I)]	$R_1 = 0.0312$ $wR_2 = 0.0618$
R indices (all data)	$R_1 = 0.0570$ $wR_2 = 0.0692$
Largest diff. peak and hole	0.455 and −0.531 e$Å^{-3}$

2.6.4 Crystallographic data for 31

Table 2.9: Crystal data and structure refinement for **31**.

Empirical formula	$C_{65}H_{79}N_3O_7$
Formula weight	1014.31
Temperature	150(2) K
Wavelength	0.71073 Å
Crystal system	Monoclinic
Space group	$P2_1/c$
Unit cell dimensions	$a = 12.6560(1)$Å; $\alpha = 90°$
	$b = 35.8240(3)$Å; $\beta = 95.486(1)°$
	$c = 13.2220(1)$Å; $\gamma = 90°$
Volume	5967.25(8) $Å^3$
Z	4
Density (calculated)	1.129 Mg/m^3
Absorption coefficient	0.073 mm^{-1}
F(000)	2184
Crystal size	0.35 x 0.20 x 0.10 mm
Theta range for data collection	3.53 to 27.44°
Index ranges	$-16 \leq h \leq 16$; $-46 \leq k \leq 46$; $-17 \leq l \leq 17$
Reflections collected	82356
Independent reflections	13578 [R(int) = 0.0853]
Reflections observed (>2σ)	8449
Data Completeness	0.994
Absorption correction	None
Refinement method	Full-matrix least-squares on F^2
Data / restraints / parameters	13578 / 0 / 692
Goodness-of-fit on F^2	1.017
Final R indices [I>2σ(I)]	$R_1 = 0.0554$ $wR_2 = 0.1134$
R indices (all data)	$R_1 = 0.1104$ $wR_2 = 0.1355$
Largest diff. peak and hole	0.400 and -0.331 $eÅ^{-3}$

2.6.5 Crystallographic data for 32 (xylene inclusion complex)

Table 2.10: Crystal data and structure refinement for **32 (xylene inclusion complex)**.

Empirical formula	$C_{84}H_{94}N_4O_8$
Formula weight	1287.63
Temperature	150(2) K
Wavelength	0.71073 Å
Crystal system	Triclinic
Space group	P-1
Unit cell dimensions	$a = 10.8820(1)$ Å; $\alpha = 101.083(1)°$
	$b = 15.1550(1)$ Å; $\beta = 91.568(1)°$
	$c = 22.8020(2)$ Å; $\gamma = 91.306(1)°$

Volume	3687.41(5) Å^3
Z	2
Density (calculated)	1.160 Mg/m^3
Absorption coefficient	0.074 mm^{-1}
F(000)	1380
Crystal size	0.60 x 0.50 x 0.50 mm
Theta range for data collection	3.51 to 27.65°
Index ranges	−14<=h<=14; −19<=k<=19; −28<=l<=29
Reflections collected	56708
Independent reflections	16861 [R(int) = 0.0392]
Reflections observed (>2σ)	12748
Data Completeness	0.980
Absorption correction	Semi-empirical from equivalents
Max. and min. transmission	0.97 and 0.91
Refinement method	Full-matrix least-squares on F^2
Data / restraints / parameters	16861 / 0 / 863
Goodness-of-fit on F^2	1.026
Final R indices [I>2σ(I)]	R$_1$ = 0.0639 wR$_2$ = 0.1668
R indices (all data)	R$_1$ = 0.0860 wR$_2$ = 0.1864
Largest diff. peak and hole	1.093 and −0.562 eÅ^{-3}

2.6.6   Crystallographic data for 32 (DMF inclusion complex)

Table 2.11: Crystal data and structure refinement for **32 (DMF inclusion complex)**.

Empirical formula	C$_{79}$H$_{91}$N$_5$O$_9$
Formula weight	1254.57
Temperature	150(2) K
Wavelength	0.71073 Å
Crystal system	Monoclinic
Space group	P21/c
Unit cell dimensions	a = 17.1160(2)Å; α = 90°
	b = 13.4260(1)Å; β = 94.738(1)°
	c = 30.6690(4)Å; γ = 90°
Volume	7023.63(13) Å^3
Z	4
Density (calculated)	1.186 Mg/m^3
Absorption coefficient	0.077 mm^{-1}
F(000)	2688
Crystal size	0.25 x 0.20 x 0.10 mm
Theta range for data collection	3.56 to 27.49°
Index ranges	−22<=h<=22; −17<=k<=17; −39<=l<=39
Reflections collected	101843
Independent reflections	16068 [R(int) = 0.0878]
Reflections observed (>2σ)	8887
Data Completeness	0.996

Absorption correction	Semi-empirical from equivalents
Max. and min. transmission	1.00 and 0.96
Refinement method	Full-matrix least-squares on F^2
Data / restraints / parameters	16068 / 12 / 863
Goodness-of-fit on F^2	1.013
Final R indices [I>2σ(I)]	$R_1 = 0.0646$ $wR_2 = 0.1336$
R indices (all data)	$R_1 = 0.1375$ $wR_2 = 0.1630$
Largest diff. peak and hole	0.343 and -0.376 eÅ^{-3}

2.6.7   Crystallographic data for 37

Table 2.12: Crystal data and structure refinement for **37**.

Empirical formula	$C_{152}H_{174}N_{16}O_{18}$
Formula weight	2513.07
Temperature	150(2) K
Wavelength	0.71073 Å
Crystal system	Triclinic
Space group	P-1
Unit cell dimensions	a = 17.8530(1)Å; α = 100.136(1)°
	b = 20.9960(2)Å; β = 103.846(1)°
	c = 21.7370(2)Å; γ = 109.330(1)°
Volume	7169.76(10) Å^3
Z	2
Density (calculated)	1.164 Mg/m^3
Absorption coefficient	0.077 mm^{-1}
F(000)	2684
Crystal size	0.30 x 0.30 x 0.25 mm
Theta range for data collection	3.86 to 27.48^o
Index ranges	-22<=h<=23; -27<=k<=27; -28<=l<=28
Reflections collected	136944
Independent reflections	32677 [R(int) = 0.0592]
Reflections observed (>2σ)	20477
Data Completeness	0.994
Absorption correction	None
Refinement method	Full-matrix least-squares on F^2
Data / restraints / parameters	32677 / 3 / 1731
Goodness-of-fit on F^2	1.016
Final R indices [I>2σ(I)]	$R_1 = 0.0715$ $wR_2 = 0.1760$
R indices (all data)	$R_1 = 0.1207$ $wR_2 = 0.2085$
Largest diff. peak and hole	1.031 and -0.476 eÅ^{-3}

2.6.8   Crystallographic data for 46

Table 2.13: Crystal data and structure refinement for **46**.

Empirical formula	$C_9H_{11}N_3O_4$
Formula weight	225.21
Temperature	150(2) K
Wavelength	0.71073 Å
Crystal system	monoclinic
Space group	C2/c
Unit cell dimensions	a = 15.5904(13) Å; α = 90°
	b = 9.6611(8) Å; β = 112.550(1)°
	c = 13.7196(11) Å; γ = 90°
Volume	1908.5(3) Å^3
Z	8
Density (calculated)	1.568 Mg/m^3
Absorption coefficient	0.125 mm^{-1}
F(000)	944
Crystal size	0.31 x 0.23 x 0.10 mm
Crystal description	yellow block
Theta range for data collection	2.54 to 30.56°
Index ranges	−22<=h<=22; −13<=k<=13; −19<=l<=19
Reflections collected	11025
Independent reflections	2907 [R(int) = 0.0359]
Data Completeness	0.999
Absorption correction	multi-scan
Refinement method	full-matrix least-squares on F^2
Data / restraints / parameters	2907 / 0 / 148
Goodness-of-fit on F^2	1.030
Final R indices [I>2σ(I)]	R_1 = 0.0445 wR_2 = 0.1204
R indices (all data)	R_1 = 0.0585 wR_2 = 0.1307
Largest diff. peak and hole	0.387 and −0.456 eÅ^{-3}

2.6.9   Crystallographic data for 47

Table 2.14: Crystal data and structure refinement for **47**.

Empirical formula	$C_9H_{12}ClN_3O_4$
Formula weight	261.67
Temperature	150(2) K
Wavelength	0.71073 Å
Crystal system	Triclinic
Space group	P-1
Unit cell dimensions	a = 5.8346(5) Å; α= 105.3490(10)°
	b = 8.1575(8) Å; β= 92.1640(10)°
	c = 11.8171(11) Å; γ = 91.2740(10)°

Volume	541.69(9) Å^3
Z	2
Density (calculated)	1.604 Mg/m^3
Absorption coefficient	0.361 mm^{-1}
F(000)	272
Crystal size	.35 x .21 x .02 mm^3
Crystal description	colourless lath
Theta range for data collection	1.79 to 28.99°
Index ranges	−7<=h<=7, −11<=k<=11, −16<=l<=16
Reflections collected	5798
Independent reflections	2834 [R(int) = 0.0247]
Completeness to theta = 28.99°	98.5 %
Absorption correction	Semi-empirical from equivalents
Max. and min. transmission	0.8622 and 0.7575
Refinement method	Full-matrix least-squares on F^2
Data / restraints / parameters	2834 / 0 / 160
Goodness-of-fit on F^2	1.047
Final R indices [I>2σ(I)]	$R_1 = 0.0374$ w$R_2 = 0.0915$
R indices (all data)	$R_1 = 0.0504$ w$R_2 = 0.0976$
Largest diff. peak and hole	0.428 and −0.270 eÅ^{-3}

2.6.10 Crystallographic data for 48

Table 2.15: Crystal data and structure refinement for **48**.

Empirical formula	$C_{18}H_{24}Cl_2CuN_6O_{17}$
Formula weight	730.87
Temperature	150(2) K
Wavelength	0.71073 Å
Crystal system	Monoclinic
Space group	C2/c
Unit cell dimensions	a = 10.2850(5) Å; α = 90°
	b = 14.9501(7) Å; β = 92.915(1)°
	c = 18.1501(9) Å; γ = 90°
Volume	2787.2(2) Å^3
Z	4
Density (calculated)	1.742 Mg/m^3
Absorption coefficient	1.066 mm^{-1}
F(000)	1492
Crystal size	0.19 x 0.13 x 0.10 mm^3
Crystal description	green block
Theta range for data collection	2.25 to 28.32°
Index ranges	−13<=h<=13,−19<=k<=19,−24<=l<=24
Reflections collected	14156
Independent reflections	3472 [R(int) = 0.0268]
Completeness to theta = 27.50°	100.0 %

Absorption correction	Semi-empirical from equivalents
Max. and min. transmission	0.9009 and 0.8231
Refinement method	Full-matrix least-squares on F^2
Data / restraints / parameters	3472 / 68 / 245
Goodness-of-fit on F^2	1.073
Final R indices [I>2σ(I)]	$R_1 = 0.0327$ $wR_2 = 0.0914$
R indices (all data)	$R_1 = 0.0384$ $wR_2 = 0.0951$
Largest diff. peak and hole	0.421 and -0.434 $e\text{Å}^{-3}$

2.6.11 Crystallographic data for 49

Table 2.16: Crystal data and structure refinement for **49**.

Empirical formula	$C_9H_{11}CuN_3O_5$
Formula weight	304.75
Temperature	150(2) K
Wavelength	0.71073 Å
Crystal system	Orthorhombic
Space group	Pbca
Unit cell dimensions	a = 13.5511(6) Å; α= 90°
	b = 10.4268(4) Å; β= 90°
	c = 14.7843(6) Å; γ = 90°
Volume	2088.94(15) Å^3
Z	8
Density (calculated)	1.938 Mg/m^3
Absorption coefficient	2.111 mm^{-1}
F(000)	1240
Crystal size	0.22 x 0.19 x 0.10 mm^3
Crystal description	orange/brown plate
Theta range for data collection	2.76 to 30.57°
Index ranges	$-19{<}{=}h{<}{=}19$, $-14{<}{=}k{<}{=}14$, $-21{<}{=}l{<}{=}21$
Reflections collected	23011
Independent reflections	3203 [R(int) = 0.0428]
Completeness to theta = 30.57°	99.8 %
Absorption correction	Semi-empirical from equivalents
Max. and min. transmission	0.8167 and 0.6538
Refinement method	Full-matrix least-squares on F^2
Data / restraints / parameters	3203 / 3 / 169
Goodness-of-fit on F^2	1.034
Final R indices [I>2σ(I)]	$R_1 = 0.0332$ $wR_2 = 0.0962$
R indices (all data)	$R_1 = 0.0439$ $wR_2 = 0.1027$
Largest diff. peak and hole	0.490 and -0.762 $e\text{Å}^{-3}$

2.6.12 Crystallographic data for 64

Table 2.17: Crystal data and structure refinement for **64**.

Empirical formula	$C_{69}H_{84}Cl_2N_6O_{18}$
Formula weight	1356.32
Temperature	150(2) K
Wavelength	0.71073 Å
Crystal system	Monoclinic
Space group	$P2_1/c$
Unit cell dimensions	a = 25.8174(18) Å; α= 90°
	b = 12.9239(9) Å; β= 109.574(1)°
	c = 23.2764(16) Å; γ = 90°
Volume	7317.6(9) Å^3
Z	4
Density (calculated)	1.231 Mg/m^3
Absorption coefficient	0.159 mm^{-1}
F(000)	2872
Crystal size	0.47 x 0.25 x 0.18 mm^3
Crystal description	colourless block
Theta range for data collection	1.67 to 26.00°
Index ranges	$-31 <= h <= 31$, $-15 <= k <= 15$, $-28 <= l <= 28$
Reflections collected	62134
Independent reflections	14360 [R(int) = 0.0452]
Completeness to theta = 26.00°	100.0 %
Absorption correction	Semi-empirical from equivalents
Max. and min. transmission	0.9720 and 0.9291
Refinement method	Full-matrix least-squares on F^2
Data / restraints / parameters	14360 / 30 / 955
Goodness-of-fit on F^2	1.026
Final R indices [I>2σ(I)]	$R_1 = 0.0726$ w$R_2 = 0.2109$
R indices (all data)	$R_1 = 0.1085$ w$R_2 = 0.2426$
Largest diff. peak and hole	0.824 and -0.673 eÅ^{-3}

3. Results and Discussion

3.1   Introduction

This thesis presents the results of an investigation into the development of novel metal ion binders using the *tert*-butyl-calix[4]arene as a macrocyclic scaffold with scope for providing indicative properties to show that complexation of metal ions takes place. Using standard Schiff-base and amide formation techniques, novel ligands were prepared. A summary of the work completed and presented in this thesis is displayed in Scheme 3.1 and Scheme 3.2.
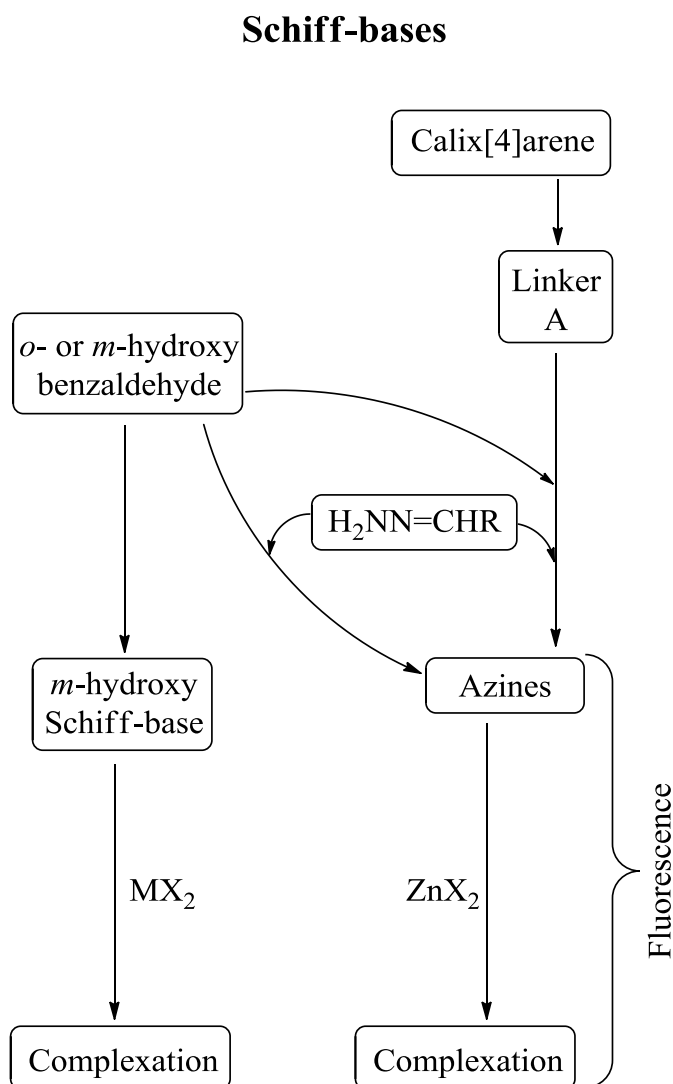
Schiff-bases

Scheme 3.1: Overview of work carried out in this thesis using Schiff-base containing molecules.

Initial work focused on the preparation of a novel class of Schiff-base ligands based on the *m*-hydroxybenzaldehyde moiety. Using various diamines, compartmental ligands

were prepared and used in the preparation of their corresponding copper(II), nickel(II) and zinc(II) coordination complexes.

In extending this theme, another benzaldehyde (salicylaldehyde) was used in the preparation of a novel macromolecular Schiff-base family of compounds. The majority of these contained the azine functional group, thus providing donor atoms for metal ion complexation. This family of calix[4]arene azines and their benzazine analogues were both screened for any potential fluorescence characteristics. In addition to the free ligands, several zinc(II) complexes of the previously described ligands were also prepared and subsequently screened for any fluorescence activity.

Amides
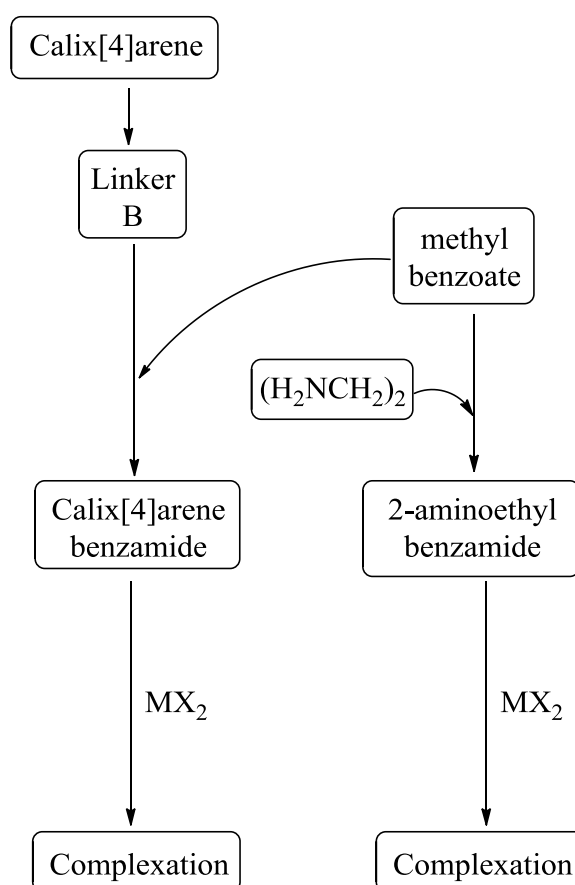
Scheme 3.2: Overview of work carried out in this thesis using benzamide containing molecules.

As an aside to the above approach using Schiff-base ligands, a second synthetic scheme was laid out using amides as points of construction. Potential problems with facile hydrolysis of the ligand (which was the case with some of the Schiff-base

ligands) were eliminated. The new benzamide ligand contained a potential ambidentate binding site and this feature was exploited with several copper(II) nickel(II) and zinc(II) coordination complexes successfully prepared.

The final approach involved the use of the novel amide ligand outlined above and its attachment to the calix[4]arene macrocycle to prepare novel calix[4]arene amide metal ion binders. The novel amide ligand was screened against a family of sodium(I), silver(I) and zinc(II) metal salts to determine if the new ligand could successfully interact with the metal ion.

3.2   Synthesis and characterisation of *m*-hydroxysal ligands

Initially it was decided to design model compounds with imine functional groups. Salicylaldehyde is a common building block for use in the synthesis of Schiff-base ligands. A quick search through the literature reveals an extensive range of compounds that are based on this simple molecule. This extended family of compounds have found use in transition metal catalysis and model systems, among others.[2,8] However the use of its *meta* substituted analogue is far less prevalent in coordination chemistry. It was therefore decided to base the design of these metal ion binders on *meta*-hydroxybenzaldehyde.

Three aliphatic diamines, ethylene diamine (en) (1,2-diaminoethane), 1,3-diaminopropane (dap) and 3,3'-diamino-*N*-methyldipropylamine (dmda) were chosen for this study. It was postulated that the binding characteristics of the salen (formed from salicylaldehyde and an alkyl or aryl diamine) ligand could be compared to its lesser used analogue, the *meta*-hydroxy derivative. Standard Schiff-base preparations were used in the synthesis of ligands **1**, **2** and **3**, with two equivalents of the aldehyde reacting with one equivalent of the diamine in a condensation reaction, as shown in Scheme 3.3. In all cases the reaction progression/completion was monitored by ^{1}H NMR spectroscopy.

The ^{1}H NMR spectrum of *meta*-hydroxybenzaldehyde reactant exhibited an aldehydic proton signal at 9.93 ppm. This aldehydic proton signal was not present in the ^{1}H NMR spectrum of **1** shown in Figure 3.1. Instead, a singlet at 8.24 ppm representing the signal for the imine hydrogen was present and this was considered indicative of

ligand formation. The IR spectrum of ligand **1** confirms this hypothesis with the replacement of the carbonyl stretch of the aldehyde functional group of the reactant at 1668 cm^{-1} with an imine stretch at 1647 cm^{-1}. **1** was isolated as a white solid, was a symmetrical molecule and its ^{13}C NMR spectrum showed 8 resonance peaks which indicated that the molecule contained a plane of symmetry.
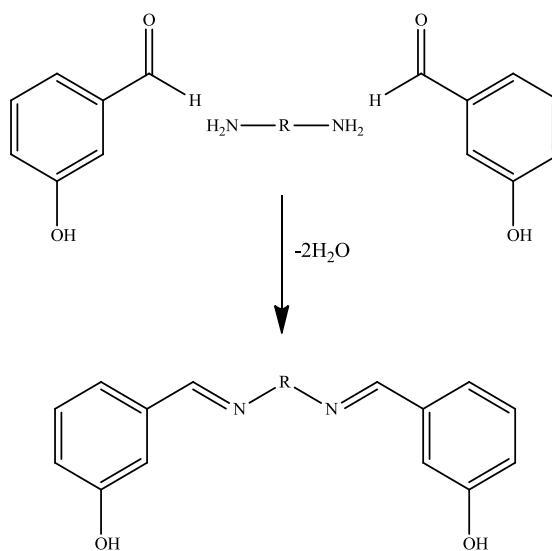
R = (CH$_2$)$_n$ with n =2 for **1**, n = 3 for **2**,
and R = (CH$_2$)$_3$NMe(CH$_2$)$_3$ for **3**

Scheme 3.3: Synthesis of *m*-hydroxysal ligands **1**, **2** and **3** using various diamines.

It was hoped that by increasing the length of the aliphatic chain linking the two iminophenol moieties, enough flexibility would be introduced into the backbone of the ligand to enable donation into the metal from the nitrogen and oxygen donor atoms, without excessive strain on the ligand. It was for this reason that 1,3-diaminopropane was used in the preparation of **2**. Similar analysis was carried out on the formation and characterisation of ligand **2**, with an imine proton resonance at 8.33 ppm replacing the aforementioned aldehydic proton at 9.93 ppm in the ^{1}H NMR spectrum. The IR spectrum showed the characteristic C=N imine stretch at 1650 cm^{-1}. The ^{13}C NMR spectrum showed 9 resonance peaks which demonstrated that a plane of symmetry existed within the molecule. Spectral analysis of the white precipitate was corroborated by microanalysis which revealed that the white solid consisted of four molecules of ligand to one molecule of water.
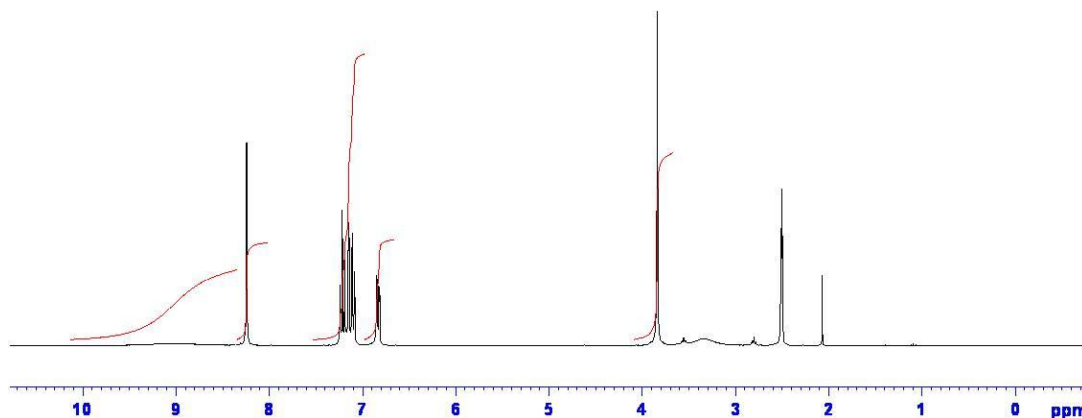
Figure 3.1: ^{1}H NMR spectrum of **1** run in d_6-DMSO showing imine resonance at 8.24 ppm with a residual acetone peak at approx. 2ppm.

Ligand **3** proved to be slightly more problematic to synthesise than either **1** or **2** as it was formed as a yellow viscous oil, which proved difficult to both handle and purify. It was synthesised, like **1** and **2**, in a protic solvent, but where these ligands afforded white solids, no precipitate was forthcoming with **3**. The solvent and volatiles were removed under reduced pressure and the flask dried to a constant weight. As before, the appearance of the imine proton at 8.21 ppm in the ^{1}H NMR spectrum confirmed the formation of the ligand with the IR spectrum confirming its synthesis with the imine C=N stretch at 1645 cm^{-1}. Microanalysis confirmed the constitution of the oil with half a molecule of solvent (methanol) present per molecule of product.

3.3   Reactions of ligands 1, 2 and 3

3.3.1   Overview

Metal complexation reactions were carried out between ligands **1**, **2** and **3** and the metal acetate, chloride and perchlorate derivatives of the copper(II), nickel(II) and zinc(II) ions. These reactions were carried out in solvents such as methanol, ethanol, acetonitrile or pyridine. Each of these reactions gave one of the following possible results: (a) hydrolysis of the ligand and no metal ion complexation with the subsequent diamine, (b) ligand hydrolysis and complexation of the metal ion to the cleaved diamine, or (c) metal complex formation with the Schiff-base ligands. The reactions are summarised in Table 3.1. In the cases of the nickel and copper complexation reactions, vibrant colour changes were observed, changing from the initial light yellow

or colourless solution of the starting ligand to a deep blue or blue/green colour. An immediate change in the colour of the solution resulted in all these cases. In the case of the zinc reactions no colour change was observed but upon complexation a light yellow or colourless solid precipitated from the reaction solution.

Table 3.1 Summary of metal complexation reactions of ligands **1**, **2** and **3**.

Entry No.	Ligand	Metal salt	Solvent	Result
4	1	$CuCl_2 \cdot 2H_2O$	MeOH	Metal-amine complex
5	1	$Cu(ClO_4)_2 \cdot 6H_2O$	EtOH	Metal-amine complex
6	1	$Cu(O_2CCH_3)_2 \cdot H_2O$	EtOH	Ligand hydrolysis
7	1	$NiCl_2 \cdot 6H_2O$	MeOH	Ligand hydrolysis
8	1	$Ni(ClO_4)_2 \cdot 6H_2O$	MeOH	Ligand hydrolysis
9	1	$Ni(O_2CCH_3)_2 \cdot 4H_2O$	EtOH	Metal-amine complex
10	1	$ZnCl_2$	MeOH	Metal complex formation
11	1	$Zn(O_2CCH_3)_2 \cdot 2H_2O$	MeOH	Ligand hydrolysis
12	1	$Cu(O_2CCH_3)_2 \cdot py$	Pyridine	Ligand hydrolysis
13	2	$CuCl_2 \cdot 2H_2O$	MeOH	Metal-amine complex
14	2	$Cu(ClO_4)_2 \cdot 6H_2O$	MeOH	Ligand hydrolysis
15	2	$Cu(O_2CCH_3)_2 \cdot H_2O$	MeOH	Metal-amine complex
16	2	$NiCl_2 \cdot 6H_2O$	MeOH	Ligand hydrolysis
17	2	$Ni(ClO_4)_2 \cdot 6H_2O$	EtOH	Metal-amine complex
18	2	$Ni(O_2CCH_3)_2 \cdot 4H_2O$	EtOH	Metal-amine complex
19	2	$ZnCl_2$	MeOH	Complex decomposed
20	2	$Zn(O_2CCH_3)_2 \cdot 2H_2O$	MeOH	Ligand hydrolysis
21	3	$CuCl_2 \cdot 2H_2O$	MeOH	Metal-amine complex
22	3	$Cu(ClO_4)_2 \cdot 6H_2O$	MeOH	Ligand hydrolysis
23	3	$Cu(O_2CCH_3)_2 \cdot H_2O$	MeOH	Ligand hydrolysis
24	3	$NiCl_2 \cdot 6H_2O$	MeOH	Ligand hydrolysis
25	3	$Ni(ClO_4)_2 \cdot 6H_2O$	EtOH	Ligand hydrolysis
26	3	$Ni(O_2CCH_3)_2 \cdot 4H_2O$	EtOH	Ligand hydrolysis
27	3	$ZnCl_2$	MeOH	Complex decomposed
28	3	$Zn(O_2CCH_3)_2 \cdot 2H_2O$	MeOH	Ligand hydrolysis

3.3.2   Ligand hydrolysis and cleavage

Hydrolysis of the Schiff-base ligands proved highly problematic with cleavage of the imine bond occurring under mild conditions. Although anhydrous solvents were used throughout, the commercially obtained metal salts, as their hydrated forms, supplied

enough water into the system for hydrolysis of the imine bond to occur. The problem was exacerbated by the presence of the metal cations which have Lewis acid properties and can accelerate this bond cleavage. The mechanism for imine formation (acid catalyst and dehydration) and its reversible reaction (aqueous acid) are shown in Scheme 3.4.

In the cases where no metal complexation took place, hydrolysis of the ligand was determined by extraction of the reaction solution with dichloromethane and subsequent evaporation of the extractant to yield a yellow solid or oil which corresponded to the starting material, *m*-hydroxybenzaldehyde. This was identified by the aldehydic proton at 9.93 ppm in the ^{1}H NMR spectrum.
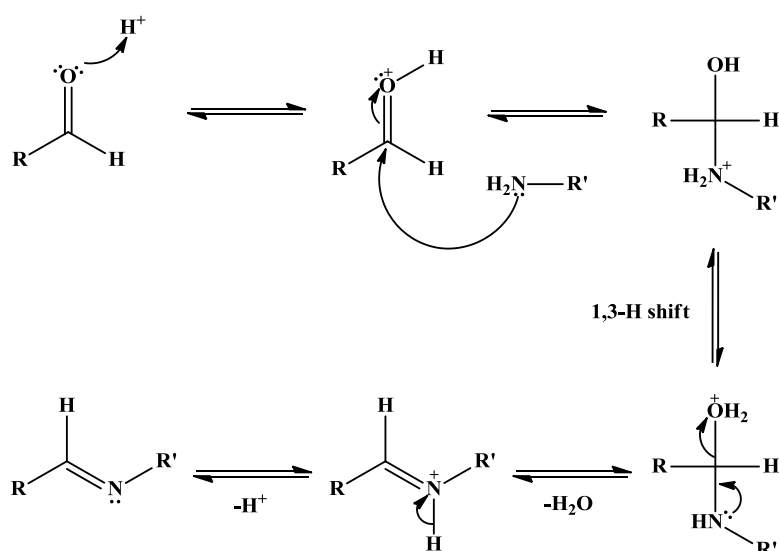
Scheme 3.4 Mechanism of imine formation.

Although imine hydrolysis occurred in the majority of cases for the copper(II) and nickel(II) complexation reactions, the free diamine did not always complex to the metal ion. This was the case for compounds **6**-**8**, **12**, **14**, **16**, **20** and from **22**-**26**.

3.3.3 Copper(II) and nickel(II) amine complexes

Highly coloured solutions were observed in all cases involving the copper(II) and nickel(II) salts, with several reactions furnishing blue or purple crystalline solids upon reduction of the reaction solution after several days. In all cases described in this Section, unless otherwise stated, complexation of the metal ion occurred as a result of

hydrolysis of the imine bond in the Schiff-bases which made the diamine available for reaction.

Reaction of **1** with copper(II) chloride dihydrate in methanol yielded a light blue solid, which was analysed using IR spectroscopy and found to be the copper(II) chloride complex of ethylene diamine (en): [Cu(en)]Cl$_2$: **4**. The spectrum compared well with data previously reported in the literature.[98] A similar case occurred with the complexation of **1** and copper(II) perchlorate hexahydrate in ethanol. The liberated diamine formed a complex with the copper(II) salt to give [Cu(en)](ClO$_4$)$_2$: **5**, as a purple solid. IR spectral data matched those previously published.[98] No complexation was observed when copper(II)acetate monohydrate and **1** were stirred together in ethanol.

The complexation reactions of the nickel(II) salts with ligand **1** were to prove equally fruitless. No complexation occurred when nickel(II) chloride and nickel(II) perchlorate were added to **1** in reactions **7** and **8** respectively. A reaction did occur when nickel(II) acetate was added to **1** giving a light green solid which analysed as the nickel amine complex [Ni(en)](O$_2$CCH$_3$)$_2$: **9**. An IR spectrum of the complex obtained was in good agreement with previously published values.[99]

Complexation reactions of **2** were carried out with the same metal salts used in the complexation reactions with **1**. The copper(II) complexation reactions were carried out in methanol but the issue of ligand hydrolysis and cleavage did not improve, affording the free diamine 1,3-diaminopropane (dap) the opportunity to bind to the metal ions. In the case of the reactions of **2** with copper(II) chloride dihydrate and copper(II) acetate monohydrate, metal amine complexes **13** and **15** were formed respectively, being isolated as a dark green solid for the former and as a blue/purple crystalline solid for the latter. Blue crystals of **15**, grown from acetonitrile proved to be suitable for X-ray crystal structure determination, and their structure will be discussed later in Section 3.3.5. The magnetic susceptibility of **15** was determined and found to be 1.88 B.M. and is in good agreement with the spin only formula calculation for a copper(II) ion of 1.73 B.M. Zeleňák and co-workers have previously prepared [Cu(dap)]Cl$_2$, **13**, and the prepared solid matched the IR data published.[100] No reaction was observed in the attempted preparation of the coordination complex of **2** with copper(II) perchlorate hexahydrate in methanol.

The reactions of the nickel(II) salts with **2** produced a similar story, with hydrolysis of the ligand and subsequent complexation of the freed amine occurring in cases of nickel(II) perchlorate and nickel(II) acetate, and no reaction was observed when **2** was mixed with a methanolic solution of nickel(II) chloride hexahydrate. The nickel(II) amine complexes formed were identified as **17** and **18** by IR spectral data. The IR data compares favourably with those previously published: complex **17** was previously prepared by Magee *et al.*[101] while **18** has been reported by Mitra *et al.*[99]

After the disappointing results of the complexation reactions of **2** with the various copper(II) and nickel(II) salts, save for the crystal structure obtained of **15**, the approach was taken to prepare a 3-hydroxy Schiff-base analogue of **1** and **2** with three nitrogen donors instead of the previous attempt of using only two, thereby providing a potential tridentate bridge between the phenol rings. From this new plan, ligand **3** was prepared and attempts made to prepare its copper(II) and nickel(II) derivatives, as previously described for ligands **1** and **2**. Unfortunately, it seems that the extra nitrogen present only decreased the binding ability of the ligand as in the majority of cases the starting materials were recovered. In the rare case where reaction with a metal salt actually took place, hydrolysis of the imine bond occurred to give *m*-hydroxybenzaldehyde and 3,3'-diamino-*N*-methyldipropylamine, (dmda) mirroring the previous problems of ligand stability observed with **1** and **2**.

The only redeeming factor of the copper(II) and nickel(II) reactions carried out with **3** was the complex prepared from the reaction of **3** with copper(II) chloride dihydrate. The complexation was done in methanol and when no precipitate was forthcoming the solvent was allowed to evaporate, after which acetonitrile was added to the residue resulting in an immediate precipitation of a brown solid that analysed as *m*-hydroxybenzaldehyde. The filtrate (a blue green solution) was allowed to reduce over several days. This resulted in the formation of dark blue/green crystals which were suitable for X-ray crystallographic analysis. The X-ray structure of **21**, a copper-amine complex, will be discussed in due course. IR and microanalytical data corroborated the X-ray structural results. A peak at 2256 cm^{-1} was identified as the CN nitrile stretch of the acetonitrile trapped in the matrix. The magnetic susceptibility of the solid was determined to be 1.67 B.M. and was in good agreement with the calculated theoretical value of 1.73 B.M.

The failure of the copper and nickel complexation reactions led to a different approach. Since all the metal salts used thus far had been hydrated derivatives, and water was required for hydrolysis of the ligands, it was decided to prepare a metal salt that did not have any water molecules present. To this end the pyridine derivative of copper(II) acetate monohydrate was prepared. Testing the hypothesis, this pyridine copper derivative was stirred with **1** in anhydrous pyridine. No identifiable product was forthcoming on reduction of the solvent over several days.

3.3.4   Zinc(II) reactions of 1, 2 and 3

The results previously mentioned in Section 3.3.3 led to the use of various zinc salts which could be obtained commercially in an anhydrous state. The reactions of ligands **1**, **2** and **3** with either zinc(II) chloride or zinc(II) acetate dihydrate generally resulted in the formation of a complex with the appropriate ligand. In only one case did the zinc ion fail to bind. This occurred with zinc(II) acetate in the presence of **3**, however most of the complexes were unstable in either air or water and resulted in decomposition of the complex. This would suggest that the water in the reaction flask coordinating to the metal complex is responsible for the break-up of the ligands rather than the water present in the solvent. The one exception to this observation was the reaction of **1** with zinc(II) chloride which formed a complex which was sufficiently air and water stable for analysis to be carried out. The complex formed had a metal-to-ligand ratio of 1:1. The ^{1}H NMR spectrum of **10** showed that the phenolic proton was still present in the complex but had altered from a broad signal at 9.03 ppm in the ^{1}H NMR spectrum of **1** to a sharp singlet at 9.55 ppm. This would suggest that the zinc was binding to the ligand through the phenolic OH rather than through the imine nitrogen. The ^{1}H NMR spectrum of the product also ruled out that the precipitate formed was not a mixture of the starting materials. The IR spectrum of **10** supported this binding mode as the imine C=N stretch at 1641 cm^{-1} had not shifted significantly from its original value of 1647 cm^{-1} in the IR spectrum of **1**. The product **10**, a 1:1 complex has two plausible structures, as shown in Figure 3.2.

It could exist as a dimer, with two ligands face to face and two zinc(II) chloride molecules bridging the ligands through the phenolic OHs. The other possible structure is a polymeric orientation, where the ligands are linked together by coordinating to

zinc(II) chloride *via* the phenolic oxygen. This creates a 'chain-like' polymeric structure and due to the poor solubility of **10** was therefore proposed as the most likely structure.
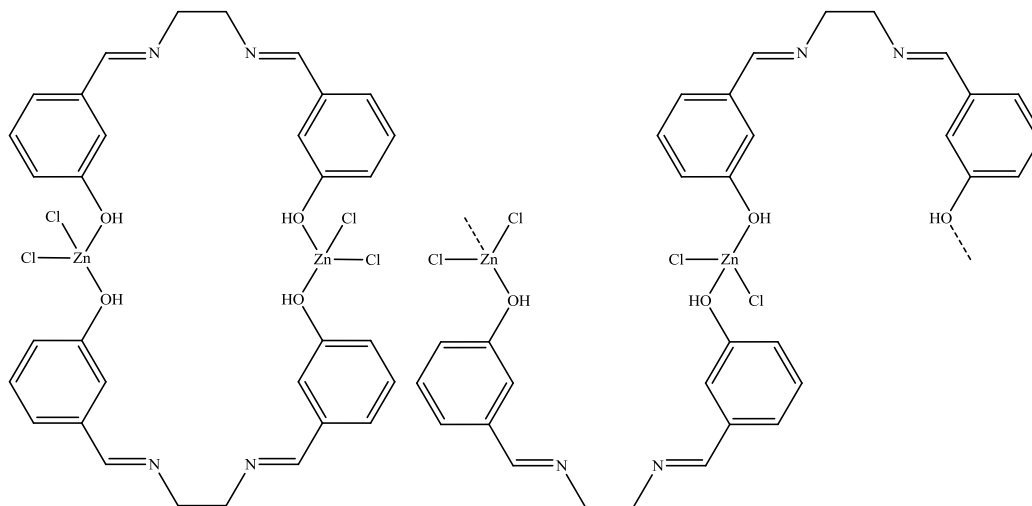
Figure 3.2: Possible structures for **10**.

3.3.5   X-Ray crystal structure of 15

Ligand **2** was reacted with copper(II) acetate monohydrate in methanol which resulted in the hydrolysis of the imine bond to give 1,3-diaminopropane (dap) and *m*-hydroxybenzaldehyde. The result of this hydrolysis was that the free diamine complexed with the copper(II) salt to give **15**, a blue green solid. Crystals suitable for X-ray crystallographic analysis were grown by slow evaporation of an acetonitrile solution of the product. The X-ray structure revealed that the product consisted of two metal complexes, one of which was a monomer and the other a dimeric species, along with two molecules of water trapped in the lattice. There is extensive hydrogen bonding in the lattice.

The monomeric unit, as shown in Figure 3.3, contains a five-coordinate copper(II) centre: Cu(2), with the diamine binding in a bidentate fashion, one water molecule and two monodentate acetate counterions occupying the five sites. The geometry of five-coordinate compounds can be described by the Addison parameter τ, which is an index of distortion from the square pyramidal to trigonal bypyramidal geometry. The value τ can be calculated from the following: $\tau = (\beta - \alpha)/60$, where β and α are the two largest coordination angles, $\tau = 0$ for square pyramidal and $\tau = 1$ for trigonal

bipyramidal.[111] The copper(II) centre occupies a slightly distorted square pyramidal orientation denoted by a value of $\tau = 0.05$.
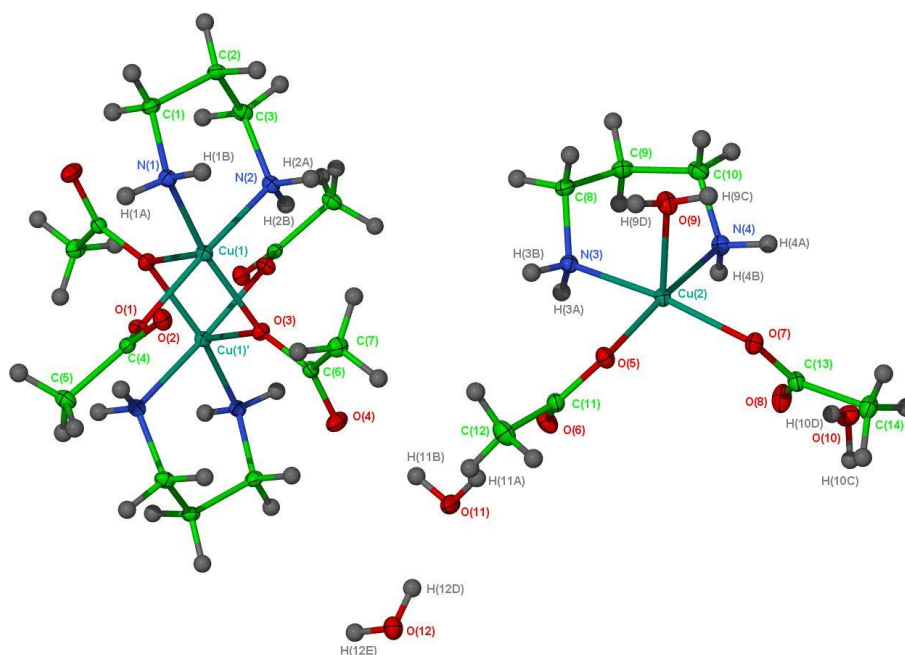
Figure 3.3: X-ray crystal structure of **15**.

The synthesis of the complex $[Cu(dap)](O_2CCH_3)_2$ has been reported previously by Zeleňák *et al.*[100] but their four-coordinate copper(II) complex was highly sensitive to humidity and necessitated a desiccator for storage. Attempts by the group to grow crystals of the acetate complex from diffusion of carbon tetrachloride into a methanolic solution of the acetate complex resulted in the formation of $[Cu(dap)]Cl_2$, with the chloride counterions being supplied by the carbon tetrachloride.

The other copper(II) complex in the crystal lattice was a dimer. As depicted in Figure 3.3, each copper occupies a slightly distorted square pyramidal geometry (denoted by $\tau = 0.16$) by binding to the bidentate 1,3-diamino propane, one monodentate acetate and two bridging monodentate acetate groups. The acetate oxygen bridging the two copper(II) ions results in bond lengths for the Cu(1)-O(3) and O(3)-Cu(1)' moieties of 2.0153(9) and 2.2873(9) Å respectively. Acetate-bridged copper(II) dimer units are well known and the bond lengths mentioned above are within the range reported (1.96-2.37 Å) for this acetate-copper(II) binding mode.[112] Elemental analysis of a sample dried in the oven revealed the loss of three molecules of water: the two lattice water molecules along with the copper-bound water.

3.3.6   X-ray crystal structure of 21

Ligand **3** was reacted with copper(II) chloride dihydrate in methanol. This formed a blue solution which was allowed to reduce over several days. The solution was replenished with acetonitrile and allowed to stand. Small blue/green crystals appeared in the reaction vessel within two hours, formed as a result of the hydrolysis of the ligand to give *m*-hydroxybenzaldehyde and dmda. The blue crystals were determined to be $[[Cu(dmda)(\mu\text{-}Cl)]Cl_2]\cdot[CuCl_2]\cdot2[Cu(dmda)]Cl_2\cdot2H_2O\cdot CH_3CN$, **21**, with its formation resulting from hydrolysis of the ligand and binding of the free triamine to the copper(II) chloride.
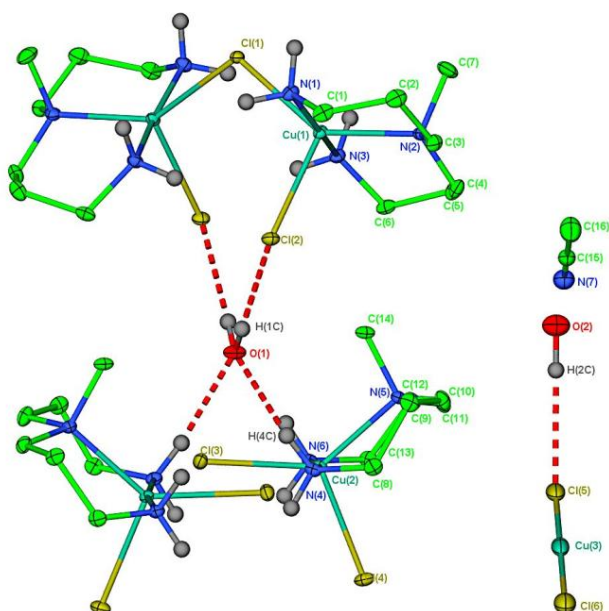
Figure 3.4: X-ray crystal structure of **21** showing the asymmetric unit.

Figure 3.4 illustrates that the crystal lattice consists of two $Cu(dmda)Cl_2$ molecules, one chloro-bridged $[Cu(dmda)(\mu\text{-}Cl)Cl_2]^+$ cation, one unusual $CuCl_2$ species, and three solvent molecules, two of which are water and one of which is acetonitrile. The water molecule was assigned by the clear identification of the water hydrogens in the case of O(1). In the case of O(2), only one hydrogen was identified, as seen in Figure 3.4, suggesting the presence of a hydroxide anion required to balance the cationic chloro-bridged species. The other option for an anionic counterion is the $CuCl_2$ unit which could possess an anionic charge whilst leaving the second solvent species O(2) neutral. Efforts to determine the anionic species will be discussed at the end of this Section.

The monochloro-bridged structure containing Cu(1), shown in Figure 3.4, is an unusual arrangement as examples of the dichloro-bridged species are much more abundant in the literature.[113] The mono-chloro bridged orientation is rare by comparison, with only a few being reported.[114] The coordination geometry about the Cu(1) centre contains the tridentate 3,3'-diamino-N-methyldipropylamine (dmda), two chlorine atoms, one bridged, one unbridged, and lies between trigonal bipyramidal and square pyramidal, as denoted by the Attison parameter $\tau = 0.45$. The Cu(1)-Cl(1) bond length is 2.482(4) Å and is comparable to monochloro-bridged Cu-Cl-Cu species previously reported.[114] The Cu(1)-Cl(1) bond length is also significantly shorter than the typical Cu(II)-Cl bond length for dichloro-bridged species, which are generally in the region of 2.7-3.0 Å.[113] The angle of the Cu(1)-Cl(1)-Cu(1)' moiety is 111.11(2)^{o} and is significantly narrower than bond angle range of 142-149° described previously.[114] This may be a result of the non-bridging chlorides participating in hydrogen bonding with the adjoining water O(1)H(1C)···Cl(2) with the chlorine atoms functioning as molecular tweezers.

The second complex is a Cu(dmda)Cl$_2$ species with no bridging chlorines. The five-coordinate Cu(2) centre lies between a trigonal bipyramidal and square pyramidal geometry, as denoted by its Attison parameter, $\tau = 0.57$. This complex has been prepared previously and characterised by X-ray crystallography.[115] An important point to note is that, although very similar to **21**, the method by McCasland *et al.*[115] resulted in the copper(II) ion occupying a slightly distorted square pyramidal geometry ($\tau = 0.09$) with a MeN-Cu-Cl angle of 158.23° whereas the coordination geometry in our case about the Cu(2) atom suggests that it lies approximately midway between square pyramidal and trigonal bipyramidal with a significantly narrower MeN(5)-Cu(2)-Cl(3) angle of 135.79(4)°. This may be as a result of hydrogen bonding interactions between the water molecule O(1) and the terminal amine groups N(4)H(4C)···O(1). These bonding interactions bring two of the copper complexes in close proximity to each other resulting in steric hindrance which may force the copper(II) centre out of the square pyramidal geometry into the hybrid geometry shown.

In the preparation of the Cu(dmda)Cl$_2$ species, McCasland *et al.*[115] did not show any evidence of a chloro-bridged dimer. This would suggest that the *m*-hydroxybenzaldehyde from the hydrolysed ligand has some role in the formation of

the chloro-bridged complex. This theory is reinforced when attempts to prepare **21** from 3,3'-diamino-N-methyldipropylamine and copper(II) chloride in methanol and acetonitrile resulted in the formation of a blue solution from which a blue crystalline solid precipitated and was identified to be the Cu(dmda)Cl$_2$ species, with no evidence of the chloro-bridged species formed.

Analysis of the crystal packing of **21**, illustrated in Figure 3.4, shows that the water molecule O(1) has a dual role. Firstly, and as mentioned previously, the hydrogen atoms are involved in hydrogen bonding to a pair of chlorine atoms, Cl(2) and Cl(2)', in the chloro-bridged cation. The lone pairs of the oxygen O(1) form a bridge between the two neutral Cu(2) copper complexes by way of hydrogen bonding to the amine hydrogen atoms (H(4C)). The second water molecule O(2), also participates in hydrogen bonding with the Cl(5) of the linear copper chloride species Cl(5)-Cu(3)-Cl(6), whilst the lone pair of the oxygen atom O(2) is involved in an interaction with the nitrogen atom of the adjoining acetonitrile molecule.
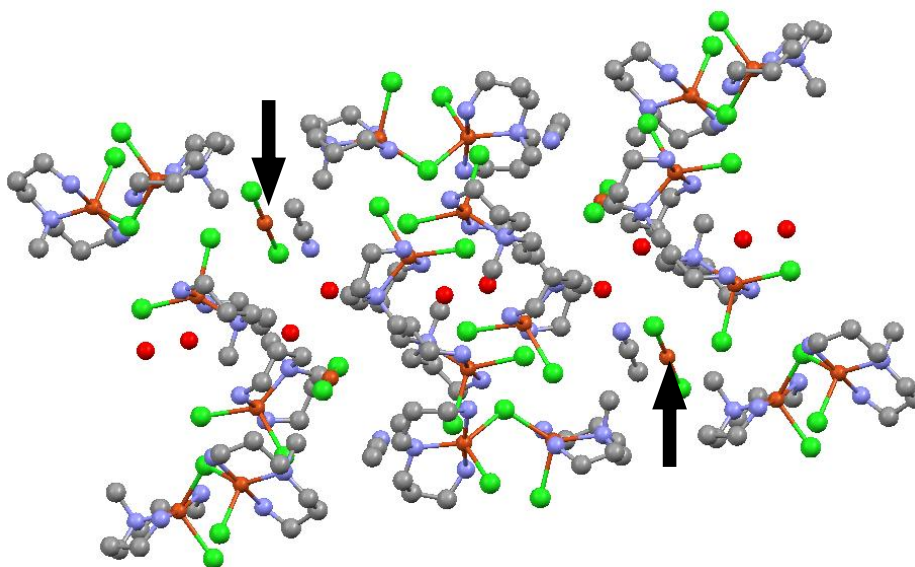
Figure 3.5: Partial packing diagram of **21** with black arrows showing location of Cu(3).

The linear copper chloride entity (highlighted in Figure 3.5 with a black arrow) proved to be difficult to acertain whether it was neutral or possessed a negative charge. The two copper Cu(3)-Cl(5) and Cu(3)-Cl(6) bond lengths are at 2.111(12) and 2.118(12) Å respectively and the Cl(5)-Cu(3)-Cl(6) bond angle of 178.84(4)° suggested an almost linear metal coordination geometry. There are quite a few examples of the [Cu(I)Cl$_2$]$^-$ in the literature,[116] but only one X-ray structure of a

two-coordinate Cu(II)Cl$_2$ species, determined by Chen and co-workers.[117] In their case weak interactions between the copper(II) atom and the donor oxygen atoms of the formadine derivative (interatomic distance of 3.157 Å) suggest that, in this case, the copper occupies a highly distorted three-coordinate geometry. In regard to the Cu(3) in **21**, by examining the crystal packing in Figure 3.5 it was determined there are no interactions of note (>4 Å) between it and any other atom, aside from the aforementioned chlorine atoms. A space fill view of the packing diagram reveals that there is no available space around the Cu(3) centre for interaction with another atom and that it is quite isolated. Attempts to determine the magnetic susceptibility of the complex using the Evans method would almost certainly expand the coordination sphere of the Cu(3) centre.

Microanalysis of an oven-dried sample of **21** revealed the loss of a molecule of acetonitrile in the drying process.

3.4 Synthesis of the calix[4]arene azines

3.4.1 Synthesis of calix[4]arene precursors

The calix[4]arene (tetramer), **27**, was synthesised using a well known procedure by Gutsche *et al.*[102] by first preparing the precursor calix[8]arene, **26**, (octamer) *via* a base catalysed condensation of paraformaldehyde and *p-tert*-butylphenol, outlined in Scheme 3.5. Analysis of the octamer by ^{1}H NMR spectroscopy showed that the macrocycle is highly symmetrical, with a single uncoupled peak representing the *tert*-butyl groups at 1.28 ppm. The aromatic protons, by virtue of the positioning of the *tert*-butyl groups, are equivalent and so resonate as singlets at 7.17 ppm. The bridging methylene groups resonate as two doublets at 3.48 and 4.39 ppm due to their diastereotopic nature, the result one proton pointing into the macrocyclic cavity, thus giving rise to two different environments for the geminal protons. The signal for the phenolic protons resonates at 9.63 ppm, as a result of the close proximity to each other, its low field position explained by extensive hydrogen bonding. Conversion of the octamer, **26** to the calix[4]arene starting material, **27**, shown in Scheme 3.5, was achieved by heating to reflux in diphenyl ether in the presence of a catalytic amount of base. The product was isolated as a white glistening solid. Symmetry was conserved in

the tetramer with the ^{1}H NMR spectrum, shown in Figure 3.6, exhibiting singlets for the *tert*-butyl groups, the aromatic protons and the phenolic protons at 1.21, 7.04 and 10.34 ppm respectively, with the phenolic proton resonance at a lower field position as a result of the OH groups' closer proximity to each other because of the reduced size of the macrocycle. The methylene protons, as in the case of the octamer, retain their diastereotopic nature, resonating as two doublets at 3.50 and 4.26 ppm.
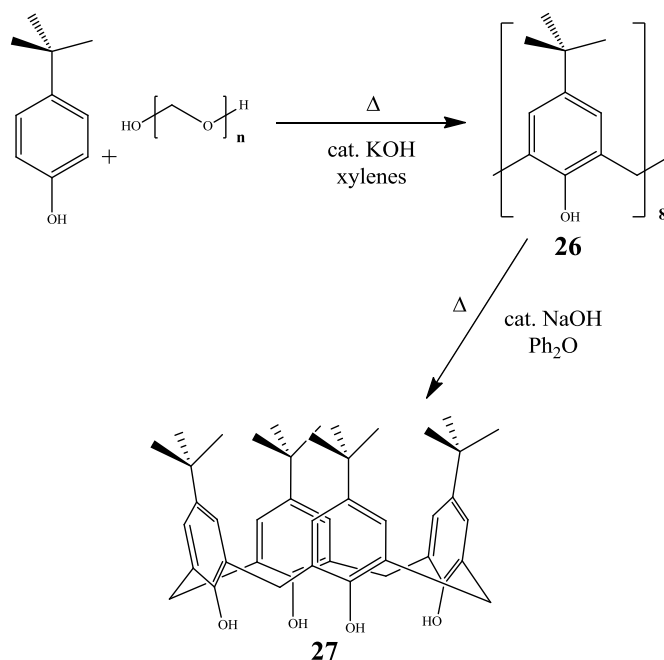
Scheme 3.5: Synthesis of calix[8]arene, **26**, and calix[4]arene, **27** showing conditions used.
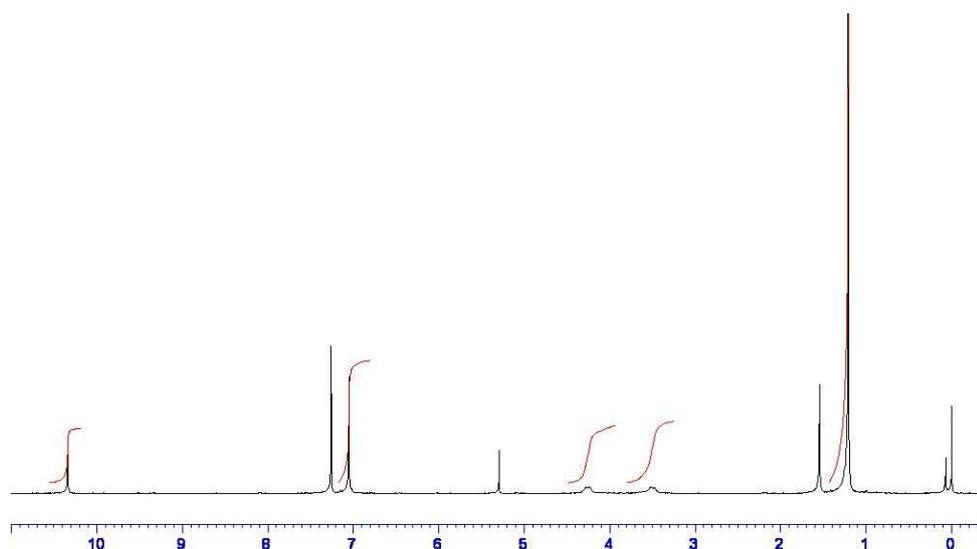
Figure 3.6: ^{1}H NMR spectrum of calix[4]arene **27** run in CDCl$_3$ with x-axis in ppm. Peak at 5.3 ppm is residual DCM from crystallisation.

Functionalisation of the tetramer at the phenolic oxygens was readily achieved using potassium carbonate as a base and the appropriate electrophile. In the synthesis of the bromoethoxy functionalised derivative, **28**, outlined in Scheme 3.6, **27** was heated to reflux in acetonitrile with the aforementioned base and a tenfold excess of 1,2-dibromoethane, for two days under nitrogen. This furnished the 1,3-distal substituted calixarene with its synthesis confirmed by analysis of its ^{1}H NMR spectrum.
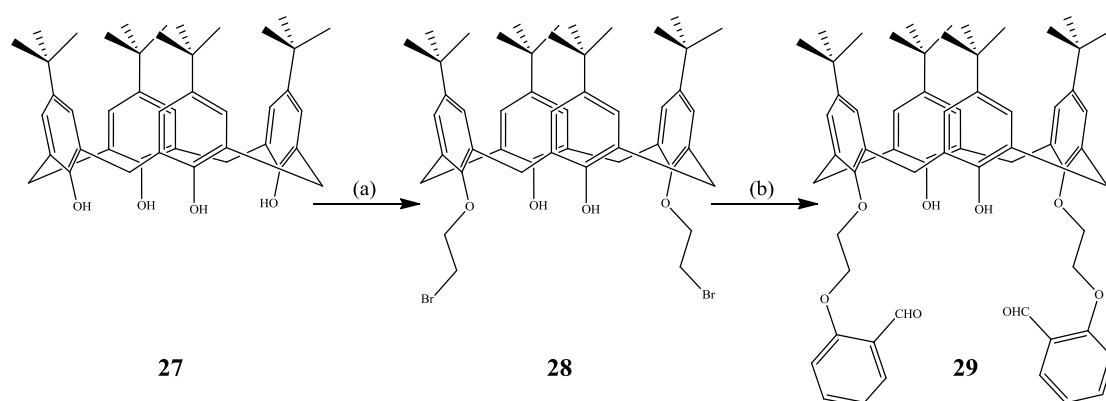
Scheme 3.6: Synthesis of calix[4]arene derivatives **28** and **29** from **27** using conditions: **(a)** 1,2-dibromoethane, K$_2$CO$_3$, CH$_3$CN, N$_2$, Δ; **(b)** salicylaldehyde, K$_2$CO$_3$, CH$_3$CN, N$_2$, Δ.

A plane of symmetry is conserved in the molecule with two singlets representing the *tert*-butyl groups at 0.95 and 1.29 ppm, one representing the unsubstituted phenol and the other representing the *tert*-butyl group attached to the phenolic ether moiety. The same applies for the aromatic protons, with singlets representing them at 6.78 and 7.06 ppm. A point of note is the large upfield shift of the phenolic hydrogen to 6.92 ppm. This is as a result of the substitution at two of the phenol groups and results in a significant reduction in the degree of hydrogen bonding in which the remaining phenolic protons can participate. From the data analysed in this project, all distal disubstituted calix[4]arene derivatives exhibited this characteristic. The ethyl fragment of the molecule is represented by the presence of two triplets at 3.84 and 4.31 ppm in the ^{1}H NMR spectrum with each of the signals situated downfield, due to their proximity to electronegative atoms, in this case O and Br. The bridging methylene protons of **28** appear as a set of doublets due to their diastereotopic nature which was explained previously. They resonate at 3.33 and 4.30 ppm and have a coupling constant of J = 13.0 Hz, a value within the range expected for coupled geminal protons.[87] The diastereotopic nature of these methylene protons is exhibited in all of

the functionalised calix[4]arene derivatives described in this thesis, with their chemical shift and coupling constant values broadly similar to those previously mentioned.

Conversion of **28** to the *o*-benzaldehyde derivative **29** was achieved by heating to reflux a mixture of **28**, potassium carbonate and salicylaldehyde in acetonitrile for 24 hours, shown in Scheme 3.6. After work up, the dialdehyde calix[4]arene was isolated as a white solid. Analysis of its ^{1}H NMR spectrum (shown in Figure 3.7) confirmed its formation, as its spectral data had previously been published.[58] The addition of the new aromatic ring resulted in three new peaks in the ^{1}H NMR spectrum, with resonances at 7.00, 7.50 and 7.83 ppm and collectively integrating for eight hydrogens. A characteristic signal of **29** is the aldehydic proton signal which resonates at 10.50 ppm. The presence of an aldehydic carbonyl is also observed in the ^{13}C NMR spectrum of **29**, resonating at 190.2 ppm and also in the IR spectrum, where the aldehydic CO stretch is observed as a strong absorption band at 1682 cm^{-1}.
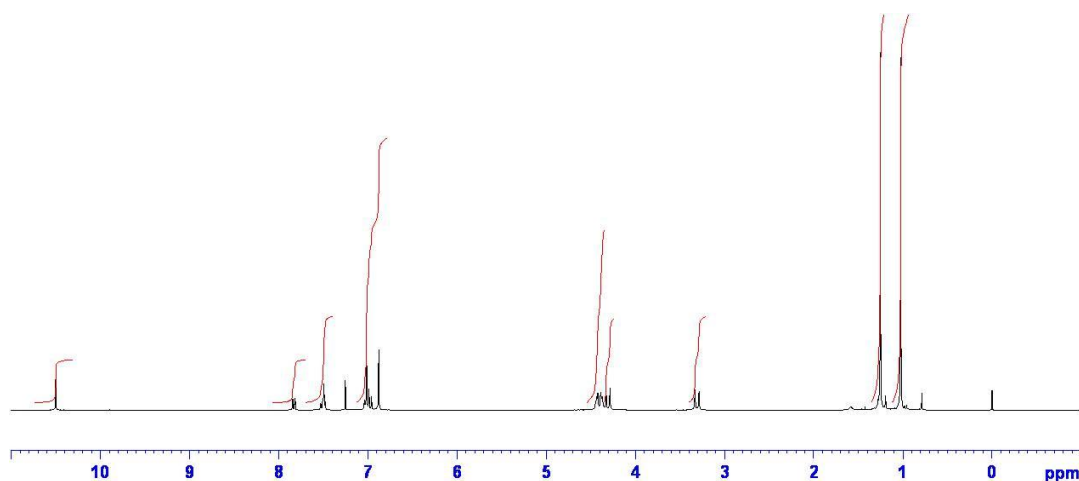
Figure 3.7: ^{1}H NMR spectrum of **29** in CDCl$_3$ showing characteristic aldehydic proton signal at 10.50 ppm along with additional aromatic proton resonances.

3.4.2   Syntheses and characterisation of calix[4]arene hydrazones and azines

The calix[4]arene aldehyde derivative **29** was used as the main building block in the preparation of the calix[4]arene azine derivatives. The synthesis of these derivatives is shown in Scheme 3.7, along with conditions required.
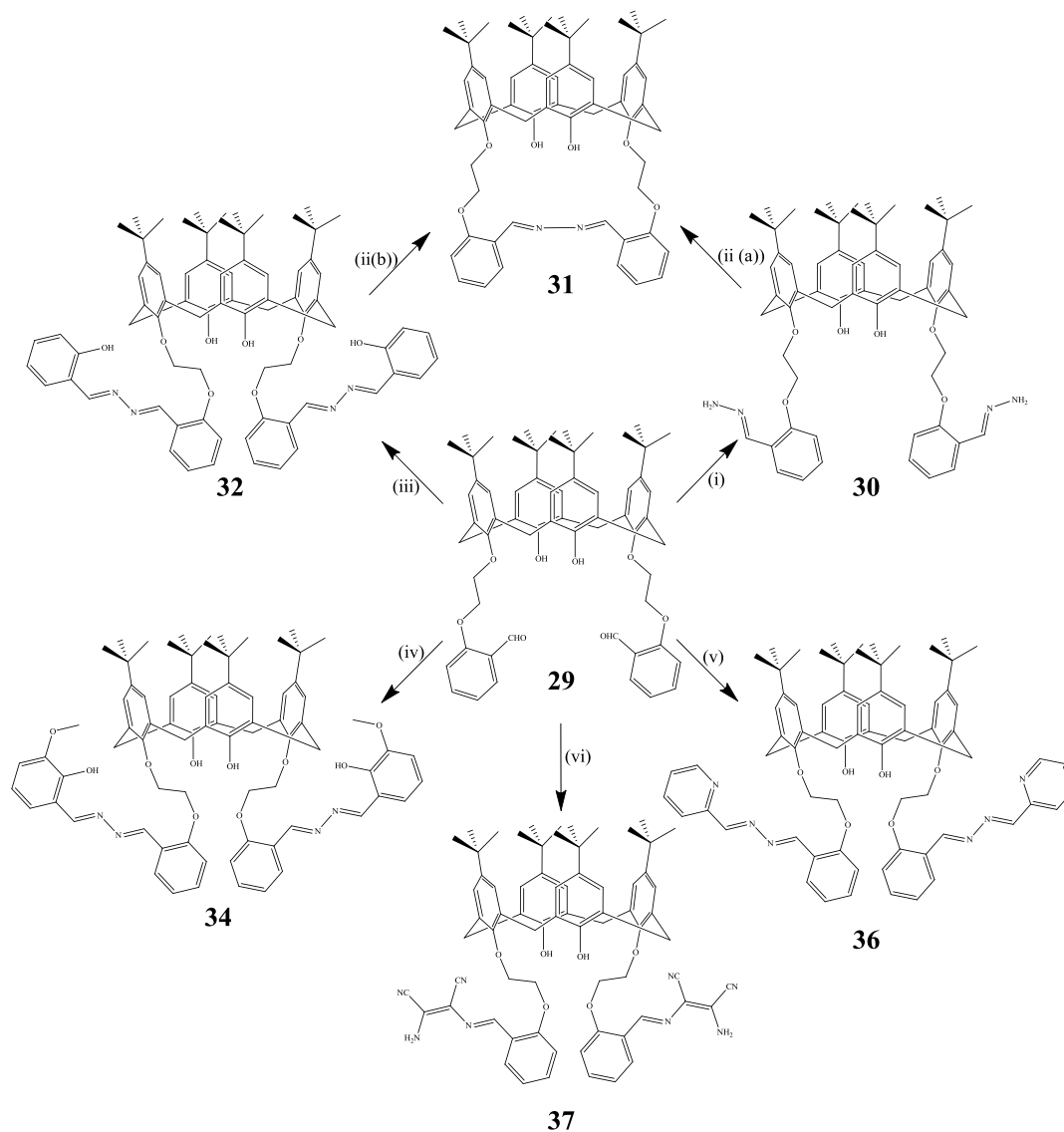
Reaction conditions:
(i): NH$_2$NH$_2$, CH$_3$CN.
(ii): (a) **30**, EtOH, Δ; (b) **32**, EtOH, Δ.
(iii): salicylaldehyde hydrazone, AcOH, EtOH.
(iv): 3-methoxysalicylaldehyde hydrazone (**33**), AcOH, EtOH, Δ.
(v): 2-pyridinecarboxaldehyde hydrazone (**35**), CH$_3$CN, Δ.
(vi): diaminomaleonitrile, AcOH, EtOH.

Scheme 3.7: Synthesis of calix[4]arenes **30-32, 34, 36** and **37** and conditions used.

The first imine formation reaction carried out was the dropwise addition of **29** to an excess of hydrazine hydrate in acetonitrile. This produced a light yellow solution

which was concentrated under reduced pressure. Ethanol was added to the concentrate to precipitate a white solid, a dihydrazone functionalised calix[4]arene **30**. Confirmation that the hydrazone was formed was by spectroscopic and analytical techniques. Microanalysis confirmed the constitution of the sample. The ^{1}H NMR spectrum of **30**, when compared to **29** reveals that the signal for the aldehydic proton is not present. It is replaced by a singlet resonating at 8.21 ppm which represents the signal for the imine proton. The appearance of a broad singlet at 4.95 ppm representing the terminal NH$_2$ protons of the hydrazone confirms that calix[4]arene **30** was formed. Confirmation that the aldehyde had reacted is provided in the ^{13}C NMR spectrum where an aldehydic carbonyl resonance, previously observed at 190.2 ppm, is not present.
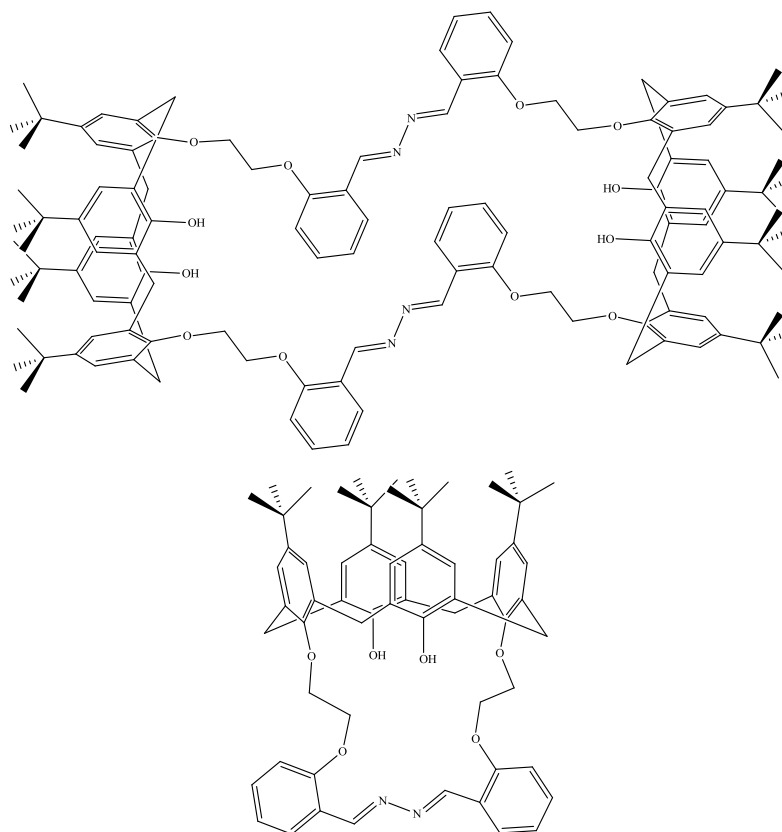
Figure 3.8: Two proposed structures for **31**.

An interesting point of note was the change in the ^{1}H NMR spectrum of **30** when it was heated to reflux in ethanol. The white solid dissolved and after an hour of heating a yellow precipitate formed. Analysis of this light yellow solid, **31**, revealed that the imine proton resonance, present in the starting molecule at 8.21 ppm, shifted downfield to 9.02 ppm and the signal for the terminal amine protons was not present.

113

The molecule still exhibited a plane of symmetry as indicated by the the number of peaks in the ^{1}H NMR and ^{13}C NMR spectrum. Condensing the information, two possible structures were proposed, as shown in Figure 3.8. In the end, the structure of **31** was confirmed by X-ray crystallography to be the intramolecular cyclisation product, the results of which will be discussed in Section 3.4.3.

Another amine derivative that was reacted with **29** was the commercially available salicylaldehyde hydrazone. An ethanolic solution of the hydrazone was stirred with the calix[4]arene aldehyde **29** with a catalytic amount of acetic acid. From the yellow solution a light yellow solid precipitated, which analysed as the calix[4]arene azine derivative, **32**, shown in Figure 3.9. Microanalysis confirmed the solid to be the hemi-hydrated species. The aldehyde signal, present in the ^{1}H NMR spectrum of **29** at 10.50 ppm, was no longer present. The ^{1}H NMR spectrum of **32**, shown in Figure 3.10, contains peaks representing the additional aromatic protons and also two singlet resonances for the two imine hydrogens at 8.64 and 9.12 ppm. The additional phenolic proton on the terminal aromatic ring is visible as a sharp singlet at 11.71 ppm. The low field chemical shift of this signal results from intramolecular hydrogen bonding with the annular imine nitrogen. Characterisation of the ligand was extended to the use of X-ray crystallography, the results of which will be discussed in due course.
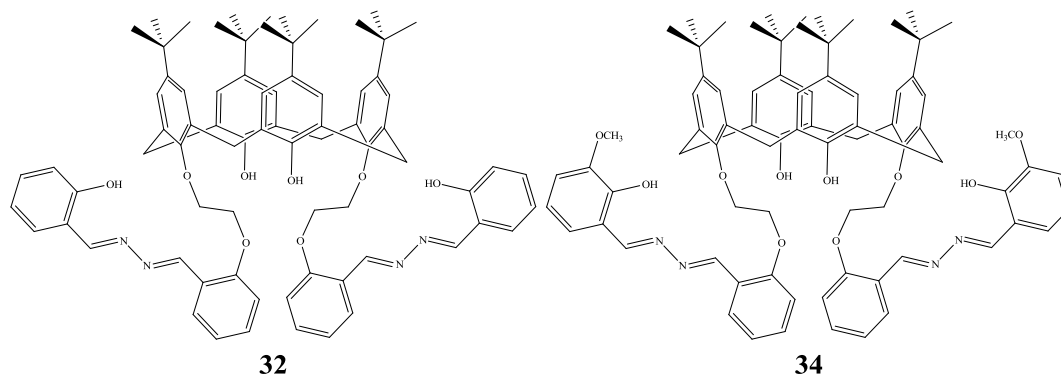
Figure 3.9: Structures of calix[4]arene azine derivatives **32** and **34**.

The range of calix[4]arene azine compounds prepared was extended through the preparation of various non-commercially available hydrazones. One of these hydrazones was *o*-vanillin hydrazone, **33**. This compound was prepared using a variation of a method in the literature to yield a yellow oil which crystallised upon

standing to give a yellow solid.[104] Formation of the hydrazone moiety was confirmed by ^{1}H NMR spectroscopy. A singlet at 7.86 ppm represented the imine proton, and a broad peak at 5.46 ppm, integrating for two hydrogens and exchanging after a D_2O shake revealed the presence of the hydrazone NH_2 protons.
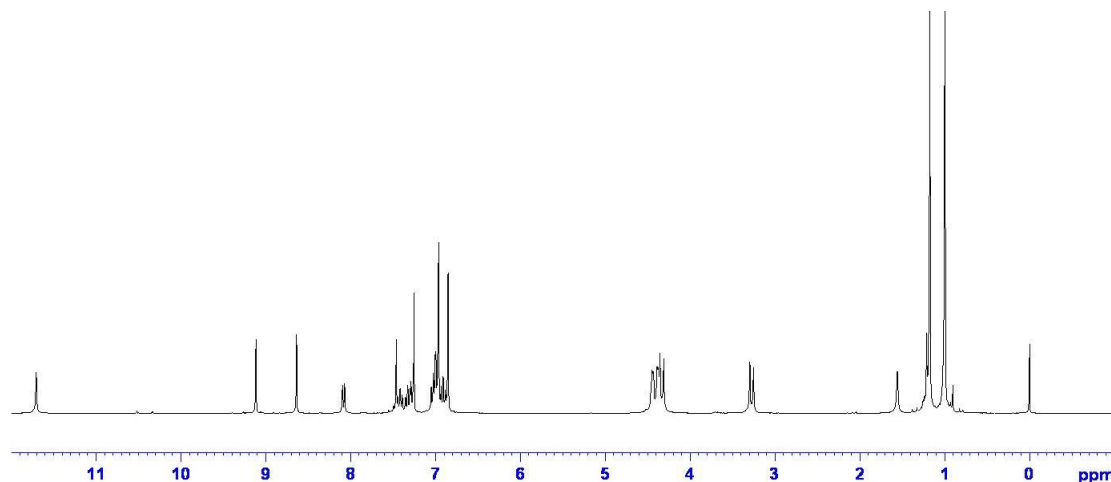
Figure 3.10: ^{1}H NMR spectrum of **32** in CDCl₃ showing terminal phenolic proton signal at 11.71 ppm. Note that the aldehydic proton signal at 10.50 is no longer present and has been replaced by two singlets representing the imine protons at 8.64 and 9.12 ppm.

Hydrazone **33** was then reacted in excess with the calix[4]arene aldehyde scaffold **29** under reflux conditions in ethanol for one hour. On cooling a yellow precipitate formed which was isolated to give the *o*-vanillin azine calix[4]arene derivative, **34**, (whose structure is shown in Figure 3.9) which analysed as the dihydrate. As previously mentioned for derivatives **30**-**32**, formation of the hydrazone was monitored by the aldehydic peak's replacement with additional imine proton resonances. For **34**, these imine protons resonated at 8.71 and 9.03 ppm. The presence of the methyl proton signal of the aryl-methoxy ether which integrates for six hydrogens and resonates at 3.94 ppm, is a distinguishing feature when compared to previously mentioned calix[4]arene azine derivatives. The *o*-vanillin phenolic proton's signal was also visible, in a similar case to **32**, it being hydrogen bound to the imine nitrogen and consequently occupying a low field position at 11.57 ppm.

Previous calix[4]arene azine derivatives mentioned relied on the use of oxygen donors on the terminal azine aromatic ring to provide ligating properties for metal binding. It was also decided to employ the use of nitrogen donors on the aforementioned annulus to provide these binding characteristics. One approach was through the synthesis of pyridyl-azine calix[4]arenes. These were prepared by first synthesising the 2-pyridine

hydrazone precursor **35**, using a modified literature preparation.[105] 2-Pyridine carboxaldehyde was reacted with hydrazine hydrate in ethanol and subsequent removal of the volatiles yielded a yellow/brown oil. Characteristic peaks in the ^{1}H NMR spectrum, such as the protons of the newly formed imine and the hydrazone NH_2 were identified, resonating at 7.83 and 5.83 ppm respectively and revealed the oil to be of sufficient purity to be used in the synthesis of the 2-pyridine azine calix[4]arene derivative, **36** as seen in Figure 3.11.
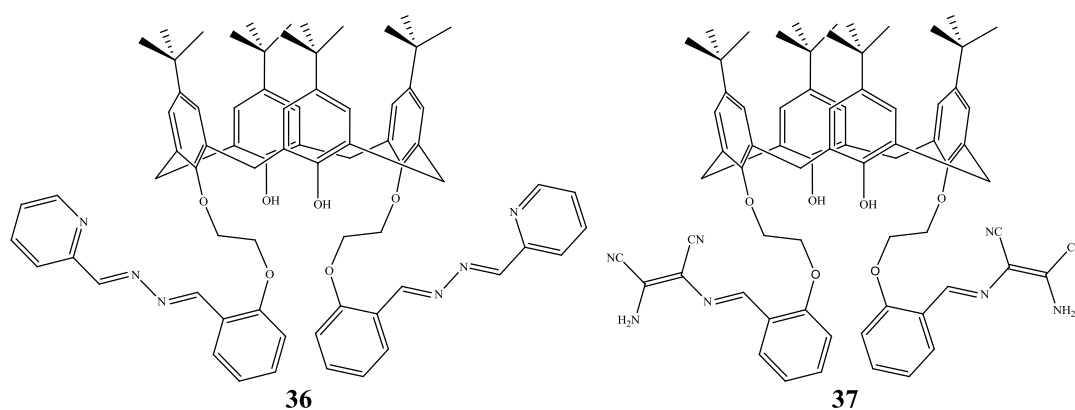
Figure 3.11: Structures of calix[4]arene azine derivatives **36** and **37**.

Using the prepared hydrazone **35**, 2-pyridine azine calix[4]arene derivative **36** was synthesised by stirring the aldehyde **29** in an acetonitrile solution of an excess amount of **35**. This generated a yellow precipitate which analysed as the 2-pyridine calix[4]arene azine **36**. Spectroscopic analysis followed a broadly similar approach mentioned previously, with the appearance of imine proton resonances at 8.66 and 9.24 ppm considered indicative of ligand formation. The ^{1}H NMR spectrum also exhibited a series of aromatic doublets and triplets, making identification of the presence of the pyridyl groups a rudimentary task.

A final calix[4]arene Schiff-base was prepared using diaminomaleonitrile. Using the same calix[4]arene aldehyde precursor as before, **29**, a yellow precipitate was formed from its reaction with diaminomaleonitrile and a catalytic amount of acid in ethanol. Analysis of the oven dried product was carried out and was found to contain 1.5 equivalents of acetic acid. This compound, **37**, shown in Figure 3.11, was unique in that it was the only derivative insoluble in CDCl$_3$ and so a ^{1}H NMR spectrum was obtained by running the sample in *d$_6$*-DMSO. The characteristic peak in the formation of **37** was the new imine proton peak at 8.76 ppm. The signal of the terminal amine

protons was also visible, resonating at 7.74 ppm. Its low field position resulted from a combination of the close proximity of the amine protons to the electron withdrawing nitrile groups and also from being situated on the periphery of the double bond's induced magnetic field. The IR spectrum also confirmed the presence of the nitrile groups, with two bands present at 2232 and 2205 cm^{-1}. The structure of **37** was ultimately defined by X-ray crystallographic analysis, the crystals for which were grown by the method of slow evaporation from a solution of ethyl acetate. The data obtained will be discussed in Section 3.4.6.

3.4.3   X-ray crystal structure of 31

Crystals of calix[4]arene azine **31** were grown by the method of slow evaporation from a dimethylformamide (DMF) solution. This yielded a crop of yellow block crystals which were subjected to X-ray crystallographic analysis. The structure determined is shown in Figure 3.12. The calix[4]arene is in a cone conformation, corroborating the NMR data previously obtained. The cone is stabilised by two intramolecular hydrogen bonds between the hydroxyl groups and the substituted oxygens: O(3)H(3)···O(1) and O(6)H(6)···O(4) exhibiting values of 2.673 and 2.740 Å respectively. These values are within the range of previously published hydrogen bonding interactions for the lower rim hydroxyl groups on a calix[4]arene.[118]

The calix[4]arene formed an inclusion complex with the DMF, with one molecule (highlighted in orange) of the solvent trapped in the macrocyclic cavity. DMF trapped in a calix[4]arene cavity has been reported previously for several different derivatives of the macrocycle.[119,120] In this case the DMF was situated within the cavity in such a manner that one of the methyl groups attached to the nitrogen pointed directly into the cavity whereas the carbonyl group was pointing away from the cavity as observed by Takemura *et al*.[120] A CH···π interaction was observed between the NMe carbon C(65) of the DMF and its hydrogens and the aromatic ring of the calix[4]arene cavity wall. The contacts between C(65) and the benzene ring C(1)-C(2)-C(3)-C(4)-C(5)-C(6) (plane 1) are 3.84 and 3.92 Å; the contacts between C(65) and the benzene ring C(34)-C(35)-C(36)-C(37)-C(38)-C(39) (plane 2) are 3.92 and 4.10 Å. The methyl protons H(65C) and H(65A) have distances of approximately 2.88 and 2.86 Å to planes 1 and 2 respectively.
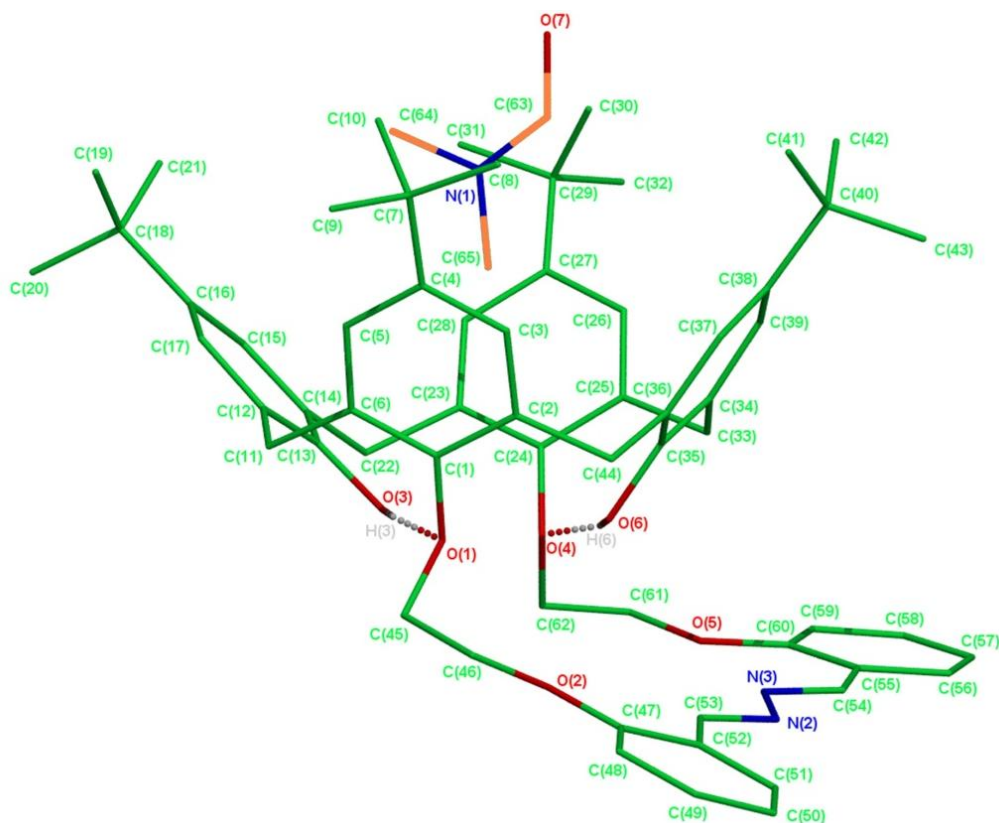
Figure 3.12: X-ray structure of **31** showing an inclusion molecule of DMF (coloured in orange) in the calix[4]arene cavity.

3.4.4   X-ray structure of 32 (xylene inclusion complex)

Compound **32**, a yellow solid, was recrystallised from xylenes by the method of slow evaporation to give yellow blocks. X-ray crystallographic analysis was performed on these crystals and the structure of **32** was determined, as shown in Figure 3.13. The calix[4]arene is in the cone conformation with the two pendant arms folded back against the wall of the macrocycle. The cone is stabilised by two intramolecular hydrogen bonds between the two hydroxyl groups on the calix[4]arene scaffold and the ether oxygens: O(1)H(1)···O(3) and O(2)H(2)···O(5) showing values of 2.809 and 2.796 Å respectively. There are additional hydrogen bond interactions between the terminal hydroxyl proton of the azine arm and the imine nitrogen. The interactions, O(7)H(7)···N(1) and O(8)H(8)···N(3), of distance 2.641 and 2.642 Å respectively, form a *pseudo* six-member ring which is exhibited in most *o*-hydroxy substituted Schiff-base derivatives.[121]

118
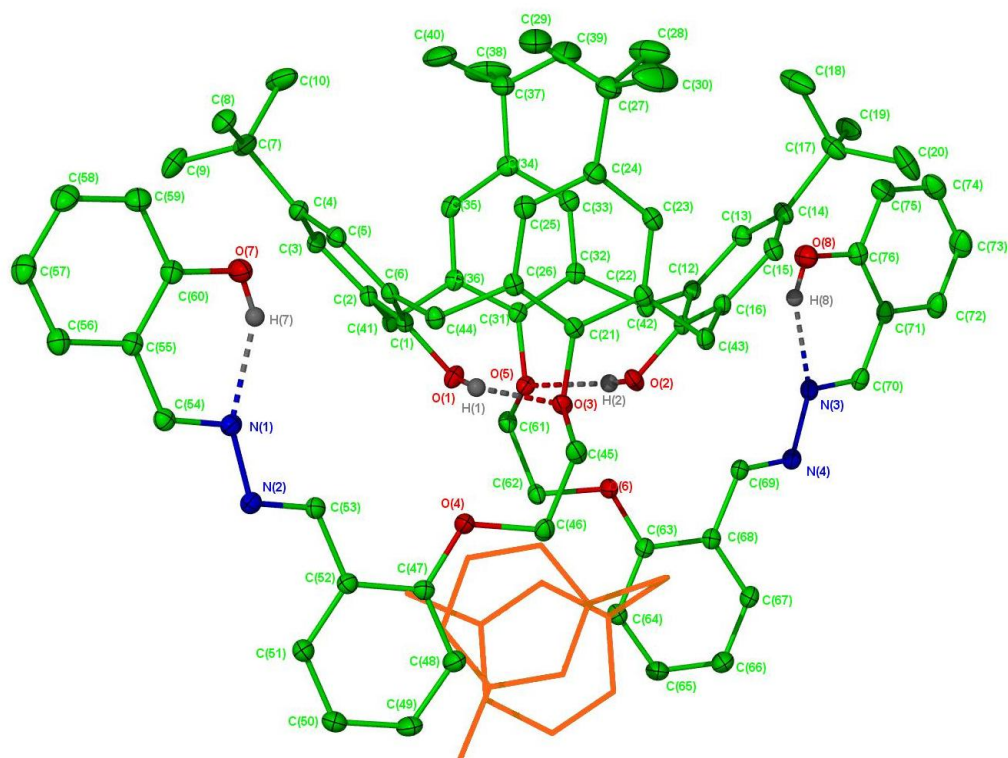
Figure 3.13: X-ray crystal structure of **32** (crystallised from xylenes) showing an inclusion molecule of *m*-xylene (disordered) in orange situated between the benzene rings of the pendant arms.

The molecule formed an inclusion complex with a molecule of *m*-xylene situated between the two aromatic rings of the azine moieties. The average distance between the centroid of the two calix[4]arene benzene rings and the centroid of the *m*-xylene is 4.9 Å. This aromatic 'sandwich', clearly seen in Figure 3.14, could lead to the orientation of the planar azine arms to be folded back up against the wall of the macrocycle. This lower rim orientation where the arms are folded back has been previously observed, but in these previous cases the pendant arms were attached to the calix[4]arene *via* amide bonds.[122] The amide proton was able to form a hydrogen bonding interaction with the phenolic oxygen atom on the calix[4]arene lower rim which held the arm in the described orientation.

Curious about the origin of this folded conformation, and to test the hypothesis that the inclusion molecule of *m*-xylene was responsible for its folded back form, **32** was crystallised from a non-aromatic solvent: DMF.
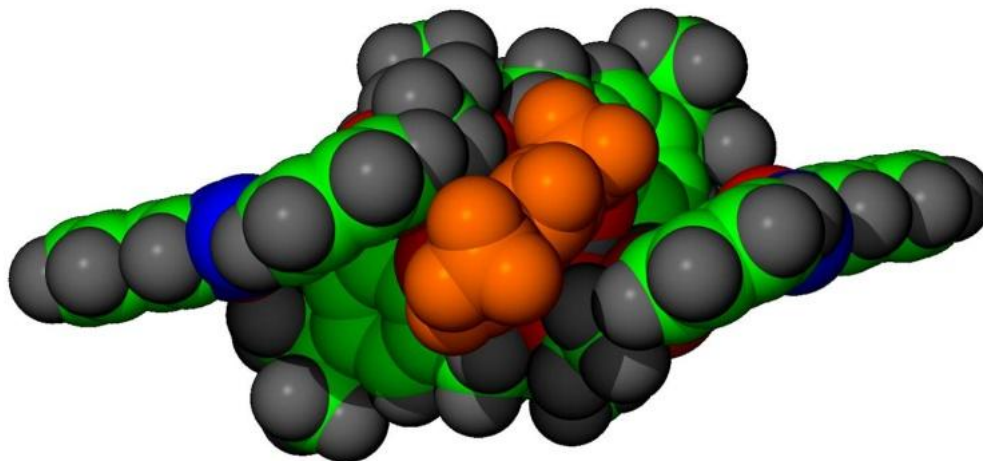
Figure 3.14: Space-fill view of **32** (crystallised from xylenes) from the bottom showing the position of the inclusion molecule *m*-xylene (in orange) between the pendant arms.

3.4.5   X-ray crystal structure of 32 (DMF inclusion complex)

Crystals of calix[4]arene azine **32** were grown by the method of slow evaporation from a dimethylformamide (DMF) solution. This yielded a crop of yellow block crystals which were subjected to X-ray crystallographic analysis. The structure determined is shown in Figure 3.15. The calix[4]arene is in the cone conformation, its structure corroborating the NMR data discussed previously. The macrocyclic orientation is stabilised by two intramolecular hydrogen bonds at the lower rim between the substituted oxygens and the unsubstituted hydroxyl groups. These two interactions, O(2)H(2)···O(1) and O(4)H(4)···O(3), have distances of 2.706 and 2.747 Å respectively.

Hydrogen bonding also exists at the terminal ring of the azine arms with an interaction detected between the hydroxyl group and the imine nitrogen, with O(7)H(7)···N(2) and O(8A)H(8A)···N(4) having respective values of 2.678 and 2.650 Å, which are similar to the values mentioned previously with the xylene inclusion derivative of **32**.

The calix[4]arene was crystallised from a DMF solution and formed an inclusion complex with the solvent. The DMF sat in the calix[4]arene macrocyclic cavity (highlighted in orange), in a manner that was identical to the inclusion complex it formed with **31**, i.e. one of the methyl groups attached to the nitrogen pointed directly into the cavity whereas the carbonyl group was pointing away from the cavity. A CH···π interaction was observed between the NMe carbon C(79) of the DMF and its

hydrogens and the aromatic ring of the calix[4]arene cavity wall. The contacts between C(79) and the benzene ring C(1)-C(2)-C(3)-C(4)-C(5)-C(6) (plane 1) are 3.73 and 3.91 Å; the distances between C(79) and the benzene ring C(34)-C(35)-C(36)-C(37)-C(38)-C(39) (plane 2) are 3.91 and 4.05 Å. The methyl protons H(79C) and H(79A) have distances of approximately 2.76 and 2.78 Å to planes 1 and 2 respectively.
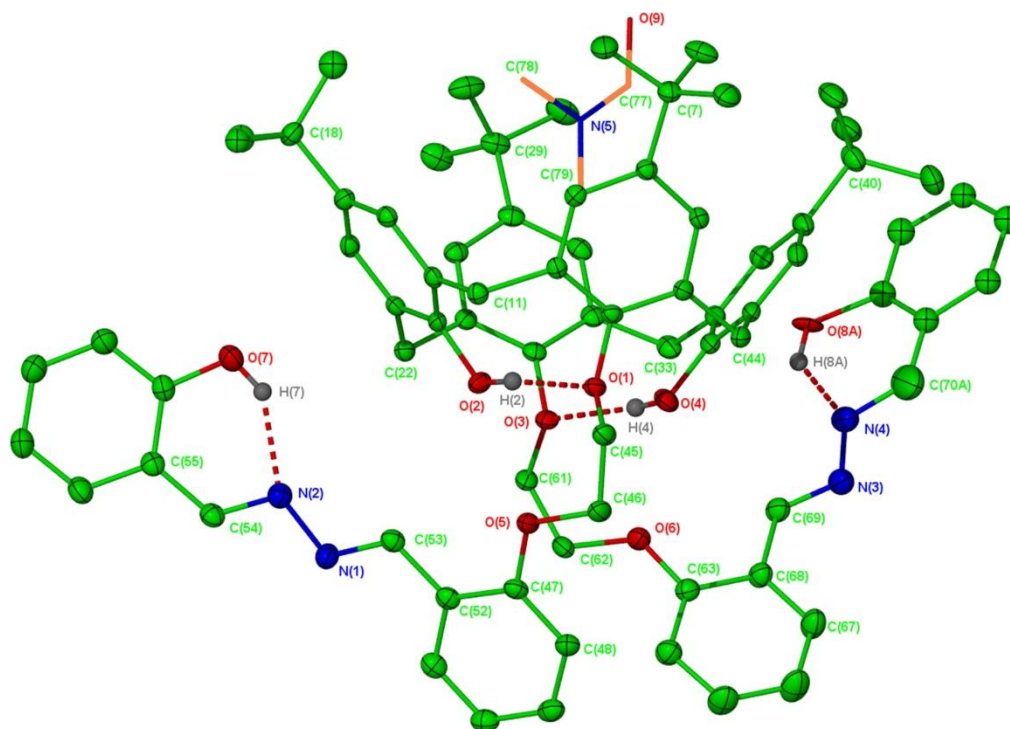
Figure 3.15: X-ray crystal structure of **32** (crystallised from DMF) showing inclusion molecule of DMF (in orange) situated in the calix[4]arene cavity.

The original objective of crystallising **32** in solvent that did not contain any aromatic ring was to determine the reason for the orientation of the pendant arms at the lower rim. When **32** was crystallised from xylenes, an inclusion complex was formed with *m*-xylene situated between the aromatic rings of the azine arms, as seen in Figure 3.13 and to determine if the solvent at the lower rim was responsible for their orientation. As can be seen in Figure 3.15, the azine arms adopt a configuration that is very similar to the xylene derivative, thus ruling out solvent effects as the reason for their configuration. As mentioned *vide supra*, the azine groups are attached to the macrocycle *via* an ethoxy ether linkage which does not provide ample opportunity for configuration-coaxing hydrogen bonding, as in the cases previously mentioned with amide bonds.[122] The reasons may be due to the simple explanation of steric clashing

between the two arms and that by adopting this folded-back style such interactions can be minimised.

One other explanation for the folded back azine groups lies in an observation of the space fill model of the xylene inclusion complex (Figure 3.14) which is viewed from beneath. The view of O(5) and O(6), which are both connected to methylene units, are in close proximity to each other with a distance of 2.91 Å between them and may lend to the possibility that an interaction is holding them in this position. The crystal packing revealed no obvious π-π interactions between the molecules. The azine arms however, if the ethoxy linkers are ignored, are almost planar. This suggested that there is π-conjugation extending throughout the azine arm. This type of conjugation has been previously reported.[123]

3.4.6   X-ray crystal structure of 37

Crystals of the calix[4]arene maleonitrile derivative, **37** were grown from an ethyl acetate solution using the method of slow evaporation to yield yellow crystals suitable for crystallographic analysis. The structure determined as seen in Figure 3.16 supported the spectral data previously obtained. The crystal also contained three molecules of ethyl acetate (not shown) trapped in the matrix.

The orientation of **37** is different to the structures of the calix[4]arene azines previously discussed. The calix[4]arene macrocycle is in a distorted cone conformation compared to the true cone conformer shown for azines **31** and **32**. This distorted cone, like previous examples, is stabilised by the intramolecular hydrogen bonding between the phenolic groups on the lower rim. These interactions, O(1)H(1)···O(2) and O(3)H(3)···O(4), have values of 2.798 and 2.991 Å respectively. The crystal structure of **37** is the only example in the class of calix[4]arene azines studied where the macrocycle does not form an inclusion complex with the solvent. A feature similar to the azine derivatives is the planar nature of the arms, with the exception of the ethoxy chains. Again, this can be explained by the conjugation that is present throughout the arm.
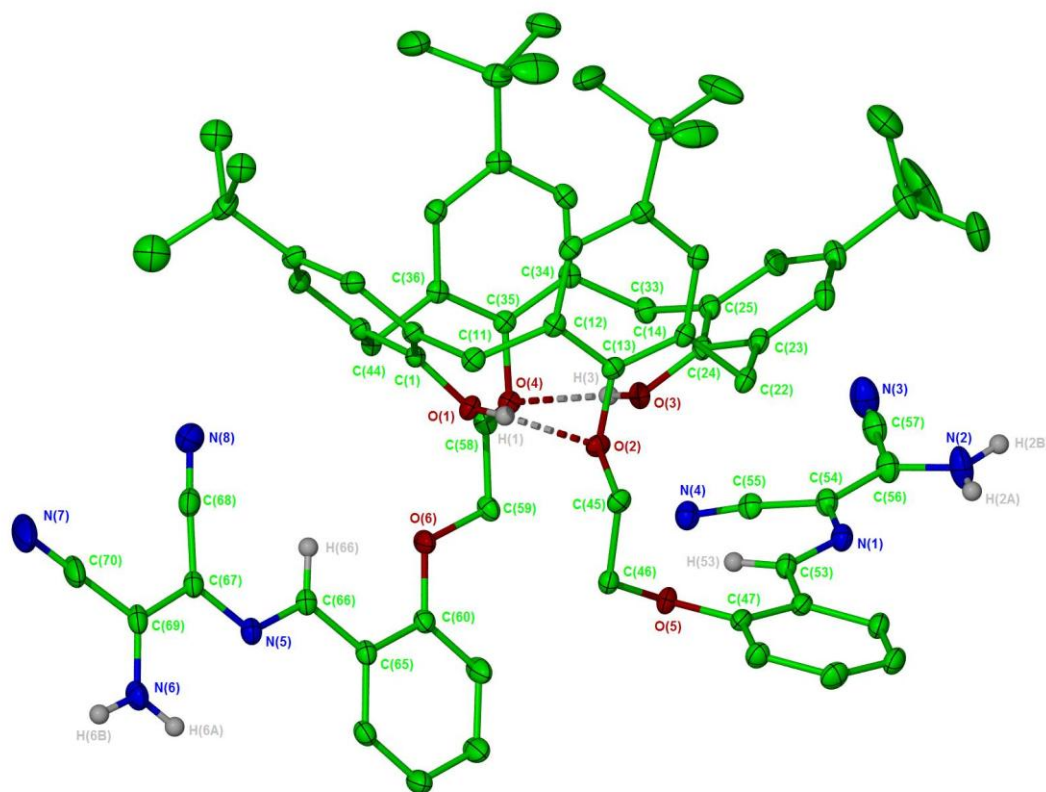
Figure 3.16: X-ray crystal structure of **37** with three molecules of ethyl acetate solvent omitted for clarity.

3.5   Benzazine model complexes

3.5.1   Overview

While the calix[4]arene azine derivatives were being prepared it was decided to determine whether the calix[4]arene scaffold had any effect on the properties, both binding and luminescent, of the azine pendant arms. To this end the following selection of benzazines were prepared using similar procedures to their calix[4]arene analogues described in Section 3.4. These model complexes were reacted with the same zinc(II) salts, namely the chloride, acetate and perchlorate salts.

3.5.2   Synthesis of hydrazone precursors 33, 35 and 39

The preparation of the hydrazone precursors has already been discussed earlier in this chapter. Aside from the commercially available salicylaldehyde hydrazone, **33**, **35** and **39** were prepared in a similar manner, i.e. the appropriate aldehyde was added

dropwise to an excess of hydrazine hydrate, and after the appropriate reaction time, evacuation of the flask was carried out to remove the volatiles. The hydrazones were usually isolated as brown or yellow oils, the exception being **33**, which crystallised to give a yellow solid.

3.5.3 Synthesis and characterisation of benzazines 38 and 40 and attempted synthesis of 2-pyridine azine derivative

The first benzazine model complex to be prepared was the salicylazine derivative **38**, whose structure is shown in Figure 3.17. Using a methyl group to 'tie up' one of the hydroxy groups, *o*-methoxybenzaldehyde was employed, the methoxy group acting as mimic of the ethoxy linker in the calix[4]arene derivatives. The commercially available salicylaldehyde hydrazone was stirred in an ethanolic solution with *o*-methoxybenzaldehyde to yield a yellow crystalline precipitate, which was removed by filtration. *o*-Methoxybenzaldehyde had a peak in its ^{1}H NMR spectrum at 10.44 ppm, which represented the aldehydic proton resonance. This signal was not present in the ^{1}H NMR spectrum of **38**. Instead, a resonance signal appearing as a singlet was present at 9.05 ppm, which was assigned to an imine proton signal. This, along with another resonance peak at 8.76 ppm which represented the other chemically inequivalent imine, confirmed the formation of **38**.
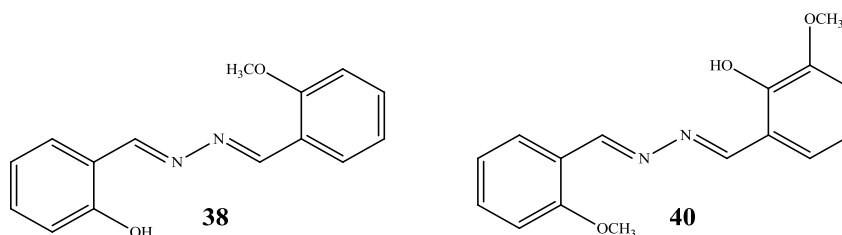
Figure 3.17: Structure of benzazine derivatives **38** and **40**.

The ^{1}H NMR spectrum (shown in Figure 3.18) also exhibited a broad singlet resonance at 11.89 ppm which represented the phenolic proton. Its low field resonance was explained by its ability to participate in hydrogen bonding with the imine nitrogen to form a *pseudo* six-member ring. The ^{13}C NMR spectrum confirmed that no plane of symmetry existed within the molecule, with 15 signals representing the different carbons. The presence of the aliphatic methyl group was observed *via* its resonance peak at 55.6 ppm. This corroborated the signal in the ^{1}H NMR spectrum for the methyl

protons, in which a signal integrating to three hydrogens was observed at 3.91 ppm. Microanalysis confirmed the constitution of the yellow solid.
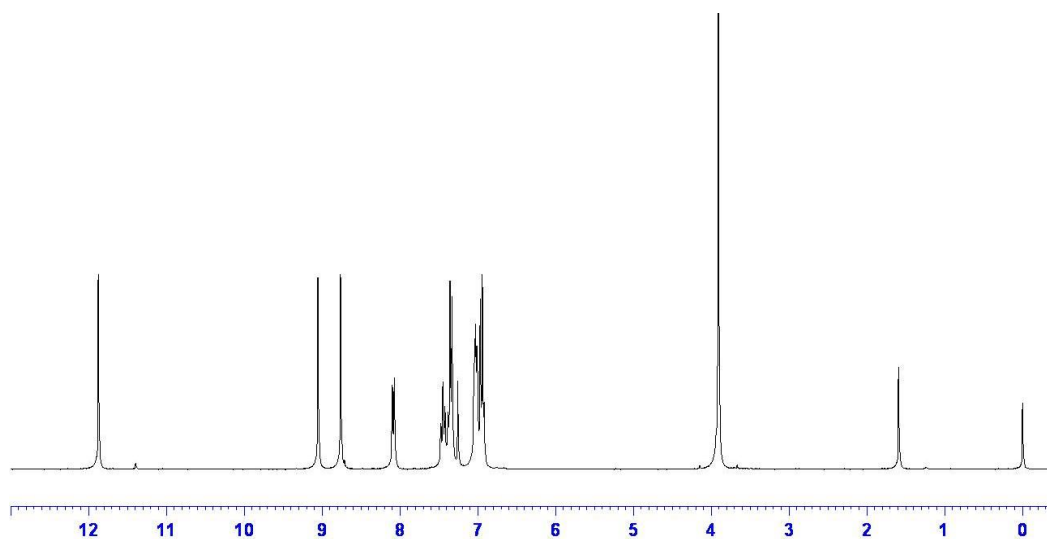
Figure 3.18: ^{1}H NMR spectrum of **38** run in CDCl$_3$ with x-axis in ppm showing phenolic proton signal at 11.89 ppm. Also present is the methoxy protons resonance at 3.91 ppm.

Compound **38** was prepared using a commercially available hydrazone. However, this luxury was not afforded for the *o*-vanillin derivative **40**, whose structure is shown in Figure 3.17. This was prepared using the 2-methoxybenzaldehyde hydrazone, **39** and an ethanolic solution of *o*-vanillin which formed a yellow solid within 5 minutes. Analysis of this yellow solid was performed using NMR and IR spectroscopy. Composition of the sample by microanalysis corroborated the spectroscopic data. The ^{1}H NMR spectrum of the *o*-vanillin reactant showed an aldehydic proton resonance at 9.91 ppm. Monitoring the azine formation by ^{1}H NMR spectroscopy showed the aldehyde being consumed *via* the disappearance of aldehyde proton peak and the concurrent appearance of a singlet at 8.75 ppm which represented the proton on the newly formed imine functional group.

The formation of an imine was also displayed in the IR spectrum of **40**. In the IR spectrum of *o*-vanillin a strong absorption band was observed for the C=O aldehydic stretch at 1666 cm^{-1}. This band was not present in the IR spectrum of **40**. However, a strong absorbance band was observed at 1621 cm^{-1} to represent the C=N imine stretching mode. Distinguishing between the two inequivalent imine absorption bands proved difficult to assign with any certainty. Like **38**, **40** does not have a plane of symmetry and this was shown by the presence of sixteen signals in the ^{13}C NMR

spectrum. Microanalysis corroborated the spectral data in ascertaining the composition of the yellow solid.

Attempts to synthesise and isolate an asymmetric 2-pyridine azine derivative (shown in Figure 3.19) using 2-pyridinecarboxaldehyde hydrazone, **35**, and 2-methoxybenzaldehyde resulted in failure. On each occasion no precipitate was forthcoming and analysis of the oily residue which remained after removal of the volatiles revealed a mixture of products, most probably formed as a result of hydrolysis of the reactant hydrazone to give the free hydrazine followed by consecutive imine formation of one of the two possible symmetrical azines, i.e. the 2-methoxybenzazine or the 2-pyridine azine, whose structures are shown in Figure 3.19.
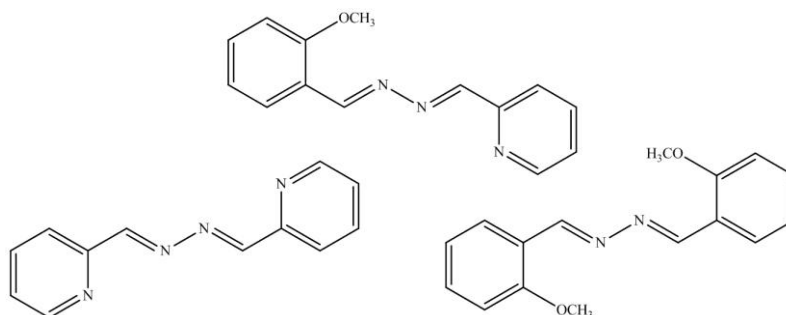
Figure 3.19: Structure of desired asymmetric azine (top) and products formed: 2-pyridine azine (left) and 2-methoxybenzazine (right).

3.6 Metal complexes of calix[4]arene azines and benzazine model complexes

3.6.1 Overview

The model azine complexes and their calix[4]arene derivatives were prepared to determine their effectiveness as zinc(II) ionophores and their subsequent fluorescent properties in binding the metal ion. Exhaustive zinc(II) complexation reactions were carried out using the ligands mentioned in Sections 3.4.2 and 3.5.3. In most cases interaction between the ligand and the metal ion was observed using ^{1}H NMR spectroscopy. Unfortunately, the complexation products isolated were also characterised as having impurities, as seen in the ^{1}H NMR spectra and in some cases by microanalysis.

The lack of pure complexes made the comprehensive evaluation of the influence of the calix[4]arene macrocycle impossible. Using the examples that have been prepared, it is possible to gauge whether the calix[4]arene scaffold is having an effect on the luminescent properties of the benzazine moieties.

In the few cases where pure metal complexes were obtained, as presented below, spectroscopic examination of their fluorescent properties was carried out.

3.6.2   Zinc(II) calix[4]arene complex 41

In an ethanolic suspension of **32**, sodium hydroxide was used to deprotonate the phenoxide which was situated on the pendant arms. The yellow solid quickly dissolved upon addition of the base. To this sodium analogue was added an ethanolic solution of zinc(II) perchlorate. After stirring overnight a neon yellow solid had formed. This analysed as the zinc complex of **32**, with two zinc ions being complexed by each pendant arm, as shown in Figure 3.20. Compound **41** consisted of the zinc ion bound to the terminal imine moiety, in a classic bidentate fashion. The remaining two coordination sites on the metal were occupied by a water molecule and a hydroxide ion, which along with the deprotonated phenol balanced the charge on the zinc(II) cation.
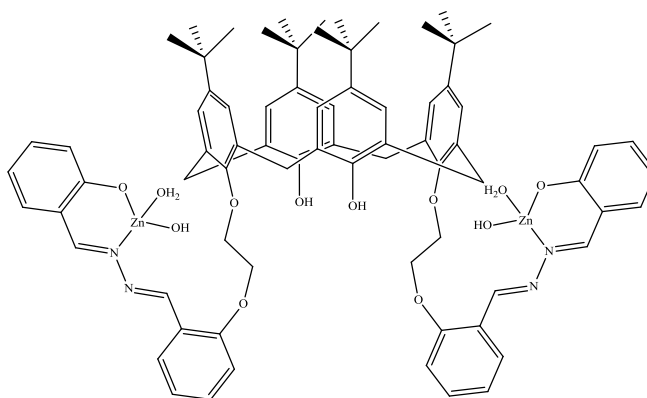
Figure 3.20: Proposed structure of calix[4]arene zinc complex **41**.

The structure was proposed using the information available, namely elemental analysis and spectroscopic data, both ^{1}H NMR and IR spectroscopy. The IR spectrum of **41** revealed that the perchlorate counterion was no longer present, by virtue of the absence of an absorption band at 1089 cm^{−1}. The HOH bending mode of the coordinated water,

which was present in the IR spectrum of the starting material (zinc(II) perchlorate hexahydrate) at 1616 cm^{-1}, was not identified in the IR spectrum of **41** due to overlapping bands from the C=N stretches of the azine moiety. Metal hydroxo complexes exhibit MOH bending modes below 1200 cm^{-1},[124] however assignment of this band in the calix[4]arene product proved difficult due to the overlapping absorption bands of the ligand itself. The imine stretch, present in the IR spectrum of **32** at 1624 cm^{-1} has now shifted to the slightly lower wavenumber of 1618 cm^{-1}.

The ^{1}H NMR spectrum of **41** exhibited several notable differences when compared to the ^{1}H NMR spectrum of the calix[4]arene starting material **32**, both of which are shown in Figure 3.21. The signal for the terminal phenolic proton, which was present at 11.17 ppm in the d_6-DMSO ^{1}H NMR spectrum of **32** is no longer observed. This would suggest that the zinc(II) ion was bound at this site. This hypothesis was supported by the observed chemical shift of the imine proton signals. These singlet signals, present in the d_6-DMSO ^{1}H NMR spectrum of the starting material at 8.86 and 9.16 ppm, had now shifted upfield to 8.11 and 9.03 ppm respectively. Whereas the consensus for the coordination complex might be for the imine peaks to occupy a lower field position than the free ligand, this unusual trend had been observed in the literature with very similar azine derivatives.[80]
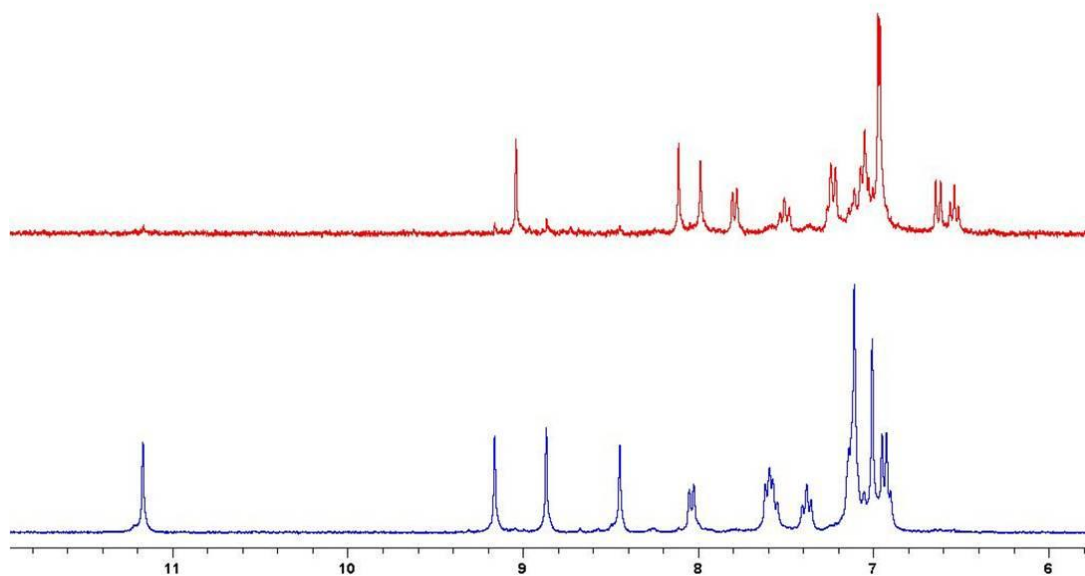
Figure 3.21: Partial ^{1}H NMR spectra of **32** (blue trace) and its zinc(II) perchlorate complex **41** (red trace) run in d_6-DMSO with x-axis scale in ppm

A point of note would be the exceptionally poor solubility of **41**. NMR spectra required solvation of **41** in hot d_6-DMSO to run successfully. Several deuterated solvents were tried, with the aforementioned dimethyl sulphoxide the only one that was successful. A possible explanation is that **41** may be a coordination polymer, with the free imine nitrogen occupying a fifth coordination site on the zinc ion, by virtue of the geometry about the imine bond which occupies a *trans*-orientation (as seen from the obtained X-ray crystal structures of **32**) and results in the protrusion of the lone pair outwards. This results in a sterically unhindered nitrogen and is as a consequence available to donate into the metal coordination sphere *via* its lone pair. This would most likely result in a polymeric network (a section of which is shown in Figure 3.22) of five-coordinate zinc complexes linked by the calix[4]arene scaffold. This is reasonable, as five-coordinate zinc(II) complexes are common in the literature.[125]
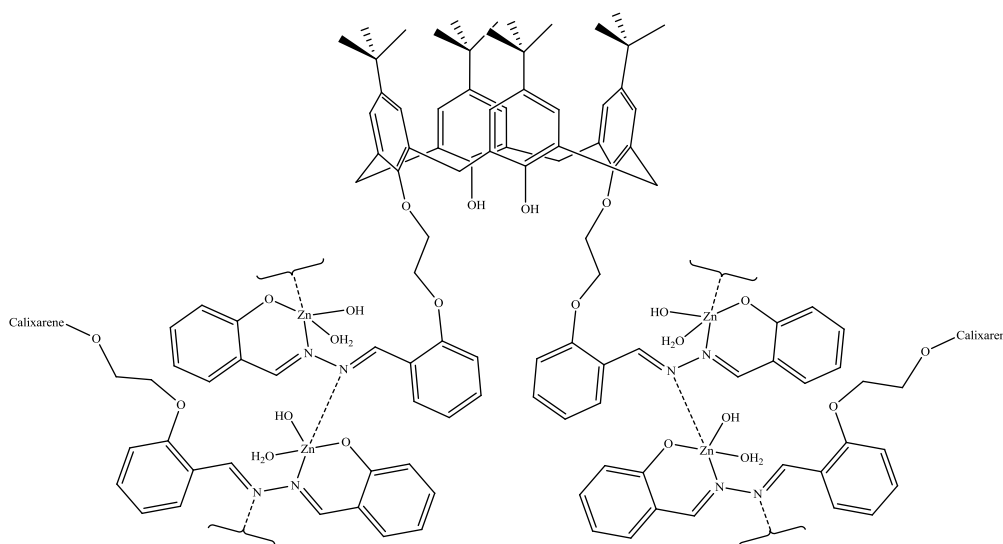
Figure 3.22: Proposed polymeric structure of **41** showing interactions between adjacent complexes to give 5-coordinate zinc(II) centres.

3.6.3   Zinc(II) calix[4]arene complex 42

Using the same ligand **32**, a different zinc salt was used, to determine whether the perchlorate ion had any influence on the coordination geometry adopted by the metal. To this end, zinc(II) chloride was chosen. As was the case with the formation of **41**, **42** was formed from an ethanolic suspension of **32** to which sodium hydroxide solution was added to deprotonate the terminal phenolic proton which was situated on the pendant arms. This formed the soluble sodium analogue to which was added an

ethanolic solution of zinc(II) chloride. Stirring the mixture for 75 minutes resulted in formation of a yellow precipitate. This neon yellow solid was analysed by NMR and IR spectroscopy and also its composition was determined by elemental analysis.

Microanalysis of the yellow solid revealed that it consisted of the ligand with three zinc ions incorporated into the structure, as shown in Figure 3.23, forming a trinuclear species. Two of the metal ions could be assigned to the azine binding site, whilst the final zinc ion is most likely bound by the ethereal oxygens on the ethoxy linker. Metathesis of the counterion has occurred in a similar fashion to **41**, with a hydroxide anion replacing the chloride in this case. The IR spectrum of **42** displayed the same characteristics as that of **41**, with a shift in the imine stretch migrating toward a lower wavenumber. Whilst the reference value for the imine stretch in the IR spectrum of **32** at 1624 cm^{-1}, a value of 1619 cm^{-1} was recorded for the imine vibration in the zinc complex.
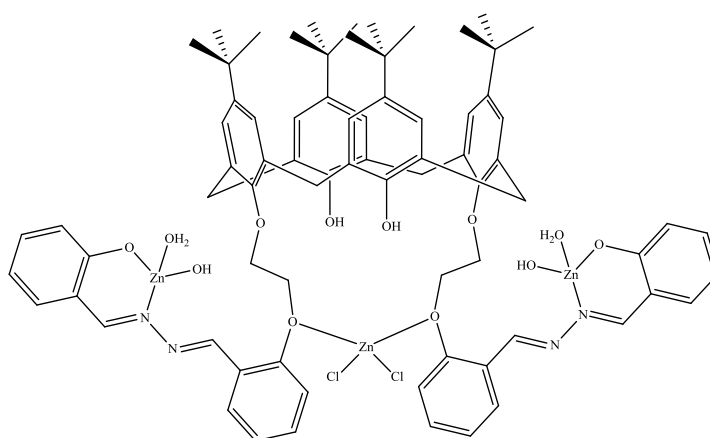
Figure 3.23: Proposed structure of **42** showing positions of zinc(II) ions at the pendant arms and at the lower oxygens of the ethoxy linker.

Analysis of the ^{1}H NMR spectrum of **42** revealed several noticeable differences when compared to the corresponding spectrum of **41**. Firstly, the ethyl linker, observed in all previous cases as a single multiplet signal, has now resolved into two separate signals: one at 4.16 ppm and the other at 4.50 ppm, both signals integrating for four protons. This substantial difference in chemical shift would suggest that the zinc ion is bound through one of the ethereal oxygen pairs, with the lower oxygen pair being the most likely donor atoms due to potential steric crowding if the calix[4]arene oxygens were employed. This binding resulted in chemically inequivalent ether oxygens, with one pair of oxygens binding to the metal ion, which resulted in a partial positive charge on

the oxygen atom due to the Lewis acid nature of the zinc(II) chloride. As a consequence, this resulted in a more deshielded environment for the adjoining CH_2 protons. The second pair of oxygens, which provided the link to the calix[4]arene, were not involved in complexation and so occupied a higher field position. As before, the terminal phenolic proton signal was not observed, so it was postulated that this was the site where the zinc ions were bound. The imine proton signals, resonating at 8.86 and 9.16 ppm in the d_6-DMSO ^{1}H NMR spectrum of **32**, have shifted as a result of the imine nitrogen binding to the zinc ion, with two resonances observed at 8.21 and 9.30 ppm, mirroring the trend reported in the literature.[80]

3.6.4   Zinc(II) benzazine complex 43

Using the azine model complex **38** in a suspension with ethanol and some sodium hydroxide to deprotonate the phenol hydrogen, **43** was prepared by adding a solution of zinc(II) chloride to the sodium azine derivative. This resulted in formation of a yellow solid within two minutes. This yellow solid was isolated and its composition determined by NMR and IR spectroscopy along with microanalysis. The yellow solid consisted of two ligands of **38** surrounding a zinc core, with coordination to the metal through the bidentate site (i.e. through the phenoxide oxygen and the imine nitrogen) in a similar fashion to that observed with the calix[4]arene derivatives. Unlike the calix[4]arene derivatives however, a second equivalent of **38** was employed by the zinc ion to occupy its coordination sphere. This suggested that the calix[4]arene had an influence on the binding mode of the pendant arm. It maybe just a simple matter of steric interaction that a similar coordination sphere was not observed in the cases of **41** and **42** simply because the sheer bulk of the macrocycle prevents the type of close arrangement that was observed for the less hindered model azine derivative **43**.

Microanalysis revealed that the yellow solid consisted of two equivalents of metal complex (1:2 metal-to-ligand ratio) with three equivalents of water. From the IR spectral data and elemental analysis, it is probable that **43** is either the four- or the five-coordinate species shown in Figure 3.24. The water molecules may be bound to the zinc or they may be in the lattice, without a definitive X-ray crystal structure it is impossible to be certain.

The IR spectral data of **43** suggested that the five-coordinate species was the most likely structure. The imine C=N stretch, present in the free ligand as a strong absorption band at 1622 cm^{-1}, now exhibited a lower wavenumber, as expected, in the IR spectrum of the product at 1615 cm^{-1} indicating that the imine was involved in metal coordination. The HOH bending mode of the bound water was most likely represented by the new absorption band observed at 1582 cm^{-1}.
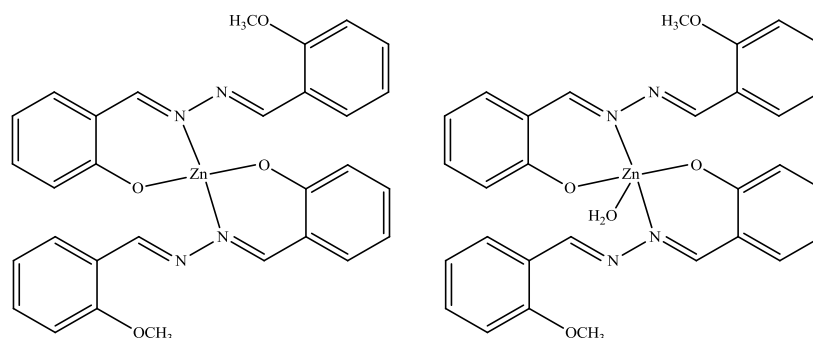
Figure 3.24: Proposed structures of **43** showing four- (left) and five-coordinate species (right).

The ^{1}H NMR spectrum of **43** reveals that a plane of symmetry was present throughout the molecule, as displayed by the number of inequivalent proton resonances observed. The most telling signal was the peak representing the aryl-methoxy protons. This signal integrated to six hydrogens and was unsplit (i.e. a singlet), so showing that the two ligands bind in a symmetrical fashion. The binding site was determined by the absence of the phenolic proton signal in the metal complex **43** but which was present at 11.29 ppm in the d_6-DMSO ^{1}H NMR spectrum of the starting material: **38**. The signal for the imine protons had also shifted, from exhibiting resonances at 8.97 and 8.94 ppm in the d_6-DMSO ^{1}H NMR spectrum of **38** to the slightly lower field shift of 9.04 and 8.96 ppm.

3.6.5   Zinc(II) benzazine complex 44

Ligand **40** was initially synthesised to function as a model complex for calix[4]arene derivative **34**. Unfortunately no zinc coordination compounds were isolated from complexation reactions involving the calix[4]arene. Since **40** was a novel compound, it was decided to determine whether the additional methoxy group, present as a result of the use of *o*-vanillin as a precursor, would have any effect on the complexation properties of the imine/phenoxy binding site and also to determine its fluorescent

properties. To this end, complex **44** was prepared as a yellow solid by using a similar preparation to the zinc azine model complexes previously described. Treating a suspension of **40** in ethanol with sodium hydroxide to deprotonate the phenol moiety and generate the sodium salt analogue, an ethanolic solution of zinc(II) acetate was added to the yellow solution. After three days stirring at room temperature, the resultant yellow precipitate was isolated and characterised by microanalysis along with spectral characterisation using NMR and IR spectroscopy.

The yellow solid was determined using elemental analysis to have a metal-to-ligand ratio of 1:2, resulting in a broadly similar complex to the example described in the previous Section. Similarly to the case of **43** it is difficult to determine without the aid of a X-ray crystal structure whether the water is bound to the metal (giving a five-coordinate complex) or if it is free in the lattice (yielding a four-coordinate species). Based on general trends for the coordination sphere of zinc ions it most likely exists as the five-coordinate species.[19] It consists, as shown in Figure 3.25, of a symmetrical coordination complex with two molecules of ligand **40** wrapped around a zinc ion core, with coordination to the metal provided through the imine nitrogen and phenolic oxygen donor atoms. The coordination sphere about the zinc ion is completed by the binding of a single molecule of water to give a five-coordinate metal centre.
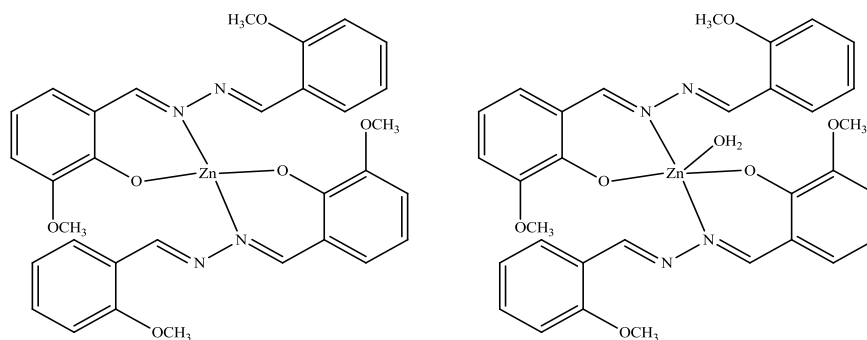
Figure 3.25: Proposed structures of **44** showing four- (left) and five-coordinate species (right).

The ^{1}H NMR spectrum of **40** was carried out in d_6-DMSO for comparative purposes with the zinc complexation product. The ligand exhibited a resonance at 11.08 ppm which integrated for one hydrogen and represented the phenol proton. This signal was not observed in the ^{1}H NMR spectrum of **44**. This would suggest that the phenolic oxygen is involved in binding the zinc ion. The imine nitrogens are involved in ligation of the metal and, as a consequence, are responsible of the shift observed in the

imine proton resonances. The ligand **40** exhibited these signals at 8.96 and 8.94 ppm in its ^{1}H NMR spectrum. After metal complexation these peaks shifted to resonances of 8.60 and 9.04 ppm.

The IR spectrum also revealed that the imine nitrogen is implicated in the metal binding. The IR spectrum of **44** showed a strong absorption band at 1615 cm^{-1} which represented the C=N stretch of the imine involved in complexation. This value is in contrast to the free ligand, which exhibited a value of 1621 cm^{-1} for the imine absorption. The IR spectrum also showed an additional absorption band at 1583 cm^{-1} which has a similar value to the absorption band observed for the bound water HOH bending mode in the IR spectrum of **43**. Since there was no lattice water present in the sample, unlike **43**, it would seem reasonable to assign this band to the vibrational mode of the coordinated water.

3.6.6   Zinc(II) benzazine complex 45

On preparation of calix[4]arene **36**, a 2-pyridine benzazine derivative, it was decided to prepare the corresponding model complex for comparative purposes, as in the previous cases. This involved synthesising a ligand containing, like **38** and **40**, a benzene ring with a hydrazone appendage and a methoxy group in the *ortho* position. Attempts to prepare this compound involved adding 2-pyridinecarboxaldehyde to 2-methoxysalicylaldehyde hydrazone, **39**, in typical reaction conditions (dry ethanol) for Schiff-base formation. After approximately 30 minutes a yellow solid precipitated from the amber solution. After isolation, the yellow solid was analysed by ^{1}H NMR spectroscopy. This revealed the yellow solid to be the dipyridyl azine derivative, most probably formed as a result of residual water in the system which caused hydrolysis of the imine bond of **39** to produce the free hydrazine which subsequently condensed with two equivalents of 2-pyridinecarboxaldehyde to give the azine. This structure has been previously reported and characterised in the literature.[126] Reduction of the filtrate revealed that the liberated 2-methoxybenzaldehyde had performed a similar action to the 2-pyridinecarboxaldehyde. A yellow solid, lighter in colour than the pyridine azine, was isolated and found to be the dimethoxy benzazine derivative. Like the corresponding pyridine hydrazone, this compound has been previously reported and has found use as a fluorescent sensor,[81] and has also been characterised by Fu using

134

X-ray crystallography.[127] Additional attempts were made to prepare the asymmetric azine starting from 2-pyridinecarboxaldehyde hydrazone, **35** and 2-methoxybenzaldehyde, but these too proved fruitless, yielding the same symmetric undesirables. The reaction time was curtailed, with the aim of stopping the reaction when the desired product was formed before hydrolysis of the ligand could occur. No precipitation had occurred when the reaction flask was evacuated to remove the volatiles. Analysis of this brown viscous oil by ^{1}H NMR spectroscopy revealed that the reaction had not proceeded cleanly and that formation of the symmetric undesirables had already commenced. The summary of the reactions attempted are shown in Scheme 3.8.
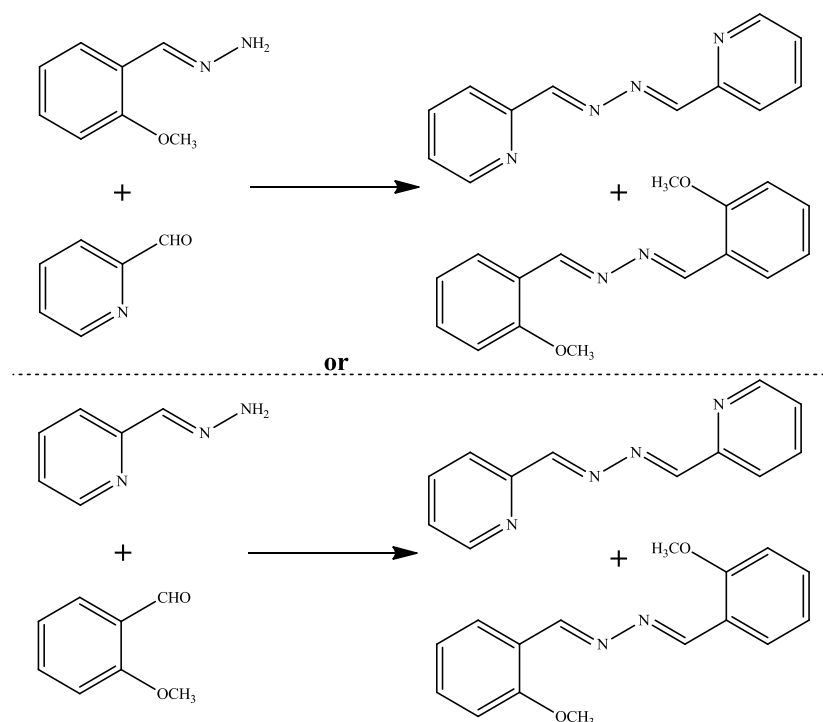
Scheme 3.8: Attempted reactions and products of preparation of model azine of **36**.

From initial unsuccessful attempts to prepare the ligand, it was decided to make the ligand *in situ* without isolating it and react it immediately with the metal salt so that the complexed metal would add some much needed stability to the ligand. It was decided to prepare the ligand using neat 2-pyridinecarboxaldehyde hydrazone **35** and neat 2-methoxybenzaldehyde, thereby bypassing the possibility of introducing water to the system *via* a solvent carrier. This mixture turned pale yellow and after five minutes a solution of zinc(II) chloride was added, which resulted in the immediate formation of a yellow/orange precipitate. This solid analysed using NMR and IR spectroscopy along

with microanalysis as the required product **45**, shown in Figure 3.26, to be an asymmetric Schiff-base complexed to the zinc(II) ion. It was difficult to assign the appropriate aromatic proton peaks and the imine peaks in the ^{1}H NMR spectrum as the corresponding spectrum for the free ligand was not available. To ensure that the solid obtained was not simply a mixture of the symmetrical azines, seen in Scheme 3.3, that formed their respective zinc coordination complexes, complexation reactions were also carried out with zinc(II) chloride and the corresponding symmetric azine. It was surprising to note that from the ^{1}H NMR data obtained, it appeared that in each case, no metal binding had occurred. This was unusual, particularly in the case of the pyridine azine, since several metal coordination complexes of the symmetrical pyridine azine ligand have been reported.[128]
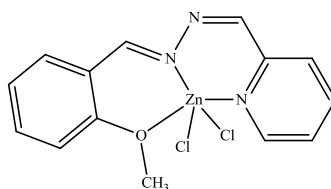
Figure 3.26: Proposed structure of **45**.

The IR spectrum of **45** had a strong absorption band present at 1623 cm^{-1} and 1594 cm^{-1}, which corresponded to the C=N stretching modes of the imines and the C=N vibration mode of the pyridine ring. These are within the ranges observed for the azine complexes previously prepared. It is difficult to assign the relevant absorption bands as there is no spectral data for the free ligand, so basing these values on similar complexes, it would seem reasonable to propose the assignments mentioned above for these vibration modes.

A similar dilemma existed for assignment of the resonance peaks in the ^{1}H NMR spectrum of **45**. Based on the spectral data obtained for the two symmetric azines, the chemical shift of these proton resonances could be estimated. Since both imine protons were the only low field protons that were not affected by spin-spin coupling, their signals could be assigned as singlets at 8.60 and 8.97 ppm. Due to steric constraints it is reasonable to say that the imine nitrogen involved in coordination to the metal was the one nearest the 2-methoxybenzene derivative. This resulted in the formation of two six-member rings in the complex, which is preferable to the case that would arise if the metal was bound through the imine nitrogen closest to the pyridine ring. This would

result in the formation of a five- and an eight-member ring in the molecule. The methoxy protons were assigned as a singlet appearing at 3.90 ppm.

3.7 Fluorescent properties of azines and their metal complexes

3.7.1 Overview

Although not all zinc(II) azine complexes prepared were of sufficient purity by NMR and IR spectroscopy as well as elemental analysis, those that were pure were screened for potential fluorescent characteristics. Some of the calix[4]arene azines that were prepared were not subjected to examination because the azine moiety is not contained in these, namely the calix[4]arene hydrazone, **30** and the calix[4]arene Schiff-base amine prepared from diaminomaleonitrile, **37**. The selection of fluorophores presented in this thesis focus on those derivatives that bound the zinc(II) ion. To compare and contrast whether the calix[4]arene macrocycle had any diminishing or enhancing effect on the emission characteristics, a family of benzazines were prepared as model complexes, along with their subsequent zinc(II) coordination complexes. Successfully prepared azines and zinc(II) coordination complexes and their corresponding fluorescent properties are summarised in Table 3.2.

Table 3.2: Absorption maximum of UV absorption spectrum (λ_{abs}) was used as an excitation parameter to generate emission spectrum with maximum (λ_f^{em}). Emission maximum was used as an emission parameter to generate excitation spectrum with maximum (λ_f^{ex}). Data were obtained for calix[4]arene azine derivatives and their zinc(II) complexes, along with free benzazine derived ligands and their corresponding zinc(II) complexes. In a single case, No Fluorescence was Observed (NFO).

Sample No.	λ_{abs} (nm)	λ_f^{em} (nm)	λ_f^{ex} (nm)
32	352	544	351, 289
34	324	415	301
36		NFO	
38	356	433	293, 340
40	340	437	340, 274
41	365	505	470
42	418	504	411
43	409	493	409
44	336	431	317
45	366	418	358

3.7.2   Fluorescence of calix[4]arene azine ligands 32, 34 and 36

Calix[4]arene azines **32**, **34** and **36** (structures shown in Figure 3.27) contain potential fluorophoric moieties. Benzazine derivatives resembling the pendant arms have been subjected to spectroscopic analysis using time resolved fluorescence spectroscopy.[80] The presence of the calix[4]arene macrocycle caused the observation of an additional absorption band with a λ_{max} at 280 nm. The value corresponded favourably to values previously published.[39] This absorption band may overlap with some of the absorption bands of the azine moiety.
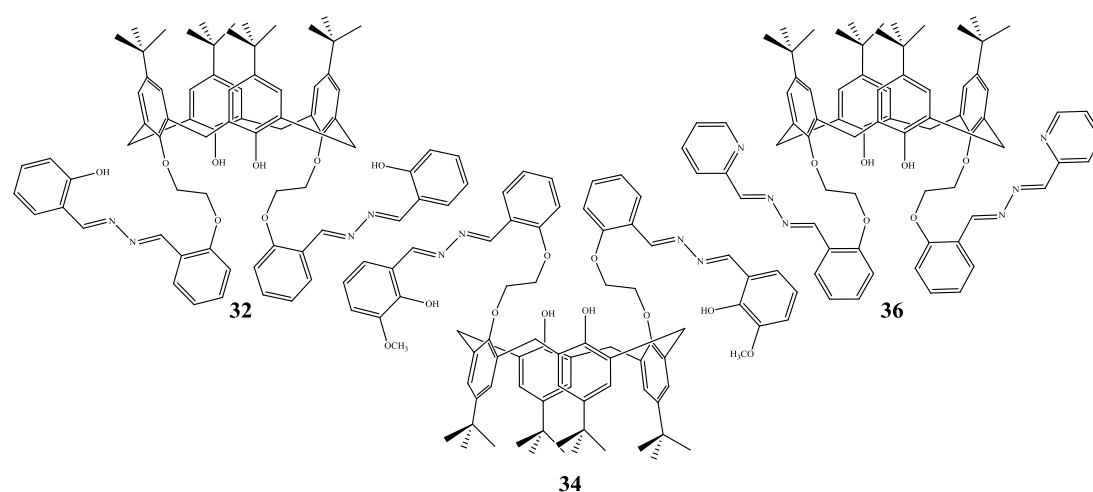
Figure 3.27: Calix[4]arene azine derivatives **32**, **34** and **36** used in fluorescence studies

Calix[4]arene azine derivative **32** was the first ligand to be examined, and yielded encouraging results. Excitation of the sample at 352 nm yielded an emission spectrum with broad bands at 442, 544 and 574 nm, with a fluorescence maximum at 544 nm. The emission maximum was chosen as the emission parameter for the excitation spectrum. The excitation spectrum of **32** revealed two excitation bands, one at 351 nm and a second, stronger band at 289 nm. To eliminate the possibility that the band at 289 nm was a contribution from the calix[4]arene macrocycle, a corresponding excitation spectrum was obtained of the unfunctionalised calix[4]arene (tetramer), **27**, and was subtracted from the excitation spectrum of **32**. The new compound spectrum showed a reduction in the two original observed excitation bands, showing that the calix[4]arene itself was contributing to the strength of the excitation bands. The UV absorption spectrum of **32** also contained the longer wavelength absorption band at 352 nm. The excitation and emission spectra of **32** are displayed in Figure 3.28.
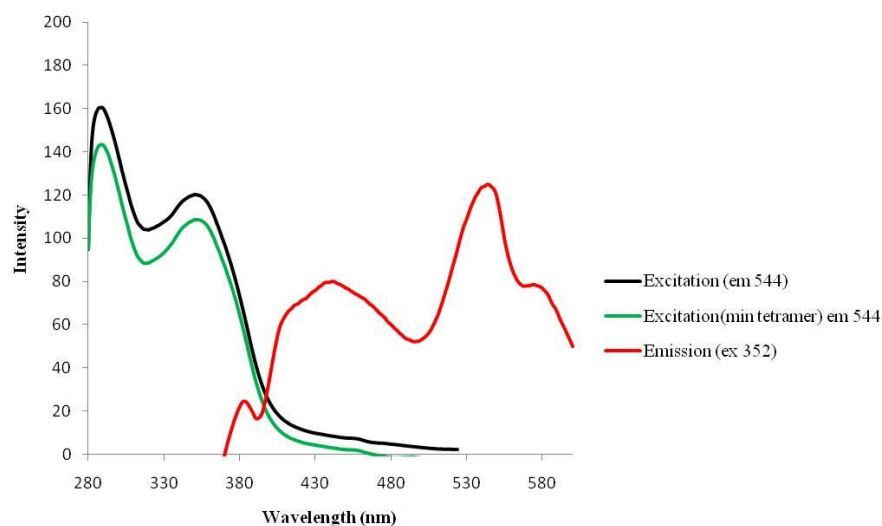
Figure 3.28: Excitation spectra of **32** (black trace with λ_{em} = 544 nm), **32** minus unfunctionalised tetramer (green trace with λ_{em} = 544 nm) and an emission spectrum obtained for **32** (red trace with λ_{ex} = 352 nm). All samples were run as 10 μM solutions in DMSO.

Calix[4]arene azine, **34**, did not display a similar emission spectrum to **32**, even though the only difference between them is a methoxy group situated *ortho* to the hydroxyl moiety on the pendant arms. A single emission band at 415 nm was observed after excitation at 324 nm. The excitation spectrum displayed a very intense band at 301 nm with a shoulder at 307 nm. Subtraction of the excitation spectrum of the tetramer at the same emission wavelength (415 nm) resulted in a large reduction in the intensity of the excitation bands, as displayed in Figure 3.29. Given that no further emission was observed above 550 nm it could be argued that the methoxy group is facilitating non-radiative relaxation. The UV absorption spectrum of **34** exhibited an absorption maximum at 324 nm.

For the third calix[4]arene azine examined, a 2-pyridine azine was used to give the calix[4]arene azine **36**. Its UV absorption spectrum showed two strong absorption bands at 296 and 334 nm. Using these to obtain an emission spectrum, it was found that no emission took place. The reasons for this are probably the pyridine nitrogen, whose lone pair most likely participates in an $n \rightarrow \pi^*$ transition. $n \rightarrow \pi^*$ transitions are slow, due to their low molar absorption coefficients. As a result of this slow uptake, the radiative lifetime of $n \rightarrow \pi^*$ transitions is up to 100 times longer than that of the lowest energy $\pi \rightarrow \pi^*$ transition. Because the lifetime is so long it cannot compete with non-radiative processes which are generally 100 times faster.[66]
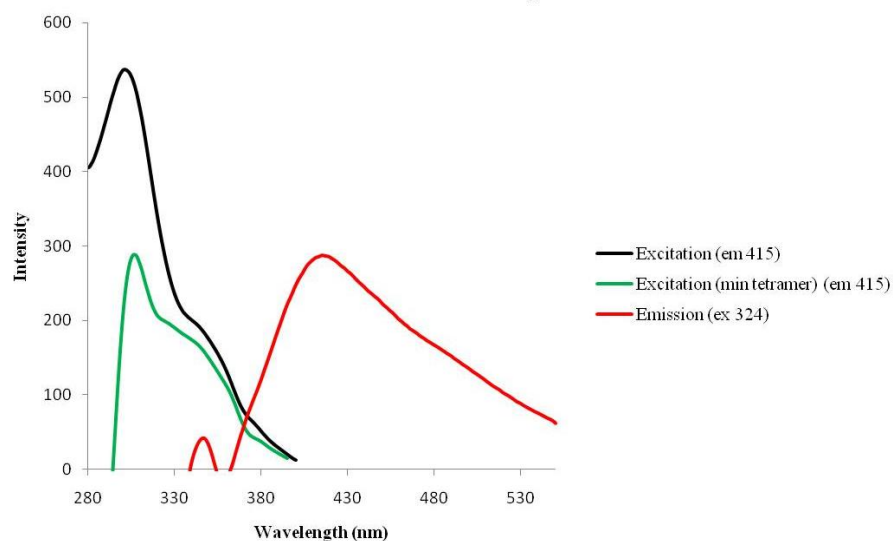
Figure 3.29: Excitation spectra of **34** (black trace with λ_{em} = 415 nm), **34** minus unfunctionalised tetramer (green trace with λ_{em} = 415 nm) and an emission spectrum of **34** (red trace with λ_{ex} = 324 nm). All samples were run as 10 μM solutions in DMSO.

3.7.3   Fluorescence of benzazine ligands 38 and 40

Taking the two novel prepared ligands **38** and **40**, it was decided to examine their fluorescent properties and if the calix[4]arene macrocycle had any effect on their emission or excitation. Using a methyl ether to simulate the ethoxy linker to the lower rim of the calix[4]arene, **38** and **40** were easily prepared. The structures of **38** and **40** are displayed in Figure 3.30.
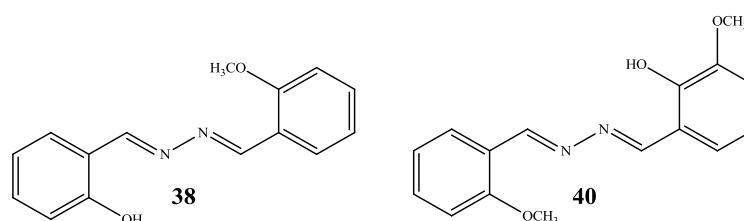
Figure 3.30: Compounds **38** and **40** used as model ligands for calix[4]arene azine derivatives **32** and **34** respectively.

Azine **38**, a model of calix[4]arene azine **32**, was the first benzazine to be scrutinised. Its emission spectrum (excited at 356 nm) displayed a strong but broad band with a plateau from 412 to 433 nm, the latter value being the peak with the greatest intensity. A noticeable difference in the emission spectrum is the absence of a strong band at 544 nm, a band that was present in the emission spectrum of **32**. In addition to the band at 412 nm, a shoulder is also observed at 390 nm. The excitation spectrum of **38** shows

two intense bands, one at 340 nm and another, more intense band at 293 nm. The excitation and emission spectra of **38** are displayed in Figure 3.31. The UV absorption spectrum of **38** exhibited several broad bands, with an absorption maximum at 356 nm.
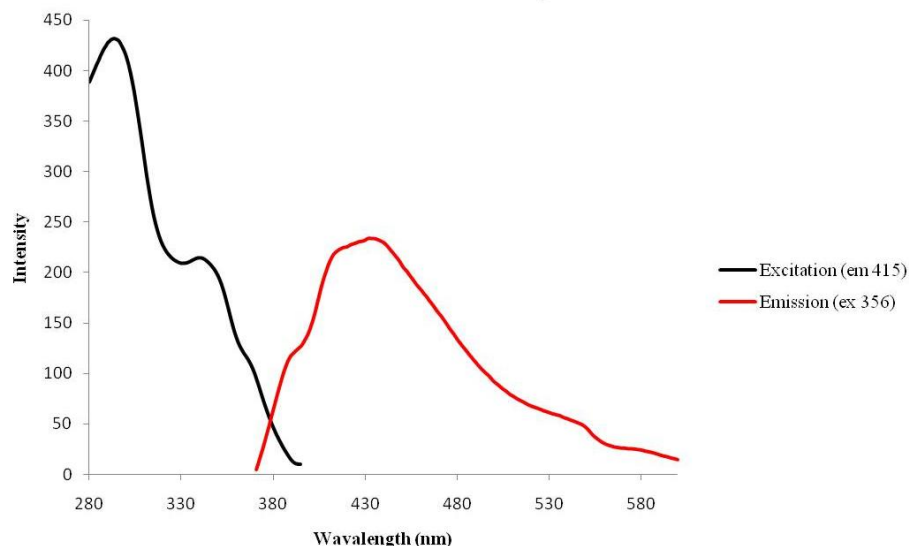
Figure 3.31: Excitation (black trace with λ_{em} = 415 nm) and emission (red trace with λ_{ex} = 356 nm) spectra of **38**. Sample was run as a 10 μM solution in DMSO.
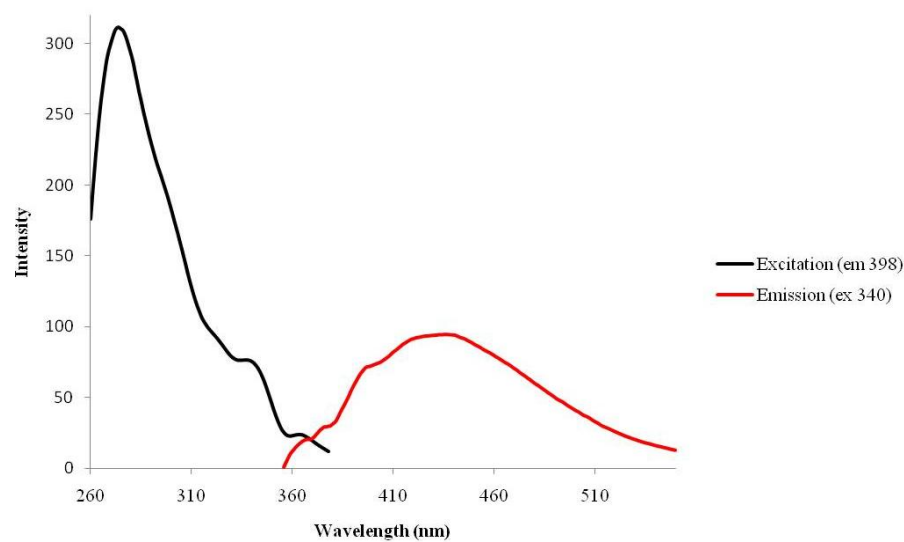
Figure 3.32: Excitation (black trace with λ_{em} = 398 nm) and emission (red trace with λ_{ex} = 340 nm) spectra of **40**. Sample was run as a 10 μM solution in DMSO.

In the case of comparing **40** with its calix[4]arene azine counterpart **34**, the emission spectrum of **40**, shown in Figure 3.32, is not markedly different to that shown by the other model azine **38**, although the bands observed are far less intense. The emission spectrum of **40** showed a very broad emission band with three discernible shoulders

141

present at 398, 422 and the most intense at 437 nm. The most distinguishable peak was at 398 nm and was used as the chosen wavelength to determine the excitation spectrum of **40**. It yielded an excitation spectrum with a single intense band at 274 nm with numerous less intense, broad side bands. One of these was distinguishable with an absorption maximum at 340 nm. A band at 340 nm was also the absorption maximum in the UV spectrum of benzazine **40**.

A direct comparison to the calix[4]arene derivative, **36** could not be made as the successful preparation of its benzazine analogue was not achieved.

3.7.4   Fluorescence of zinc(II) calix[4]arene and zinc(II) benzazine complexes 41, 42, 43, 44 and 45

After preparing and determining the fluorescent properties of both the calix[4]arene azines and their model benzazine counterparts, the focus moved to preparing the zinc(II) coordination complexes of these ligands. Successful isolation of the coordination complexes was partial, with only five complexes, **41**, **42**, **43**, **44** and **45** prepared, the proposed structures of which are displayed in Figure 3.33.
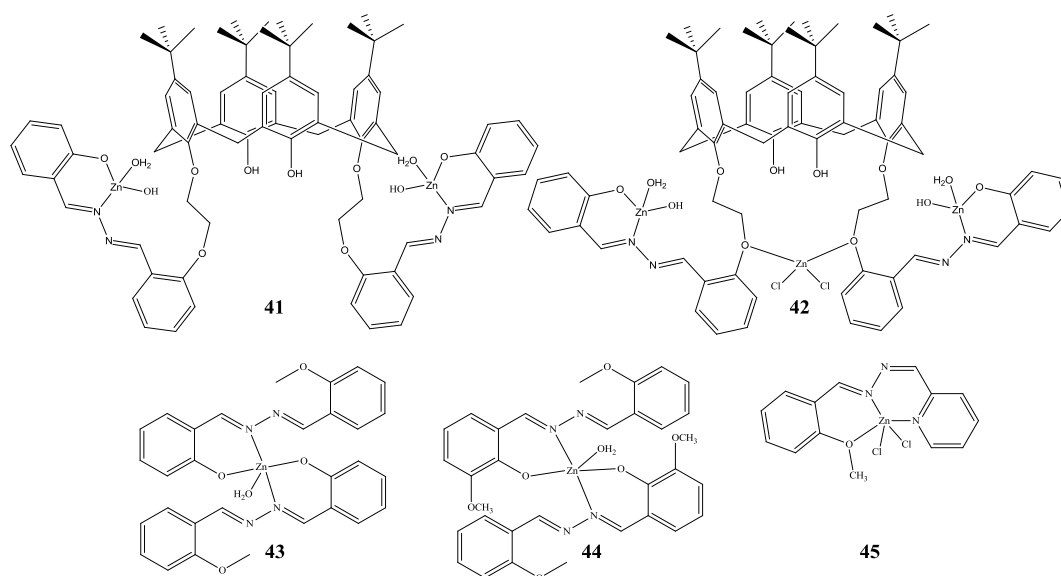
Figure 3.33: Proposed structures of zinc(II) azine complexes **41**, **42**, **43**, **44** and **45** used in fluorescence studies.

The zinc(II) coordination complexes proved to be much less soluble in a variety of solvents and it was for this reason that DMSO was chosen as the solvent in which to

conduct fluorescence studies. It also allowed direct comparison with the free ligands as solvent effects could be ignored.

Using the NMR and IR spectroscopic data as well as microanalysis, it was postulated that **41** had two zinc(II) ions present with one each distributed per pendant arm. The emission spectrum of **41** displayed a single band at 505 nm with excitation at 365 nm and showed an increase in emission intensity from the corresponding band in the free ligand **32**. The excitation spectrum was similarly uncomplicated with a single excitation band at 470 nm, but was far less intense, the intensity was scaled up by a factor of 100 to give the display shown in Figure 3.34. An indicator of the difference in fluorescence intensity between the free ligand and the ligand with the zinc(II) ion bound is the image in Figure 3.34 that shows ligand **32** and its zinc complex **41** under a UV lamp with a wavelength at 365 nm. The image shows the very noticeable difference in intensity upon binding the zinc(II) ion, something that could be of use if the calix[4]arene azine were to be developed as a selective fluorionophore.
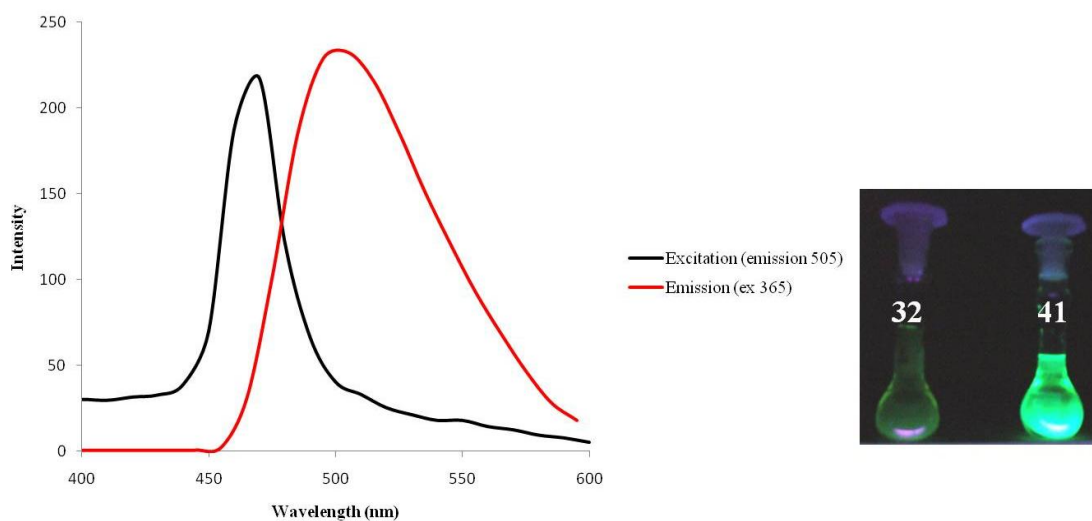
Figure 3.34: Excitation (black trace with λ_{em} = 505 nm) and emission (red trace with λ_{ex} = 365 nm) spectra of **41**. Sample was run as a 10 μM solution of its proposed structure in DMSO. The excitation spectrum was scaled up in intensity by a factor of 100. Also is physical appearance of DMSO solution of ligand **32** and its zinc(II) complex **41** under a UV lamp.

The trinuclear complex **42** was similar in that only one emission band was observed, at almost exactly the same emission wavelength as for **41**: at 504 nm. Similarly, the intensity of the emission was greater than that of the free ligand **32**. The emission band also had no observable side bands or shoulders. The excitation spectrum of **42**, however, was more complicated than the corresponding spectrum for **41** in that, in

addition to a broad, intense excitation band at 411 nm, also present was another broad and strong excitation band with a maximum intensity at 285 nm along with a weaker but discernible shoulder at approximately 316 nm. Both the excitation and emission spectra are displayed in Figure 3.35. From comparing the emission spectra of **41** and **42** it suggests that the third zinc atom situated between the pendant arms is not influencing fluorescent properties of the ligand. The UV absorption spectrum showed several strong absorption bands at 404, 344 and the most intense band at 292 nm.
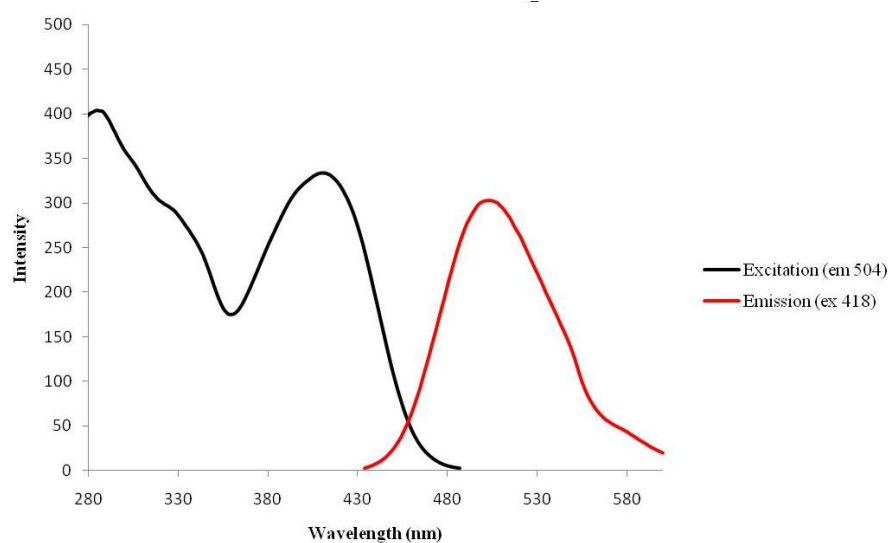
Figure 3.35: Excitation (black trace with λ_{em} = 504 nm) and emission (red trace with λ_{ex} = 418 nm) spectra of **42**. Sample was run as a 10 μM solution of its proposed structure in DMSO.

Given that the calix[4]arene azine zinc(II) complexes exhibited decent fluorophoric activity it could be assumed that the excitation and emission characteristics of the model benzazine zinc(II) coordination complexes would be somewhat similar. This proved to be the case for **43**, with a single broad, intense emission band detected at 493 nm when excited at 409 nm. A disappointing feature of the emission of the zinc(II) complex was that the intensity of the emission band was not augmented on zinc(II) complexation. The corresponding excitation spectrum of **43** similarly showed a strong, broad excitation band that dominated the spectrum at 409 nm. In addition to this, there are several weaker broader emission bands, two of whom may be identified at 300 and 328 nm. The excitation and emission spectra for **43** are shown in Figure 3.36. The UV absorption spectrum of **43** shows little absorption above 360 nm, with absorption maxima at 284 nm and 332 nm.
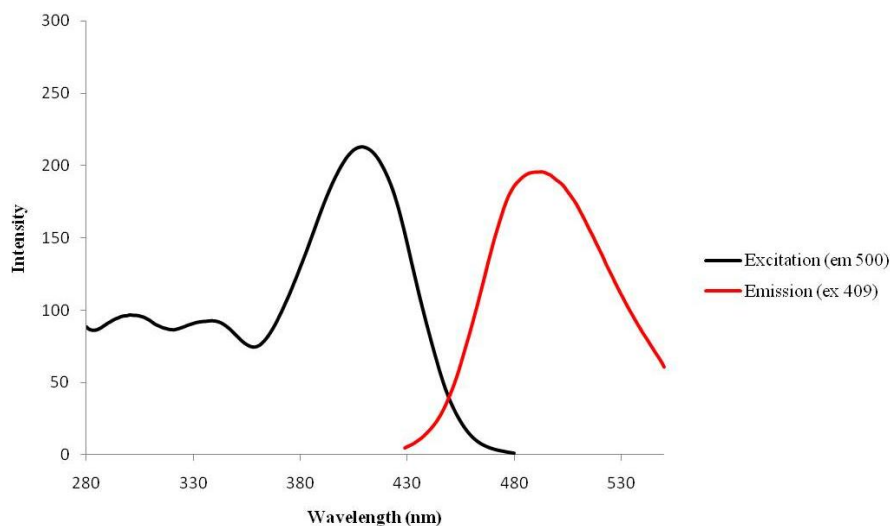
Figure 3.36: Excitation (black trace with λ_{em} = 500 nm) and emission (red trace with λ_{ex} = 409 nm) spectra of **43**. Sample was run as a 10 μM solution of its proposed structure in DMSO.

Encouraged by the fluorescence spectra obtained for **43**, it was hoped that the reaction of zinc(II) acetate with benzazine ligand **40** would yield another fluorescent coordination complex, that of **44**. Preparation of complex **44** was achieved in low to moderate yield. The emission spectrum of **44** shows a single broad emission band with a maximum intensity at 431 nm after excitation of the sample at 336 nm. There are some poorly defined shoulders on the emission band and assigning wavelengths to these proved difficult because of their weak intensities. One differing feature from the case of **44** when compared to **43** is that the intensity of the emission on complexation of the zinc(II) increases. This is in contrast to **43**, where no increase in the intensity of the emission is observed. Obtaining an excitation spectrum of **44** using 431 nm as an emission parameter yielded a single strong excitation band with a maximum intensity at 317 nm. The excitation and emission spectra of **44** are shown in Figure 3.37. Examining the UV absorption spectrum shows several weak bands with a maximum absorption at 336 nm.

The final zinc(II) complex to be examined was the compound prepared by the *in situ* formation of the 2-pyridine-2'-methoxybenzazine derivative, shown in Figure 3.38, followed by a solution of zinc(II) chloride to give the zinc(II) adduct, **45** as an orange solid. This yielded an emission peak with a maximum intensity at 418 nm, as can be seen in Figure 3.39. From this emission maximum the corresponding excitation spectrum was obtained. The excitation spectrum of **45** displayed two bands, one at 358

145

nm and another, stronger band at 286 nm, both of which are shown in Figure 3.39. The UV absorption spectrum of **45** exhibited several broad bands with the most intense band at 336 nm. A second, much weaker band was observed at 418 nm.
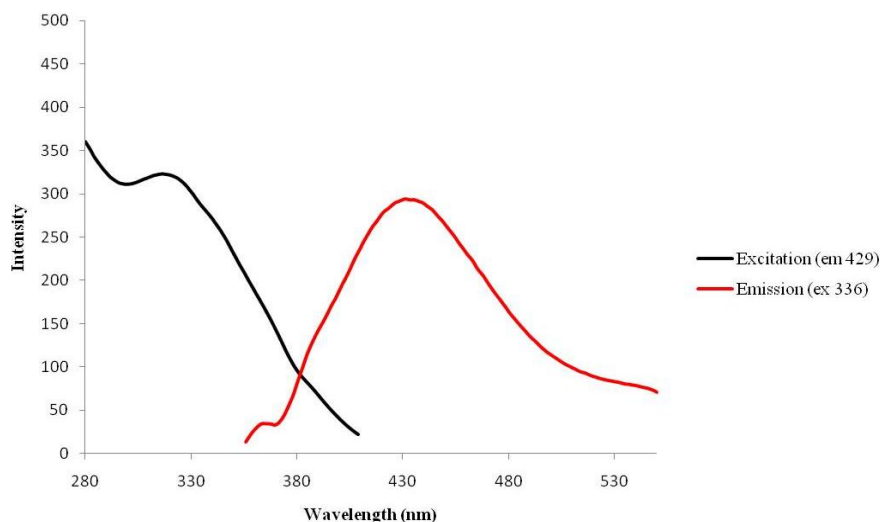
Figure 3.37: Excitation (black trace with λ_{em} = 429 nm) and emission (red trace with λ_{ex} = 336 nm) spectra of **44**. Sample was run as a 10 μM solution of its proposed structure in DMSO.
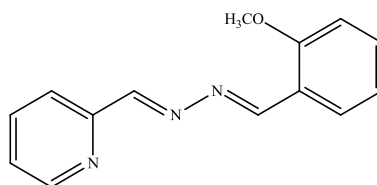
Figure 3.38: Azine derivative prepared *in situ* prior to addition of a solution of zinc(II) chloride to form the adduct complex **45**.
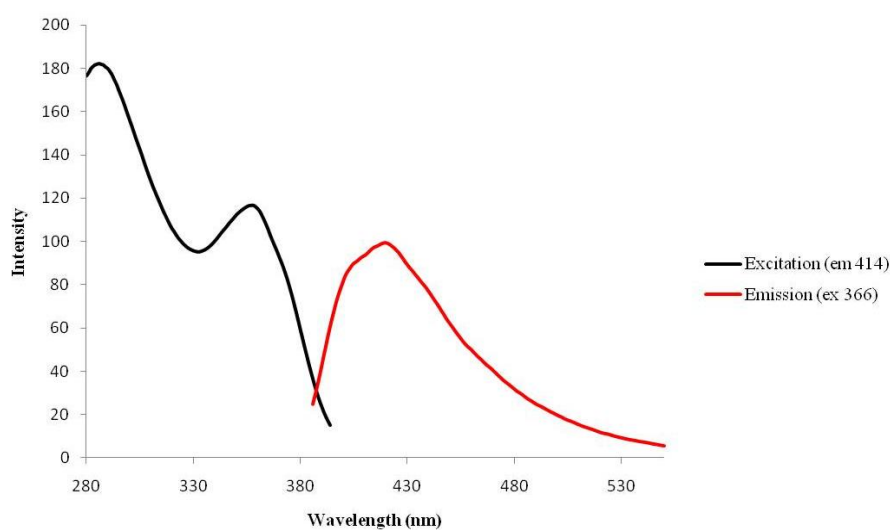
Figure 3.39: Excitation (black trace with λ_{em} = 414 nm) and emission (red trace with λ_{ex} = 366 nm) spectra of **45**. Sample was run as a 10 μM solution of its proposed structure in DMSO.

It would seem that when the lone pair on the pyridine nitrogen is occupied in binding to the metal, some fluorescence is observed. From these observations it can be proposed that the n $\rightarrow \pi^*$ transition is no longer the lowest energy transition. It has swapped with the lowest $\pi \rightarrow \pi^*$ transition meaning that radiative decay processes (emission) can now compete with the previously dominant non-radiative processes thus switching 'on' the fluorescence.

3.8 Synthesis and properties of 2-hydroxy-5-nitrobenzamide ligands and their metal complexes

3.8.1 Overview

The low solubility of the azines and their metal complexes, even in polar solvents like DMSO, led to the development of a metal binding site based on the amide moiety. This functional group provides, like the imine, a nitrogen donor atom. In conjunction with an adjacent oxygen, its binding possibilities extend to it acting as an ambidentate ligand, as shown in Figure 3.40, donating through either the amide nitrogen or the carbonyl oxygen. The amide functional group also has the added attraction of being far less susceptible to hydrolysis than the imine. Amides will hydrolyse, but require far more stringent conditions to do so. The presence of a donor atom at the *ortho* position is retained, by virtue of the oxygen atom of the hydroxy group. The nitro group, being of a polar nature, was expected to provide some much needed hydrophilic property to the ligand, as was the terminal amine which has hydrophilic character.
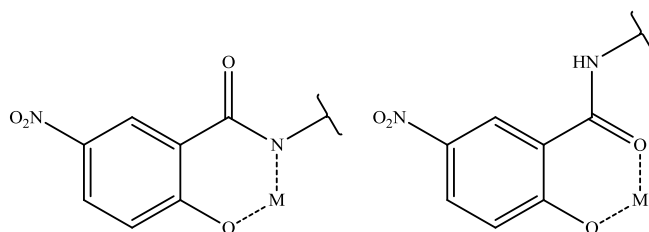
Figure 3.40: Possible bidentate binding modes of amide moiety with an adjacent oxygen atom.

The ligands prepared were *N*-(2-aminoethyl)-2-hydroxy-5-nitrobenzamide: **46**, and its hydrochloride salt: **47**, from commercially available starting materials and were characterised by NMR and IR spectroscopy and X-ray crystallography.

Metal complexation reactions were carried out using **46** in either a metal-to-ligand ratio of 1:2 or 2:1 with the following metal salts: copper(II) perchlorate hexahydrate, copper(II) chloride dihydrate, copper(II) acetate monohydrate, zinc(II) perchlorate hexahydrate, zinc(II) chloride and zinc(II) acetate dihydrate. Other complexation reactions were performed, but these gave less encouraging results and involved the use of the following: nickel(II) perchlorate hexahydrate, nickel(II) chloride hexahydrate, nickel(II) acetate tetrahydrate, manganese(II) perchlorate hexahydrate, manganese(II) chloride hexahydrate, manganese(II) acetate tetrahydrate, iron(III) perchlorate hexahydrate, iron(III) chloride hexahydrate and silver(I) perchlorate. The full range of complexation reactions carried out is summarised in Scheme 3.9.
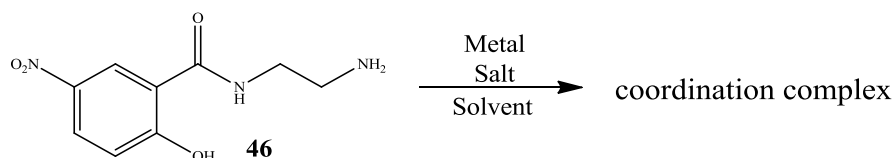
Scheme 3.9: Summary of complexation reactions carried out using ligand **46** (left) with metal ions being either Cu^{+2}, Ni^{+2}, Zn^{+2}, Mn^{+2}, Fe^{+3} or Ag^+ and the counterion being either AcO^-, Cl^- or ClO_4^-. Reaction solvents were either H_2O or CH_3CN.

Reactions were performed in two solvents: water or acetonitrile, to determine whether solvent effects were responsible for the orientation of the metal's coordination mode. A stoichiometric amount of base (supplied in the form of sodium hydroxide) was required for certain complexation reactions, namely the reactions with nickel(II) perchlorate and chloride, and the zinc(II) and silver(I) metal salts mentioned above. The complexation reactions involving the manganese(II) salts resulted in no reaction occurring. Iron(III) salts gave a dark red/orange solution when carried out in water. Several attempts were made to initiate precipitation of the benzamide complex, including anion metathesis, but all attempts were unsuccessful.

X-ray crystal structures of copper benzamide complexes were determined in two cases, a six-coordinate octahedral complex and a four-coordinate square planar complex, both of which will be discussed in detail later in Sections 3.8.12 and 3.8.13.

148

3.8.2 Synthesis and characterisation of *N*-(2-aminoethyl)-2-hydroxy-5-nitrobenzamide, 46, and its hydrochloride salt, 47

Ligand **46** was synthesised from the commercially available starting materials, methyl-2-hydroxy-5-nitrobenzoate and ethylene diamine. These were heated to reflux for four hours in a 1:1 toluene:methanol solvent mixture, as outlined in Scheme 3.10. On reaching reflux temperature a yellow precipitate formed. After cooling the yellow suspension was filtered to isolate the yellow solid. The mono benzamide product was formed exclusively, with no di-benzamide by-product formation taking place, the reasons for which will be explained at a later stage. The dried powder was analysed using NMR spectroscopy and found to be the required product.
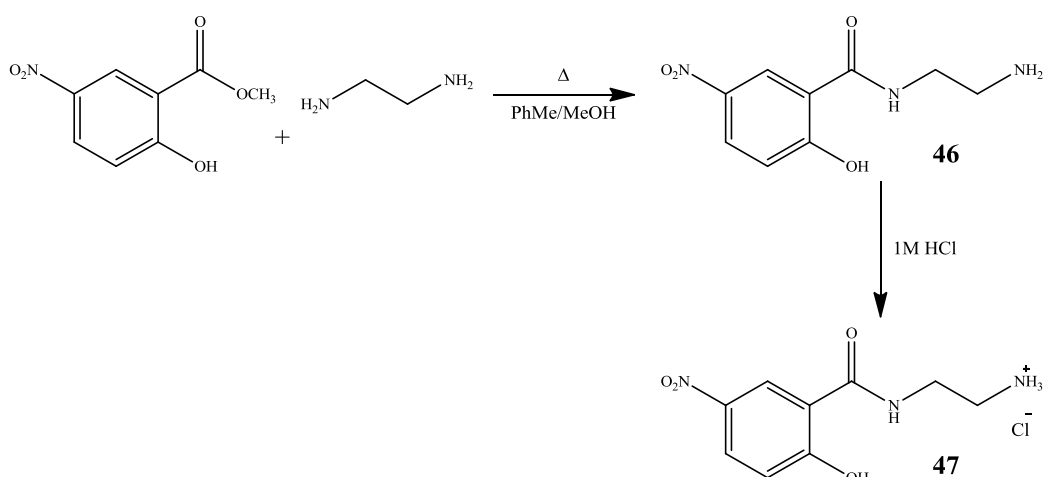
Scheme 3.10: Synthesis of ligands **46** and **47** showing reactants and conditions used.

The ^{1}H NMR spectrum of the benzoate starting material showed a signal representing the methyl protons of the ester group at 3.91 ppm. This peak was not present in the ^{1}H NMR spectrum of the product (shown in Figure 3.41). Instead it was replaced by a triplet at 11.43 ppm, which represents the hydrogen of the newly formed amide. Also present were two additional signals in the spectrum which were a multiplet at 3.50 ppm and a triplet at 2.96 ppm, both representing the protons of the CH_2 groups. The triplet represents the CH_2 bonded to the terminal amine, but coupling to the NH_2 protons is not exhibited in the splitting pattern. The aromatic region shows three signals that represent the aromatic protons. The splitting pattern corresponds well with the substitution pattern of the ring. The chemical shifts of these protons, which are labelled H_a, H_b and H_c, as shown in Figure 3.42, are in good agreement with the electronic effects of the amide, nitro and hydroxyl functional groups. H_a resonates at

8.65 ppm and its signal appears as a doublet with a coupling constant J_{ab} = 3.3 Hz, which is within the range for *meta* coupled protons. The signal for H_b appears as a doublet of doublets at 7.80 ppm courtesy of it coupling to both H_a and H_c. The magnitude of the coupling constants for H_b are the reciprocal coupling constant J_{ba} = 3.3 Hz and the *ortho* coupling value of J_{bc} = 9.5 Hz, both of which are within expected ranges. H_c resonates at 6.27 ppm and its signal is observed as a doublet with a coupling constant of J_{cb} = 9.5 Hz. The phenolic proton is not observed in the spectrum, but because the sample was run in d_6-DMSO, it is assumed that it is hidden by the water peak.
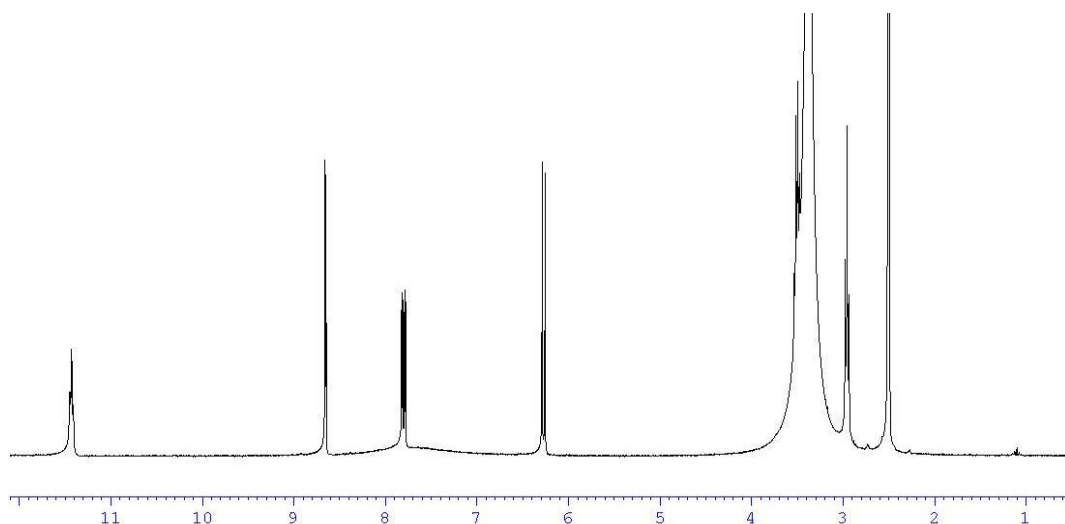
Figure 3.41: ^{1}H NMR spectrum of **46** run in d_6-DMSO with x-axis in ppm.
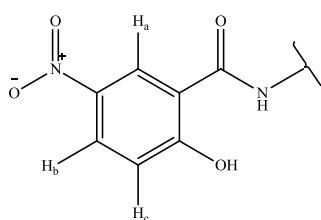
Figure 3.42: Numbering key for protons on aromatic ring of **46**.

The ^{13}C NMR spectrum supports the data provided by the ^{1}H NMR spectrum, with 9 peaks present thereby confirming that asymmetry exists within the molecule. The ^{13}C NMR spectrum also exhibits a peak at 178.2 ppm, which represents the amide carbonyl carbon. This peak was observed instead of the ester carbonyl peak at 166.2 ppm, which is present in the ^{13}C NMR spectrum of the benzoate starting material.

The IR spectrum of the starting material contains a strong absorption band at 1679 cm^{-1} which is indicative of the carbonyl C=O stretch of the ester. In the IR spectrum of **46**, the ester carbonyl stretch has been replaced by a strong absorption band at 1626 cm^{-1} which represented the C=O stretch of the amide. One of the NO stretches of the nitro was also assigned as a strong absorption band that was present at 1298 cm^{-1}, however due to overlapping bands it proved difficult to assign the second stretch of the nitro group with any confidence. Recrystallisation of **46** from water yielded crystals suitable for X-ray diffraction. The results of this will be discussed in Section 3.8.3. Elemental analysis confirmed the constitution of the yellow solid to be consistent with those calculated.

The hydrochloride salt of **46** was prepared by adding a hydrochloric acid solution to an aqueous suspension of **46**, as shown in Scheme 3.10. This addition resulted in the dissolution of the yellow reactant and disappearance of the yellow colour. The colourless solution was allowed to reduce and this resulted in the precipitation of a white solid, which analysed as the hydrochloride salt, **47**. The NMR and IR spectral data of the white solid confirmed its constitution.

The ^{1}H NMR spectrum differed from **46** in that the signal representing the phenolic proton was now visible, occupying a downfield position at 13.45 ppm. The amide proton's resonance had shifted to a more upfield position and resonated at 9.28 ppm. The ethyl fragment's CH$_2$ protons were also visible as two multiplets at 3.61 and 3.02 ppm, their splitting altered by virtue of the newly protonated amine NH$_2$, which is now existing as an ammonium R-NH$_3^+$. The R-NH$_3^+$ protons themselves were exhibited by the broad signal visible at 8.17 ppm whose downfield position confirmed the deshielding effect of the full positive charge situated on the nitrogen atom. The aromatic region retained the three signals for the aromatic protons, as mentioned in the discussion of **46**.

The ^{13}C NMR spectrum of **47** was broadly similar to its parent compound **46**. The amide carbon signal now occupied an upfield position, moving from 178.2 to 166.9 ppm, the reasons for which will be revealed later in Sections 3.8.3 and 3.8.4 when the X-ray structures of **46** and **47** will be discussed. The spectrum contained nine signals, representing the nine inequivalent carbons and confirming the existence of asymmetry within the ligand.

The IR spectrum showed a strong absorption band at 1641 cm^{-1} which corresponded to the C=O stretch of the amide. The microanalytical results confirmed the white solid to be **47**, which is consistent with calculated values.

3.8.3   X-ray crystal structure of 46

Ligand **46** was isolated as a yellow solid. The solid was soluble in hot water and a hot saturated solution was prepared. Crystals suitable for X-ray crystallographic analysis were grown from a cooled solution by the method of slow evaporation. The structure, shown in Figure 3.43, exists as a zwitterion, with the hydroxyl proton migrating to the terminal amine nitrogen N(3) to form the cationic ammonium ion. This also explains why the signal for the hydroxyl proton is not observed in the ^{1}H NMR spectrum. The proton migration also explains why the asymmetric monoamide derivative was preferentially formed and not the symmetrical diamide. The first amide bond is formed and the proton is transferred to the terminal amine. This confers a full positive charge on the nitrogen, which renders it non-nucleophilic and prevents the diamide derivative from forming.
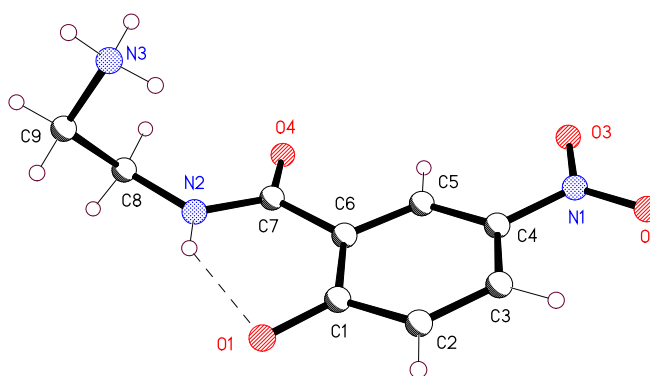
Figure 3.43: X-ray crystal structure of **46**.

There is a hydrogen bond interaction between the oxygen anion and the amide hydrogen, N(2)H(2)···O(1) with a value of 2.7047(15) Å. The proton is shown by a difference map to be localised on the amide nitrogen, revealing that the oxygen O(1) possesses a negative charge. The phenoxy bond (O(1)C(1) is very short at 1.3003(16) Å when compared to the typical C-O bond length of a phenol moiety, which is 1.362 Å.[129]

There is extensive hydrogen bonding in the crystal lattice forming either six-, eight-, or fourteen-member ring systems. The terminal ammonium group is involved in three hydrogen bonds, as can be seen in Figure 3.44. Two of the protons form interactions with the phenoxy oxygen of adjacent benzamide molecules, while the third interaction is with a neighbouring amide carbonyl oxygen. The benzamide molecules form a layered structure, with the amide, nitro group and aromatic ring all lying in the same plane. The aliphatic chain with the ammonium nitrogen lies outside this plane. The aromatic rings overlap each other, forming layers held together by π-stacking interactions with an average centroid to centroid distance of 3.427 Å. The aplanar ammonium group link these layers together by their hydrogen bonding, which was described previously.
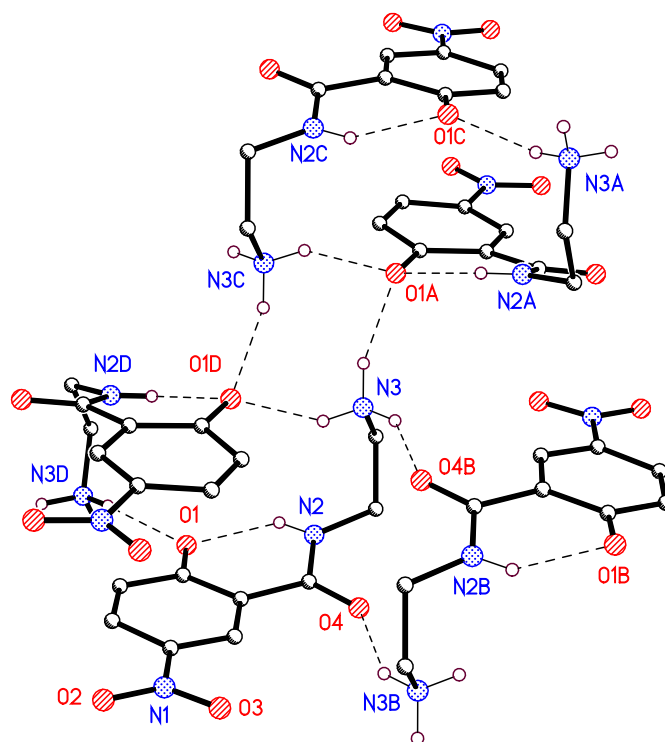
Figure 3.44: Partial packing diagram for **46** showing hydrogen bonding interactions.

3.8.4   X-ray crystal structure of 47

The hydrochloride salt, **47**, was prepared by adding 1 M hydrochloric acid solution to an aqueous suspension of **46**. Initially, the acid was added until the solid disappeared and was then followed by the disappearance of the yellow colour from solution. The solvent from this colourless solution was allowed to reduce after which a white solid

precipitated. Crystals suitable for X-ray crystallographic analysis were grown from an aqueous solution of **47** by the method of slow evaporation

The structure, shown in Figure 3.45 is a charged species and contrasts to the zwitterionic nature of **46**. The proton, previously absent in **46**, has been restored to the phenoxy oxygen and now participates in a hydrogen bond (O(1)H(1)···O(4)) with the amide oxygen. This bond has a value of 2.547(2) Å. The hydrogen H(1) which is localised on the oxygen O(1), results in the lengthening of the O(1)C(1) bond to 1.339(2) Å, and compares favourably with the average phenoxy C-O bond length of 1.362 Å.[129]
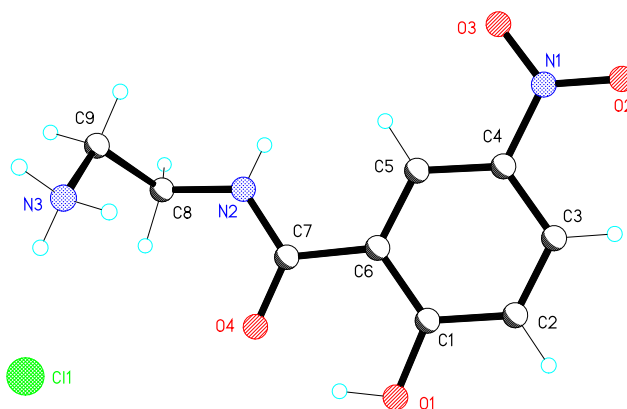
Figure 3.45: X-ray crystal structure of **47**.

A point of note is the orientation of the amide arm. The carbonyl has rotated inward toward the phenolic oxygen to form a hydrogen bond. This is in contrast with the conformation adopted by the amide moiety in the X-ray crystal structure of **46**. In this case the carbonyl group is pointing outward and away from the phenolic oxygen. This would suggest that the amide, along with the adjacent phenoxy oxygen, provides a potential ambidentate metal binding site simply by varying the pH of the reaction system which can coordinate to a metal ion through the phenolic oxygen and through either the nitrogen or the oxygen atom of the amide.

The crystal packing, shown in Figure 3.46 consists of sheets of the molecule held together by hydrogen bonding and runs diagonally across the unit cell. The chloride anion functions as a hydrogen bond acceptor, with interactions between it and three symmetry-related $R-NH_3^+$ groups at an average distance of 3.175 Å. The cations are

paired by two symmetry-related hydrogen bonds: N(2)H(2)⋯O(3) with a distance of 2.999 Å.
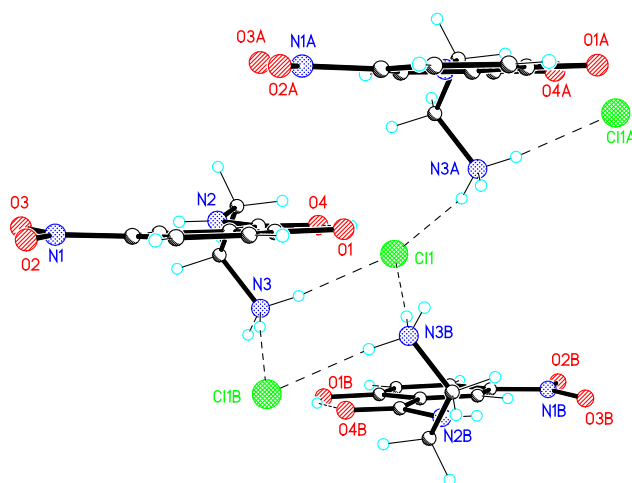
Figure 3.46: Partial crystal packing diagram for **47** showing hydrogen bonding interactions.

3.8.5   Reactions of copper(II) perchlorate hexahydrate and benzamide 46

Copper(II) complexes of **46** were prepared from aqueous solutions of the copper(II) salts and the benzamide ligand in either a 1:2 or 2:1 metal-to-ligand ratio.

A copper(II) perchlorate solution was added to an aqueous solution of **46** in a 2:1 metal-to-ligand ratio to form a green solution. Upon reduction of the solvent a green crystalline solid, **48**, precipitated as shown in Figure 3.47.
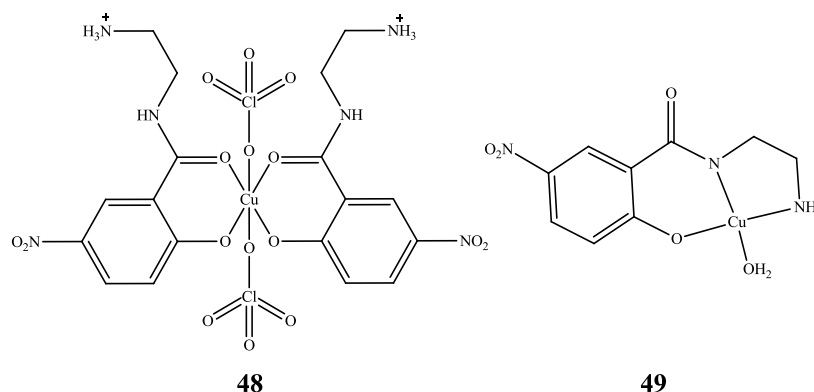
Figure 3.47: Structures of two isolated products from the reaction of **46** with copper(II) perchlorate hexahydrate: a green solid **48** and a brown solid, **49**.

IR spectroscopy revealed that the C=O stretch of the amide shifted from 1626 cm^{-1} in the starting material to a lower wavenumber (1610 cm^{-1}) in the copper(II) complex.

This indicates a weakening of the amide bond, suggesting it forms a coordination bond to the metal ion. The starting copper(II) perchlorate has a strong absorption band at 1081 cm^{-1} due to the perchlorate anion. A strong absorption band was also present at 1075 cm^{-1} in the IR spectrum of **48** which suggests that the perchlorate anion is present in the complexation product. Microanalysis of the green solid suggests a complex with a metal-to-ligand ratio of 1:2. Crystals suitable for X-ray crystallographic analysis were grown using the slow evaporation technique from an aqueous solution of **48**. This analysed as the bis(*O,O'*-2-hydroxy-5-nitro(*N*-2-aminoethyl)benzamide) copper(II) perchlorate complex **48**, shown in Figure 3.47 and whose structure will be discussed in Section 3.8.12.

A similar reaction was also carried out to form **49** with the only alteration being a 1:2 metal-to-ligand ratio. This resulted in the formation of a brown solid along with the precipitation of surplus starting material. The brown solid was isolated and characterised to be **49**, whose structure is shown in Figure 3.47. Its IR spectrum revealed several noticeable differences to the IR spectrum of **48**. The strong absorption band at 1075 cm^{-1}, characteristic of the perchlorate anion is now absent in the new product **49**. In addition, the C=O amide stretch is present as a medium absorption band at 1609 cm^{-1}, having shifted from 1626 cm^{-1}, the corresponding position of the C=O absorption band in the starting material. The weak absorption suggests that the amide is involved in extensive hydrogen bonding. Microanalysis of the brown solid showed that the perchlorate was not present and suggested that the benzamide ligand possessed a formal charge of −2 to form a complex with the copper(II) ion. This hypothesis was proven correct when the X-ray crystal structure of the brown solid **49** was solved. The X-ray data will be discussed in Section 3.8.13.

Metal complexation reactions were also carried out in acetonitrile. This gave a green precipitate that analysed very similar to **48** with an acetonitrile molecule included in the matrix.

3.8.6   Reactions of copper(II) chloride dihydrate and benzamide 46

Copper(II) chloride dihydrate was reacted with **46** in a 2:1 metal-to-ligand ratio in water. This resulted in a green solution, followed by the formation of a green precipitate. The green solid was removed by filtration and dried to give **50**. The IR

spectrum of the complex was very similar to **48**, apart from the obvious differences in the anions. This would suggest that the copper(II) ion is occupying a coordination mode very similar to the copper(II) perchlorate analogue, i.e. an octahedral geometry, with the two chloride ions occupying the axial positions.

The reaction was repeated in acetonitrile giving a light green solid. Using IR spectroscopy, the solid analysed was very similar to the green solid formed in the aqueous preparation: **50**. Microanalysis confirmed the composition of the sample to be identical to **50**.

3.8.7   Reactions of copper(II) acetate monohydrate and benzamide 46

Copper(II) acetate was dissolved in water and added to the suspension of **46** in a similar manner to the copper(II) perchlorate and copper(II) chloride benzamide complexes. This resulted in the immediate precipitation of a purple/brown solid with a near identical IR spectrum to **49**. Microanalysis confirmed that the brownish solid was the square planar copper(II) complex of *N*-(2-aminoethyl)-5-nitro-2-hydroxybenzamide. At no point was the formation of a six-coordinate copper(II) species detected.

This copper(II) acetate complexation reaction was also performed in acetonitrile, and yielded a green solid: **51** illustrated in Figure 3.48. The IR spectrum reveals that the solid is not the square planar copper(II) complex **49**. There are strong absorption bands at 1600 cm^{-1} which is a similar absorption band for the amide C=O stretch observed in the metal complexes prepared above, and also a band at 1573 cm^{-1} which may or may not overlap with the acetate anion. Based on literature wavenumber values for the acetate O-C=O stretching modes, it is most likely that the acetate anion occupies a bridging role.[124] This results in the formation of an acetate bridged symmetrical dinuclear copper(II) complex, shown in Figure 3.48. This is a plausible structure as bridging acetate ions are well known.[130] Microanalysis of the solid supports the proposed structure with the *N*-(2-aminoethyl)-5-nitro-2-hydroxybenzamide molecule functioning as a tridentate ligand. A molecule of solvent (acetonitrile) completes the coordination sphere, giving the copper(II) cation an octahedral environment. Attempts were made to grow crystals of **51** from other solvent systems, but proved fruitless.
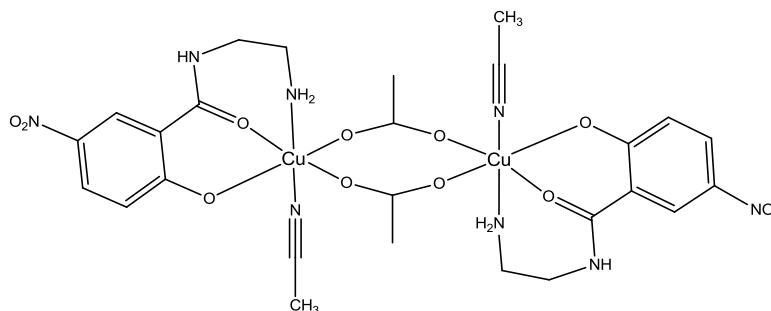
Figure 3.48: Proposed structure of **51** from the reaction of **46** and copper(II) acetate in an acetonitrile solvent showing both the bridging acetate anions and coordinated solvent.

3.8.8   Reaction of nickel(II) perchlorate hexahydrate and benzamide 46

The nickel(II) perchlorate reaction required the use of sodium hydroxide to enable complexation to occur. Trial reactions showed that the nickel(II) ion did not complex to the benzamide ligand without the presence of the base. Successful complexation of the metal produced a light green solid: **52** whose proposed structure is shown in Figure 3.49.
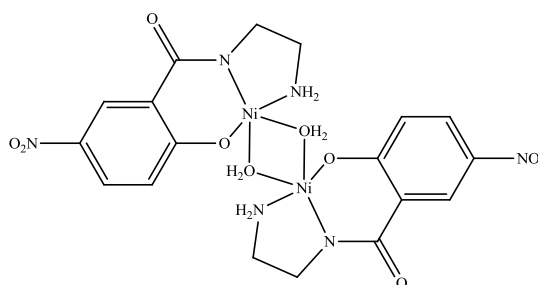
Figure 3.49: Proposed structure of **52**.

The IR spectrum confirmed the loss of the perchlorate counterion by the absence of the strong absorption band in the region around 1100 cm^{-1}. The C=O amide absorption band, present at 1626 cm^{-1} in the IR spectrum of **46** has been replaced by a strong absorption band at 1611 cm^{-1} in the IR spectrum of **52**. Its shift to a lower wavenumber results from the amide nitrogen's donation into the nickel(II) ion and results in the weakening of the C=O bond. Microanalysis of the green solid supported the spectroscopic evidence of the absence of the perchlorate ion. The bridging water ligands mean that each nickel(II) centre most likely exhibits a highly distorted trigonal bipyramidal geometry, owing to the conformational constraints imposed by the tridentate benzamide ligand. Bridging water molecules between metal centres have

158

been observed previously.[131] The proposed complex (a dinuclear coordination compound) is supported by the magnetic susceptibility data obtained which gives a value of 2.79 B.M. and compares favourably with the ideal value for a nickel(II) ion centre (using the spin only formula) of 2.83 B.M.

3.8.9 Reaction of nickel(II) chloride hexahydrate and benzamide 46

A similar procedure to that for the nickel(II) perchlorate reaction with the benzamide ligand was used in the preparation of **53**. Immediately after the addition of the nickel(II) chloride solution a yellow/brown solid formed. This solid was dried and was analysed using IR spectroscopy, microanalysis and magnetic susceptibility. The IR spectrum revealed that the amide moiety is involved in metal ligation, the result of which saw the amide carbonyl stretch shifting to a lower wavenumber: 1615 cm^{-1}. Microanalysis reveals the presence of a coordinated water molecule, and a 1:1 metal-to-ligand ratio. Based on trends in the literature, the proposed structure of the complex, shown in Figure 3.50, is most likely a dinuclear chloride bridged dimeric species, where the metal ion is in an octahedral geometry.[132]
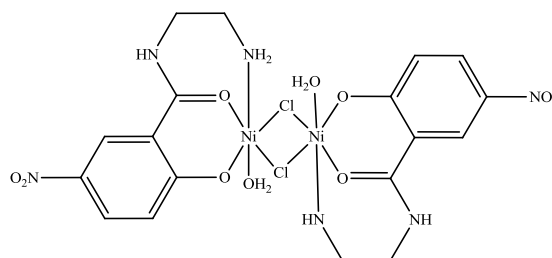
Figure 3.50: Proposed structure of **53**.

The magnetic susceptibility measurements confirm the presence of the nickel(II) ion with a magnetic moment of 3.45 B.M.

3.8.10 Reaction of nickel(II) acetate tetrahydrate and benzamide 46

The nickel(II) acetate complexation reaction was the only nickel derivative that did not require sodium hydroxide in the system for complexation to occur. The reaction proceeded readily using solutions of the benzamide and nickel(II) acetate. A precipitate started to form from the solution within two minutes and was removed by filtration within ten minutes. This yellow/green solid, **54**, was shown using

microanalysis to be the only mononuclear complex in this series of reactions, with a metal-to-ligand ratio of 1:2. The proposed structure is shown in Figure 3.51.
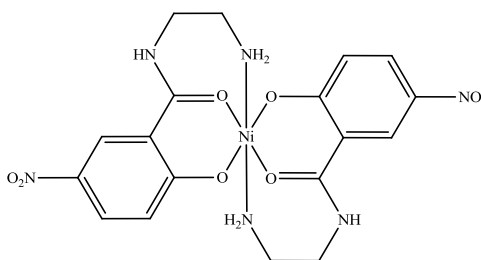
Figure 3.51: Proposed structure of **54**.

The IR spectrum of the green solid revealed that, as with the case of the previous nickel(II) complexes, the amide is involved in binding to the metal, shown by its lower wavenumber of 1614 cm^{-1}. The two benzamide ligands function in a tridentate fashion, with the amide and phenoxy functional groups situated opposite each other thus forming the asymmetric skeleton of the complex of the proposed structure. The octahedral coordination sphere is completed by the terminal amine groups occupying the two axial positions. Magnetic susceptibility measurements confirmed the presence of only one nickel(II) ion, with a magnetic moment reading of 3.03 B.M. which, similar to the nickel(II) derivatives previously discussed, compares favourably to the calculated value of 2.83 B.M.

3.8.11 Reaction of zinc(II) perchlorate hexahydrate and zinc(II) acetate dihydrate with benzamide 46

Preparation of the zinc coordination compounds required the use of sodium hydroxide, as no complexation was observed in the absence of the base. The aqueous zinc perchlorate solution was added to the alkaline benzamide solution (prepared by adding a stoichiometric equivalent of base to the ligand) and resulted in the immediate precipitation of a yellow solid. After an hour the solid, **55**, shown in Figure 3.52, was isolated and dried. The diamagnetic nature of zinc(II) compounds allowed the use of ^{1}H NMR spectroscopy to study the complex in solution. Poor solubility necessitated the use of d_6-DMSO to dissolve the sample.

The ^{1}H NMR spectrum of **55** showed several differences from the corresponding spectrum of **46**. The most obvious change is the signal representing the amide proton

resonance, present in the proton spectrum of the starting material at 11.43 ppm ,is not observed in the ^{1}H NMR spectrum of **55**. Its absence is corroborated by the splitting pattern of the proton signals that represent the ethyl chain. These CH_2 groups are observed as multiplets and triplets in the ^{1}H NMR spectrum of the benzamide, but are now represented by broad signals in the corresponding spectrum of **55**. Also, the three aromatic proton resonances are still visible. The coordination of the metal to the benzamide ligand resulted in all the proton resonances exhibiting a lower field chemical shift.
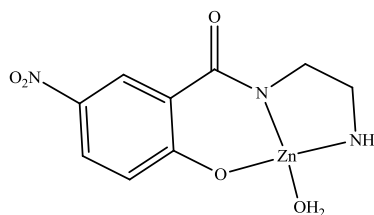
Figure 3.52: Proposed structure of **55**.

The IR spectrum of **55** reveals the absence of the perchlorate anion, shown by the lack of strong absorbance bands around 1100 cm^{-1}, demonstrates that the ligand is functioning as a dianion, with the loss of protons from the hydroxy and amide functional groups providing the necessary charge. The spectrum is quite similar in appearance to the IR spectrum of **49**, whose X-ray crystal structure has been determined. The copper(II) ion is situated in a square planar environment with the benzamide taking the role as an anionic tridentate ligand. A single molecule of water completes the coordination sphere. Using this information, along with corroborating microanalytical results, the proposed structure of **55** places the zinc(II)ion in a square planar environment as seen in Figure 3.52, with the ligand playing an identical role to the copper(II) complex derivative. A single molecule of water, as before, occupies the fourth coordination site.

A similar result was obtained with zinc(II) acetate dihydrate. Using the same conditions, apart from the metal salt used, the reaction of **46** with zinc(II) acetate dihydrate in the presence of sodium hydroxide yielded the same metal complex as seen when zinc(II) perchlorate was used, i.e. complex **55** was formed. IR spectroscopic data and microanalysis of the yellow solid was used to confirm this.

3.8.12 X-ray crystal structure of 48

Complex **48** was prepared using a 2:1 metal-to-ligand ratio of copper(II) perchlorate hexahydrate and ligand **46** in water to give a green solution. Slow evaporation of the solvent yielded green crystals suitable for crystallographic analysis, and subsequent structural characterisation of **48**.

The asymmetric unit, as seen in Figure 3.53, shows the copper(II) ion in an octahedral environment with two perchlorate ions occupying the axial positions with the two ligands forming an equatorial plane. The charge of the complex is balanced by virtue of protonation of the amine group, forming the R-NH$_3^+$ ammonium and the copper(II) cation, which are counter balanced by the two phenoxy moieties and the perchlorate anions. The perchlorate anions are disordered and were modelled with a 60:40 occupancy over two overlapping sites. The benzamide ligands are orientated such that the aliphatic arms lie on the same side. In effect they are *cis* to each other, but point in opposite directions to each other. It could be expected that having the ligands bind in such a way would result in the pendant arms occupying space on opposite sides, or *trans* to each other and would consequently reduce the likelihood of steric clashing of the pendant arms. The fact that this does not occur suggests that the hydrogen bonding interaction between the ammonium group N(3) and the water molecule O(1W) is in some way responsible for its orientation.
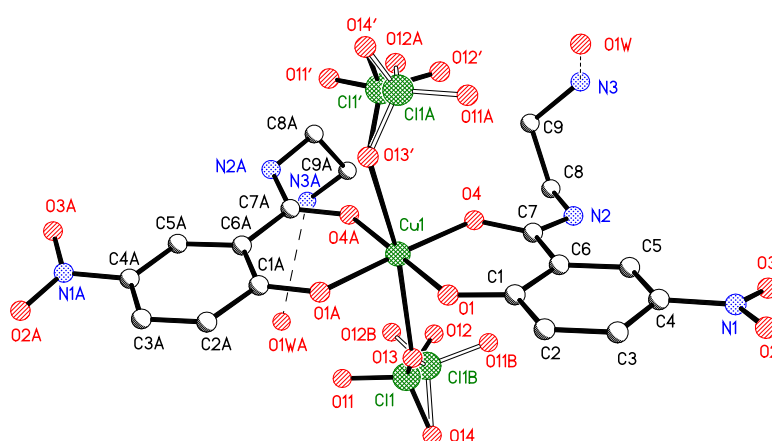
Figure 3.53: X-ray crystal structure of **48**.

Analysis of the crystal packing diagram reveals an intricate web of hydrogen bonding interactions, with the molecules linked into hydrogen bonded chains by the water solvate molecule, as shown in Figure 3.54. Intermolecular interactions also occur

between the ammonium groups and adjacent amide carbonyl and phenoxy atoms, as well as between the amide nitrogen and an adjoining perchlorate oxygen and these are not displayed for clarity purposes.
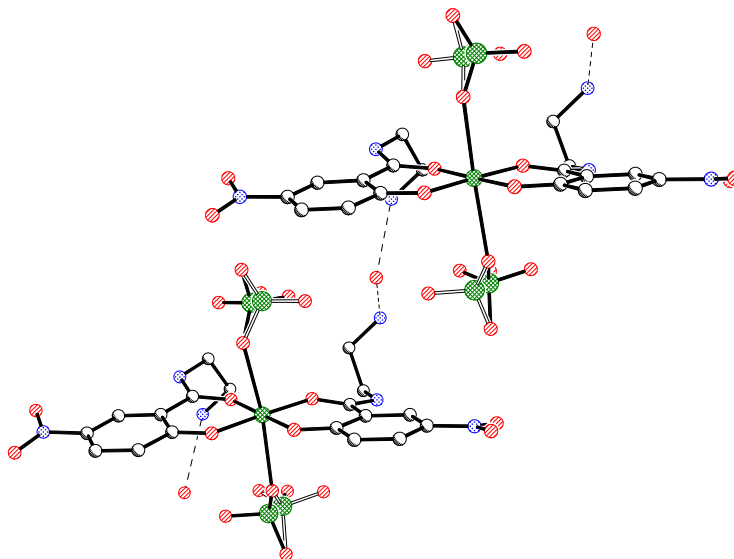
Figure 3.54: Partial crystal packing diagram of **48** showing hydrogen bonding interactions.

3.8.13 X-ray crystal structure of 49

Whereas **48** was prepared using **46** and copper(II) perchlorate hexahydrate in a 2:1 metal-to-ligand ratio, **49** was similarly prepared using the same reactants but in a metal-to-ligand ratio of 1:2. This yielded a brown solid: the copper(II) complex, shown in Figure 3.55, along with the precipitation of excess ligand. The brown solid was isolated and crystals of it that were suitable for X-ray crystallographic analysis were grown from an aqueous solution using the slow evaporation method.
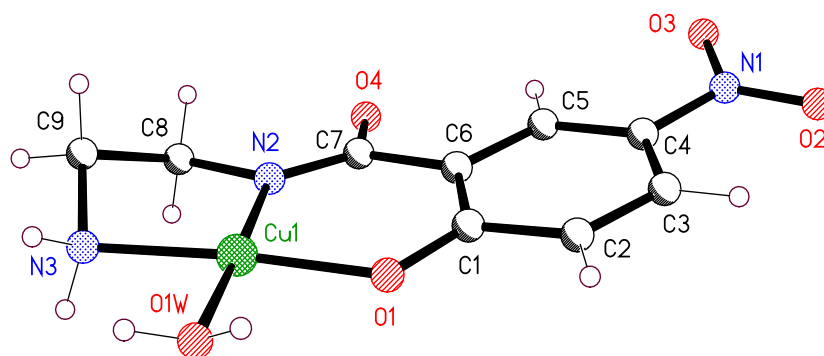
Figure 3.55: X-ray crystal structure of **49**.

The asymmetric unit, shown in Figure 3.55, revealed that the copper(II) ion is situated in a square planar geometry, with the ligand also supplying the counter anionic charges *via* its deprotonated phenol and amide moieties. These two charged atoms provide two coordination sites with the remaining two filled by the terminal amine and a solvent water molecule. Deprotonation of compartmental ligands, and as a consequence the demonstration of similar binding modes, are frequently observed in the literature, although in some cases the proton is lost through the introduction of a base, such as piperidine or triethylamine.[94,133] This mode of coordination through the deprotonated amide has also been observed before in hydroxamic acids, although in their case deprotonation more commonly occurs at the terminal hydroxide, with subsequent ligation of the metal occurring *via* the oxygens of the amide and the terminal hydroxide. As a result of this, the hydroxamate forms stable five-member chelate rings.[134] This type of coordination (through the amide carbonyl oxygen) mode would be unsuitable in the case of **49**, as it would form comparatively unstable six- and seven-member chelate rings, as opposed to the five- and six-member rings observed.
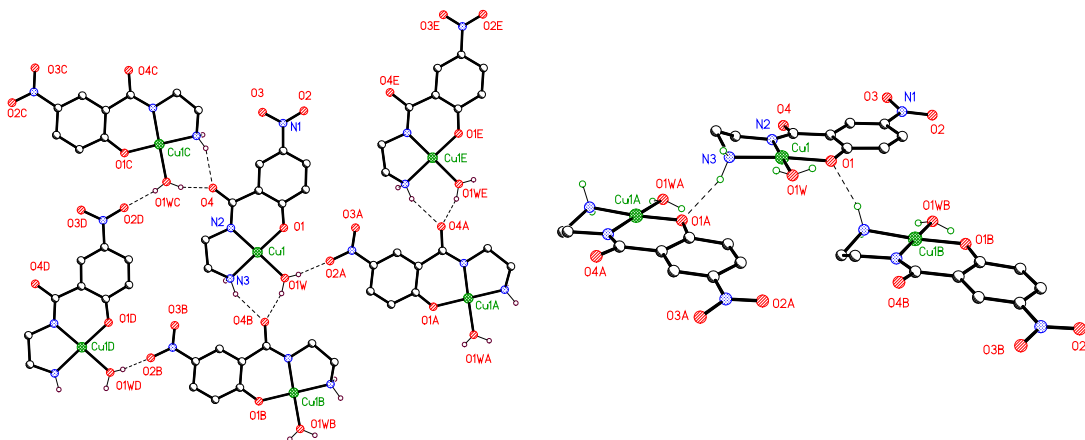
Figure 3.56: Partial crystal packing diagrams of **49** showing hydrogen bonding interactions.

Analysis of the crystal packing, as seen from two different angles in Figure 3.56, reveals that the overall structure consists of double layers composed of hydrogen bonding interactions between the bound water molecule and adjacent nitro and amide functional group of neighbouring molecules. The amine group is also implicated in hydrogen bonding interactions with the carbonyl oxygen of adjoining molecules. The amine group forms an additional hydrogen bond to an adjoining phenoxide oxygen, thereby forming the double layer sandwich. As a result of these aforementioned

interactions, there is no possible interaction between the copper ion and any other atom, which supports the fact that it lies in a 4-coordinate square planar geometry.

3.9 Synthesis and properties of calix[4]arene benzamide ligands and their metal complexations

3.9.1 Overview

From the complexation reactions performed using **46** and the various metal salts the next logical step with the ligand was to attach it to the calix[4]arene scaffold. This however would create a crucial difference when compared with the free ligand. From the crystal structure of **49** it can be seen that the terminal amine is involved in ligation of the metal ion. From this data it was decided to proceed regardless. The bidentate site between the phenolic oxygen and the amide nitrogen would seem to be sufficient to bind metals without the requirement of having a free terminal amine. Indeed, it has already been shown in this thesis that it is not compulsory to have a free amine for metal binding to occur. From the X-ray crystal structure, **48**, the free amine is protonated, rendering it unable to function as a ligand, but the ligand is able to bind through the previously described bidentate site regardless. The only unknown was the possible effect that the calix[4]arene itself could exert on the binding character of the benzamide moiety through either its steric bulk or by competitive binding through the phenolic oxygens.

The original synthetic strategy was to use the original calix[4]arene aldehyde, **29**, to synthesise the calix[4]arene imine derivative of **46** by linking the terminal amine by formation of an imine with the aldehyde moiety, as outlined in Scheme 3.11. This would ensure that the 'adjusted' amine would still have metal binding properties through its lone pair. Furthermore, with the amide attached, the linker imine could be selectively reduced in the presence of the amide to form a secondary amine which would still be able to bind metal ions, like the well known ligand *N,N,N',N'*-tetramethylethylenediamine (TMEDA).[135]

No reaction was observed between the amine and the aldehyde in ethanol, even at reflux temperature. The use of pyridine was employed to raise the pH of the system,

thereby liberating the terminal amine from the ammonium ion. Again, no reaction was observed. Consensus of opinion about imine formation is that it involves the use of an acid catalyst for the reaction to proceed.[87] Since the imine did not form using the pyridine with the free amine nor was its formation observed with the zwitterionic species it was decided to design a new synthetic route toward the macromolecular version of **46**.
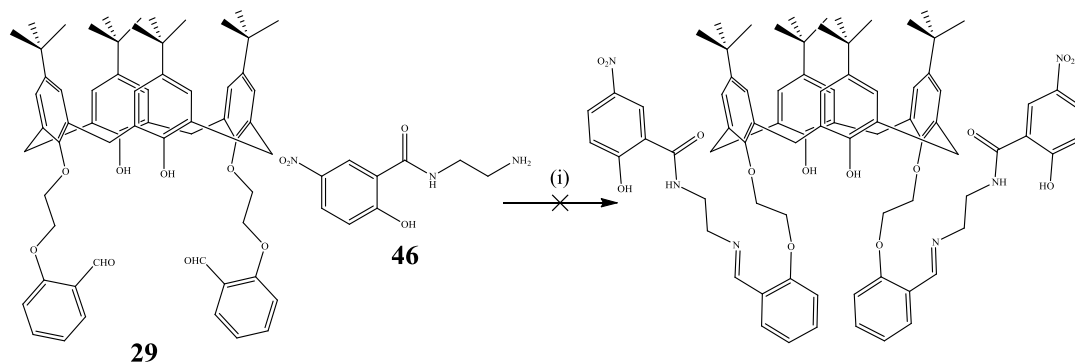
Scheme 3.11: Failed synthesis of calix[4]arene amide/imine derivative using calix[4]arene dialdehyde **29** and benzamide **46** along with conditions used:
(i) = ethanol, Δ. **or** ethanol, pyridine, Δ.

The reasons to change the macromolecular derivative to attach **46** were twofold: previous issues with imine bond stability, mainly because of hydrolysis, as discussed previously in Section 3.3.2 and also the problems highlighted in preparing the imine derivative in the previous paragraph. It was decided to employ the use of an amide linker to attach **46** to the calix[4]arene. This would satisfy one of the problems of using imines, i.e. it would ensure that the ligand was robust enough to withstand mild aqueous conditions. It was also hoped that the newly formed amide moiety itself would participate in ligation of any metal ions it was exposed to.

The initial amide building strategy, shown in Scheme 3.12, was to use the well-known 'scaffold building block' calix[4]arene diethyl ester **56** to attach the benzamide to the calix[4]arene. This would form the diamide calix[4]arene **65**, from which metal complexation reactions could be carried out. This synthetic strategy did not provide the desired product. Because of the zwitterionic nature of **46**, it was not able to participate in nucleophilic attack toward the ester carbonyl, and so prevented amide formation from occurring. It was then decided to prepare a more electrophilic carbonyl derivative of **56** by converting the ester group to an acid chloride which gave **58**. This more reactive calix[4]arene, along with the use of dried pyridine as a solvent was expected

to make the terminal amine available to function as a nucleophile toward the electrophilic carbonyl. This also proved unsuccessful.
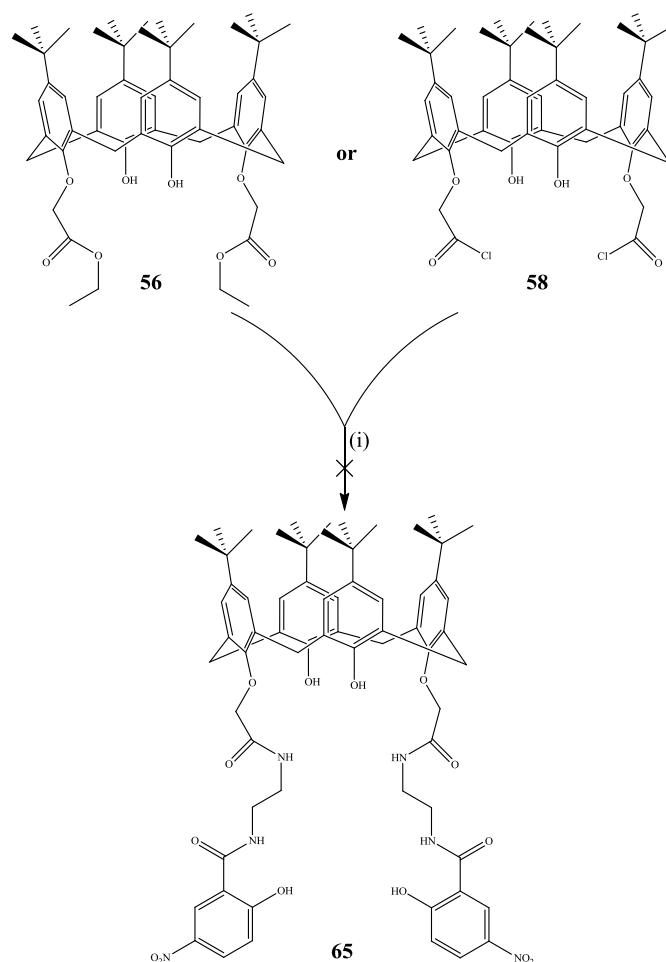
Scheme 3.12: Failed synthetic strategy for preparation of **65** with conditions used: (i) = benzamide **46**, pyridine.

The failure to couple **46** to the calix[4]arene directly *via* an amide linkage resulted in the implementation of a new synthetic strategy, shown in Scheme 3.13. The approach involved protecting the problematic phenol on the nitrobenzamide ring with a durable aryl-methyl ether. The synthesis called for the building of the end product sequentially, firstly by attaching an *N*-Boc-mono-protected ethylene diamine derivative, **59**, to the macrocycle. This yielded the *N*-Boc ethylamide calix[4]arene **60**, which was then deprotected using trifluoroacetic acid (TFA) to give the free amine, **61**. Subsequent reaction of **61** with 2-methoxy-5-nitrobenzoyl chloride, **63**, gave the desired product, albeit in a protected form. Complexation reactions were performed on this ligand to determine its metal binding properties. Deprotection of the aryl-methyl ether with

boron tribromide afforded the desired product, **65**, and its metal binding characteristics were determined.
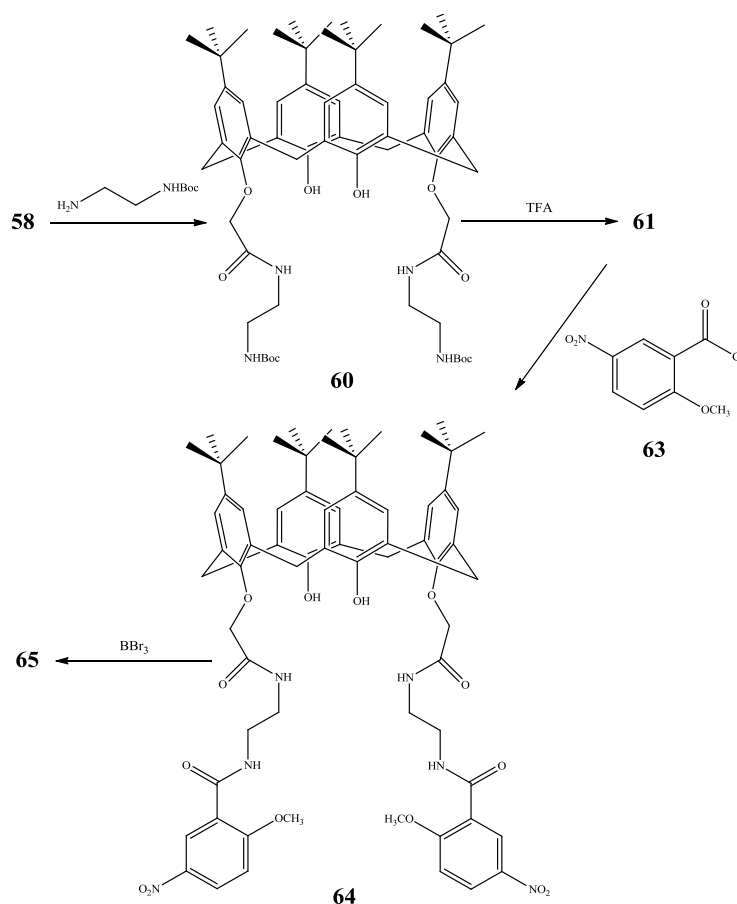
Scheme 3.13: Alternate synthetic strategy for synthesis of **65** showing intermediates and conditions to be used.

3.9.2   Synthesis of calix[4]arene *diester* 56, *diacid* 57, and *diacid chloride* 58

Starting from the parent calix[4]arene (tetramer), **27**, the difunctionalised calix[4]arene diethyl ester, **56**, was prepared using a literature method involving the use of potassium carbonate, ethyl bromoacetate and acetonitrile under reflux conditions under a blanket of nitrogen.[48] This yielded a white solid in a 57 % yield.

Analysis of the ^{1}H NMR spectrum in CDCl$_3$, which is displayed in Figure 3.57, revealed it to be the desired product. The ethyl ester produces a characteristic splitting pattern as a result of the CH$_2$ and CH$_3$ protons coupling to each other. These signals, which resonate at 1.32 and 4.39 ppm are observed as a triplet (for the terminal methyl) and a quartet (for the CH$_2$) with their relative field positions a result of their proximity

to the ester oxygen and carbonyl. The reaction produces the 1,3-distal substituted product, and a plane of symmetry throughout the molecule is displayed by the two resonances for the *tert*-butyl protons, seen in the ^{1}H NMR spectrum at 0.97 and 1.26 ppm, as well as the two signals observed for the aromatic protons of the calix[4]arene. Similar to previous cases, these singlets resonate at 6.81 and 7.02 ppm, which are appropriate chemical shifts for aromatic hydrogens. The methylene groups also exhibit their diastereotopic nature (which has already been previously observed), splitting to form a set of doublets resonating at 3.31 and 4.44 ppm with a coupling constant of $J =$ 13.1 Hz, a value within the range expected for a saturated carbon with coupling geminal protons. The methylene group linking the aryl oxygen on the lower rim with the ester moiety is observed as a singlet at 4.72 ppm, its low field position resulting from deshielding effects of the carbonyl group and the adjoining phenolic oxygen.
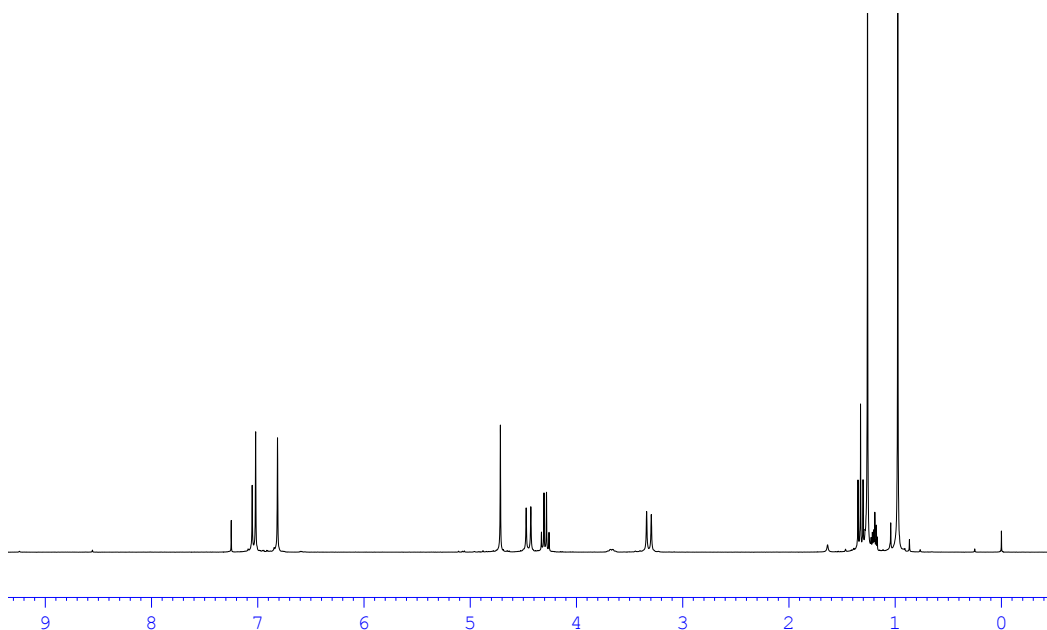
Figure 3.57: ^{1}H NMR spectrum of **56** run in CDCl$_3$ with x-axis in ppm.

The ^{13}C NMR spectrum also shows that a plane of symmetry is exhibited throughout the molecule, with 17 resonances observed. The ester carbonyl is resonating at 169.3 ppm, appropriate for this type of carbon. The IR spectrum of **56** also displays the presence of the ester group with a strong absorption band present at 1759 cm^{-1}, which is representative of the C=O stretching mode. The OH stretch of the hydroxyl group on the lower rim of the calix[4]arene is observed at 3421 cm^{-1}.

Using the prepared diester, attempts were made to couple the benzamide ligand to the calix[4]arene. By adding pyridine it was hoped that it could remove the proton from the ammonium ion to generate the free amine and so present the nucleophile to yield the amide product. Unfortunately, the same result persisted with the ester as with the aldehyde, that is, no reaction between the two substrates occurred.

It was postulated that the ester carbonyl carbon (like the aldehyde) was simply not electrophilic enough for the amine to attack. To rectify this, the acid chloride analogue of the ester derivative was prepared, thus supplying a much more reactive species than the ester. To carry out this transformation, the carboxylic acid derivative was prepared by heating **56** to reflux temperature in the presence of an excess amount of sodium hydroxide in ethanol for 24 hours, using a variation of a procedure published by Collins *et al*.[48] This mixture was treated with hydrochloric acid to liberate the free acid from its sodium salt equivalent. The calix[4]arene diacid **57**, was isolated as a white solid.

Its spectral data is in good agreement with literature values.[48] The main difference in the ^{1}H NMR spectrum is that the peaks representing the ethyl fragment of the ester, present in the ^{1}H NMR spectrum of **56** as a triplet and a quartet, are no longer observed in the ^{1}H NMR spectrum of **57**. There are still two signals representing the *tert*-butyl protons at 1.07 and 1.26 ppm, as well as the two resonances for the aromatic protons at 6.96 and 7.06 ppm. In the ^{13}C NMR spectrum the newly formed carboxylic acid carbon is exhibited at 170.1 ppm.

The IR spectrum supports the NMR data which suggests formation of the carboxylic acid. There is a strong absorption band shown at 1747 cm^{-1}, which represents the C=O stretching mode of the carboxyl group. The shift to a lower wavenumber is expected upon hydrolysis of the ester group, where the C=O stretch was present at 1759 cm^{-1}.

The calix[4]arene carboxylic acid derivative **57** was prepared as an intermediate to the calix[4]arene acid chloride. The acid chloride **58** was prepared using a modification of a preparation by Collins *et al*. by heating to reflux a solution of **57** in neat thionyl chloride under a calcium chloride guard tube.[48] After cooling the volatiles were removed under reduced pressure to yield an off-white solid. This analysed as the required product by ^{1}H NMR and IR spectroscopy.

170

The ^{1}H NMR spectrum of **58** was similar to that previously published. The sensitivity of the molecule to hydrolysis meant that a suitable ^{13}C NMR spectrum could not be obtained. The IR spectrum confirmed the formation of the acid chloride functional group, with its C=O stretch shown as a strong absorption band at 1813 cm^{-1}.

All of the above calix[4]arene derivatives were previously reported in the literature and did not require further characterisation.

Using the acid chloride **58** as a 'terminus' the benzamide ligand was built out from the calix[4]arene starting with the ethyl chain.

3.9.3 Synthesis of *N*-Boc(2-aminoethyl)amine 59, and calix[4]arene derivatives *N*-Boc ethylamine 60, and TFA salt amine 61

The reaction of ethylene diamine with **58** to form the 1,3-distal disubstituted amine was initially attempted using an excess of the diamine to force the formation of the desired product: the *N*-(2-aminoethyl)amide. This reaction was unsuccessful because formation of the intramolecular diamide dominates over the intermolecular derivative as outlined in Scheme 3.14. This diamide has been prepared previously in the literature using the calix[4]arene diester derivative **56**.[61]

Taking the previous results into account it was decided to protect one of the amine groups. The protecting group used was the *tert*-butylcarbamate (Boc) moiety. It is cleavable under mild acid conditions and thus provided a suitable route toward the desired calix[4]arene amide. Using Boc anhydride as a reactant, ethylene diamine was mono protected in good yield using a procedure by Eisenführ *et al*. to yield a yellow oil.[108]

The ^{1}H NMR spectrum of the mono Boc-protected diamine **59** contained a peak integrating for nine protons at 1.45 ppm which represented the protons of the *tert*-butyl groups. The proton of the carbamate NH appeared as a broad signal at 5.13 ppm, its low field position a result of its proximity to the carbonyl moiety. The ethyl group's inequivalent CH$_2$ fragments were observed as two multiplets, both integrating for two hydrogens and resonated at 2.79 and 3.16 ppm. A coupling constant of $J = 5.8$ Hz was observed between these two CH$_2$ groups.
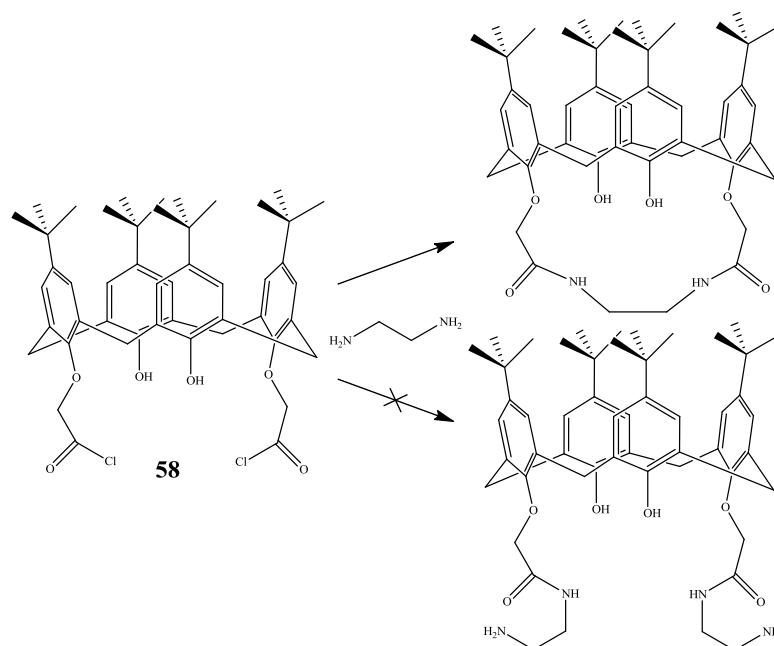
Scheme 3.14: Attempted synthesis of calix[4]arene *N*-2-aminoethylamide.

The ^{13}C NMR spectrum exhibits five peaks, as expected. The carbamate's carbonyl carbon has a chemical shift of 156.2 ppm, making its identification trivial as the other four resonance peaks appear below 80 ppm.

The C=O stretching mode of the carbamate is visible in the IR spectrum of **59**. It is shown as a strong absorption band at 1707 cm^{-1}.

Coupling the mono Boc-protected diamine **59** to the acid chloride calix[4]arene **58** proved straightforward as outlined in Scheme 3.15. A preparation by Chen *et al.* was used to effect this transformation.[89] This was carried out in dry DCM at 0 °C followed by the addition of methanol after an overnight stir to precipitate a white solid: **60**.

Analysis of the white solid by NMR and IR spectroscopy reveals that the data compares well with the previously published data. The ^{1}H NMR spectrum of **60** reveals the presence of three *tert*-butyl group signals: two representing the butyl groups' protons on the upper rim of the macrocycle and the third (at 1.34 ppm) representing the *tert*-butyl protons of the Boc group. Evidence of the newly formed amide is present in the ^{1}H NMR spectrum, with its NH proton resonating as a multiplet at 8.98 ppm. The signal of the NH proton of the carbamate moiety, which was present in the ^{1}H NMR spectrum of **59** at 5.13 ppm, is now observed as a multiplet at 5.09 ppm. Both NH signals integrate for two protons. The aliphatic ethyl group is

represented as two broad signals at 3.53 and 3.34 ppm, with both signals integrating for four hydrogens. The calix[4]arene itself has all its usual representative signals: the aforementioned *tert*-butyl groups at 1.07 and 1.25 ppm and the aromatic protons are observed at 6.97 and 7.07 ppm. These are all observed as singlets. The methylene bridge proton resonances are also present, resonating at 3.44 and 4.16 ppm as doublets due to their diastereotopic nature. The coupling constant is measured to be $J = 13.3$ Hz.
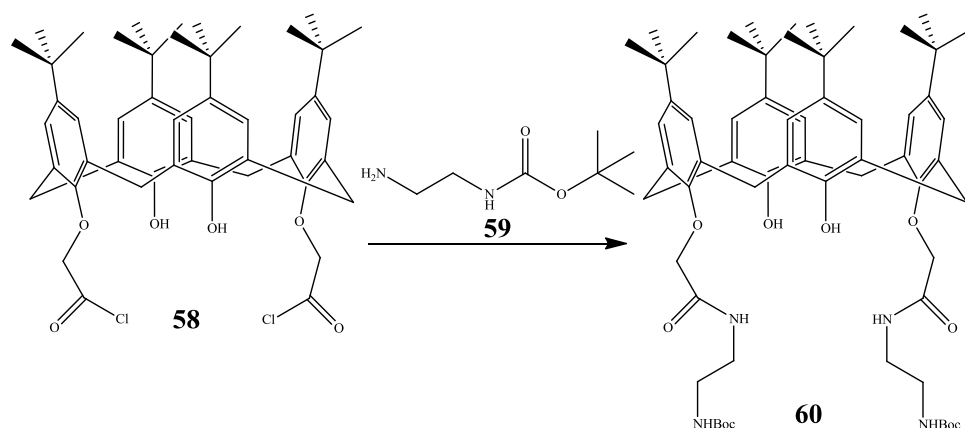
Scheme 3.15: Synthesis of *N*-Boc calix[4]arene **60**.

The ^{13}C NMR spectrum also reveals the presence of the newly formed amide. Its carbonyl carbon resonates at 168.7 ppm, with the carbamate carbonyl's signal visible at 155.9 ppm. The IR spectrum of **60** also exhibits a band representing the C=O stretching mode at 1694 cm^{-1}. The carbamate C=O stretch is still visible at 1708 cm^{-1}. The presence of the calix[4]arene means that assignment of other vibrational bands is difficult.

Removal of the Boc group was carried out in DCM with the use of trifloroacetic acid (TFA) according to a method previously published by Chen *et al.*[89] This furnished the trifluoroacetate salt of the deprotected amine **61**, in quantitative yield. The off-white solid was analysed by NMR and IR spectroscopy. The ^{1}H NMR spectrum of **61** is shown in Figure 3.58.

^{1}H NMR spectral data compared favourably to the published data. The signal for the protons of the *tert*-butyl carbamate group, which was in the ^{1}H NMR spectrum of **60** as a singlet at 1.34 ppm, is now no longer present. In addition, the broad signal representing the NH proton of the protected amine is also not observed. Instead there is a broad signal at 7.34 ppm and integrates to six protons and is probably representative

of the unprotected amine which has been protonated by the TFA (shown in Figure 3.59), thus forming the ionic product. The presence of the counterion is exhibited in the ^{19}F NMR spectrum of **61**, with a signal for the fluorine atoms of the trifluoroacetate CF$_3$ observed at −75.5 ppm.
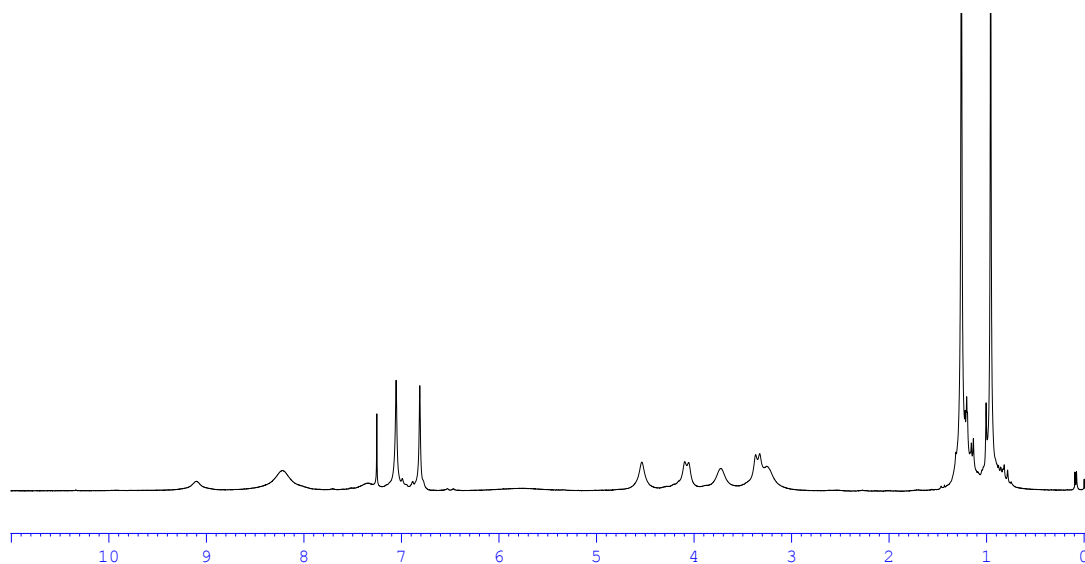
Figure 3.58: ^{1}H NMR spectrum of **61** run in CDCl$_3$ with x-axis in ppm.

The IR spectrum of **61** no longer contains the carbamate carbonyl C=O stretch at 1708 cm^{-1}, indicating that successful deprotection of the amine had occurred. Successful completion of the transformation was also supported by the ^{13}C NMR spectrum of **61**, which no longer had the carbamate carbonyl signal present at 155.9 ppm.
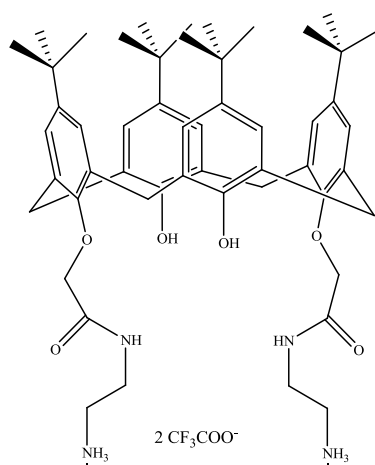
Figure 3.59: Deprotected ethyl amine calix[4]arene **61**.

3.9.4 Synthesis of 5-nitro-2-methoxybenzoic acid 62, and 5-nitro-2-methoxybenzoyl chloride 63

The synthesis of these two derivatives has been completed previously by de Paulis *et al.*[109] The commercially available methyl-2-methoxy-5-nitrobenzoate was used as starting material. An excess of sodium hydroxide solution was added to a methanolic solution of the ester. The mixture was heated to reflux for five hours after which the solution was cooled, concentrated on a rotary evaporator and the residue treated with 6 M hydrochloric acid to liberate the acid from its sodium analogue. The white solid was isolated by filtration. As an aside, when attempts were made to prepare the carboxylic acid, ethanol was used as a solvent. It was found that, even with a stoichiometric equivalent of base, formation of a by-product occurred. Its structure was determined using NMR and IR spectroscopy.

The starting ester had two methyl groups present and their protons were represented in its ^{1}H NMR spectrum by two singlets, each integrating to three protons. These resonated at approximately 3.93 and 4.04 ppm. On reaction with sodium hydroxide in ethanol, the expected hydrolysis of the ester occurs, along with a side reaction to give an alternate product. The ^{1}H NMR spectrum of this alternate derivative showed that the methyl ester had been hydrolysed, as judged by the absence of the methyl proton signal. The methoxy signal of the methyl-aryl ether was also absent. Instead of the methoxy protons' singlet resonance, a quartet at 4.43 ppm and a triplet at 1.62 ppm were observed with these new signals integrated for two and three hydrogens respectively. This side product, 2-ethoxy-5-nitrobenzoic acid, resulted from the action of sodium ethoxide (formed *in situ*) on the starting material. Using the electron withdrawing ability of the nitro group to stabilise the intermediate, as outlined in Scheme 3.16, the ethoxide ion functioned as a nucleophile, attacking the aromatic carbon attached to the methoxy moiety. This aromatic carbon is deshielded (the result of the nitro group's *meta*-directing effects) by the ring's electronic effects which enhanced its electrophilicity. The ethoxide ion attacked this carbon and the resultant intermediate was stabilised by the nitro group. Expulsion of the methoxy anion occurred as a result of it being a weaker base than the ethoxide. Of course, all of this was avoided by using methanol as a solvent, giving exclusive formation of the desired product: 5-nitro-2-methoxybenzoic acid, **62**, whose structure is shown in Figure 3.60.
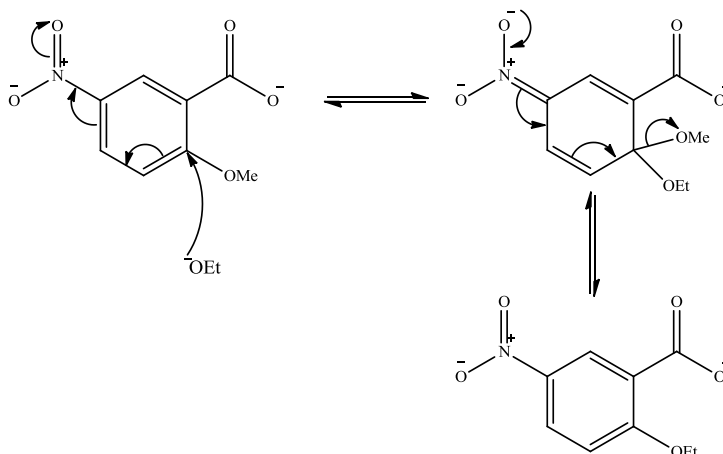
Scheme 3.16: Proposed mechanism for formation of 2-ethoxy-5-nitrobenzoic acid.

Once the carboxylic acid derivative **62** was prepared, it was a trivial task to convert it to its acyl chloride derivative, using a variation of a literature preparation.[136] Using thionyl chloride, 5-nitro-2-methoxybenzoyl chloride, **63**, was prepared in quantitative yield. The off-white solid was characterised by NMR and IR spectroscopy.

The ^{1}H NMR spectrum of **63**, whose structure is shown in Figure 3.60, did not exhibit the broad resonance for the carboxyl proton that was present at 13.30 ppm in the ^{1}H NMR spectrum of **62**. The proton signals for the aromatic hydrogens are more deshielded, resonating at lower field positions at 7.14, 8.47 and 9.56 ppm, when compared to the aromatic proton signals of **62**, which resonated at 7.36, 8.39 and 8.45 ppm. This difference could be due to the electronic effects of a more electron withdrawing substituent in the shape of the acid chloride moiety, when compared to the carboxylic acid functional group.
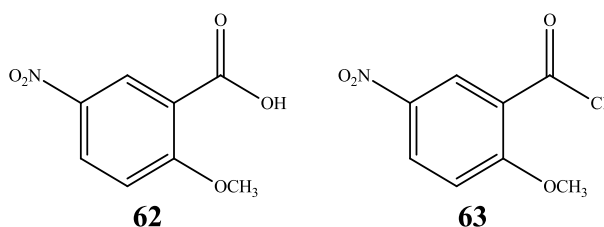
Figure 3.60: Structures of 2-methoxy-5-nitrobenzoic acid, **62** and 2-methoxy-5-nitrobenzoyl chloride, **63**.

It was a surprise when postulating these effects that, in the ^{13}C NMR spectrum of **63** the carbonyl signal of the acid chloride resonated at 163 ppm. This was unexpected considering that the chemical shift of the carboxylic acid carbon signal was at 165

ppm, it would be expected for the acid chloride carbonyl to have a larger chemical shift than this because of its more deshielded nature. One possible explanation may be that hydrolysis of the acid chloride took place in the NMR sample tube from the residual water in the deuterated solvent. This would yield the carboxylic acid derivative, a possibility that supports the small chemical shift observed of the carbonyl carbon peak.

The IR spectrum of **63** made for easy confirmation that the acid chloride moiety had formed. The C=O stretch of the carboxylic acid was present in the IR spectrum of **62** at 1705 cm^{-1}. This band was not present in the IR spectrum of **63**. Instead, a band representing the C=O stretching mode of the acid chloride moiety was present at 1776 cm^{-1}.

Using the acid chloride **63** as a reactive intermediate, the benzamide calix[4]arene derivatives **64** and **65** were prepared.

3.9.5 Synthesis and characterisation of 2-methoxy-5-nitrobenzamide calix[4]arene 64

The novel calix[4]arene derivative, **64**, was prepared from a coupling reaction between 2-methoxy-5-nitrobenzoyl chloride, **63**, and the TFA salt of 2-aminoethylbenzamide calix[4]arene, **61**. This reaction was carried out in dry dichloromethane with the addition of dry triethylamine (performing a dual role) to liberate the terminal amine from its trifluoroacetic acid salt and to neutralise the hydrogen chloride formed during the coupling reaction. Compound **64**, whose structure is displayed in Figure 3.61, was isolated as a white solid after precipitation with acetone. The solid was characterised by NMR and IR spectroscopy as well as elemental analysis.

The ^{1}H NMR spectrum of **64** revealed that coupling of the benzoyl chloride to the calix[4]arene was successful, as characterised by the appearance of an amide hydrogen resonance: a multiplet at 8.08 ppm. The original amide signal that was present in the ^{1}H NMR spectrum of **61** at 9.11 ppm was still present in the product and had barely moved, with a chemical shift of 9.12 ppm. The aromatic region was more complicated as a result of the addition of the 2-methoxy-5-nitrobenzamide moiety, with three additional signals representing the aromatic protons resonating at 6.78, 8.14 and 9.00

ppm. The substitution orientation of the aromatic ring was confirmed by measuring the coupling *J* values of the protons signals, as discussed in Section 3.8.2. The signals for the aromatic protons of the calix[4]arene were present and resonated as singlets at 6.85 and 6.88 ppm. The calix[4]arene itself, aside from the aforementioned aromatic peaks, were represented by signals for the phenolic proton (at 7.92 ppm), the protons of the two *tert*-butyl groups (at 1.03 and 1.20 ppm) and the diastereotopic protons of the bridging methylene group (doublets at 3.24 and 4.05 ppm with a coupling constant value of *J* = 13.2 Hz). The ethyl linkage between the two amides was represented in the ^{1}H NMR spectrum by two multiplets, each one for each of the inequivalent CH_2 fragments and they resonated at 3.70 and 3.78 ppm. The signal for the methoxy group's protons was present at 3.98 ppm and was unsplit.
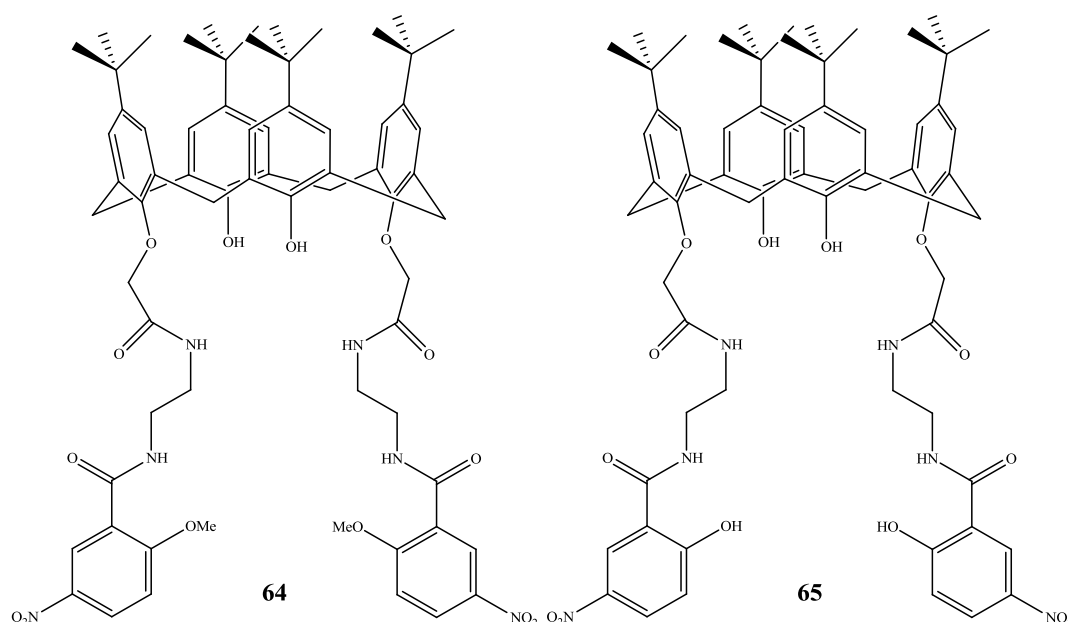
Figure 3.61: Calix[4]arene derivatives **64** and **65**.

Elemental analysis confirms the constitution of the white solid. Crystals of **64** were grown from a dichloromethane methanol solution, some of which were of sufficient quality to subject to X-ray crystallographic analysis, the results of which will be discussed in Section 3.9.7.
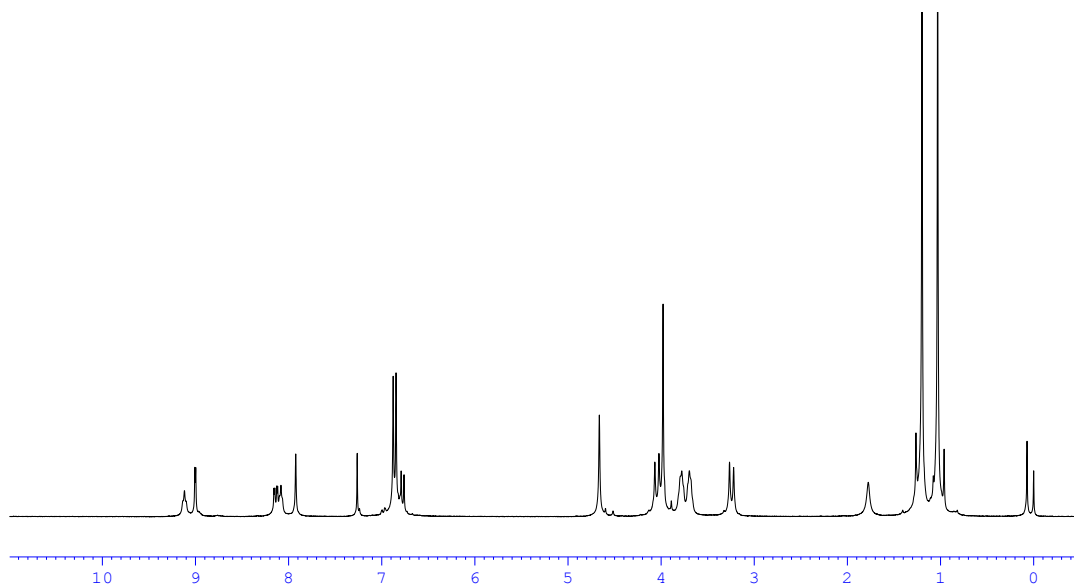
Figure 3.62: ^{1}H NMR spectrum of **64** run in CDCl$_3$ with x-axis in ppm.

3.9.6 Synthesis and characterisation of 2-hydroxy-5-nitrobenzamide calix[4]arene 65

Deprotection of the methoxy-aryl ether was achieved using a Lewis acid: boron tribromide, in a dichloromethane solution. The reaction was completed after an overnight stir that followed an addition of a commercially prepared solution of boron tribromide in dichloromethane (1 M) to a solution of **64** in dichloromethane. The addition of methanol gave **65**, whose structure is shown in Figure 3.61, as a white solid in 33 % yield after workup. The white solid was characterised by NMR and IR spectroscopy, as well as obtaining its mass spectrum.

The ^{1}H NMR spectrum of **65** (displayed in Figure 3.63) revealed that successful cleavage of the methyl ether had occurred, as denoted by the presence of a singlet resonance peak at 13.48 ppm. The large chemical shift of this signal was probably as a result of the proximity of the amide moiety on the aromatic ring, which would allow for hydrogen bonding to occur between the amide carbonyl oxygen and the phenoxy hydrogen, as outlined in Figure 3.64. The methyl protons' peak that was present at 3.98 ppm in the ^{1}H NMR spectrum of **64** was now not observed in the product. Further evidence of the presence of the phenoxy derivative was the upfield shift of the aromatic proton signals which resonated at 9.00, 8.14 and 6.78 ppm in the ^{1}H NMR spectrum of **64**, to a slightly more shielded position at 8.64, 8.02 and 6.79 ppm. This

response was expected of their chemical shift when substituting a slightly weaker donating ring substituent for a stronger donating one, i.e. exchangeing OCH_3 for OH.
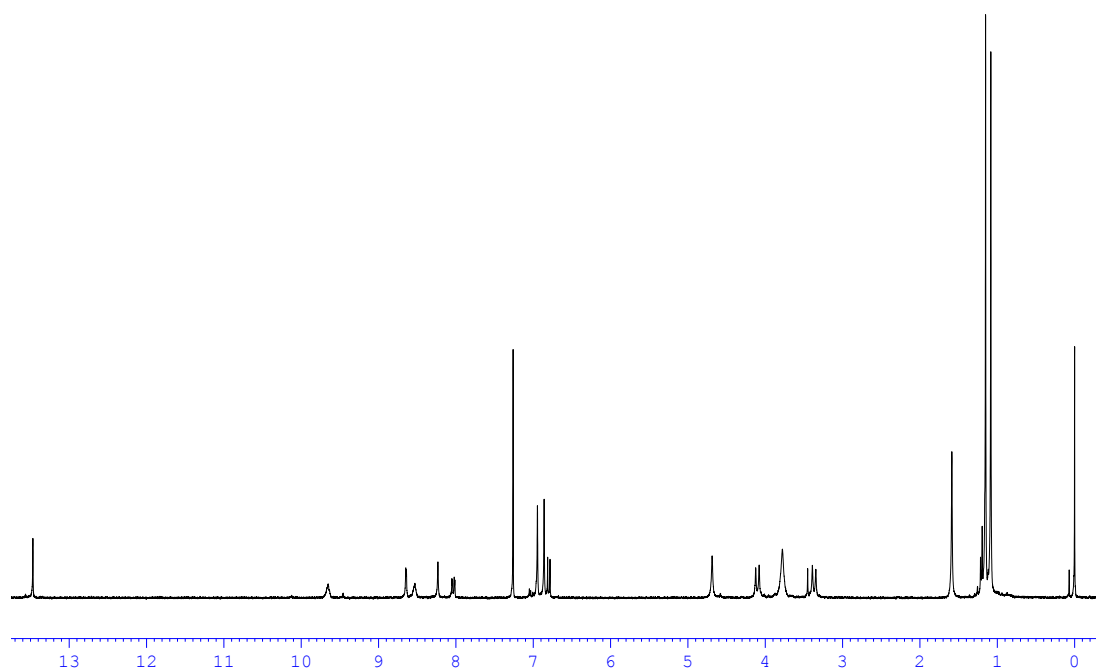
Figure 3.63: ^{1}H NMR spectrum of **65** run in CDCl$_3$with x-axis in ppm.

Confirmation that the methyl group was removed was also provided in the ^{13}C NMR spectrum of **65**. The methyl carbon resonance, which was present in the ^{13}C NMR spectrum of **64** at 55.6 ppm was not present in the ^{13}C NMR spectrum of the product, thus confirming cleavage of the ether moiety.
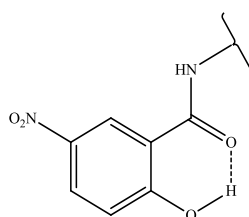
Figure 3.64: Benzamide moiety of **65** showing H-bonding interactions.

The ether CO vibration modes could not be assigned with any confidence in the IR spectrum of **64** so the absence of these bands in the deprotected ether did not result in any noticeable difference in the spectrum of **65** as the CO stretching region contained overlapping bands that represented the calix[4]arene and ligand vibration modes, both moieties of which contain CO fragments.

The mass spectrum of **65** contained a major peak at 1201.5526, which corresponded to the $(M + Na)^+$ ion. The protonated species $(M + H)^+$ ion was also detected at 1179.5704.

3.9.7   X-ray crystal structure of 64

Calix[4]arene **64** was isolated as a white solid. Colourless crystals of **64** were grown from a dichloromethane and methanol solution by the method of slow evaporation and proved suitable for X-ray crystallographic analysis. The structure determined is shown in Figure 3.65. The calix[4]arene is in a cone conformation, which follows the trend of the calix[4]arene derivatives' orientations previously exhibited in this thesis. The cone is stabilised by two intramolecular hydrogen bonds between the hydroxyl groups and the substituted oxygens: O(1B)H(1B)···O(1C) and O(1D)H(1D)···O(1A) exhibiting values of 2.739(3) and 2.710(3) Å respectively. These values are within the range of previously published hydrogen bonding interactions for the lower rim hydroxyl groups on a calix[4]arene.[118]
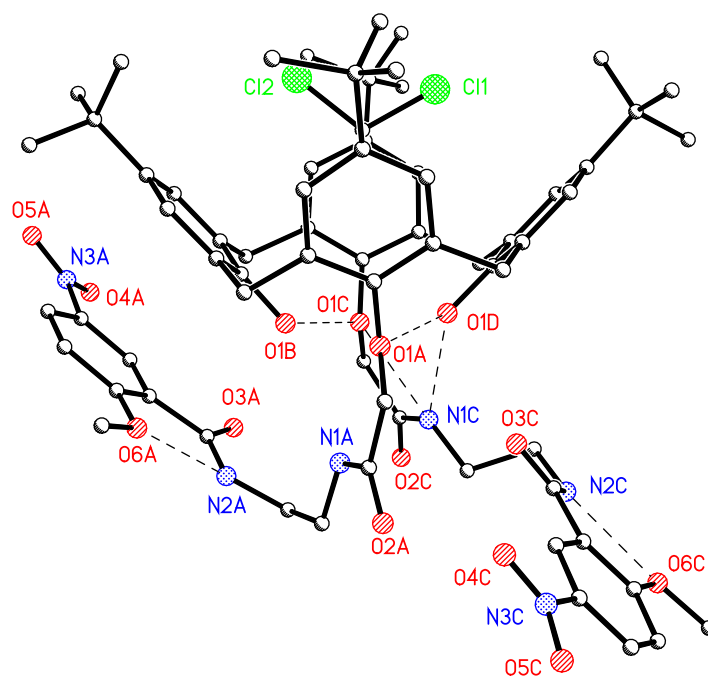
Figure 3.65: X-ray crystal structure of **64**.

Hydrogen bonding occurs at several additional sites. The amide moieties nearest the calix[4]arene macrocycle participate in hydrogen bonding with the lower rim oxygens. These interactions, N(1C)H(1C)···O(1C) and N(1C)H(1C)···O(1D) (of magnitude

2.605(3) and 2.967(3) Å respectively) are partially responsible for the orientation of the pendant arms, with one pointing upwards and the other downwards. Additional hydrogen bonding is observed at the aromatic ring containing the nitro functional group, with interactions between the aryl-methyl ether's oxygen and the adjacent amide proton on the two pendant arms: N(2A)H(2A)···O(6A) and N(2C)H(2C)···O(6C) exhibiting distances of 2.664(4) and 2.978(3) Å respectively. All of the above hydrogen bond distances are within the accepted range for these types of interactions.[137]

The orientation of the pendant arms also facilitates π-stacking interactions in the crystal packing. The calix[4]arenes lie in double layers facing each other with the *tert*-butyl groups pointing outwards. The pendant arm that has swung upwards forms a short chain by way of π-stacking interactions with one of the aromatic rings of the calix[4]arene cavity wall and one of the pendant arms of an adjacent molecule. This bimolecular species interacts, by π-stacking, with a second bimolecular species to form a short six-member π-π stack, thereby linking the two layers together. These resulting interactions are displayed in Figure 3.66. The π-π interactions between each of the six rings are 3.544, 3.705, 3.603, 3.705 and 3.544 Å respectively. As a result, each calix[4]arene molecule interacts with three adjacent units.

The calix[4]arene itself crystallised as an inclusion complex, as shown in Figure 3.65, with a molecule of dichloromethane (DCM) situated within the macrocyclic cavity. The hydrogens of the DCM are situated in such a way as to interact with the π systems of two of the aromatic rings that make up part of the calix[4]arene's wall. The hydrogen-bonding distances to the centre of the two aromatic rings are 2.548 and 2.616 Å respectively. DCM-calix[4]arene inclusion complexes have been reported in the literature previously, with the calix[4]arene binding in a similar fashion to that observed in the above case.[138]

Using the crystallographic data obtained, it was postulated that with this calix[4]arene derivative it would be possible to sequester metal ions from solution, ideally with some selectivity. To this end, metal complexation studies were carried out with metal-ligand complex formation detected using ^{1}H NMR spectroscopy.
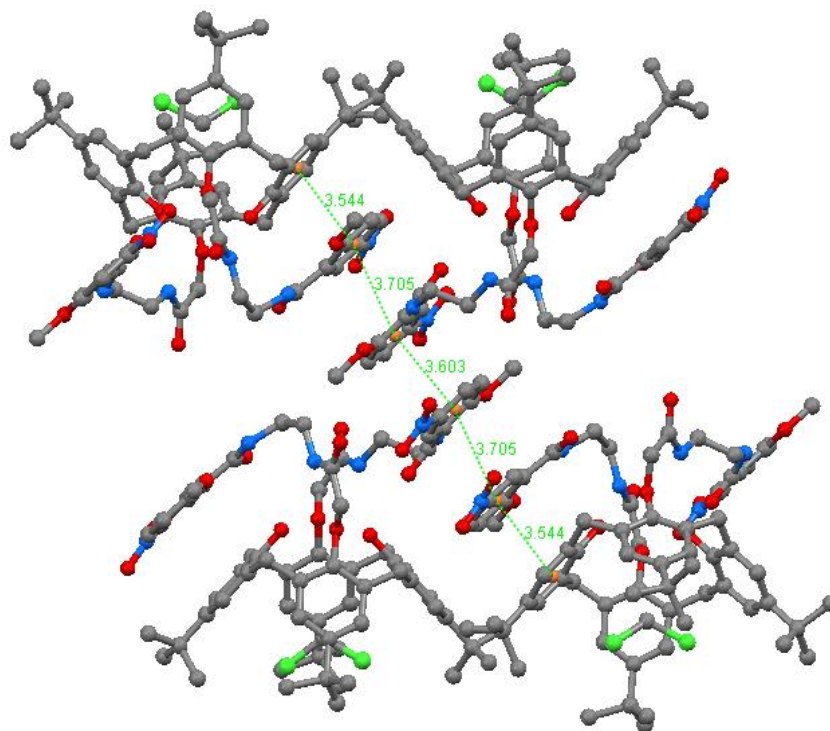
Figure 3.66: Partial packing diagram of **64** showing π-stacking interactions within the double
layer with centroid (orange) to centroid distances displayed.

3.9.8   Metal complexation reactions of 64

Due to the relatively poor solubility of metal salts in CDCl$_3$, metal complexation
reactions were performed in d_6-DMSO. The ^{1}H NMR spectrum of calix[4]arene
derivative **64** was first obtained in the deuterated solvent, then an excess of the
appropriate metal salt solution (also in d_6-DMSO) was added to the ligand. In the case
of silver(I) acetate, the metal salt was added as an aqueous solution because of the very
limited solubility of the silver(I) salt in d_6-DMSO although this resulted in inaccurate
comparisons between the silver titration and its sodium and zinc equivalent titrations.
The ^{1}H NMR spectrum of the mixture was obtained and then compared with the
corresponding spectrum of the starting material. A summary of the metal complexation
reactions carried out is shown in Table 3.3.

Table 3.3: Summary of metal complexation reactions of **64**.

Metal Salt	Metal Equivalents	Solvent
NaClO$_4$·6H$_2$O	5.0	d_6-DMSO
NaO$_2$CCH$_3$·3H$_2$O	5.0	d_6-DMSO
Zn(O$_2$CCH$_3$)$_2$·2H$_2$O	5.0	d_6-DMSO

ZnCl$_2$	5.0	d_6-DMSO
Zn(ClO$_4$)$_2$·H$_2$O	6.0	d_6-DMSO
AgClO$_4$	6.0	d_6-DMSO
AgO$_2$CCH$_3$	2.0	d_6-DMSO/H$_2$O

In all of the cases listed in Table 3.3 no shift of the calix[4]arene peaks was detected. Considering the number of potential binding sites on the ligand, this is a surprising result. The tetra functionalised ester derivative by McKervey *et al.* is a good example of a metal ion binder with a particular affinity for alkali metal ions.[139] This ester derivative binds by using the lone pairs of the carbonyl oxygens to bind the appropriate metal ion. As a result, it was hoped that by using this calix[4]arene ester derivative as a template it would be expected that the tetra-amide calix[4]arene derivative **64** would display some kind of binding action toward the metals mentioned in Table 3.3, which were introduced as their corresponding salt. In addition to the amides' oxygens, the amide nitrogen (if deprotonated) also has the potential to bind metal ions, as examples in the literature are a testament to.[83,84] To ensure that the solvent was not responsible for a cage effect around the metal cation, deuterated acetonitrile was used as an alternative solvent in a test case. In this instance no shift in the ligand's peaks were observed in its ^{1}H NMR spectrum.

To determine whether the binding ability of the benzamide moiety was affected by the protected phenol group, the methyl ether was cleaved and the deprotected benzamide calix[4]arene was subjected to complexation studies with the same array of metal salts used for **64**. Thus, the ability of calix[4]arene **65** to bind metal ions was determined

3.9.9   Metal complexation reactions of 65

3.9.9.1   Overview

The failure of **64** to show any evidence of complexation properties led to the deprotection of the methyl ether. The hydroxy derivative, **65**, which possesses a labile proton, has upon deprotonation the potential to function as an anionic ligand. To this end, metal salt titrations, using a similar method to that for **64**, were performed. A known amount of the starting ligand was dissolved in d_6-DMSO (for reasons mentioned in 3.9.8). The parent solution was titrated against a known concentration of

the metal salt in the same solvent (except in the case of silver(I) acetate, for reasons of poor solubility). The use of an NMR spectrometer limited the range of metal salts that could be used to those with exclusively diamagnetic character. To determine the scope of binding character of **65**, some sodium(I) and silver(I) salts were employed in addition to the main metal of focus which was zinc(II). To determine whether the anion had any influence on whether the metal ion would bind or not, a selection of anions was used, namely acetate, chloride and perchlorate ions, to counter the metal cations. A summary of metal salts employed and their amounts used are shown in Table 3.4.

Table 3.4: Summary of metal salts, solvents and stoichiometric equivalents used for determining binding properties of **65**.

Metal Salt	Metal Equivalents (up to)	Solvent
$NaClO_4 \cdot 6H_2O$	5.0	d_6-DMSO
$NaO_2CCH_3 \cdot 3H_2O$	5.0	d_6-DMSO
$Zn(O_2CCH_3)_2 \cdot 2H_2O$	5.0	d_6-DMSO
$ZnCl_2$	5.0	d_6-DMSO
$Zn(ClO_4)_2 \cdot H_2O$	5.0	d_6-DMSO
$AgClO_4$	5.0	d_6-DMSO
AgO_2CCH_3	1.6	d_6-DMSO/H_2O

The experimental results presented previously in this thesis show that, when chloride and perchlorate metal salts are used, no shift of the ligand's peaks in the ^{1}H NMR spectra were observed. This is surprising since it was postulated that the removal of the methyl moiety would afford favourable binding characteristics similar to that shown by **46**, where both chloride and perchlorate metal salts bind with ease.

3.9.9.2   Complexation studies of zinc(II) acetate with 65

Additional metal salt titrations were carried out using a solution of zinc(II) acetate and this yielded a change in the ^{1}H NMR spectrum of **65**. A suggestion that the acetate was effecting an alteration of **65** in solution was the observed change in colour of the solution. The original ligand, whose solution exhibited a very pale yellow colour, altered on contact with the acetate solution to give a much stronger yellow colour. This colour change was very noticeable, even in the presence of substoichiometric amounts of the metal salt. Aliquots of the metal salt solution were continually added, with each

sequential addition monitored for alterations in the ^{1}H NMR spectrum up to one equivalent of metal. On addition of excess equivalents of zinc(II) acetate, additional changes in the ^{1}H NMR spectrum were not observed. This suggests that the zinc(II) ion was binding in a 1:1 metal-to-ligand ratio, with the pendant arms working in tandem to provide an *O,O,O,O*-tetradentate coordination site. This type of coordination mode with *ortho*-hydroxy benzamides and zinc(II) salts has been reported previously.[140] A proposed structure of the zinc(II) calix[4]arene complex is displayed in Figure 3.67.
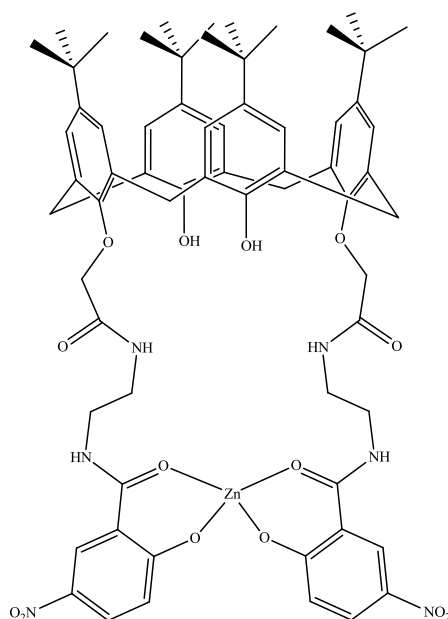
Figure 3.67: Proposed structure of **65** with one equivalent of zinc(II) acetate. Excess amounts of zinc(II) acetate do not alter chemical shifts in ^{1}H NMR spectrum.

A comparison of the ^{1}H NMR spectrum of **65** and that of the same ligand with one full equivalent of zinc(II) acetate added is shown in Figure 3.68. The most noticeable change between the two spectra was the signal that was present in the ^{1}H NMR spectrum of the ligand at 13.94 ppm was not present after the addition of the zinc(II) solution. This suggested that the zinc may have bound to the *ortho*-hydroxy benzamide moiety in an *O,O-* bidentate fashion, analogous to that displayed in the X-ray crystal structure of **48**. Evidence that the calix[4]arene's pendant arm was functioning with only one site of deprotonation was the continued presence of the amide protons, whose representative signals were observed at 9.38 and 9.02 ppm in the ^{1}H NMR spectrum of the starting material and who diverged in the corresponding ^{1}H NMR spectrum on addition of the zinc(II) solution to 10.29 and 8.76 ppm respectively. The increased

difference in their resonance positions would suggest that only one of the amide functional groups was participating in binding the zinc(II) ion.
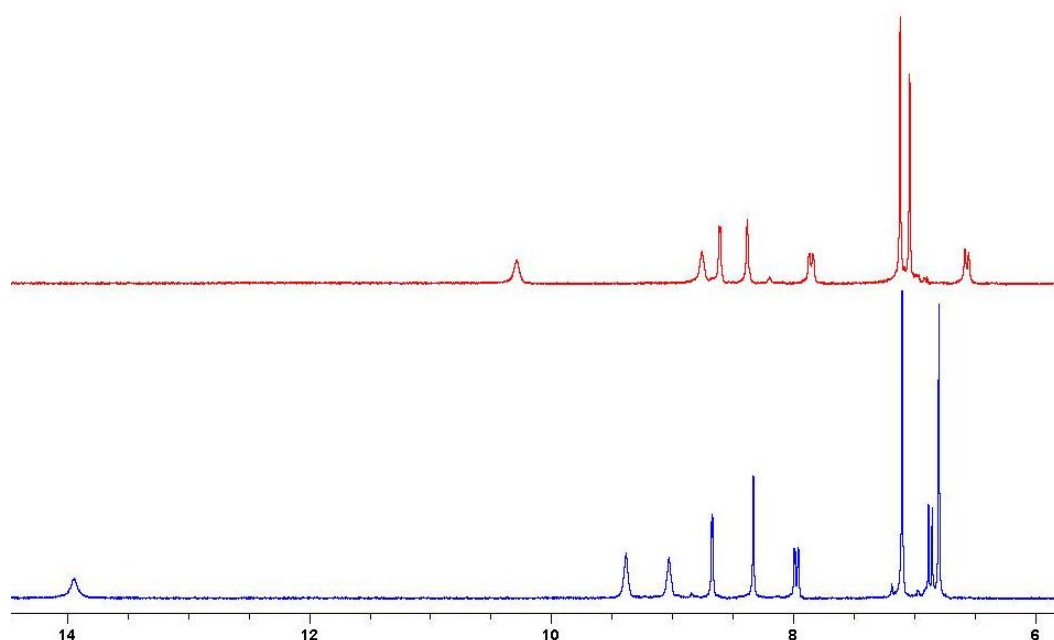
Figure 3.68: Partial ^{1}H NMR spectra of **65** (shown in blue trace) and of **65** with the addition of one equivalent of zinc(II) acetate (shown in red trace) in d_6-DMSO with x-axis scale in ppm.

3.9.9.3 Complexation studies of sodium(I) acetate with 65

To ascertain whether ligand **65** binds selectively to zinc(II) acetate, sodium(I) acetate was used in the same manner as its zinc(II) analogue. Suggestive complexation of the ligand was provided by a similar colour change to that observed on addition of zinc(II) acetate, i.e. alteration of the colour from a light yellow hue to a much stronger yellow colour. Titrations were carried out in an identical manner to that for the zinc(II) acetate complexation and it was found that the sodium(I) ion complexes to **65** in a metal-to-ligand ratio of 2:1, suggesting that each pendant arm binds one sodium ion apiece, as displayed by the proposed structure in Figure 3.69.

Similar to the binding studies on zinc(II) acetate, the phenolic proton signal at 13.94 ppm present in the ^{1}H NMR spectrum of the ligand was not observed, suggesting that the metal may be binding at this site. Again, similar to the zinc(II) acetate case, the two signals for the amide protons were still present in the ^{1}H NMR spectrum of the 2:1 metal salt-to-ligand solution. They shifted in a similar manner to that observed for the zinc(II) complex with the amide protons' signals diverging from 9.38 and 9.02 ppm to

11.27 and 8.80 ppm respectively, as shown in Figure 3.70. In an identical manner to that postulated for the complexed zinc(II) ion, it is proposed that the sodium(I) ion was bound in a bidentate *O,O*- coordination mode, with additional solvent molecules filling the metal ion's coordination sphere as outlined in Figure 3.69. Sodium(I) generally occupies a maximum coordination number of six,[19] a consequence of its small size and thus resulting in the postulate that the final four coordination sites were occupied by either water or d_6-DMSO donors.
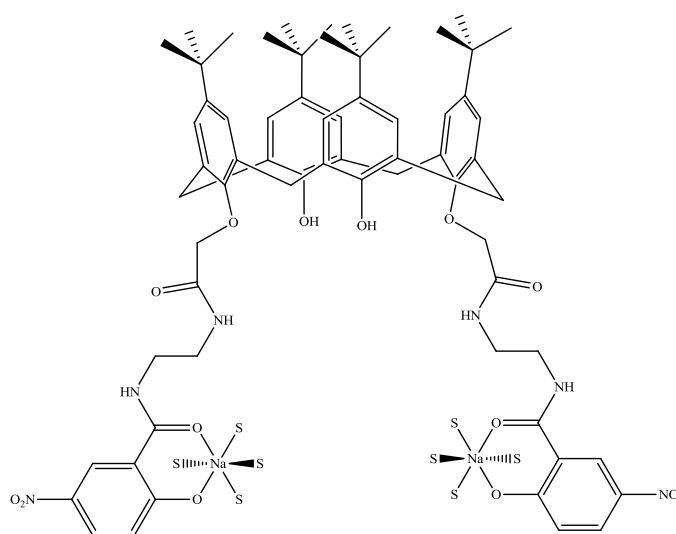
Figure 3.69: Proposed structure of sodium coordination complex of **65** with 2 eq. sodium(I) acetate added, with S denoting donor solvent molecules.
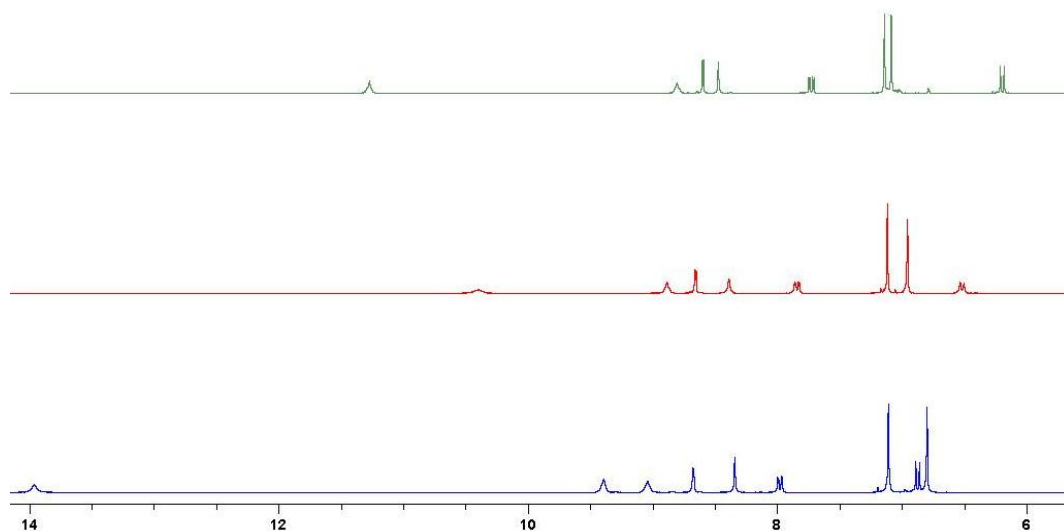
Figure 3.70: Partial ^{1}H NMR spectra of **65** (shown in blue trace), **65** and the addition of 1 equivalent of sodium(I) acetate (shown in red trace) and **65** and the addition of 2 equivalents of sodium(I) acetate (shown in green trace) in d_6-DMSO with x-axis scale in ppm.

3.9.9.4   Complexation studies of silver(I) acetate with 65

The successful binding of **65** to both the zinc(II) and sodium(I) salts encouraged the expansion of the investigation to ascertain whether another transition metal, silver(I) would interact with the ligand. Following the same trend as both the zinc(II) and sodium(I) analogues, the only silver(I) salt to show any type of interaction with the ligand was silver(I) acetate. Prior to the silver(I) acetate reaction, a similar reaction using silver(I) perchlorate showed no effect on the chemical shift of the ligand upon addition of excess amounts.

Solubility issues with the silver(I) acetate salt in d_6-DMSO meant that an aqueous solution of silver(I) acetate was used in the metal salt titrations with **65**. This alteration resulted in inaccurate comparisons of the spectral data because of the different solvent environments. However it was decided to monitor the alteration of the ligand's peaks on addition of the metal salt. It was postulated that when no further shift in the peaks occurred it implies that the ligand was unable to bind to any additional metal ions added in its presence. From the experimental set up (identical to the zinc(II) and sodium(I) titrations except for the solvent) and chemical shifts of the ligand's signals in the ^{1}H NMR spectrum it is suggested that the ligand interacted with the silver(I) ion. Additional changes (including the intensification of the yellow colour in the sample) were also noted. The signal of the phenolic hydrogen on the pendant arm observed in the ^{1}H NMR spectrum of the ligand at 13.94 ppm had, like all previous cases in the presence of a metal acetate salt, disappeared. Given that the silver ion possesses a +1 charge, this would suggest that the silver ion was shared between the ligands, thus forming a long chain polymer, with a possible repeat unit which is shown in Figure 3.71. Formation of coordination polymers have been observed before with ligands binding silver(I) ions.[141] Support for this theory also came in the physical appearance of the NMR sample. As the acetate solution was added upon completion of the addition of one full equivalent of silver(I) acetate, a yellow solid was formed in the sample tube. Attempts were made to redissolve this solid, but to no avail. Prior to the formation of this precipitate, the ^{1}H NMR spectrum of the metal-to-ligand mixture showed that many of the signals representing the protons on the pendant arms had altered to give a very broad appearance, again supporting the theory that polymer formation had occurred.

The rest of the signals in the ^{1}H NMR spectrum of the metal and ligand mixture suggested an analogous binding mode was used by the ligand in this case also. The amide protons that were present in the ^{1}H NMR spectrum of **65** at 9.38 and 9.02 ppm had diverged to 10.89 and 8.92 ppm respectively, as can be seen in Figure 3.72, upon addition of one metal salt equivalent. This conveyed that the metal, as in the two previous cases, sat in an *O,O*- bidentate coordination sphere. The silver ion may be encapsulated by an additional donor from an adjacent molecule of **65**. A representation of this binding mode is shown in Figure 3.71.
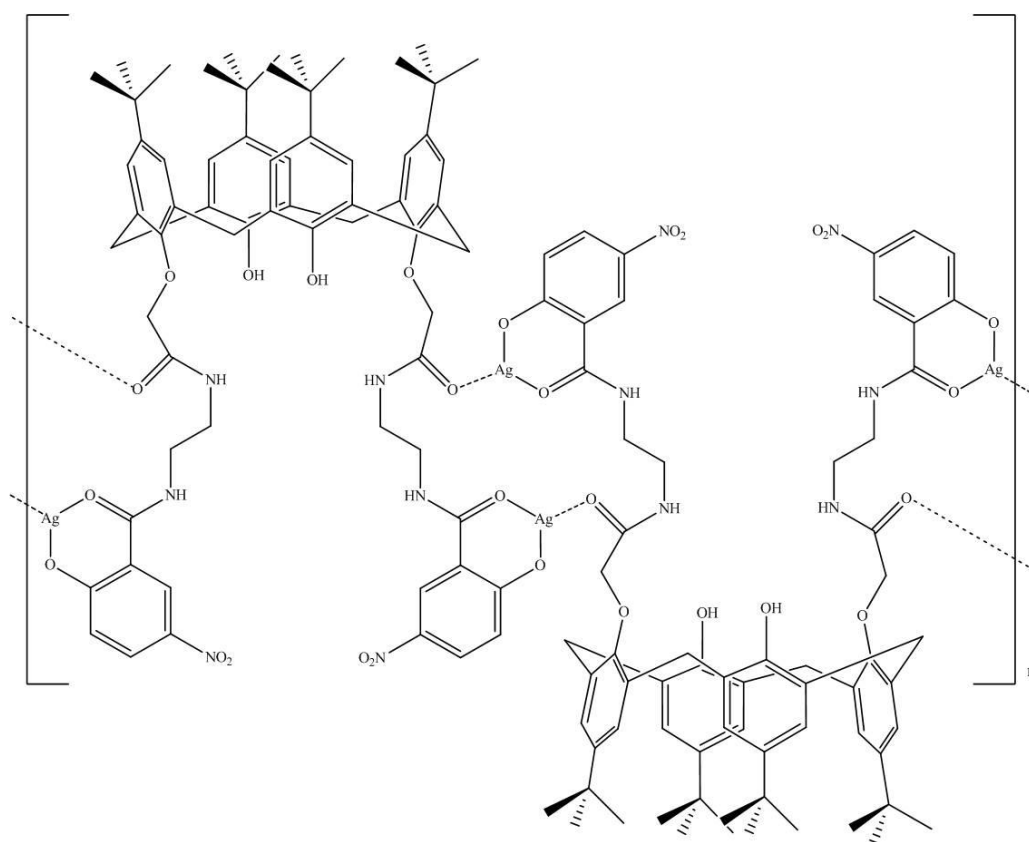
Figure 3.71: Possible repeat unit of proposed polymeric structure for complex formed from **65** and the addition of silver(I) acetate. Poor solubility of complex also supports a proposed polymeric structure.
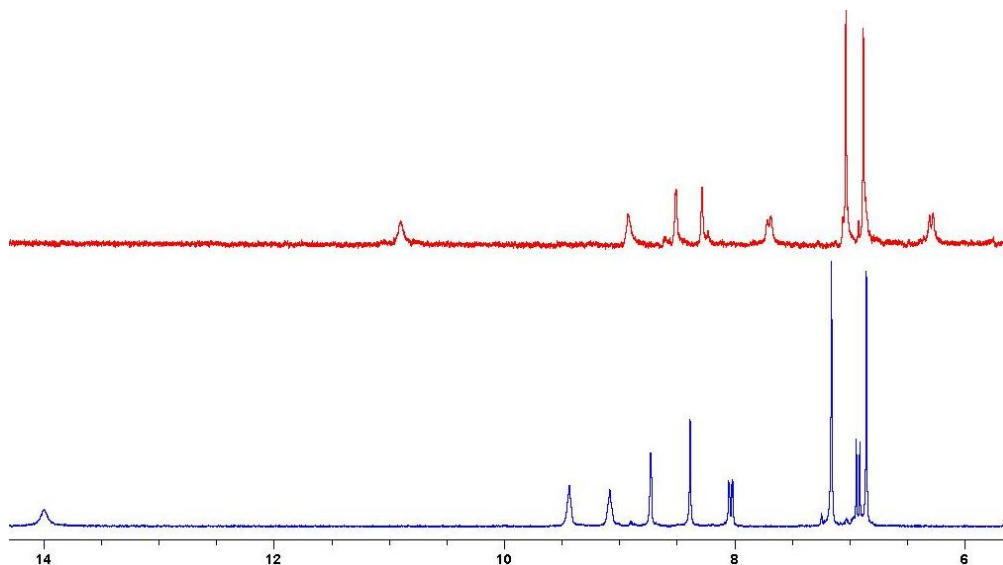
Figure 3.72: Partial ^{1}H NMR spectra of **65** (shown in blue trace), **65** and the addition of 1 equivalent of silver(I) acetate (shown in red trace) and **65** in a d_6-DMSO/H$_2$O mixture with x-axis scale in ppm.

3.9.9.5   Explanation for selectivity of 65 for metal acetates

Examining the results of the metal complex titrations with **65**, it becomes clear that the ligand binds exclusively to metal acetates. An explanation for this trend can be found by the relative basicity of the metal cations' counterions, namely the acetate, perchlorate and chloride anions. By using known pK_a values determined in DMSO for analogous compounds, it is possible to show why the acetate salts are the only ones to bind to **65**. Ligand **65** has a *para*-nitrophenol moiety on its pendant arm and has an approximate pK_a of 10.8 in DMSO.[142] In reality the pK_a of **65** is probably even lower, as the presence of the amide *ortho* to the hydroxyl would also contribute toward the stability of the conjugate base (i.e. the phenoxide), thus enhancing the acidity of the phenol and lowering the pK_a even further.

Acetic acid, whose conjugate base is the acetate anion, has a pK_a of 12.3 in DMSO.[142] This would suggest that the acetate anion is more basic than the ligand (**65**), specifically the nitrophenol moiety. From this information it can be proposed that the acetate anion, a sufficiently strong base, is able to deprotonate the nitrophenol moiety to give the corresponding phenoxide. The charged species, being a much stronger donor, is now able to bind to the metal cation, in a way that the neutral ligand could not. Evidence of the crucial role of the counterion in facilitating metal binding arises when the acetate salts are compared with their chloride and perchlorate counterparts.

191

Hydrochloric acid (pK_a of 1.8 in DMSO (−8.0 in H$_2$O))[142] and perchloric acid (pK_a of −10 in H$_2$O)[142] are both stronger acids than acetic acid, meaning that both the chloride and perchlorate anions would be weaker bases than the acetate anion. This suggests that the chloride anion is not sufficiently strong to remove the proton from the nitrophenol moiety. Failure to deprotonate the phenol means that the neutral ligand is not a strong enough ligand to bind to the metal cation. The same case occurs for the perchlorate anion, which is an even weaker base than the chloride.
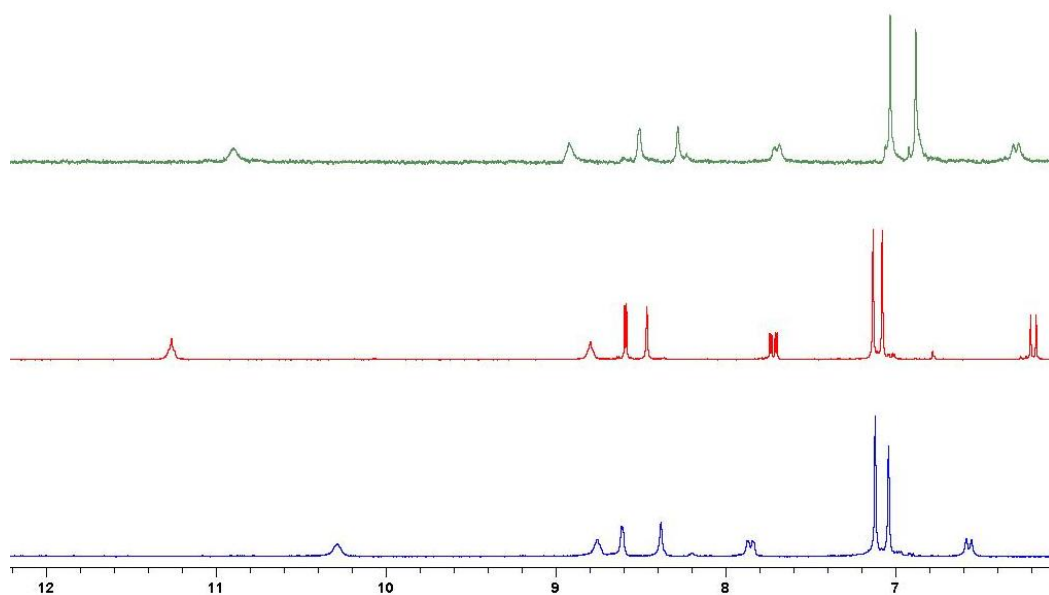
Figure 3.73: Partial ^{1}H NMR spectra of **65** with zinc(II) acetate (blue trace), sodium(I) acetate (red trace) and silver(I) acetate (green trace) with x-axis scale in ppm.

Using the three separate metals also rules out the possibility that the acetate anion is functioning as a 'naked anion' and that no complexation of the metal cation is occurring. By comparing the three ^{1}H NMR spectra of the metal titrations it can be seen that obvious variations occur in the spectra. This suggests that the metal ion is forming a coordination complex with the charged ligand. Partial ^{1}H NMR spectra of the three acetate titrations are shown in Figure 3.73 displaying how emphatic the differences between the metals are though the different solvent environment used in the silver(I) titration means that accurate comparisons between the NMR data cannot be made.

4. Conclusions

The goal of the work carried out in this thesis was to prepare an array of novel ligands based on either a Schiff-base or amide design. Some of these ligands were attached to the calix[4]arene macrocycle to prepare macromolecular derivatives. Several of these ligands were examined for potential fluorescent character. All were subjected to complexation studies resulting in the formation and characterisation of novel coordination complexes. Sodium(I), nickel(II), copper(II), zinc(II) and silver(I) metal salts were employed in these complexation reactions.

Using *meta*-hydroxybenzaldehyde, three (two novel) Schiff-base ligands were prepared in good yield with isolation of the products a straightforward task. The isolated ligands were stable for an extended period. Complexation reactions were carried out using nickel(II), copper(II) and zinc(II) metal ion salts, with the counterions being acetate, chloride and perchlorate. In every case except one, hydrolysis of the Schiff-base ligands occurred. Precautions were taken to exclude moisture but the use of hydrated metal salts defeated these measures. The single case where complexation was determined to be successful was with the use of an anhydrous metal salt: zinc(II) chloride. The zinc(II) salt formed a coordination polymer with two phenol ether oxygens on adjacent ligand molecules, thus bridging two Schiff-base molecules. Aside from this success, only metal-amine complexes were isolated. The use of effective drying agents or the wider availability of anhydrous metal salts may prove to bear more fruitful results if used with these ligands, along with extending the range of metal salts used.

In two cases, complexation between a Schiff-base ligand derivative and a metal salt yielded metal-amine complexes whose X-ray crystal structures were obtained. One contained a dinuclear copper(II) dimer bound to 1,3-diaminopropane (dap) with two bridging acetate ions. In the crystal was also a mononuclear copper(II) complex bound to dap with two monodentate acetate ions and a coordinated water. The mononuclear complex adopted a distorted square pyramidal geometry. The second X-ray crystal structure isolated contained a pentanuclear copper(II) matrix, the result of the reaction of copper(II) chloride and a hydrolysed Schiff-base that produced 3,3'-diamino-N-methyldipropylamine (dmda). The unit cell contained a dinuclear chloride bridged metal amine species, two mononuclear metal amine species and an unusual two-coordinate copper centre. It is not clear if the copper ion is copper(II) or copper(I) but based on literature trends for copper(I) species this was deemed to be the likely

oxidation state of the copper centre, with a counter ion hydroxide balancing the charges.

The very limited success of the *meta*-hydroxy Schiff-base family resulted in the re-evaluation of progressing to synthesis a macrocyclic derivative. To this end *ortho*-hydroxybenzaldehyde was used as a substitute. Using an ethyl linker to the lower rim of the calix[4]arene, **29** was prepared in moderate yield. Using this as a template, a family of compounds were prepared from the macromolecular aldehyde. Some of them were found to be unstable under reflux conditions and conversion of these from a hydrazone and an acyclic azine (in separate cases) to a communal product that was characterised by X-ray crystallography to be a cyclic azine. Binding studies on this macromolecular bicycle revealed it to be poor at the complexation of metal ions.

The family of azines produced three additional X-ray crystal structures. One of these azines, **32** was crystallised initially from xylenes with the pendant arms folded upwards against the wall of the calix[4]arene. It was found to have formed an inclusion complex with a molecule of xylene sandwiched between the pendant arms, the result it was thought of π-π stacking interactions. Crystallisation also took place of the same molecule from a non-aromatic solvent: *N,N*-dimethylformamide (DMF). The folded upwards orientation of the pendant arms persisted in this environment leading to the theory that an interaction exists between the hydroxyl group on the azine and the wall of the calix[4]arene. Molecular modelling may cast some light on the reasons for the calix[4]arene azine adopting this orientation

The family of acyclic calix[4]arene azines fared better than the cyclic derivative when subjected to complexation reactions. Two zinc(II) calix[4]arene azine complexes (a dinuclear and a trinuclear) were prepared and were both found to exhibit fluorescent properties. The free ligands and the zinc(II) complexes were both found to have some degree of fluorescent activity and in all cases an enhancement of emission occurred on complexation of the zinc(II) ion. The range of azines could be expanded to determine the scope of the fluorescent properties of this class of macrocyclic compound.

Model complexes (benzazines) of the pendant arms were also prepared to determine whether the calix[4]arene had any effect on the fluorescent properties of the pendant arms. Complexation of the zinc(II) salts was successful yielding several novel zinc(II)

azine complexes. Fluorescent studies on these azines aligned itself to the trend exhibited by the zinc(II) calix[4]arene azine complexes in that there is an increase in the emission intensity on complexation of the zinc(II) ion when compared to the emission strength of the free ligands. It would seem that the calix[4]arene macromolecule has little effect on the fluorescent characteristics of the azine moiety, although the substituents on the benzazine aromatic rings do.

Aside from imine donor ligands, a set of metal complexes using a benzamide ligand were also prepared. The synthesis of *N*-(2-aminoethyl)-2-hydroxy-5-nitrobenzamide **46** was accomplished using unprotected ethylene diamine (en) and methyl-2-hydroxy-5-nitrobenzoate in good yield. The amide was found to function as a zwitterionic species. The hydrochloride salt of **46** was also prepared using a facile procedure. The zwitterion and its hydrochloride salt differed in the orientation of the amide group, thus possessing potential ambidentate character. Both species were found to be soluble in water and were also characterised by X-ray crystallography. As a result of its solubility, subsequent metal complexation reactions of **46** were carried out in water.

Copper(II), nickel(II) and zinc(II) complexes were prepared of the benzamide ligand **46**. Two of these yielded X-ray grade crystals and their structures subsequently solved. Both products were produced from a reaction of **46** with copper(II) perchlorate. An octahedral mononuclear complex with two equivalents of **46** occupying the equatorial positions as neutral donors with coordinated perchlorate anions situated in the axial coordination sites when the metal salt-to-ligand ratio is 2:1, formed. The second copper(II) complex was a square planar complex with **46** functioning as a charged ligand with deprotonation occurring at both the phenol and at the amide proton. Experimental conditions required the use of a metal salt-to-ligand ratio of 1:2. Copper(II) acetate exclusively produced the four-coordinate square planar complex whilst reaction of **46** with copper(II) chloride produced the six-coordinate analogue of the octahedral copper(II) perchlorate complex. Reaction of copper(II) acetate with the ligand in acetonitrile yielded a proposed dinuclear acetate bridged species with the ligand. Formation of the zinc(II) complexes of **46** required the use of a base to effect complexation. In all cases regarding the zinc(II) complexes exclusive formation of the zinc(II) derivative of the square planar copper(II) complex occurred. Further work is required to determine the scope of the metal binding abilities of **46** and also the reason behind the production of two separate copper(II) complexes.

To prepare the macromolecular version of **46**, a point of attachment had to be provided on the lower rim of the calix[4]arene. Calix[4]arene diester derivative **56** was prepared to allow attachment to occur. No reaction occurred. The use of base was tried to produce the free amine from the zwitterion, but to no avail. Converting **56** to a diacid chloride provided a more reactive substrate but this yielded similar results when attempting to join **46** to it. From here it was decided to build the ligand sequentially out from the acid chloride terminus. Mono-Boc-protected ethylene diamine successfully coupled to **56**. Facile deprotection with trifluoroacetic acid furnished the free amine. This coupled successfully to **63** in reasonable yield to give **64**. Liberating the phenol from its methyl ether protecting group was achieved through the use of boron tribromide to give the macromolecular analogue of **46**: calix[4]arene derivative **65**. Improved synthetic methods for the efficient production of **65** are needed to produce appropriate quantities for exhaustive metal complexation studies.

Preliminary metal complexation studies were carried out on both **64** and **65**. Binding studies based on peak shifts in ^{1}H NMR spectra were carried out and yielded approximate information about the ratio of metal ion take up per ligand. **64**, with its aryl-methyl ether *ortho* to the benzamide failed to display any sort of interaction with any of the metal ions present in solution, judging by the absence of changes in its ^{1}H NMR spectrum. The metal salts used were sodium(I), silver(I) and zinc(II) metal salts with either acetate, chloride or perchlorate counterions. Deprotected of the methyl ether was by the method mentioned in the previous paragraph to yield **65**, whose complexation studies yielded much more encouraging results. Using the same array of metal salts as with **64**, it was found that the ligand only interacts with the metal cation when the counterion of the metal was the acetate. The use of relative pK_a values help explain this selectivity. Future work could vary the substituents on the aromatic ring to tune the acidity of the phenolic proton. This could further enhance the selectivity of **65** in the preparation and development of a highly selective ion binder.

Bibliography

1. K. C. Gupta, A. Kumar Sutar and C.-C. Lin, *Coord. Chem. Rev.*, 2009, **253**, 1926; Y. Kou, J. Tian, D. Li, W. Gu, X. Liu, S. Yan, D. Liao and P. Cheng, *Dalton Trans.*, 2009, 2374.

2. D. Iyaguchi, S. Kawano, K. Takada and E. Toyota, *Bioorg. & Med. Chem.*, 2010, **18**, 2076.

3. N. P. Kushwah, M. K. Pal, A. P. Wadawale and V. K. Jain, *J. Organomet. Chem.*, 2009, **694**, 2375; J.-C. Andrez, *Tet. Lett.*, 2009, **50**, 4225; Y. Zhang, L. Xiang, Q. Wang, X.-F. Duan and G. Zi, *Inorg. Chim. Acta*, 2008, **361**, 1246.

4. N. Singh, M. S. Hundal, G. Hundal and M. Martinez-Ripoll, *Tetrahedron*, 2005, **61**, 7796.

5. P. A. Vigato, S. Tamburini and L. Bertolo, *Coord. Chem. Rev.*, 2007, **251**, 1311; P. A. Vigato, S. Tamburini and P. Guerriero, *Coord. Chem. Rev.*, 1995, **139**, 17.

6. T. M. Ross, S. M. Neville, D. S. Innes, D. R. Turner, B. Moubaraki and K. S. Murray, *Dalton Trans.*, 2010, **39**, 149.

7. G. Nocton, P. Horeglad, V. Vetere, J. Pecaut, L. Dubois, P. Maldivi, N. M. Edelstein and M. Mazzanti, *J. Am. Chem. Soc.*, 2009, **132**, 495.

8. E. N. Jacobsen, W. Zhang, A. R. Muci, J. R. Ecker and L. Deng, *J. Am. Chem. Soc.*, 1991, **113**, 7063.

9. K. C. Gupta and A. K. Sutar, *Coord. Chem. Rev.*, 2008, **252**, 1420.

10. L. Li, Y.-Q. Dang, H.-W. Li, B. Wang and Y. Wu, *Tet. Lett.*, 2010, **51**, 618.

11. L. C. Nathan, J. E. Koehne, J. M. Gilmore, K. A. Hannibal, W. E. Dewhirst and T. D. Mai, *Polyhedron*, 2003, **22**, 887.

12. E. J. Campbell and S. T. Nguyen, *Tet. Lett.*, 2001, **42**, 1221.

13. L. T. Taylor and W. M. Coleman, *J. Am. Chem. Soc.*, 1970, **92**, 1449; P. Chakraborty, S. K. Chandra and A. Chakravorty, *Inorg. Chem.*, 1994, **33**, 4959.

14. J. Chakraborty, A. Ray, G. Pilet, G. Chastanet, D. Luneau, R. F. Ziessel, L. J. Charbonniere, L. Carrella, E. Rentschler, M. S. E. Fallah and S. Mitra, *Dalton Trans.*, 2009, 10263; C. S. Marvel, S. A. Aspey and E. A. Dudley, *J. Am. Chem. Soc.*, 1956, **78**, 4905.

15. H. J. Banbery, F. McQuillan, T. A. Hamor, C. J. Jones and J. A. McCleverty, *J. Chem. Soc., Dalton Trans.*, 1989, 1405.

16. A. E. Frost and H. H. Freedman, *J. Org. Chem.*, 1959, **24**, 1905.

17. I. I. Ebralidze, G. Leitus, L. J. W. Shimon, Y. Wang, S. Shaik and R. Neumann, *Inorg. Chim. Acta*, 2009, **362**, 4713; G. K. Patra and I. Goldberg, *Eur. J. Inorg. Chem.*, 2003, **2003**, 969; M. Mukhopadhyay, M. M. Reddy, G. C. Maikap and J. Iqbal, *J. Org. Chem.*, 1995, **60**, 2670.

18. I. Correia, A. Dornyei, T. Jakusch, F. Avecilla, T. Kiss and J. C. Pessoa, *Eur. J. Inorg. Chem.*, 2006, **2006**, 2819.

19. F. A. Cotton and G. Wilkinson, 'Advanced Inorganic Chemistry' John Wiley & Sons, 5ᵗʰ ed., 1988, New York.

20. M. G. Gichinga and S. Striegler, *J. Am. Chem. Soc.*, 2008, **130**, 5150; S.-Y. Ku, K.-T. Wong and A. J. Bard, *J. Am. Chem. Soc.*, 2008, **130**, 2392; E. C. Constable, G. Zhang, C. E. Housecroft, M. Neuburger, S. Schaffner and W.-D. Woggon, *New Jour. Chem.*, 2009, **33**, 1064.

21. L. T. Yildirim, R. Kurtaran, H. Namli, A. D. Azaz and O. Atakol, *Polyhedron*, 2007, **26**, 4187.

22. P. J. McCarthy, R. J. Hovey, K. Ueno and A. E. Martell, *J. Am. Chem. Soc.*, 1955, **77**, 5820.

23. M. Asadi, K. A. Jamshid and A. H. Kyanfar, *Inorg. Chim. Acta*, 2007, **360**, 1725; D. Cunningham, J. F. Gallagher, T. Higgins, P. McArdle, J. McGinley and M. O' Gara, *J. Chem. Soc., Dalton Trans.*, 1993, 2183.

24. S. Anbu, M. Kandaswamy and B. Varghese, *Dalton Trans.*, 2010, **39**, 3823.

25. P. Mukherjee, M. G. B. Drew and A. Ghosh, *Eur. J. Inorg. Chem.*, 2008, **2008**, 3372.

26. V. A. Soloshonok, T. U. Boettiger and S. B. Bolene, *Synthesis*, 2008, **2008**, 2594.

27. Y. N. Belokon, N. B. Bespalova, T. D. Churkina, I. Císařová, M. G. Ezernitskaya, S. R. Harutyunyan, R. Hrdina, H. B. Kagan, P. Kočovský, K. A. Kochetkov, O. V. Larionov, K. A. Lyssenko, M. North, M. Polášek, A. S. Peregudov, V. V. Prisyazhnyuk and Š. Vyskočil, *J. Am. Chem. Soc.*, 2003, **125**, 12860.

28. T. K. Ellis and V. A. Soloshonok, *Synlett*, 2006, **2006**, 0533.

29. S. Brooker, P. D. Croucher, T. C. Davidson, G. S. Dunbar, C. U. Beck and S. Subramanian, *Eur. J. Inorg. Chem.*, 2000, **2000**, 169.

30. G. A. Lawrance, M. Maeder, T. M. Manning, M. A. O' Leary, B. W. Skelton and A. H. White, *J. Chem. Soc., Dalton Trans.*, 1990, 2491.

31. R. Ocampo and W. R. Dolbier Jr, *Tetrahedron*, 2004, **60**, 9325.

32. H. E. Simmons and R. D. Smith, *J. Am. Chem. Soc.*, 1958, **80**, 5323; M. Nakamura, A. Hirai and E. Nakamura, *J. Am. Chem. Soc.*, 2003, **125**, 2341.

33. K. Soai and S. Niwa, *Chem. Rev.*, 1992, **92**, 833.

34. S. J. Lippard and E. M. Nolan, *Acc. Chem. Res.*, 2009, **42**, 193.

35. S. J. Lippard and S. C. Burdette, *Coord. Chem. Rev.*, 2001, **216-217**, 333.

36. X.-X. Sun, C.-M. Qi, S.-L. Ma, H.-B. Huang, W.-x. Zhu and Y.-C. Liu, *Inorg. Chem. Commun.*, 2006, **9**, 911.

37. E. C. Escudero-Adán, J. Benet-Buchholz and A. W. Kleij, *Eur. J. Inorg. Chem.*, 2009, **2009**, 3562.

38. K. G. Vladimirova, A. Y. Freidzon, O. V. Kotova, A. A. Vaschenko, L. S. Lepnev, A. A. Bagatur'yants, A. G. Vitukhnovskiy, N. F. Stepanov and M. V. Alfimov, *Inorg. Chem.*, 2009, **48**, 11123.

39. C. D. Gutsche, 'Calixarenes: An Introduction' Royal Society of Chemistry, 2nd ed., 2008, Cambridge.

40. J. W. Cornforth, P. D. Hart, G. A. Nicholls, R. J. W. Rees and J. A. Stock, *Br. J. Pharmacol. Chemother.*, 1955, **10**, 73.

41. G. D. Andreetti, R. Ungaro and A. Pochini, *J. Chem. Soc., Chem. Commun.*, 1979, 1005.

42. C. D. Gutsche, M. Iqbal and D. Stewart, *J. Org. Chem.*, 1986, **51**, 742.

43. C. D. Gutsche, A. E. Gutsche and A. I. Karaulov, *J. Inclusion Phenom. Macrocyclic Chem.*, 1985, **3**, 447.

44. C. D. Gutsche, D. E. Johnston and D. R. Stewart, *J. Org. Chem.*, 1999, **64**, 3747.

45. P. D. Harvey, *Coord. Chem. Rev.*, 2002, **233-234**, 289.

46. C. Wieser, C. B. Dieleman and D. Matt, *Coord. Chem. Rev.*, 1997, **165**, 93.

47. B. S. Creaven, D. F. Donlon and J. McGinley, *Coord. Chem. Rev.*, 2009, **253**, 893.

48. E. M. Collins, M. A. McKervey, E. Madigan, M. B. Moran, M. Owens, G. Ferguson and S. J. Harris, *J. Chem. Soc., Perkin Trans. 1*, 1991, 3137.

49. S. Veravong, V. Ruangpornvisuto, B. Poipoosananakaton, M. Sukwattanasinitt and T. Tuntulani, *ScienceAsia*, 2000, **26**, 163.

50.   J. Luo, L.-C. Shen and W.-S. Chung, *J. Org. Chem.*, 2009, **75**, 464; M. Lankshear, I. Dudley, K. M. Chan, A. Cowley, S. Santos, V. Felix and P. Beer, *Chem.-Eur. J.*, 2008, **14**, 2248.

51.   C. Jeunesse, C. Dieleman, S. Steyer and D. Matt, *J. Chem. Soc., Dalton Trans.*, 2001, 881; S. Steyer, C. Jeunesse, D. Matt, R. Welter and M. Wesolek, *J. Chem. Soc., Dalton Trans.*, 2002, 4264.

52.   H. Al-Saraierh, D. O. Miller and P. E. Georghiou, *J. Org. Chem.*, 2005, **70**, 8273.

53.   S. Chowdhury, J. N. Bridson and P. E. Georghiou, *J. Org. Chem.*, 2000, **65**, 3299.

54.   S. O'Malley, B. Schazmann, D. Diamond and K. Nolan, *Tet. Lett.*, 2007, **48**, 9003; N. Kerdpaiboon, B. Tomapatanaget, O. Chailapakul and T. Tuntulani, *J. Org. Chem.*, 2005, **70**, 4797.

55.   R. Patel, J. Panchal, V. Rana and S. Menon, *J. Inclusion Phenom. Macrocyclic Chem.*, 2010, **66**, 285.

56.   Y. Liu, B.-T. Zhao, H.-Y. Zhang, T. Wada and Y. Inoue, *J. Chem. Soc., Perkin Trans. 2*, 2001, 1219.

57.   B. S. Creaven, M. Deasy, P. M. Flood, J. McGinley and B. A. Murray, *Inorg. Chem. Commun.*, 2008, **11**, 1215.

58.   R. Seangprasertkij, Z. Asfari, F. Arnaud, J. Weiss and J. Vicens, *J. Inclusion Phenom. Macrocyclic Chem.*, 1992, **14**, 141.

59.   R. Seangprasertkij, Z. Asfari, F. Arnaud and J. Vicens, *J. Org. Chem.*, 1994, **59**, 1741.

60.   N. Singh, G. W. Lee and D. O. Jang, *Tetrahedron*, 2008, **64**, 1482.

61.   V. Böhmer, G. Ferguson, J. F. Gallagher, A. J. Lough, M. A. McKervey, E. Madigan, M. B. Moran, J. Phillips and G. Williams, *J. Chem. Soc., Perkin Trans. 1*, 1993, 1521.

62.   H. M. Chawla, S. P. Singh and S. Upreti, *Tetrahedron*, 2006, **62**, 9758.

63.   A. D. Bond, B. S. Creaven, D. F. Donlon, T. L. Gernon, J. McGinley and H. Toftlund, *Eur. J. Inorg. Chem.*, 2007, **2007**, 749.

64.   C. Gaeta, M. De Rosa, M. Fruilo, A. Soriente and P. Neri, *Tetrahedron: Asymmetry*, 2005, **16**, 2333.

65.   A. Sharma and S. G. Schulman, 'Introduction to Fluorescence Spectroscopy' John Wiley & Sons, 1st ed., 1999, New York.

66.   B. Valeur, 'Molecular Fluorescence Principles and Applications' John Wiley & Sons, 1st ed., 2002, Weinheim.

67.   J. R. Lakowicz, 'Principles of Fluorescence Spectroscopy' Springer, 3rd ed., 2006, New York.

68.   H. A. Clark, R. Kopelman, R. Tjalkens and M. A. Philbert, *Anal. Chem.*, 1999, **71**, 4837; B. Cohen and D. Huppert, *J. Phys. Chem. A*, 2001, **105**, 7157.

69.   N. Boens, W. Qin, N. Basarić, A. Orte, E. M. Talavera and J. M. Alvarez-Pez, *J. Phys. Chem. A*, 2006, **110**, 9334.

70.   P. Nandhikonda, M. P. Begaye and M. D. Heagy, *Tet. Lett.*, 2009, **50**, 2459; I. Stoll, J. Eberhard, R. Brodbeck, W. Eisfeld and J. Mattay, *Chem.-Eur. J.*, 2008, **14**, 1155; R. D. Carpenter and A. S. Verkman, *Org. Lett.*, 2010, **12**, 1160; S. J. M. Koskela, T. M. Fyles and T. D. James, *Chem. Commun.*, 2005, 945.

71.   C. Bazzicalupi, A. Bencini, S. Biagini, A. Bianchi, E. Faggi, C. Giorgi, M. Marchetta, F. Totti and B. Valtancoli, *Chem.-Eur. J.*, 2009, **15**, 8049; F. Pina, M. Bernardo and E. García-España, *Eur. J. Inorg. Chem.*, 2000, **2000**, 2143; J. Pina, J. Seixas de Melo, F. Pina, C. Lodeiro, J. C. Lima, A. J. Parola, C. Soriano, M. P. Clares, M. T. Albelda, R. Aucejo and E. García-España, *Inorg. Chem.*, 2005, **44**, 7449.

72.   S. Goswami and R. Chakrabarty, *Tet. Lett.*, 2009, **50**, 5910.

73.   S. J. Bullock, C. E. Felton, R. V. Fennessy, L. P. Harding, M. Andrews, S. J. A. Pope, C. R. Rice and T. Riis-Johannessen, *Dalton Trans.*, 2009, 10570.

74.   G. De Santis, L. Fabbrizzi, M. Licchelli, C. Mangano, D. Sacchi and N. Sardone, *Inorg. Chim. Acta*, 1997, **257**, 69.

75.   J. S. Kim and D. T. Quang, *Chem. Rev.*, 2007, **107**, 3780; I. Leray and B. Valeur, *Eur. J. Inorg. Chem.*, 2009, **2009**, 3525.

76.   S. Y. Park, J. H. Yoon, C. S. Hong, R. Souane, J. S. Kim, S. E. Matthews and J. Vicens, *J. Org. Chem.*, 2008, **73**, 8212.

77.   T. Gruber, C. Fischer, M. Felsmann, W. Seichter and E. Weber, *Org. Biomol. Chem.*, 2009, **7**, 4904.

78.   E. L. Que, D. W. Domaille and C. J. Chang, *Chem. Rev.*, 2008, **108**, 1517.

79.   T. Hirano, K. Kikuchi, Y. Urano, T. Higuchi and T. Nagano, *Angew. Chem., Int. Ed.*, 2000, **39**, 1052.

80.   H. Görner, S. Khanra, T. Weyhermuller and P. Chaudhuri, *J. Phys. Chem. A*, 2006, **110**, 2587.

81. W. Tang, Y. Xiang and A. Tong, *J. Org. Chem.*, 2009, **74**, 2163.

82. N. L. Fry, M. J. Rose, C. Nyitray and P. K. Mascharak, *Inorg. Chem.*, 2008, **47**, 11604.

83. M. Wood, D. Leitch, C. Yeung, J. Kozak and L. Schafer, *Angew. Chem., Int. Ed.*, 2007, **46**, 354.

84. G. Zi, F. Zhang, L. Xiang, Y. Chen, W. Fang and H. Song, *Dalton Trans.*, 2010, **39**, 4048.

85. L. Stoicescu, C. Duhayon, L. Vendier, A. Tesouro-Vallina, J. P. Costes and J. P. Tuchagues, *Eur. J. Inorg. Chem.*, 2009, **2009**, 5483.

86. J. March, 'Advanced Organic Chemistry' John Wiley & Sons, 3rd ed., 1985, New York.

87. J. Clayden, N. Greeves, S. Warren and P. Wothers, 'Organic Chemistry' Oxford University Press, 1st ed., 2001, Oxford.

88. M. Kunishima, C. Kawachi, J. Monta, K. Terao, F. Iwasaki and S. Tani, *Tetrahedron*, 1999, **55**, 13159.

89. Q. Y. Chen and C. F. Chen, *Eur. J. Org. Chem.*, 2005, 2468.

90. T. Kido, Y. Ikuta, Y. Sunatsuki, Y. Ogawa, N. Matsumoto and N. Re, *Inorg. Chem.*, 2002, **42**, 398; Y. Zou, W.-L. Liu, S. Gao, C.-S. Lu, D.-B. Dang and Q.-J. Meng, *Polyhedron*, 2004, **23**, 2253.

91. P. A. Vigato and S. Tamburini, *Coord. Chem. Rev.*, 2008, **252**, 1871.

92. W.-L. Liu, Y. Zou, C.-L. Ni, Z.-P. Ni, Y.-Z. Li, Y.-G. Yao and Q.-J. Meng, *Polyhedron*, 2004, **23**, 849.

93. J.-P. Costes, L. Vendier and W. Wernsdorfer, *Dalton Trans.*, 2010, **39**, 4886.

94. O. Rotthaus, O. Jarjayes, F. Thomas, C. Philouze, C. P. del Valle, E. Saint-Aman and J.-L. Pierre, *Chem.-Eur. J.*, 2006, **12**, 2293.

95. T. C. Harrop, M. M. Olmstead and P. K. Mascharak, *Inorg. Chem.*, 2006, **45**, 3424.

96. S. Osa, Y. Sunatsuki, Y. Yamamoto, M. Nakamura, T. Shimamoto, N. Matsumoto and N. Re, *Inorg. Chem.*, 2003, **42**, 5507.

97. N. Nishat, M. M. Haq, T. Ahamad and V. Kumar, *J. Coord. Chem.*, 2007, **60**, 85.

98. P. Sarmah, S. Singha, R. Chakrabarty, S. J. Bora and B. K. Das, *Indian Jour. Chem. Section A. Bio-org, Bio-inorg, Phys, Theoret. & Anal. Chem.*, 2007, **46(A)**, 1929.

99. S. Mitra, G. De and N. R. Chaudhuri, *Thermochim. Acta*, 1983, **66**, 187.

100. V. Zeleňák, A. Orendáčová, I. Císařová, J. Černák, O. V. Kravchyna, J. H. Park, M. Orendáč, A. G. Anders, A. Feher and M. W. Meisel, *Inorg. Chem.*, 2006, **45**, 1774.

101. S. P. Roe, J. O. Hill and R. J. Magee, *Monatsh. Chem.*, 1991, **122**, 467.

102. C. D. Gutsche, B. Dhawan, K. H. No and R. Muthukrishnan, *J. Am. Chem. Soc.*, 1981, **103**, 3782.

103. Z. T. Li, G. Z. Ji, C. X. Zhao, S. D. Yuan, H. Ding, C. Huang, A. L. Du and M. Wei, *J. Org. Chem.*, 1999, **64**, 3572.

104. B. de Castro, C. Sousa and C. Freire, *Molecules*, 2003, **8**, 894.

105. H. H. Szmant and C. M. Harmuth, *J. Am. Chem. Soc.*, 1959, **81**, 962.

106. K. Aoki, S. Shimizu, K. Satake, S. Yamazaki and N. Hatakeyama, *Jp. Pat.*, 52-156827, 1977.

107. E. M. Collins, M. A. McKervey and S. J. Harris, *J. Chem. Soc., Perkin Trans. 1*, 1989, 372.

108. A. Eisenführ, P. S. Arora, G. Sengle, L. R. Takaoka, J. S. Nowick and M. Famulok, *Bioorg. & Med. Chem.*, 2003, **11**, 235.

109. T. de Paulis, A. Janowsky, R. M. Kessler, J. A. Clanton and H. E. Smith, *J. Med. Chem.*, 1988, **31**, 2027.

110. G. M. Sheldrick, *Acta Cryst. Section A*, 2008, **64**, 112.

111. A. W. Addison, T. N. Rao, J. Reedijk, J. Vanrijn and G. C. Verschoor, *J. Chem. Soc., Dalton Trans.*, 1984, 1349; G. A. van Albada, I. Mutikainen, U. Turpeinen and J. Reedijk, *Inorg. Chem. Commun.*, 2006, **9**, 1067.

112. S. J. Brown, X. Tao, D. W. Stephan and P. K. Mascharak, *Inorg. Chem.*, 1986, **25**, 3377; B. Sarkar, M. G. B. Drew, M. Estrader, C. Diaz and A. Ghosh, *Polyhedron*, 2008, **27**, 2625; G. Mezei, M. Rivera-Carrillo and R. G. Raptis, *Inorg. Chim. Acta*, 2004, **357**, 3721.

113. A. M. Prokhorov, D. N. Kozhevnikov, V. L. Rusinov, O. N. Chupakhin, I. V. Glukhov, M. Y. Antipin, O. N. Kazheva, A. N. Chekhlov and O. A. Dyachenko, *Organometallics*, 2006, **25**, 2972; A. Bernalte-García, A. M. Lozano-Vila, F. Luna-Giles and R. Pedrero-Marín, *Polyhedron*, 2006, **25**, 1399; J. M. Veauthier, E. Tomat, V. M. Lynch, J. L. Sessler, U. Mirsaidov and J. T. Markert, *Inorg. Chem.*, 2005, **44**, 6736.

114. M. Du, Y. M. Guo, X. H. Bu, J. Ribas and M. Monfort, *New Jour. Chem.*, 2002, **26**, 939; X.-J. Zhao, M. Du, Y. Wang, J.-H. Guo and X.-H. Bu, *Inorg. Chim. Acta*, 2005, **358**, 4481.

115. A. K. McCasland, N. W. Alcock and D. H. Busch, *Acta Cryst. Section C*, 1998, **54**, 1837.

116. L. Wang, R.-B. Huang, L.-S. Long, L.-S. Zheng, E.-B. Wang and Z.-X. Xie, *J. Coord. Chem.*, 2005, **58**, 1439 ; F. Mohr, S. A. Binfield, J. C. Fettinger and A. N. Vedernikov, *J. Org. Chem.*, 2005, **70**, 4833; S. H. Oakley, M. P. Coles and P. B. Hitchcock, *Inorg. Chem.*, 2004, **43**, 5168.

117. C.-W. Yeh, H.-L. Hu, R.-H. Liang, K.-M. Wang, T.-Y. Yen, J.-D. Chen and J.-C. Wang, *Polyhedron*, 2005, **24**, 539.

118. N. Singh, M. Kumar and G. Hundal, *Tetrahedron*, 2004, **60**, 5393; B. S. Creaven, M. Deasy, J. F. Gallagher, J. McGinley and B. A. Murray, *Tetrahedron*, 2001, **57**, 8883; R. Dorta, L. J. W. Shimon, H. Rozenberg, Y. Ben-David and D. Milstein, *Inorg. Chem.*, 2003, **42**, 3160; X. Zeng, H. Sun, L. Chen, X. Leng, F. Xu, Q. Li, X. He, W. Zhang and Z.-Z. Zhang, *Org. Biomol. Chem.*, 2003, **1**, 1073; P. R. A. Webber, A. Cowley, M. G. B. Drew and P. D. Beer, *Chem.-Eur. J.*, 2003, **9**, 2439.

119. M. Pietraszkiewicz, O. Pietraszkiewicz, W. Kolodziejski, K. Wozniak, N. Feeder, F. Benevelli and J. Klinowski, *J. Phys. Chem. B*, 2000, **104**, 1921.

120. H. Takemura, T. Iwanaga and T. Shinmyozu, *Tet. Lett.*, 2005, **46**, 6687.

121. P. A. Vigato and S. Tamburini, *Coord. Chem. Rev.*, 2004, **248**, 1717.

122. J.-M. Kim, S. J. Min, S. W. Lee, J. H. Bok and J. S. Kim, *Chem. Commun.*, 2005, 3427; S. K. Kim, S. H. Kim, H. J. Kim, S. H. Lee, S. W. Lee, J. Ko, R. A. Bartsch and J. S. Kim, *Inorg. Chem.*, 2005, **44**, 7866; P. A. Gale, Z. Chen, M. G. B. Drew, J. A. Heath and P. D. Beer, *Polyhedron*, 1998, **17**, 405.

123. A. I. Costa and J. V. Prata, *Supramolecular Chemistry*, 2008, **20**, 95 ; X. H. Sun, C. S. Chan, M. S. Wong and W. Y. Wong, *Tetrahedron*, 2006, **62**, 7846; R. Nakamura, A. Ikeda, L. D. Sarson and S. Shinkai, *Supramolecular Chemistry*, 1998, **9**, 25

124. K. Nakamoto, 'Infrared and Raman Spectra of Inorganic and Coordination Compounds' Wiley-Interscience, 3, 1977, New York.

125. E. Almaraz, W. S. Foley, J. A. Denny, J. H. Reibenspies, M. L. Golden and M. Y. Darensbourg, *Inorg. Chem.*, 2009, **48**, 5288; B.-H. Ye, X.-Y. Li, I. D.

Williams and X.-M. Chen, *Inorg. Chem.*, 2002, **41**, 6426; H. Adams, N. A. Bailey, D. E. Fenton and Q. Y. He, *J. Chem. Soc., Dalton Trans.*, 1995, 697; E. Szlyk, A. Wojtczak, A. Surdykowski and M. Gozdzikiewicz, *Inorg. Chim. Acta*, 2005, **358**, 467.

126. A. R. Kennedy, K. G. Brown, D. Graham, J. B. Kirkhouse, M. Kittner, C. Major, C. J. McHugh, P. Murdoch and W. E. Smith, *New Jour. Chem.*, 2005, **29**, 826.

127. Z. W. Fu, *Acta Cryst. Section E*, 2007, **63**, O2993.

128. G. Mahmoudi and A. Morsali, *Polyhedron*, 2008, **27**, 1070; D. A. Edwards, G. M. Hoskins, M. F. Mahon, K. C. Molloy and G. R. G. Rudolph, *Polyhedron*, 1998, **17**, 2321; W. J. Stratton and D. H. Busch, *J. Am. Chem. Soc.*, 1958, **80**, 3191.

129. F. H. Allen, O. Kennard, D. G. Watson, L. Brammer, A. G. Orpen and R. Taylor, *J. Chem. Soc., Perkin Trans. 2*, 1987, S1.

130. P. Mukherjee, O. Sengupta, M. G. B. Drew and A. Ghosh, *Inorg. Chim. Acta*, 2009, **362**, 3285; K. S. Bharathi, A. K. Rahiman, K. Rajesh, S. Sreedaran, P. G. Aravindan, D. Velmurugan and V. Narayanan, *Polyhedron*, 2006, **25**, 2859; C. P. Pradeep, P. S. Zacharias and S. K. Das, *Inorg. Chem. Commun.*, 2006, **9**, 1071.

131. J.-H. Zhou, R.-M. Cheng, Y. Song, Y.-Z. Li, Z. Yu, X.-T. Chen and X.-Z. You, *Polyhedron*, 2006, **25**, 2426; D. Lee, P.-L. Hung, B. Spingler and S. J. Lippard, *Inorg. Chem.*, 2002, **41**, 521.

132. P. K. Dhara, S. Sarkar, M. G. B. Drew, M. Nethaji and P. Chattopadhyay, *Polyhedron*, 2008, **27**, 2447; S. Senda, Y. Ohki, T. Hirayama, D. Toda, J.-L. Chen, T. Matsumoto, H. Kawaguchi and K. Tatsumi, *Inorg. Chem.*, 2006, **45**, 9914; K. O. Joung, C. J. O'Connor, E. Sinn and R. L. Carlin, *Inorg. Chem.*, 1979, **18**, 804.

133. J. Y. Yang and D. G. Nocera, *Tet. Lett.*, 2008, **49**, 4796; J.-P. Costes, S. Shova and W. Wernsdorfer, *Dalton Trans.*, 2008, 1843.

134. C. J. Marmion, D. Griffith and K. B. Nolan, *Eur. J. Inorg. Chem.*, 2004, **2004**, 3003.

135. C. Comuzzi, A. Melchior, P. Polese, R. Portanova and M. Tolazzi, *Eur. J. Inorg. Chem.*, 2002, **2002**, 2194; J. C. Friese, A. Krol, C. Puke, K. Kirschbaum

and D. M. Giolando, *Inorg. Chem.*, 2000, **39**, 1496; A. S. Hay, *J. Org. Chem.*, 1962, **27**, 3320.

136. T. Depaulis, A. Janowsky, R. M. Kessler, J. A. Clanton and H. E. Smith, *J. Med. Chem.*, 1988, **31**, 2027.

137. C. Bilton, F. H. Allen, G. P. Shields and J. A. K. Howard, *Acta Cryst. Section B*, 2000, **56**, 849.

138. C. Dielemann, D. Matt, P. G. Jones and H. Thonnessen, *Acta Cryst. Section C*, 2003, **59**, O247.

139. E. M. Collins, F. Arnaudneu, M. Deasy, G. Ferguson, S. J. Harris, B. Kaitner, A. J. Lough, M. A. McKervey, E. Marques, B. L. Ruhl, M. J. Schwingweill and E. M. Seward, *J. Am. Chem. Soc.*, 1989, **111**, 8681.

140. C. Suksai, S. Watchasit, T. Tuntulani and C. Pakawatchai, *Acta Cryst. Section E*, 2008, **64**, M884.

141. R. Rowan, T. Tallon, A. M. Sheahan, R. Curran, M. McCann, K. Kavanagh, M. Devereux and V. McKee, *Polyhedron*, 2006, **25**, 1771.

142. D. A. Evans and D. H. Ripin, *Evans' pK$_a$ tables*, http://www2.lsdiv.harvard.edu/labs/evans/pdf/evans_pKa_table.pdf, Date accessed:20-09-2010.

Appendix

- **Crystallographic data recorded for 15**

Table 0.1: Atomic coordinates (*10^4) and equivalent isotropic displacement parameters (Å^2 * 10^3) for **15**. U(eq) is defined as one third of the trace of the orthogonalised Uij tensor.

Atom	x	y	z	U(eq)
Cu(1)	−84(1)	1737(1)	−240(1)	20(1)
Cu(2)	5008(1)	4264(1)	2301(1)	21(1)
O(1)	−878(1)	1821(1)	389(1)	25(1)
O(2)	−734(1)	4162(1)	715(1)	27(1)
O(3)	633(1)	487(1)	688(1)	23(1)
O(4)	1517(1)	99(1)	1952(1)	34(1)
O(6)	3731(1)	2917(1)	3084(1)	34(1)
O(7)	5945(1)	5028(1)	3243(1)	27(1)
O(8)	6500(1)	2883(1)	3703(1)	40(1)
O(9)	4892(1)	6251(1)	1544(1)	33(1)
O(10)	7594(1)	521(1)	3890(1)	37(1)
O(11)	2758(1)	754(1)	3395(1)	38(1)
O(12)	1987(1)	1194(1)	4602(1)	31(1)
N(1)	−583(1)	3433(1)	−959(1)	23(1)
N(2)	753(1)	1391(1)	−838(1)	23(1)
N(3)	4051(1)	3263(1)	1449(1)	25(1)
N(4)	5836(1)	3349(1)	1814(1)	27(1)
C(1)	−741(1)	3257(2)	−1870(1)	25(1)
C(2)	58(1)	2940(2)	−2075(1)	24(1)
C(3)	441(1)	1469(2)	−1763(1)	27(1)
C(4)	−1076(1)	2968(2)	702(1)	22(1)
C(5)	−1790(1)	2801(2)	1056(1)	30(1)
C(6)	1171(1)	924(2)	1366(1)	23(1)
C(7)	1374(1)	2516(2)	1428(1)	30(1)
C(8)	4049(1)	3269(2)	570(1)	29(1)
C(9)	4822(1)	2543(2)	472(1)	33(1)
C(10)	5625(1)	3361(2)	888(1)	32(1)
C(11)	3704(1)	4264(2)	3072(1)	25(1)
C(12)	3022(1)	5028(2)	3306(1)	37(1)
C(13)	6510(1)	4223(2)	3724(1)	26(1)
C(14)	7224(1)	4984(2)	4358(1)	34(1)
O(5)	4216(1)	5058(1)	2857(1)	27(1)

Table 0.2: Bond lengths (Å) and angles (°) for **15**.

Cu(1)-O(1)	1.9550(10)	Cu(1)-N(2)	2.0013(12)
Cu(1)-N(1)	2.0022(12)	Cu(1)-O(3)	2.0153(9)
Cu(1)-O(3)#1	2.2873(9)	Cu(2)-O(7)	1.9854(10)
Cu(2)-O(5)	1.9984(10)	Cu(2)-N(4)	2.0167(13)
Cu(2)-N(3)	2.0172(12)	Cu(2)-O(9)	2.2140(11)
O(1)-C(4)	1.2772(17)	O(2)-C(4)	1.2445(17)
O(3)-C(6)	1.2820(16)	O(3)-Cu(1)#1	2.2873(9)
O(4)-C(6)	1.2400(17)	O(6)-C(11)	1.2482(18)
O(7)-C(13)	1.2792(17)	O(8)-C(13)	1.2416(19)
N(1)-C(1)	1.4840(18)	N(2)-C(3)	1.4841(18)
N(3)-C(8)	1.4815(19)	N(4)-C(10)	1.488(2)
C(1)-C(2)	1.521(2)	C(2)-C(3)	1.530(2)
C(4)-C(5)	1.511(2)	C(6)-C(7)	1.511(2)
C(8)-C(9)	1.523(2)	C(9)-C(10)	1.518(2)
C(11)-O(5)	1.2718(18)	C(11)-C(12)	1.505(2)
C(13)-C(14)	1.510(2)		

I

O(1)-Cu(1)-N(2)	172.80(4)	O(1)-Cu(1)-N(1)	93.89(5)
N(2)-Cu(1)-N(1)	92.81(5)	O(1)-Cu(1)-O(3)	86.95(4)
N(2)-Cu(1)-O(3)	87.40(4)	N(1)-Cu(1)-O(3)	163.11(4)
O(1)-Cu(1)-O(3)#1	86.57(4)	N(2)-Cu(1)-O(3)#1	88.02(4)
N(1)-Cu(1)-O(3)#1	117.23(4)	O(3)-Cu(1)-O(3)#1	79.66(4)
O(7)-Cu(2)-O(5)	88.45(4)	O(7)-Cu(2)-N(4)	89.90(5)
O(5)-Cu(2)-N(4)	175.48(5)	O(7)-Cu(2)-N(3)	172.16(5)
O(5)-Cu(2)-N(3)	90.06(5)	N(4)-Cu(2)-N(3)	91.01(5)
O(7)-Cu(2)-O(9)	93.97(4)	O(5)-Cu(2)-O(9)	90.81(4)
N(4)-Cu(2)-O(9)	93.50(5)	N(3)-Cu(2)-O(9)	93.74(5)
C(4)-O(1)-Cu(1)	124.82(9)	C(6)-O(3)-Cu(1)	126.50(9)
C(6)-O(3)-Cu(1)#1	132.74(9)	Cu(1)-O(3)-Cu(1)#1	100.34(4)
C(13)-O(7)-Cu(2)	123.10(9)	C(1)-N(1)-Cu(1)	116.41(9)
C(3)-N(2)-Cu(1)	116.78(9)	C(8)-N(3)-Cu(2)	117.45(9)
C(10)-N(4)-Cu(2)	117.20(9)	N(1)-C(1)-C(2)	112.04(11)
C(1)-C(2)-C(3)	113.72(12)	N(2)-C(3)-C(2)	112.11(11)
O(2)-C(4)-O(1)	124.50(13)	O(2)-C(4)-C(5)	120.46(13)
O(1)-C(4)-C(5)	115.03(13)	O(4)-C(6)-O(3)	122.68(13)
O(4)-C(6)-C(7)	120.48(12)	O(3)-C(6)-C(7)	116.85(12)
N(3)-C(8)-C(9)	112.06(12)	C(10)-C(9)-C(8)	113.47(13)
N(4)-C(10)-C(9)	111.47(13)	O(6)-C(11)-O(5)	123.92(14)
O(6)-C(11)-C(12)	119.53(14)	O(5)-C(11)-C(12)	116.54(13)
O(8)-C(13)-O(7)	124.35(13)	O(8)-C(13)-C(14)	119.16(13)
O(7)-C(13)-C(14)	116.49(13)	C(11)-O(5)-Cu(2)	122.40(9)

Symmetry transformations used to generate equivalent atoms: #1 −x,−y,−z

Table 0.3: Anisotropic displacement parameters ($\mathring{A}^2$ x 10^3) for **15**. The anisotropic displacement factor exponent takes the form: $-2\,g\pi^2$ [$h^2\,a^{*2}$ U11 + ... + 2 h k a* b* U12].

Atom	U11	U22	U33	U23	U13	U12
Cu(1)	23(1)	17(1)	21(1)	1(1)	9(1)	1(1)
Cu(2)	20(1)	18(1)	26(1)	0(1)	7(1)	0(1)
O(1)	30(1)	18(1)	29(1)	1(1)	14(1)	2(1)
O(2)	27(1)	23(1)	33(1)	−4(1)	11(1)	−4(1)
O(3)	24(1)	20(1)	22(1)	−2(1)	4(1)	−1(1)
O(4)	38(1)	30(1)	28(1)	6(1)	0(1)	−7(1)
O(6)	33(1)	23(1)	51(1)	3(1)	21(1)	−1(1)
O(7)	24(1)	23(1)	32(1)	−1(1)	4(1)	1(1)
O(8)	29(1)	24(1)	58(1)	5(1)	2(1)	1(1)
O(9)	30(1)	22(1)	46(1)	6(1)	13(1)	1(1)
O(10)	38(1)	38(1)	34(1)	4(1)	10(1)	12(1)
O(11)	34(1)	47(1)	29(1)	7(1)	3(1)	−14(1)
O(12)	28(1)	26(1)	39(1)	0(1)	9(1)	−2(1)
N(1)	24(1)	21(1)	25(1)	1(1)	9(1)	0(1)
N(2)	25(1)	18(1)	27(1)	1(1)	11(1)	0(1)
N(3)	25(1)	22(1)	27(1)	2(1)	8(1)	−1(1)
N(4)	25(1)	24(1)	31(1)	−1(1)	8(1)	2(1)
C(1)	27(1)	26(1)	21(1)	3(1)	5(1)	0(1)
C(2)	28(1)	26(1)	18(1)	0(1)	8(1)	−2(1)
C(3)	34(1)	25(1)	24(1)	−4(1)	14(1)	−2(1)
C(4)	20(1)	25(1)	18(1)	1(1)	5(1)	3(1)
C(5)	32(1)	29(1)	33(1)	3(1)	18(1)	2(1)
C(6)	22(1)	24(1)	22(1)	−1(1)	8(1)	−2(1)
C(7)	35(1)	24(1)	28(1)	−4(1)	7(1)	−6(1)
C(8)	31(1)	32(1)	24(1)	4(1)	7(1)	−2(1)
C(9)	38(1)	36(1)	24(1)	0(1)	11(1)	1(1)
C(10)	32(1)	33(1)	34(1)	5(1)	16(1)	3(1)
C(11)	23(1)	27(1)	26(1)	−1(1)	8(1)	−1(1)

II

C(12)	35(1)	34(1)	50(1)	−3(1)	24(1)	0(1)
C(13)	22(1)	25(1)	31(1)	2(1)	8(1)	0(1)
C(14)	26(1)	34(1)	35(1)	0(1)	1(1)	−1(1)
O(5)	27(1)	22(1)	34(1)	−4(1)	13(1)	−3(1)

Table 0.4: Hydrogen coordinates ($*10^4$) and isotropic displacement parameters ($\mathring{A}^2 * 10^3$) for **15**.

Atom	x	y	z	U(eq)
H(1A)	−1082	3655	−874	27
H(1B)	−233	4211	−780	27
H(2A)	1176	2056	−649	27
H(2B)	983	492	−689	27
H(3A)	4043	2318	1612	30
H(3B)	3562	3683	1465	30
H(4A)	6341	3810	2036	32
H(4B)	5910	2405	1989	32
H(1C)	−998	4150	−2160	30
H(1D)	−1141	2457	−2077	30
H(2C)	473	3701	−1824	29
H(2D)	−65	2984	−2688	29
H(3C)	15	708	−1979	32
H(3D)	910	1280	−1985	32
H(5A)	−1730	3510	1502	44
H(5B)	−1781	1825	1283	44
H(5C)	−2321	2960	614	44
H(7A)	1817	2711	1954	44
H(7B)	874	3069	1411	44
H(7C)	1565	2802	959	44
H(8A)	4022	4279	371	35
H(8B)	3544	2761	219	35
H(9A)	4870	1560	713	39
H(9B)	4752	2443	−131	39
H(10A)	6088	2917	730	38
H(10B)	5563	4372	687	38
H(12A)	2680	4317	3481	56
H(12B)	2670	5566	2823	56
H(12C)	3271	5698	3766	56
H(14A)	7105	5055	4889	51
H(14B)	7289	5954	4156	51
H(14C)	7740	4435	4441	51
H(9D)	4475(11)	6760(20)	1509(13)	43(6)
H(10D)	7297(13)	1270(20)	3888(15)	62(7)
H(11A)	3016(15)	1510(20)	3286(16)	73(8)
H(12D)	2235(14)	1120(30)	4225(13)	73(8)
H(9C)	5296(11)	6860(20)	1698(12)	47(6)
H(10C)	7643(13)	80(20)	4355(11)	53(6)
H(11B)	2389(11)	580(20)	2929(10)	43(5)
H(12E)	1590(12)	590(20)	4444(13)	51(6)

- **Crystallographic data recorded for 21**

Table 0.5: Atomic coordinates (*10^4) and equivalent isotropic displacement parameters (Å^2 * 10^3) for **21**. U(eq) is defined as one third of the trace of the orthogonalised Uij tensor.

Atom	x	y	z	U(eq)
Cu(1)	10115(1)	1825(1)	4365(1)	18(1)
Cu(2)	3749(1)	4067(1)	4265(1)	17(1)
Cu(3)	2926(1)	619(1)	2500	43(1)
Cl(1)	11345(1)	2500	5000	18(1)
Cl(2)	8277(1)	1420(1)	4763(1)	23(1)
Cl(3)	3832(1)	4108(1)	5206(1)	24(1)
Cl(4)	1743(1)	3978(1)	3911(1)	27(1)
Cl(5)	3721(1)	1672(1)	2500	47(1)
Cl(6)	2099(1)	−419(1)	2500	53(1)
O(1)	6063(2)	2500	5000	32(1)
O(2)	6672(2)	1849(2)	2500	57(1)
N(1)	10960(1)	952(1)	4635(1)	23(1)
N(2)	10149(1)	1492(1)	3592(1)	21(1)
N(3)	9531(1)	2822(1)	4194(1)	20(1)
N(4)	3877(1)	2988(1)	4357(1)	21(1)
N(5)	4993(1)	4092(1)	3651(1)	19(1)
N(6)	3669(1)	5155(1)	4306(1)	20(1)
N(7)	7743(3)	365(2)	2500	42(1)
C(1)	10724(2)	223(1)	4403(1)	29(1)
C(2)	10986(2)	228(1)	3833(1)	32(1)
C(3)	10121(2)	677(1)	3517(1)	27(1)
C(4)	9123(2)	1778(1)	3293(1)	28(1)
C(5)	8958(2)	2609(1)	3284(1)	31(1)
C(6)	8602(2)	2921(1)	3803(1)	27(1)
C(7)	11245(2)	1795(1)	3373(1)	36(1)
C(8)	4015(2)	2503(1)	3901(1)	26(1)
C(9)	5135(2)	2688(1)	3615(1)	28(1)
C(10)	5061(2)	3414(1)	3327(1)	28(1)
C(11)	4775(2)	4703(1)	3275(1)	25(1)
C(12)	4694(2)	5472(1)	3496(1)	27(1)
C(13)	3619(2)	5597(1)	3828(1)	25(1)
C(14)	6137(2)	4207(1)	3913(1)	25(1)
C(15)	8225(3)	−184(2)	2500	35(1)
C(16)	8842(3)	−881(2)	2500	50(1)

Table 0.6: Bond lengths (Å) and angles (°) for **21**.

Cu(1)-N(3)	1.9808(15)	Cu(1)-N(1)	1.9835(15)
Cu(1)-N(2)	2.0865(16)	Cu(1)-Cl(2)	2.4503(5)
Cu(1)-Cl(1)	2.4822(4)	Cu(2)-N(4)	1.9825(16)
Cu(2)-N(6)	1.9831(16)	Cu(2)-N(5)	2.1274(15)
Cu(2)-Cl(3)	2.4338(5)	Cu(2)-Cl(4)	2.4702(5)
Cu(3)-Cl(6)	2.1105(12)	Cu(3)-Cl(5)	2.1184(12)
Cl(1)-Cu(1)#1	2.4822(4)	N(1)-C(1)	1.480(2)
N(2)-C(7)	1.480(2)	N(2)-C(3)	1.495(2)
N(2)-C(4)	1.496(2)	N(3)-C(6)	1.475(2)
N(4)-C(8)	1.479(2)	N(5)-C(14)	1.485(2)
N(5)-C(10)	1.493(2)	N(5)-C(11)	1.497(2)
N(6)-C(13)	1.475(2)	N(7)-C(15)	1.139(4)
C(1)-C(2)	1.501(3)	C(2)-C(3)	1.519(3)
C(4)-C(5)	1.522(3)	C(5)-C(6)	1.514(3)
C(8)-C(9)	1.514(3)	C(9)-C(10)	1.518(3)

C(11)-C(12)	1.513(3)	C(12)-C(13)	1.513(3)
C(15)-C(16)	1.451(5)		

N(3)-Cu(1)-N(1)	166.99(7)	N(3)-Cu(1)-N(2)	93.32(6)
N(1)-Cu(1)-N(2)	95.38(7)	N(3)-Cu(1)-Cl(2)	94.62(5)
N(1)-Cu(1)-Cl(2)	91.63(5)	N(2)-Cu(1)-Cl(2)	109.22(4)
N(3)-Cu(1)-Cl(1)	83.44(5)	N(1)-Cu(1)-Cl(1)	83.68(5)
N(2)-Cu(1)-Cl(1)	139.89(4)	Cl(2)-Cu(1)-Cl(1)	110.896(17)
N(4)-Cu(2)-N(6)	169.81(7)	N(4)-Cu(2)-N(5)	93.55(6)
N(6)-Cu(2)-N(5)	92.85(6)	N(4)-Cu(2)-Cl(3)	84.64(5)
N(6)-Cu(2)-Cl(3)	85.24(5)	N(5)-Cu(2)-Cl(3)	135.79(4)
N(4)-Cu(2)-Cl(4)	92.78(5)	N(6)-Cu(2)-Cl(4)	92.44(5)
N(5)-Cu(2)-Cl(4)	110.19(4)	Cl(3)-Cu(2)-Cl(4)	114.014(18)
Cl(6)-Cu(3)-Cl(5)	178.84(4)	Cu(1)-Cl(1)-Cu(1)#1	111.11(2)
C(1)-N(1)-Cu(1)	119.17(12)	C(7)-N(2)-C(3)	109.68(16)
C(7)-N(2)-C(4)	109.50(17)	C(3)-N(2)-C(4)	105.13(14)
C(7)-N(2)-Cu(1)	105.93(12)	C(3)-N(2)-Cu(1)	114.32(12)
C(4)-N(2)-Cu(1)	112.27(12)	C(6)-N(3)-Cu(1)	120.48(12)
C(8)-N(4)-Cu(2)	120.12(12)	C(14)-N(5)-C(10)	108.99(15)
C(14)-N(5)-C(11)	109.64(15)	C(10)-N(5)-C(11)	104.98(15)
C(14)-N(5)-Cu(2)	104.59(11)	C(10)-N(5)-Cu(2)	115.78(12)
C(11)-N(5)-Cu(2)	112.82(11)	C(13)-N(6)-Cu(2)	120.01(12)
N(1)-C(1)-C(2)	110.77(17)	C(1)-C(2)-C(3)	113.58(17)
N(2)-C(3)-C(2)	116.68(16)	N(2)-C(4)-C(5)	116.78(16)
C(6)-C(5)-C(4)	113.04(17)	N(3)-C(6)-C(5)	111.56(16)
N(4)-C(8)-C(9)	110.23(16)	C(8)-C(9)-C(10)	112.69(17)
N(5)-C(10)-C(9)	116.50(17)	N(5)-C(11)-C(12)	116.84(16)
C(13)-C(12)-C(11)	113.65(17)	N(6)-C(13)-C(12)	111.13(16)
N(7)-C(15)-C(16)	179.8(4)		

Symmetry transformations used to generate equivalent atoms: #1 x,−y+1/2,−z+1

Table 0.7: Anisotropic displacement parameters ($\text{Å}^2 * 10^3$) for **21**. The anisotropic displacement factor exponent takes the form: $-2\,g\pi^2\,[\,h^2\,a^{*2}\,U11 + ... + 2\,h\,k\,a^*\,b^*\,U12]$

Atom	U11	U22	U33	U23	U13	U12
Cu(1)	18(1)	18(1)	19(1)	−2(1)	−2(1)	4(1)
Cu(2)	15(1)	18(1)	20(1)	1(1)	2(1)	0(1)
Cu(3)	27(1)	76(1)	28(1)	0	0	18(1)
Cl(1)	14(1)	21(1)	20(1)	−2(1)	0	0
Cl(2)	16(1)	22(1)	30(1)	−2(1)	0(1)	−2(1)
Cl(3)	25(1)	28(1)	20(1)	1(1)	−1(1)	−5(1)
Cl(4)	17(1)	27(1)	36(1)	5(1)	−5(1)	−2(1)
Cl(5)	27(1)	81(1)	32(1)	0	0	11(1)
Cl(6)	37(1)	79(1)	42(1)	0	0	10(1)
O(1)	18(1)	32(1)	47(1)	−3(1)	0	0
O(2)	42(2)	63(2)	67(2)	0	0	−4(1)
N(1)	23(1)	19(1)	27(1)	−2(1)	−5(1)	3(1)
N(2)	16(1)	24(1)	22(1)	−3(1)	1(1)	−2(1)
N(3)	18(1)	19(1)	24(1)	−2(1)	−3(1)	3(1)
N(4)	18(1)	21(1)	25(1)	2(1)	3(1)	−1(1)
N(5)	16(1)	20(1)	21(1)	0(1)	2(1)	0(1)
N(6)	17(1)	21(1)	23(1)	0(1)	2(1)	2(1)
N(7)	35(2)	49(2)	40(2)	0	0	−4(1)
C(1)	29(1)	18(1)	39(1)	−2(1)	−6(1)	3(1)
C(2)	29(1)	26(1)	41(1)	−12(1)	−3(1)	7(1)
C(3)	26(1)	26(1)	28(1)	−11(1)	−2(1)	1(1)
C(4)	31(1)	32(1)	21(1)	−1(1)	−8(1)	−3(1)
C(5)	36(1)	30(1)	27(1)	6(1)	−10(1)	−2(1)

C(6)	19(1)	26(1)	35(1)	4(1)	−7(1)	3(1)
C(7)	26(1)	45(1)	39(1)	−6(1)	14(1)	−8(1)
C(8)	28(1)	19(1)	31(1)	−2(1)	−2(1)	−5(1)
C(9)	30(1)	20(1)	32(1)	−6(1)	4(1)	2(1)
C(10)	36(1)	26(1)	24(1)	−7(1)	8(1)	−2(1)
C(11)	28(1)	28(1)	21(1)	5(1)	5(1)	1(1)
C(12)	27(1)	24(1)	30(1)	9(1)	5(1)	2(1)
C(13)	25(1)	22(1)	28(1)	7(1)	1(1)	2(1)
C(14)	14(1)	27(1)	35(1)	−1(1)	1(1)	1(1)
C(15)	26(2)	52(2)	26(2)	0	0	−6(2)
C(16)	53(2)	55(2)	40(2)	0	0	13(2)

Table 0.8: Hydrogen coordinates (*10^4) and isotropic displacement parameters (Å^2 * 10^3) for **21**.

Atom	x	y	z	U(eq)
H(1A)	11749	1042	4602	27
H(1B)	10802	918	4983	27
H(3C)	9267	3029	4497	24
H(3D)	10165	3095	4088	24
H(4C)	4505	2903	4572	25
H(4D)	3218	2835	4532	25
H(6A)	3019	5272	4500	24
H(6B)	4312	5310	4491	24
H(1)	9892	90	4458	35
H(2)	11214	−154	4575	35
H(2A)	10983	−285	3704	38
H(2B)	11783	429	3779	38
H(3A)	10262	573	3146	32
H(3B)	9321	502	3599	32
H(4A)	8404	1555	3438	33
H(4B)	9197	1605	2931	33
H(5A)	9700	2843	3173	37
H(5B)	8351	2733	3024	37
H(3)	8430	3452	3765	32
H(4)	7878	2674	3923	32
H(7A)	11265	1701	2999	55
H(7B)	11919	1557	3538	55
H(7C)	11276	2326	3436	55
H(8A)	3337	2565	3667	31
H(8B)	4037	1983	4015	31
H(9A)	5310	2290	3365	33
H(9B)	5789	2710	3866	33
H(10A)	5757	3455	3100	34
H(10B)	4363	3399	3100	34
H(11A)	4034	4597	3090	30
H(11B)	5411	4698	3015	30
H(12A)	5401	5569	3708	32
H(12B)	4689	5830	3207	32
H(13A)	3563	6125	3919	30
H(13B)	2910	5463	3629	30
H(14A)	6756	4253	3652	38
H(14B)	6306	3787	4138	38
H(14C)	6105	4658	4120	38
H(16A)	8768	−1113	2841	75
H(16B)	9672	−797	2423	75
H(16C)	8504	−1205	2236	75
H(1C)	6550(20)	2119(11)	4964(13)	80(11)
H(2C)	5882(10)	1790(20)	2500	81(16)

- **Crystallographic data recorded for 31**

Table 0.9: Atomic coordinates (*10^4) and equivalent isotropic displacement parameters (Å^2 * 10^3) for **31**.U(eq) is defined as one third of the trace of the orthogonalised Uij tensor.

Atom	x	y	z	U(eq)
O(1)	−818(1)	2948(1)	5326(1)	25(1)
O(2)	344(1)	2329(1)	6128(1)	27(1)
O(3)	−144(1)	3647(1)	5099(1)	33(1)
O(4)	993(1)	3847(1)	7032(1)	24(1)
O(5)	2581(1)	3686(1)	8730(1)	30(1)
O(6)	−165(1)	3222(1)	7386(1)	28(1)
O(7)	−5084(2)	4236(1)	7324(2)	126(1)
N(1)	−3644(1)	4123(1)	6488(1)	42(1)
N(2)	1823(1)	2565(1)	8853(1)	28(1)
N(3)	2105(1)	2946(1)	8962(1)	30(1)
C(1)	−1917(1)	2985(1)	5286(1)	26(1)
C(2)	−2446(1)	2873(1)	6105(1)	27(1)
C(3)	−3551(2)	2911(1)	6019(2)	35(1)
C(4)	−4118(2)	3062(1)	5165(2)	40(1)
C(5)	−3541(2)	3195(1)	4400(2)	38(1)
C(6)	−2444(2)	3165(1)	4439(1)	30(1)
C(7)	−5340(2)	3080(1)	5030(2)	53(1)
C(8)	−5838(2)	2900(1)	5907(3)	88(1)
C(9)	−5724(2)	2875(1)	4037(2)	74(1)
C(10)	−5695(2)	3490(1)	4945(2)	62(1)
C(11)	−1847(2)	3347(1)	3629(1)	33(1)
C(12)	−1635(2)	3760(1)	3826(1)	29(1)
C(13)	−801(1)	3880(1)	4518(1)	26(1)
C(14)	−575(1)	4260(1)	4636(1)	26(1)
C(15)	−1214(2)	4516(1)	4079(1)	29(1)
C(16)	−2088(2)	4410(1)	3414(1)	31(1)
C(17)	−2265(2)	4029(1)	3298(1)	32(1)
C(18)	−2771(2)	4704(1)	2807(2)	40(1)
C(19)	−3869(2)	4553(1)	2437(2)	59(1)
C(20)	−2196(2)	4828(1)	1900(2)	77(1)
C(21)	−2943(2)	5046(1)	3466(2)	65(1)
C(22)	356(1)	4380(1)	5378(1)	25(1)
C(23)	51(1)	4412(1)	6460(1)	23(1)
C(24)	328(1)	4146(1)	7211(1)	23(1)
C(25)	−105(1)	4156(1)	8143(1)	24(1)
C(26)	−735(1)	4460(1)	8347(1)	28(1)
C(27)	−970(1)	4748(1)	7654(1)	29(1)
C(28)	−587(1)	4710(1)	6710(1)	27(1)
C(29)	−1628(2)	5084(1)	7946(2)	36(1)
C(30)	−2693(2)	4949(1)	8260(2)	58(1)
C(31)	−1819(2)	5365(1)	7083(2)	56(1)
C(32)	−1018(2)	5286(1)	8854(2)	59(1)
C(33)	19(1)	3833(1)	8889(1)	25(1)
C(34)	−914(1)	3564(1)	8739(1)	23(1)
C(35)	−947(1)	3280(1)	8009(1)	22(1)
C(36)	−1800(1)	3029(1)	7904(1)	23(1)
C(37)	−2612(1)	3070(1)	8533(1)	27(1)
C(38)	−2630(1)	3356(1)	9246(1)	28(1)
C(39)	−1765(1)	3598(1)	9327(1)	26(1)
C(40)	−3529(2)	3386(1)	9938(2)	36(1)
C(41)	−4568(2)	3265(1)	9419(3)	99(1)
C(42)	−3670(3)	3780(1)	10295(3)	113(2)
C(43)	−3252(3)	3146(1)	10860(2)	127(2)

C(44)	−1859(1)	2729(1)	7088(1)	25(1)
C(45)	−435(2)	2655(1)	4708(1)	28(1)
C(46)	−379(2)	2284(1)	5239(1)	28(1)
C(47)	540(1)	2026(1)	6748(1)	24(1)
C(48)	203(2)	1666(1)	6495(2)	30(1)
C(49)	464(2)	1377(1)	7165(2)	34(1)
C(50)	1050(2)	1441(1)	8085(2)	33(1)
C(51)	1367(1)	1801(1)	8340(2)	29(1)
C(52)	1123(1)	2101(1)	7681(1)	24(1)
C(53)	1451(1)	2485(1)	7943(1)	27(1)
C(54)	2424(1)	3016(1)	9894(1)	28(1)
C(55)	2811(1)	3373(1)	10304(1)	27(1)
C(56)	3148(2)	3382(1)	11342(2)	34(1)
C(57)	3568(2)	3700(1)	11816(2)	40(1)
C(58)	3661(2)	4018(1)	11251(2)	40(1)
C(59)	3330(2)	4023(1)	10217(2)	34(1)
C(60)	2905(1)	3704(1)	9740(1)	28(1)
C(61)	2598(2)	4021(1)	8142(2)	31(1)
C(62)	2112(1)	3931(1)	7092(2)	30(1)
C(63)	−4249(2)	4077(1)	7228(2)	72(1)
C(64)	−3939(3)	4377(1)	5676(2)	87(1)
C(65)	−2658(2)	3920(1)	6462(2)	56(1)

Table 0.10: Bond lengths (Å) and angles (°) for **31.**

O(1)-C(1)	1.393(2)	O(1)-C(45)	1.442(2)
O(2)-C(47)	1.366(2)	O(2)-C(46)	1.429(2)
O(3)-C(13)	1.363(2)	O(4)-C(24)	1.398(2)
O(4)-C(62)	1.443(2)	O(5)-C(60)	1.360(2)
O(5)-C(61)	1.433(2)	O(6)-C(35)	1.363(2)
O(7)-C(63)	1.217(3)	N(1)-C(63)	1.309(3)
N(1)-C(64)	1.429(3)	N(1)-C(65)	1.449(3)
N(2)-C(53)	1.282(2)	N(2)-N(3)	1.416(2)
N(3)-C(54)	1.285(2)	C(1)-C(2)	1.387(3)
C(1)-C(6)	1.404(2)	C(2)-C(3)	1.399(3)
C(2)-C(44)	1.523(2)	C(3)-C(4)	1.388(3)
C(4)-C(5)	1.388(3)	C(4)-C(7)	1.540(3)
C(5)-C(6)	1.388(3)	C(6)-C(11)	1.517(3)
C(7)-C(8)	1.516(4)	C(7)-C(10)	1.536(3)
C(7)-C(9)	1.540(4)	C(11)-C(12)	1.520(2)
C(12)-C(17)	1.396(3)	C(12)-C(13)	1.398(2)
C(13)-C(14)	1.394(2)	C(14)-C(15)	1.388(2)
C(14)-C(22)	1.521(2)	C(15)-C(16)	1.397(3)
C(16)-C(17)	1.389(3)	C(16)-C(18)	1.539(3)
C(18)-C(20)	1.526(3)	C(18)-C(19)	1.528(3)
C(18)-C(21)	1.531(3)	C(22)-C(23)	1.522(2)
C(23)-C(28)	1.395(2)	C(23)-C(24)	1.397(2)
C(24)-C(25)	1.396(2)	C(25)-C(26)	1.390(2)
C(25)-C(33)	1.519(2)	C(26)-C(27)	1.393(3)
C(27)-C(28)	1.389(3)	C(27)-C(29)	1.534(3)
C(29)-C(31)	1.521(3)	C(29)-C(30)	1.527(3)
C(29)-C(32)	1.544(3)	C(33)-C(34)	1.524(2)
C(34)-C(39)	1.392(2)	C(34)-C(35)	1.401(2)
C(35)-C(36)	1.402(2)	C(36)-C(37)	1.390(2)
C(36)-C(44)	1.518(2)	C(37)-C(38)	1.396(3)
C(38)-C(39)	1.391(3)	C(38)-C(40)	1.531(3)
C(40)-C(41)	1.489(3)	C(40)-C(42)	1.503(3)
C(40)-C(43)	1.506(3)	C(45)-C(46)	1.499(2)
C(47)-C(48)	1.389(2)	C(47)-C(52)	1.402(2)
C(48)-C(49)	1.382(3)	C(49)-C(50)	1.382(3)

C(50)-C(51)	1.382(3)	C(51)-C(52)	1.398(2)
C(52)-C(53)	1.469(2)	C(54)-C(55)	1.455(2)
C(55)-C(56)	1.398(3)	C(55)-C(60)	1.411(3)
C(56)-C(57)	1.382(3)	C(57)-C(58)	1.373(3)
C(58)-C(59)	1.391(3)	C(59)-C(60)	1.390(3)
C(61)-C(62)	1.498(3)		

C(1)-O(1)-C(45)	115.82(13)	C(47)-O(2)-C(46)	118.09(13)
C(24)-O(4)-C(62)	115.68(13)	C(60)-O(5)-C(61)	118.30(14)
C(63)-N(1)-C(64)	120.8(2)	C(63)-N(1)-C(65)	121.4(2)
C(64)-N(1)-C(65)	117.8(2)	C(53)-N(2)-N(3)	112.18(15)
C(54)-N(3)-N(2)	109.82(15)	C(2)-C(1)-O(1)	119.80(15)
C(2)-C(1)-C(6)	121.87(17)	O(1)-C(1)-C(6)	118.13(16)
C(1)-C(2)-C(3)	117.48(17)	C(1)-C(2)-C(44)	122.17(16)
C(3)-C(2)-C(44)	120.29(17)	C(4)-C(3)-C(2)	122.7(2)
C(3)-C(4)-C(5)	117.36(18)	C(3)-C(4)-C(7)	123.1(2)
C(5)-C(4)-C(7)	119.49(19)	C(6)-C(5)-C(4)	122.65(18)
C(5)-C(6)-C(1)	117.61(18)	C(5)-C(6)-C(11)	120.26(17)
C(1)-C(6)-C(11)	121.97(17)	C(8)-C(7)-C(10)	108.7(2)
C(8)-C(7)-C(9)	109.2(2)	C(10)-C(7)-C(9)	109.1(2)
C(8)-C(7)-C(4)	112.2(2)	C(10)-C(7)-C(4)	109.43(18)
C(9)-C(7)-C(4)	108.1(2)	C(6)-C(11)-C(12)	112.93(16)
C(17)-C(12)-C(13)	118.17(17)	C(17)-C(12)-C(11)	120.28(16)
C(13)-C(12)-C(11)	121.54(16)	O(3)-C(13)-C(14)	115.24(15)
O(3)-C(13)-C(12)	124.13(16)	C(14)-C(13)-C(12)	120.61(16)
C(15)-C(14)-C(13)	118.81(16)	C(15)-C(14)-C(22)	122.11(16)
C(13)-C(14)-C(22)	119.07(15)	C(14)-C(15)-C(16)	122.73(17)
C(17)-C(16)-C(15)	116.46(17)	C(17)-C(16)-C(18)	122.50(17)
C(15)-C(16)-C(18)	120.96(16)	C(16)-C(17)-C(12)	123.10(17)
C(20)-C(18)-C(19)	109.9(2)	C(20)-C(18)-C(21)	108.6(2)
C(19)-C(18)-C(21)	107.0(2)	C(20)-C(18)-C(16)	108.82(18)
C(19)-C(18)-C(16)	111.89(16)	C(21)-C(18)-C(16)	110.67(17)
C(14)-C(22)-C(23)	112.15(14)	C(28)-C(23)-C(24)	117.66(16)
C(28)-C(23)-C(22)	119.06(15)	C(24)-C(23)-C(22)	123.17(16)
C(25)-C(24)-C(23)	121.12(16)	C(25)-C(24)-O(4)	117.60(15)
C(23)-C(24)-O(4)	121.14(16)	C(26)-C(25)-C(24)	118.16(16)
C(26)-C(25)-C(33)	119.75(16)	C(24)-C(25)-C(33)	121.90(16)
C(25)-C(26)-C(27)	122.87(17)	C(28)-C(27)-C(26)	116.54(16)
C(28)-C(27)-C(29)	123.25(17)	C(26)-C(27)-C(29)	120.21(17)
C(27)-C(28)-C(23)	123.24(17)	C(31)-C(29)-C(30)	109.39(18)
C(31)-C(29)-C(27)	112.41(17)	C(30)-C(29)-C(27)	109.50(16)
C(31)-C(29)-C(32)	107.82(19)	C(30)-C(29)-C(32)	109.00(19)
C(27)-C(29)-C(32)	108.66(17)	C(25)-C(33)-C(34)	111.55(14)
C(39)-C(34)-C(35)	118.35(16)	C(39)-C(34)-C(33)	120.22(16)
C(35)-C(34)-C(33)	121.42(16)	O(6)-C(35)-C(34)	123.49(15)
O(6)-C(35)-C(36)	116.14(15)	C(34)-C(35)-C(36)	120.35(16)
C(37)-C(36)-C(35)	118.72(16)	C(37)-C(36)-C(44)	120.70(16)
C(35)-C(36)-C(44)	120.53(15)	C(36)-C(37)-C(38)	122.81(17)
C(39)-C(38)-C(37)	116.51(16)	C(39)-C(38)-C(40)	122.31(17)
C(37)-C(38)-C(40)	121.10(17)	C(38)-C(39)-C(34)	123.20(17)
C(41)-C(40)-C(42)	106.9(2)	C(41)-C(40)-C(43)	109.5(3)
C(42)-C(40)-C(43)	107.9(3)	C(41)-C(40)-C(38)	112.24(18)
C(42)-C(40)-C(38)	111.82(18)	C(43)-C(40)-C(38)	108.40(17)
C(36)-C(44)-C(2)	110.80(14)	O(1)-C(45)-C(46)	112.51(14)
O(2)-C(46)-C(45)	106.54(14)	O(2)-C(47)-C(48)	123.89(16)
O(2)-C(47)-C(52)	115.28(15)	C(48)-C(47)-C(52)	120.83(16)
C(49)-C(48)-C(47)	119.49(17)	C(50)-C(49)-C(48)	120.95(17)
C(51)-C(50)-C(49)	119.27(18)	C(50)-C(51)-C(52)	121.49(18)
C(51)-C(52)-C(47)	117.95(16)	C(51)-C(52)-C(53)	122.14(16)
C(47)-C(52)-C(53)	119.91(16)	N(2)-C(53)-C(52)	119.99(17)
N(3)-C(54)-C(55)	126.28(17)	C(56)-C(55)-C(60)	117.74(17)

IX

C(56)-C(55)-C(54)	116.51(17)	C(60)-C(55)-C(54)	125.72(17)
C(57)-C(56)-C(55)	122.22(19)	C(58)-C(57)-C(56)	119.10(19)
C(57)-C(58)-C(59)	120.73(19)	C(60)-C(59)-C(58)	120.24(19)
O(5)-C(60)-C(59)	123.52(17)	O(5)-C(60)-C(55)	116.50(15)
C(59)-C(60)-C(55)	119.97(18)	O(5)-C(61)-C(62)	107.25(14)
O(4)-C(62)-C(61)	114.23(15)	O(7)-C(63)-N(1)	126.5(3)

Table 0.11: Anisotropic displacement parameters ($\text{Å}^2 * 10^3$) for **31**. The anisotropic displacement factor exponent takes the form: $-2 \text{g}\pi^2 [h^2 a^{*2} U11 + ... + 2 h k a^* b^* U12]$

Atom	U11	U22	U33	U23	U13	U12
O(1)	27(1)	23(1)	25(1)	−4(1)	1(1)	0(1)
O(2)	34(1)	21(1)	26(1)	0(1)	−3(1)	−2(1)
O(3)	42(1)	20(1)	33(1)	2(1)	−9(1)	−2(1)
O(4)	22(1)	22(1)	29(1)	0(1)	2(1)	1(1)
O(5)	30(1)	23(1)	34(1)	1(1)	−6(1)	0(1)
O(6)	26(1)	27(1)	34(1)	−5(1)	10(1)	−5(1)
O(7)	70(2)	149(2)	170(3)	35(2)	71(2)	35(2)
N(1)	36(1)	43(1)	49(1)	13(1)	8(1)	3(1)
N(2)	30(1)	24(1)	31(1)	−1(1)	−1(1)	−4(1)
N(3)	31(1)	25(1)	33(1)	−2(1)	−1(1)	−4(1)
C(1)	26(1)	19(1)	31(1)	−3(1)	−3(1)	−2(1)
C(2)	26(1)	20(1)	33(1)	−2(1)	−2(1)	−2(1)
C(3)	27(1)	29(1)	48(1)	1(1)	0(1)	−4(1)
C(4)	30(1)	30(1)	55(1)	3(1)	−10(1)	−3(1)
C(5)	37(1)	28(1)	46(1)	5(1)	−16(1)	−4(1)
C(6)	37(1)	21(1)	30(1)	−2(1)	−8(1)	−5(1)
C(7)	26(1)	43(1)	86(2)	7(1)	−11(1)	−2(1)
C(8)	26(1)	101(2)	136(3)	37(2)	3(2)	−3(1)
C(9)	35(1)	57(2)	122(3)	−18(2)	−29(2)	−2(1)
C(10)	38(1)	53(2)	91(2)	−6(1)	−14(1)	9(1)
C(11)	45(1)	26(1)	26(1)	−1(1)	−11(1)	−3(1)
C(12)	36(1)	24(1)	26(1)	1(1)	1(1)	−3(1)
C(13)	31(1)	25(1)	22(1)	3(1)	1(1)	1(1)
C(14)	27(1)	26(1)	24(1)	2(1)	4(1)	−2(1)
C(15)	33(1)	22(1)	33(1)	3(1)	1(1)	−3(1)
C(16)	33(1)	27(1)	33(1)	6(1)	−1(1)	−1(1)
C(17)	35(1)	32(1)	28(1)	3(1)	−6(1)	−4(1)
C(18)	39(1)	31(1)	47(1)	11(1)	−11(1)	−2(1)
C(19)	47(1)	38(1)	86(2)	11(1)	−28(1)	−1(1)
C(20)	66(2)	90(2)	72(2)	51(2)	−2(2)	14(2)
C(21)	66(2)	32(1)	91(2)	1(1)	−29(2)	12(1)
C(22)	27(1)	20(1)	28(1)	4(1)	2(1)	−3(1)
C(23)	22(1)	21(1)	27(1)	2(1)	0(1)	−4(1)
C(24)	22(1)	17(1)	28(1)	−1(1)	0(1)	−2(1)
C(25)	26(1)	23(1)	24(1)	0(1)	−2(1)	−2(1)
C(26)	32(1)	25(1)	28(1)	−1(1)	6(1)	−1(1)
C(27)	29(1)	22(1)	36(1)	−1(1)	3(1)	1(1)
C(28)	28(1)	22(1)	31(1)	5(1)	1(1)	0(1)
C(29)	39(1)	26(1)	45(1)	1(1)	11(1)	7(1)
C(30)	46(1)	38(1)	94(2)	4(1)	27(1)	12(1)
C(31)	69(2)	36(1)	65(2)	9(1)	20(1)	24(1)
C(32)	69(2)	38(1)	71(2)	−17(1)	5(1)	12(1)
C(33)	28(1)	24(1)	21(1)	1(1)	0(1)	1(1)
C(34)	26(1)	22(1)	22(1)	4(1)	0(1)	3(1)
C(35)	23(1)	22(1)	22(1)	3(1)	4(1)	5(1)
C(36)	24(1)	20(1)	26(1)	3(1)	1(1)	2(1)
C(37)	25(1)	25(1)	33(1)	4(1)	5(1)	−1(1)
C(38)	28(1)	29(1)	27(1)	6(1)	6(1)	6(1)

C(39)	32(1)	23(1)	22(1)	2(1)	3(1)	6(1)
C(40)	32(1)	40(1)	37(1)	4(1)	14(1)	7(1)
C(41)	37(2)	164(3)	103(2)	−55(2)	38(2)	−21(2)
C(42)	106(3)	70(2)	180(4)	−38(2)	109(3)	−4(2)
C(43)	100(3)	213(4)	79(2)	89(3)	69(2)	91(3)
C(44)	26(1)	21(1)	29(1)	2(1)	3(1)	−2(1)
C(45)	38(1)	25(1)	23(1)	−4(1)	4(1)	3(1)
C(46)	32(1)	23(1)	27(1)	−4(1)	−3(1)	0(1)
C(47)	24(1)	21(1)	29(1)	1(1)	7(1)	3(1)
C(48)	33(1)	24(1)	33(1)	−4(1)	1(1)	0(1)
C(49)	40(1)	21(1)	40(1)	−4(1)	4(1)	−2(1)
C(50)	38(1)	25(1)	37(1)	5(1)	4(1)	4(1)
C(51)	29(1)	28(1)	31(1)	1(1)	2(1)	3(1)
C(52)	24(1)	22(1)	28(1)	−2(1)	5(1)	1(1)
C(53)	24(1)	24(1)	32(1)	2(1)	2(1)	1(1)
C(54)	24(1)	30(1)	29(1)	1(1)	1(1)	−2(1)
C(55)	19(1)	31(1)	30(1)	−6(1)	3(1)	0(1)
C(56)	29(1)	43(1)	32(1)	−4(1)	3(1)	−3(1)
C(57)	35(1)	49(1)	34(1)	−13(1)	0(1)	0(1)
C(58)	30(1)	37(1)	50(1)	−19(1)	−5(1)	2(1)
C(59)	27(1)	27(1)	48(1)	−7(1)	−5(1)	3(1)
C(60)	16(1)	30(1)	35(1)	−7(1)	−3(1)	3(1)
C(61)	24(1)	21(1)	46(1)	3(1)	−3(1)	−1(1)
C(62)	22(1)	28(1)	39(1)	7(1)	4(1)	1(1)
C(63)	57(2)	83(2)	81(2)	30(2)	27(2)	10(2)
C(64)	103(3)	79(2)	79(2)	39(2)	−1(2)	6(2)
C(65)	38(1)	51(2)	78(2)	−15(1)	6(1)	−1(1)

Table 0.12: Hydrogen coordinates ($*10^4$) and isotropic displacement parameters ($\text{Å}^2 * 10^3$) for **31**.

Atom	x	y	z	U(eq)
H(3)	−403	3431	5082	39
H(6)	239	3409	7407	34
H(3A)	−3928	2830	6567	42
H(5)	−3912	3311	3825	46
H(8A)	−5624	3037	6535	131
H(8B)	−5599	2641	5982	131
H(8C)	−6613	2906	5773	131
H(9A)	−5498	2614	4086	110
H(9B)	−5418	2995	3466	110
H(9C)	−6500	2887	3930	110
H(10A)	−6469	3501	4815	93
H(10B)	−5370	3610	4385	93
H(10C)	−5471	3620	5582	93
H(11A)	−2264	3318	2961	40
H(11B)	−1161	3217	3596	40
H(15)	−1050	4774	4152	35
H(17)	−2841	3948	2837	39
H(19A)	−3798	4352	1944	88
H(19B)	−4304	4754	2115	88
H(19C)	−4211	4454	3016	88
H(20A)	−1495	4926	2142	115
H(20B)	−2611	5023	1524	115
H(20C)	−2114	4614	1452	115
H(21A)	−3267	4968	4076	98
H(21B)	−3413	5223	3079	98
H(21C)	−2258	5166	3665	98
H(22A)	624	4624	5161	30

H(22B)	938	4196	5361	30
H(26)	−1017	4472	8987	34
H(28)	−767	4895	6209	32
H(30A)	−3108	5164	8457	87
H(30B)	−2571	4778	8836	87
H(30C)	−3083	4820	7687	87
H(31A)	−2224	5246	6502	83
H(31B)	−1135	5452	6881	83
H(31C)	−2220	5578	7311	83
H(32A)	−319	5363	8668	89
H(32B)	−928	5116	9437	89
H(32C)	−1419	5506	9033	89
H(33A)	72	3932	9591	30
H(33B)	684	3697	8797	30
H(37)	−3180	2895	8474	33
H(39)	−1754	3795	9807	31
H(41A)	−4548	2997	9282	149
H(41B)	−4709	3401	8777	149
H(41C)	−5133	3318	9857	149
H(42A)	−3800	3945	9706	169
H(42B)	−3027	3860	10710	169
H(42C)	−4277	3791	10703	169
H(43A)	−3811	3167	11321	190
H(43B)	−2575	3229	11210	190
H(43C)	−3190	2885	10650	190
H(44A)	−2231	2508	7326	30
H(44B)	−1132	2653	6961	30
H(45A)	281	2722	4524	34
H(45B)	−911	2633	4072	34
H(46A)	−1089	2211	5426	33
H(46B)	−123	2089	4792	33
H(48)	−204	1619	5866	36
H(49)	238	1131	6990	40
H(50)	1233	1241	8537	40
H(51)	1759	1846	8978	35
H(53)	1387	2674	7437	32
H(54)	2406	2815	10362	33
H(56)	3087	3163	11734	41
H(57)	3789	3699	12523	47
H(58)	3955	4237	11570	48
H(59)	3394	4245	9836	41
H(61A)	3337	4109	8120	37
H(61B)	2187	4220	8447	37
H(62A)	2220	4146	6644	36
H(62B)	2490	3715	6833	36
H(63)	−4011	3903	7742	87
H(64A)	−4003	4241	5030	131
H(64B)	−3395	4571	5660	131
H(64C)	−4621	4493	5781	131
H(65A)	−2545	3760	7065	83
H(65B)	−2068	4097	6455	83
H(65C)	−2694	3765	5850	83

- **Crystallographic data recorded for 32 (xylene inclusion complex)**

Table 0.13: Atomic coordinates (* 10^4) and equivalent isotropic displacement parameters (Å^2 * 10^3) for **32 (xylene inclusion complex)**. U(eq) is defined as one third of the trace of the orthogonalised Uij tensor.

Atom	x	y	z	U(eq)
O(1)	14217(1)	1780(1)	6915(1)	33(1)
O(2)	15705(1)	3074(1)	8194(1)	33(1)
O(3)	12785(1)	2723(1)	7822(1)	28(1)
O(4)	11293(1)	1095(1)	7657(1)	34(1)
O(5)	17021(1)	1823(1)	7407(1)	29(1)
O(6)	18195(1)	1367(1)	8468(1)	37(1)
O(7)	9734(1)	1794(1)	5195(1)	41(1)
O(8)	20545(1)	5115(1)	8901(1)	46(1)
N(1)	9334(1)	439(1)	5746(1)	30(1)
N(2)	9420(2)	−110(1)	6177(1)	32(1)
N(3)	20528(2)	3829(1)	9536(1)	34(1)
N(4)	20196(2)	3023(1)	9719(1)	37(1)
C(1)	13979(2)	1904(1)	6346(1)	27(1)
C(2)	14907(2)	1659(1)	5938(1)	28(1)
C(3)	14708(2)	1743(1)	5346(1)	31(1)
C(4)	13621(2)	2084(1)	5145(1)	32(1)
C(5)	12726(2)	2331(1)	5567(1)	30(1)
C(6)	12878(2)	2249(1)	6163(1)	28(1)
C(7)	13497(2)	2248(2)	4502(1)	39(1)
C(8)	12203(2)	2521(2)	4349(1)	44(1)
C(9)	13801(2)	1408(2)	4045(1)	54(1)
C(10)	14415(3)	3012(2)	4446(1)	67(1)
C(11)	16147(2)	3945(1)	8299(1)	28(1)
C(12)	17366(2)	4183(1)	8213(1)	29(1)
C(13)	17722(2)	5095(1)	8335(1)	33(1)
C(14)	16915(2)	5772(1)	8544(1)	34(1)
C(15)	15704(2)	5504(1)	8628(1)	34(1)
C(16)	15302(2)	4607(1)	8503(1)	29(1)
C(17)	17284(2)	6776(1)	8622(1)	45(1)
C(18)	16740(3)	7129(2)	8085(2)	76(1)
C(19)	18672(2)	6939(2)	8645(1)	48(1)
C(20)	16788(3)	7312(2)	9206(2)	67(1)
C(21)	12798(2)	3516(1)	7591(1)	27(1)
C(22)	13304(2)	4311(1)	7931(1)	29(1)
C(23)	13264(2)	5080(1)	7680(1)	33(1)
C(24)	12782(2)	5076(1)	7108(1)	35(1)
C(25)	12335(2)	4258(1)	6777(1)	34(1)
C(26)	12329(2)	3472(1)	7009(1)	29(1)
C(27)	12752(2)	5950(1)	6860(1)	45(1)
C(28)	13995(3)	6445(2)	6967(2)	85(1)
C(29)	12517(4)	5783(2)	6185(2)	87(1)
C(30)	11764(4)	6533(2)	7163(2)	95(1)
C(31)	17328(2)	2408(1)	7024(1)	28(1)
C(32)	17974(2)	3206(1)	7267(1)	30(1)
C(33)	18246(2)	3807(1)	6898(1)	34(1)
C(34)	17875(2)	3647(1)	6297(1)	35(1)
C(35)	17229(2)	2841(1)	6071(1)	34(1)
C(36)	16935(2)	2214(1)	6423(1)	29(1)
C(37)	18138(2)	4339(2)	5904(1)	44(1)
C(38)	19441(8)	4155(7)	5675(4)	97(3)
C(39)	17951(9)	5246(4)	6244(3)	92(2)
C(40)	17269(8)	4175(5)	5347(3)	84(2)

C(41)	16143(2)	1385(1)	6159(1)	30(1)
C(42)	18261(2)	3481(1)	7934(1)	31(1)
C(43)	13955(2)	4349(1)	8534(1)	30(1)
C(44)	11909(2)	2585(1)	6613(1)	30(1)
C(45)	11673(2)	2611(1)	8127(1)	34(1)
C(46)	11562(2)	1664(1)	8225(1)	34(1)
C(47)	10888(2)	232(1)	7653(1)	31(1)
C(48)	10984(2)	−177(2)	8150(1)	42(1)
C(49)	10497(2)	−1043(2)	8111(1)	48(1)
C(50)	9931(2)	−1504(2)	7590(1)	46(1)
C(51)	9855(2)	−1102(1)	7097(1)	38(1)
C(52)	10330(2)	−231(1)	7118(1)	31(1)
C(53)	10183(2)	213(1)	6606(1)	31(1)
C(54)	8565(2)	109(1)	5316(1)	31(1)
C(55)	8278(2)	576(1)	4834(1)	29(1)
C(56)	7402(2)	192(1)	4394(1)	37(1)
C(57)	7099(2)	608(2)	3924(1)	44(1)
C(58)	7673(2)	1424(2)	3893(1)	46(1)
C(59)	8546(2)	1818(1)	4317(1)	41(1)
C(60)	8860(2)	1399(1)	4792(1)	33(1)
C(61)	17911(2)	1138(1)	7415(1)	31(1)
C(62)	17751(2)	724(1)	7954(1)	31(1)
C(63)	18297(2)	1090(1)	9001(1)	33(1)
C(64)	17842(2)	264(1)	9097(1)	42(1)
C(65)	18027(3)	36(2)	9652(1)	54(1)
C(66)	18650(3)	614(2)	10110(1)	58(1)
C(67)	19094(2)	1434(2)	10019(1)	45(1)
C(68)	18922(2)	1690(1)	9466(1)	35(1)
C(69)	19385(2)	2560(1)	9367(1)	33(1)
C(70)	21352(2)	4296(1)	9885(1)	35(1)
C(71)	21860(2)	5134(1)	9770(1)	35(1)
C(72)	22811(2)	5576(2)	10149(1)	48(1)
C(73)	23346(2)	6362(2)	10051(1)	58(1)
C(74)	22933(2)	6723(2)	9570(1)	54(1)
C(75)	21994(2)	6311(2)	9189(1)	45(1)
C(76)	21455(2)	5512(1)	9286(1)	36(1)
C(101)	14205(3)	−63(2)	8950(1)	57(1)
C(102)	14481(3)	782(2)	8828(1)	69(1)
C(103)	14553(3)	897(2)	8240(1)	61(1)
C(104)	14349(3)	166(2)	7773(1)	73(1)
C(105)	14073(3)	−679(2)	7894(1)	74(1)
C(106)	14000(3)	−794(2)	8483(1)	57(1)
C(107)	14644(6)	1675(2)	9261(2)	280(11)
C(108)	13565(4)	−1636(2)	8580(2)	95(2)
C(201)	14582(3)	540(2)	8405(2)	90(3)
C(202)	14572(4)	815(2)	9022(2)	61(2)
C(203)	14366(4)	188(3)	9383(2)	85(2)
C(204)	14169(4)	−715(3)	9126(2)	128(4)
C(205)	14180(5)	−990(2)	8508(2)	134(5)
C(206)	14386(4)	−362(2)	8148(2)	72(2)
C(207)	14367(6)	−722(3)	7488(2)	152(5)
C(208)	14767(5)	1668(3)	9276(2)	71(2)
C(38A)	19006(6)	4001(4)	5416(2)	66(3)
C(39A)	18781(5)	5247(3)	6267(2)	50(2)
C(40A)	16941(7)	4626(5)	5639(4)	65(2)

XIV

Table 0.14: Bond lengths (Å) and angles (°) for **32 (xylene inclusion complex)**.

O(1)-C(1)	1.366(2)	C(33)-C(34)	1.391(3)
O(2)-C(11)	1.369(2)	C(34)-C(35)	1.396(3)
O(3)-C(21)	1.401(2)	C(34)-C(37)	1.531(3)
O(3)-C(45)	1.435(2)	C(35)-C(36)	1.394(3)
O(4)-C(47)	1.369(2)	C(36)-C(41)	1.521(3)
O(4)-C(46)	1.430(2)	C(37)-C(39)	1.464(7)
O(5)-C(31)	1.401(2)	C(37)-C(38A)	1.500(6)
O(5)-C(61)	1.438(2)	C(37)-C(40A)	1.528(7)
O(6)-C(63)	1.363(2)	C(37)-C(38)	1.537(9)
O(6)-C(62)	1.438(2)	C(37)-C(40)	1.541(7)
O(7)-C(60)	1.350(2)	C(37)-C(39A)	1.599(5)
O(8)-C(76)	1.354(2)	C(45)-C(46)	1.498(3)
N(1)-C(54)	1.288(2)	C(47)-C(48)	1.394(3)
N(1)-N(2)	1.407(2)	C(47)-C(52)	1.399(3)
N(2)-C(53)	1.279(2)	C(48)-C(49)	1.390(3)
N(3)-C(70)	1.286(3)	C(49)-C(50)	1.379(3)
N(3)-N(4)	1.407(2)	C(50)-C(51)	1.379(3)
N(4)-C(69)	1.277(3)	C(51)-C(52)	1.399(3)
C(1)-C(2)	1.399(3)	C(52)-C(53)	1.463(3)
C(1)-C(6)	1.402(3)	C(54)-C(55)	1.448(3)
C(2)-C(3)	1.391(3)	C(55)-C(56)	1.398(3)
C(2)-C(41)	1.518(2)	C(55)-C(60)	1.407(3)
C(3)-C(4)	1.403(3)	C(56)-C(57)	1.378(3)
C(4)-C(5)	1.394(3)	C(57)-C(58)	1.389(3)
C(4)-C(7)	1.535(3)	C(58)-C(59)	1.377(3)
C(5)-C(6)	1.395(3)	C(59)-C(60)	1.395(3)
C(6)-C(44)	1.518(2)	C(61)-C(62)	1.496(3)
C(7)-C(8)	1.526(3)	C(63)-C(64)	1.394(3)
C(7)-C(9)	1.532(3)	C(63)-C(68)	1.405(3)
C(7)-C(10)	1.539(3)	C(64)-C(65)	1.384(3)
C(11)-C(12)	1.396(3)	C(65)-C(66)	1.379(3)
C(11)-C(16)	1.397(3)	C(66)-C(67)	1.379(3)
C(12)-C(13)	1.399(3)	C(67)-C(68)	1.398(3)
C(12)-C(42)	1.518(3)	C(68)-C(69)	1.460(3)
C(13)-C(14)	1.389(3)	C(70)-C(71)	1.446(3)
C(14)-C(15)	1.399(3)	C(71)-C(76)	1.402(3)
C(14)-C(17)	1.540(3)	C(71)-C(72)	1.402(3)
C(15)-C(16)	1.393(3)	C(72)-C(73)	1.374(4)
C(16)-C(43)	1.516(3)	C(73)-C(74)	1.384(4)
C(17)-C(19)	1.523(3)	C(74)-C(75)	1.379(3)
C(17)-C(18)	1.538(4)	C(75)-C(76)	1.392(3)
C(17)-C(20)	1.538(4)	C(101)-C(102)	1.3900
C(21)-C(22)	1.394(2)	C(101)-C(106)	1.3900
C(21)-C(26)	1.396(3)	C(102)-C(103)	1.3900
C(22)-C(23)	1.394(3)	C(102)-C(107)	1.5174
C(22)-C(43)	1.521(3)	C(103)-C(104)	1.3900
C(23)-C(24)	1.392(3)	C(104)-C(105)	1.3900
C(24)-C(25)	1.390(3)	C(105)-C(106)	1.3900
C(24)-C(27)	1.538(3)	C(106)-C(108)	1.4101
C(25)-C(26)	1.394(3)	C(201)-C(202)	1.3900
C(26)-C(44)	1.521(2)	C(201)-C(206)	1.3900
C(27)-C(30)	1.504(4)	C(202)-C(208)	1.3209
C(27)-C(28)	1.522(4)	C(202)-C(203)	1.3900
C(27)-C(29)	1.526(4)	C(203)-C(204)	1.3900
C(31)-C(32)	1.396(3)	C(204)-C(205)	1.3900
C(31)-C(36)	1.397(3)	C(205)-C(206)	1.3900
C(32)-C(33)	1.386(3)	C(206)-C(207)	1.4978
C(32)-C(42)	1.520(3)		

C(21)-O(3)-C(45)	111.92(13)	C(39)-C(37)-C(38)	115.7(6)
C(47)-O(4)-C(46)	117.64(14)	C(38A)-C(37)-C(38)	28.3(4)
C(31)-O(5)-C(61)	112.73(13)	C(40A)-C(37)-C(38)	134.9(5)
C(63)-O(6)-C(62)	117.93(14)	C(34)-C(37)-C(38)	105.9(3)
C(54)-N(1)-N(2)	112.04(16)	C(39)-C(37)-C(40)	108.6(5)
C(53)-N(2)-N(1)	112.38(16)	C(38A)-C(37)-C(40)	78.3(4)
C(70)-N(3)-N(4)	112.72(17)	C(40A)-C(37)-C(40)	35.7(4)
C(69)-N(4)-N(3)	112.27(17)	C(34)-C(37)-C(40)	110.6(3)
O(1)-C(1)-C(2)	116.06(16)	C(38)-C(37)-C(40)	106.3(5)
O(1)-C(1)-C(6)	123.46(16)	C(39)-C(37)-C(39A)	34.0(4)
C(2)-C(1)-C(6)	120.47(16)	C(38A)-C(37)-C(39A)	104.8(3)
C(3)-C(2)-C(1)	118.94(16)	C(40A)-C(37)-C(39A)	105.4(4)
C(3)-C(2)-C(41)	121.29(16)	C(34)-C(37)-C(39A)	113.0(2)
C(1)-C(2)-C(41)	119.56(16)	C(38)-C(37)-C(39A)	83.1(5)
C(2)-C(3)-C(4)	122.43(17)	C(40)-C(37)-C(39A)	130.5(4)
C(5)-C(4)-C(3)	116.78(17)	C(2)-C(41)-C(36)	110.38(15)
C(5)-C(4)-C(7)	122.69(17)	C(12)-C(42)-C(32)	109.73(15)
C(3)-C(4)-C(7)	120.32(17)	C(16)-C(43)-C(22)	110.24(15)
C(4)-C(5)-C(6)	122.84(17)	C(6)-C(44)-C(26)	110.74(14)
C(5)-C(6)-C(1)	118.52(16)	O(3)-C(45)-C(46)	109.46(15)
C(5)-C(6)-C(44)	120.57(16)	O(4)-C(46)-C(45)	107.55(15)
C(1)-C(6)-C(44)	120.78(16)	O(4)-C(47)-C(48)	123.31(17)
C(8)-C(7)-C(9)	107.74(18)	O(4)-C(47)-C(52)	116.30(16)
C(8)-C(7)-C(4)	112.28(17)	C(48)-C(47)-C(52)	120.38(18)
C(9)-C(7)-C(4)	111.54(18)	C(49)-C(48)-C(47)	119.22(19)
C(8)-C(7)-C(10)	109.0(2)	C(50)-C(49)-C(48)	121.1(2)
C(9)-C(7)-C(10)	108.7(2)	C(49)-C(50)-C(51)	119.4(2)
C(4)-C(7)-C(10)	107.51(17)	C(50)-C(51)-C(52)	121.15(19)
O(2)-C(11)-C(12)	123.37(16)	C(51)-C(52)-C(47)	118.66(17)
O(2)-C(11)-C(16)	116.18(16)	C(51)-C(52)-C(53)	120.95(17)
C(12)-C(11)-C(16)	120.45(16)	C(47)-C(52)-C(53)	120.28(17)
C(11)-C(12)-C(13)	118.67(17)	N(2)-C(53)-C(52)	120.22(17)
C(11)-C(12)-C(42)	120.93(16)	N(1)-C(54)-C(55)	122.08(17)
C(13)-C(12)-C(42)	120.13(17)	C(56)-C(55)-C(60)	118.92(18)
C(14)-C(13)-C(12)	122.72(18)	C(56)-C(55)-C(54)	118.89(18)
C(13)-C(14)-C(15)	116.78(17)	C(60)-C(55)-C(54)	122.18(17)
C(13)-C(14)-C(17)	122.18(18)	C(57)-C(56)-C(55)	121.2(2)
C(15)-C(14)-C(17)	120.76(18)	C(56)-C(57)-C(58)	119.1(2)
C(16)-C(15)-C(14)	122.53(18)	C(59)-C(58)-C(57)	121.2(2)
C(15)-C(16)-C(11)	118.83(17)	C(58)-C(59)-C(60)	119.9(2)
C(15)-C(16)-C(43)	121.02(16)	O(7)-C(60)-C(59)	118.56(18)
C(11)-C(16)-C(43)	119.95(16)	O(7)-C(60)-C(55)	121.81(17)
C(19)-C(17)-C(18)	108.3(2)	C(59)-C(60)-C(55)	119.63(18)
C(19)-C(17)-C(20)	107.4(2)	O(5)-C(61)-C(62)	109.83(15)
C(18)-C(17)-C(20)	109.8(2)	O(6)-C(62)-C(61)	107.70(15)
C(19)-C(17)-C(14)	112.70(18)	O(6)-C(63)-C(64)	123.97(18)
C(18)-C(17)-C(14)	107.92(18)	O(6)-C(63)-C(68)	115.74(17)
C(20)-C(17)-C(14)	110.7(2)	C(64)-C(63)-C(68)	120.28(18)
C(22)-C(21)-C(26)	121.80(17)	C(65)-C(64)-C(63)	119.4(2)
C(22)-C(21)-O(3)	120.15(16)	C(66)-C(65)-C(64)	121.0(2)
C(26)-C(21)-O(3)	118.01(15)	C(67)-C(66)-C(65)	119.8(2)
C(21)-C(22)-C(23)	117.33(17)	C(66)-C(67)-C(68)	120.9(2)
C(21)-C(22)-C(43)	122.62(17)	C(67)-C(68)-C(63)	118.62(19)
C(23)-C(22)-C(43)	119.93(16)	C(67)-C(68)-C(69)	121.13(18)
C(24)-C(23)-C(22)	123.00(18)	C(63)-C(68)-C(69)	120.25(18)
C(25)-C(24)-C(23)	117.44(18)	N(4)-C(69)-C(68)	121.56(18)
C(25)-C(24)-C(27)	122.16(19)	N(3)-C(70)-C(71)	122.05(19)
C(23)-C(24)-C(27)	120.40(18)	C(76)-C(71)-C(72)	118.8(2)
C(24)-C(25)-C(26)	122.03(18)	C(76)-C(71)-C(70)	122.52(18)
C(25)-C(26)-C(21)	118.31(17)	C(72)-C(71)-C(70)	118.7(2)
C(25)-C(26)-C(44)	119.66(17)	C(73)-C(72)-C(71)	121.0(2)

C(21)-C(26)-C(44)	121.87(16)	C(72)-C(73)-C(74)	119.3(2)
C(30)-C(27)-C(28)	110.3(3)	C(75)-C(74)-C(73)	121.4(2)
C(30)-C(27)-C(29)	109.3(3)	C(74)-C(75)-C(76)	119.4(2)
C(28)-C(27)-C(29)	105.1(3)	O(8)-C(76)-C(75)	118.3(2)
C(30)-C(27)-C(24)	109.0(2)	O(8)-C(76)-C(71)	121.65(18)
C(28)-C(27)-C(24)	110.3(2)	C(75)-C(76)-C(71)	120.1(2)
C(29)-C(27)-C(24)	112.8(2)	C(102)-C(101)-C(106)	120.0
C(32)-C(31)-C(36)	121.41(17)	C(103)-C(102)-C(101)	120.0
C(32)-C(31)-O(5)	118.06(16)	C(103)-C(102)-C(107)	111.1
C(36)-C(31)-O(5)	120.44(16)	C(101)-C(102)-C(107)	128.7
C(33)-C(32)-C(31)	118.73(17)	C(102)-C(103)-C(104)	120.0
C(33)-C(32)-C(42)	119.03(17)	C(105)-C(104)-C(103)	120.0
C(31)-C(32)-C(42)	121.89(17)	C(104)-C(105)-C(106)	120.0
C(32)-C(33)-C(34)	122.15(18)	C(105)-C(106)-C(101)	120.0
C(33)-C(34)-C(35)	117.29(18)	C(105)-C(106)-C(108)	117.6
C(33)-C(34)-C(37)	121.19(18)	C(101)-C(106)-C(108)	121.9
C(35)-C(34)-C(37)	121.50(18)	C(202)-C(201)-C(206)	120.0
C(36)-C(35)-C(34)	122.80(18)	C(208)-C(202)-C(201)	121.0
C(35)-C(36)-C(31)	117.60(17)	C(208)-C(202)-C(203)	119.0
C(35)-C(36)-C(41)	119.80(16)	C(201)-C(202)-C(203)	120.0
C(31)-C(36)-C(41)	122.48(17)	C(204)-C(203)-C(202)	120.0
C(39)-C(37)-C(38A)	131.2(4)	C(205)-C(204)-C(203)	120.0
C(39)-C(37)-C(40A)	75.6(5)	C(204)-C(205)-C(206)	120.0
C(38A)-C(37)-C(40A)	110.3(5)	C(205)-C(206)-C(201)	120.0
C(39)-C(37)-C(34)	109.7(3)	C(205)-C(206)-C(207)	116.0
C(38A)-C(37)-C(34)	112.5(2)	C(201)-C(206)-C(207)	124.0
C(40A)-C(37)-C(34)	110.5(3)		

Table 0.15: Anisotropic displacement parameters ($\text{Å}^2 * 10^3$) for **32 (xylene inclusion complex)**. The anisotropic displacement factor exponent takes the form: $-2\,g\pi^2\,[\,h^2\,a^{*2}\,U11 + ... + 2\,h\,k\,a^*\,b^*\,U12]$

Atom	U11	U22	U33	U23	U13	U12
O(1)	35(1)	39(1)	24(1)	5(1)	2(1)	9(1)
O(2)	33(1)	24(1)	39(1)	0(1)	6(1)	−2(1)
O(3)	26(1)	27(1)	31(1)	4(1)	6(1)	−2(1)
O(4)	42(1)	33(1)	27(1)	6(1)	−1(1)	−8(1)
O(5)	29(1)	29(1)	28(1)	5(1)	1(1)	6(1)
O(6)	49(1)	30(1)	30(1)	5(1)	−7(1)	−6(1)
O(7)	43(1)	39(1)	43(1)	13(1)	−9(1)	−8(1)
O(8)	43(1)	47(1)	47(1)	12(1)	−9(1)	−5(1)
N(1)	33(1)	30(1)	28(1)	6(1)	2(1)	4(1)
N(2)	37(1)	32(1)	28(1)	6(1)	2(1)	1(1)
N(3)	35(1)	34(1)	31(1)	1(1)	3(1)	−3(1)
N(4)	41(1)	37(1)	31(1)	5(1)	1(1)	−4(1)
C(1)	31(1)	25(1)	25(1)	2(1)	−1(1)	0(1)
C(2)	29(1)	27(1)	27(1)	1(1)	−2(1)	1(1)
C(3)	31(1)	35(1)	26(1)	4(1)	3(1)	0(1)
C(4)	35(1)	34(1)	27(1)	7(1)	−2(1)	−4(1)
C(5)	28(1)	29(1)	31(1)	5(1)	−4(1)	−1(1)
C(6)	28(1)	25(1)	28(1)	2(1)	0(1)	−3(1)
C(7)	39(1)	50(1)	31(1)	16(1)	−3(1)	−4(1)
C(8)	49(1)	51(1)	35(1)	14(1)	−9(1)	3(1)
C(9)	54(1)	80(2)	27(1)	9(1)	4(1)	13(1)
C(10)	66(2)	89(2)	55(2)	44(2)	−14(1)	−32(2)
C(11)	33(1)	25(1)	24(1)	2(1)	−2(1)	−2(1)
C(12)	29(1)	30(1)	26(1)	4(1)	−4(1)	−1(1)
C(13)	30(1)	33(1)	34(1)	5(1)	−4(1)	−4(1)

C(14)	36(1)	28(1)	38(1)	2(1)	−5(1)	−4(1)
C(15)	33(1)	28(1)	37(1)	0(1)	0(1)	2(1)
C(16)	30(1)	29(1)	26(1)	2(1)	−1(1)	−2(1)
C(17)	43(1)	28(1)	63(2)	8(1)	−9(1)	−5(1)
C(18)	81(2)	44(1)	107(3)	34(2)	−41(2)	−17(1)
C(19)	49(1)	36(1)	60(1)	12(1)	−5(1)	−14(1)
C(20)	60(2)	32(1)	99(2)	−14(1)	6(2)	−5(1)
C(21)	23(1)	27(1)	31(1)	3(1)	5(1)	1(1)
C(22)	25(1)	28(1)	31(1)	1(1)	5(1)	1(1)
C(23)	32(1)	27(1)	39(1)	1(1)	0(1)	−1(1)
C(24)	34(1)	31(1)	41(1)	8(1)	−1(1)	2(1)
C(25)	32(1)	35(1)	35(1)	6(1)	−1(1)	3(1)
C(26)	24(1)	30(1)	32(1)	2(1)	3(1)	2(1)
C(27)	53(1)	33(1)	50(1)	13(1)	−7(1)	0(1)
C(28)	84(2)	76(2)	107(3)	55(2)	−19(2)	−23(2)
C(29)	146(3)	53(2)	65(2)	28(2)	−10(2)	−4(2)
C(30)	113(3)	63(2)	125(3)	47(2)	43(2)	42(2)
C(31)	24(1)	31(1)	29(1)	4(1)	2(1)	6(1)
C(32)	23(1)	33(1)	32(1)	4(1)	0(1)	5(1)
C(33)	29(1)	35(1)	37(1)	6(1)	0(1)	0(1)
C(34)	33(1)	37(1)	36(1)	9(1)	2(1)	5(1)
C(35)	34(1)	38(1)	28(1)	4(1)	1(1)	6(1)
C(36)	25(1)	31(1)	29(1)	2(1)	1(1)	7(1)
C(37)	53(1)	38(1)	42(1)	15(1)	−4(1)	−4(1)
C(38)	73(5)	107(7)	136(8)	89(7)	30(5)	0(4)
C(39)	170(8)	44(3)	67(4)	25(3)	−5(5)	10(4)
C(40)	111(6)	84(5)	70(4)	53(4)	−27(4)	−28(4)
C(41)	31(1)	30(1)	27(1)	0(1)	0(1)	5(1)
C(42)	28(1)	33(1)	32(1)	3(1)	−4(1)	1(1)
C(43)	31(1)	28(1)	28(1)	0(1)	4(1)	0(1)
C(44)	26(1)	31(1)	32(1)	2(1)	0(1)	−2(1)
C(45)	32(1)	34(1)	34(1)	0(1)	12(1)	−3(1)
C(46)	34(1)	39(1)	27(1)	3(1)	5(1)	−7(1)
C(47)	32(1)	32(1)	31(1)	9(1)	3(1)	−3(1)
C(48)	50(1)	43(1)	34(1)	13(1)	−6(1)	−11(1)
C(49)	66(2)	44(1)	39(1)	22(1)	−4(1)	−10(1)
C(50)	63(2)	34(1)	43(1)	12(1)	2(1)	−10(1)
C(51)	49(1)	32(1)	33(1)	5(1)	2(1)	−4(1)
C(52)	35(1)	29(1)	29(1)	6(1)	4(1)	1(1)
C(53)	35(1)	28(1)	28(1)	3(1)	4(1)	0(1)
C(54)	31(1)	29(1)	31(1)	4(1)	4(1)	3(1)
C(55)	28(1)	31(1)	29(1)	3(1)	2(1)	5(1)
C(56)	34(1)	37(1)	38(1)	2(1)	−1(1)	2(1)
C(57)	39(1)	50(1)	40(1)	6(1)	−9(1)	6(1)
C(58)	49(1)	49(1)	42(1)	15(1)	−5(1)	14(1)
C(59)	45(1)	37(1)	44(1)	14(1)	−1(1)	6(1)
C(60)	32(1)	33(1)	33(1)	5(1)	0(1)	5(1)
C(61)	28(1)	30(1)	32(1)	2(1)	−2(1)	7(1)
C(62)	33(1)	27(1)	32(1)	2(1)	−5(1)	0(1)
C(63)	35(1)	32(1)	31(1)	6(1)	0(1)	1(1)
C(64)	53(1)	35(1)	37(1)	6(1)	−3(1)	−8(1)
C(65)	83(2)	39(1)	42(1)	14(1)	1(1)	−14(1)
C(66)	94(2)	47(1)	35(1)	14(1)	−6(1)	−10(1)
C(67)	64(2)	42(1)	29(1)	5(1)	−4(1)	−5(1)
C(68)	38(1)	34(1)	30(1)	3(1)	2(1)	1(1)
C(69)	37(1)	33(1)	27(1)	3(1)	2(1)	1(1)
C(70)	34(1)	43(1)	27(1)	2(1)	4(1)	−1(1)
C(71)	30(1)	40(1)	31(1)	−2(1)	7(1)	−3(1)
C(72)	44(1)	58(1)	39(1)	−1(1)	−1(1)	−12(1)
C(73)	48(1)	61(2)	58(2)	−1(1)	−2(1)	−21(1)
C(74)	47(1)	43(1)	69(2)	3(1)	15(1)	−12(1)

XVIII

C(75)	42(1)	41(1)	54(1)	10(1)	12(1)	3(1)
C(76)	28(1)	39(1)	39(1)	1(1)	6(1)	1(1)
C(38A)	98(7)	52(4)	57(4)	28(3)	30(4)	9(4)
C(39A)	70(4)	36(3)	45(3)	13(2)	−10(3)	−18(3)
C(40A)	67(4)	46(4)	88(6)	29(3)	−29(4)	−3(3)

Table 0.16: Hydrogen coordinates ($*10^4$) and isotropic displacement parameters ($\text{Å}^2 * 10^3$) for **32 (xylene inclusion complex)**.

Atom	x	y	z	U(eq)
H(1)	13642	1987	7135	39
H(2)	16235	2734	8018	39
H(7)	9807	1497	5468	50
H(8)	20306	4635	9001	55
H(3)	15331	1562	5068	37
H(5)	11981	2565	5443	35
H(8A)	11609	2046	4397	66
H(8B)	12163	2609	3935	66
H(8C)	12007	3083	4618	66
H(9A)	13193	927	4061	81
H(9B)	14623	1210	4138	81
H(9C)	13782	1550	3643	81
H(10A)	14332	3151	4045	100
H(10B)	15255	2823	4512	100
H(10C)	14244	3548	4745	100
H(13)	18550	5257	8273	39
H(15)	15133	5952	8777	40
H(18A)	16964	7768	8124	114
H(18B)	15842	7053	8074	114
H(18C)	17066	6790	7715	114
H(19A)	19013	6635	8268	73
H(19B)	19039	6699	8977	73
H(19C)	18859	7586	8704	73
H(20A)	17149	7093	9547	101
H(20B)	15891	7234	9202	101
H(20C)	17007	7952	9240	101
H(23)	13581	5632	7910	40
H(25)	12024	4235	6381	41
H(28A)	13991	6967	6771	127
H(28B)	14641	6039	6801	127
H(28C)	14154	6648	7398	127
H(29A)	11702	5495	6086	130
H(29B)	13145	5388	5987	130
H(29C)	12552	6357	6048	130
H(30A)	11942	6674	7595	143
H(30B)	10966	6212	7084	143
H(30C)	11739	7092	7008	143
H(33)	18700	4345	7060	41
H(35)	16978	2715	5661	40
H(38A)	19487	3522	5478	145
H(38B)	20038	4283	6012	145
H(38C)	19629	4541	5388	145
H(39A)	18557	5383	6577	138
H(39B)	17120	5280	6400	138
H(39C)	18051	5683	5981	138
H(40A)	17415	4646	5114	126
H(40B)	16413	4190	5471	126
H(40C)	17424	3587	5100	126
H(41A)	16569	1018	5822	36

H(41B)	16017	1014	6466	36
H(42A)	18195	2948	8124	37
H(42B)	19113	3731	8002	37
H(43A)	13562	4797	8841	36
H(43B)	13879	3755	8651	36
H(44A)	11753	2132	6864	36
H(44B)	11131	2669	6398	36
H(45A)	10956	2743	7885	41
H(45B)	11685	3034	8516	41
H(46A)	12341	1489	8400	41
H(46B)	10895	1608	8504	41
H(48)	11377	133	8510	50
H(49)	10555	−1322	8449	58
H(50)	9596	−2094	7571	55
H(51)	9472	−1422	6737	46
H(53)	10655	743	6591	37
H(54)	8174	−458	5315	37
H(56)	7007	−365	4418	44
H(57)	6506	339	3626	52
H(58)	7460	1717	3573	55
H(59)	8935	2374	4286	50
H(61A)	18752	1406	7424	37
H(61B)	17805	670	7049	37
H(62A)	16872	571	7995	38
H(62B)	18222	165	7916	38
H(64)	17410	−139	8785	50
H(65)	17719	−527	9718	65
H(66)	18773	447	10488	70
H(67)	19522	1830	10336	55
H(69)	19077	2786	9033	39
H(70)	21636	4084	10229	43
H(72)	23090	5328	10479	58
H(73)	23992	6655	10310	69
H(74)	23305	7265	9501	65
H(75)	21717	6571	8864	54
H(101)	14155	−142	9352	69
H(103)	14742	1475	8157	74
H(104)	14398	245	7370	87
H(105)	13933	−1178	7575	88
H(10D)	13837	1933	9351	420
H(10E)	15150	2088	9081	420
H(10F)	15050	1579	9632	420
H(10G)	13274	−2007	8199	143
H(10H)	12887	−1548	8857	143
H(10I)	14233	−1939	8751	143
H(201)	14723	969	8158	108
H(203)	14359	375	9805	102
H(204)	14028	−1144	9372	154
H(205)	14045	−1607	8333	161
H(20D)	15176	−618	7331	228
H(20E)	13743	−415	7290	228
H(20F)	14171	−1369	7411	228
H(20G)	14029	2007	9224	107
H(20H)	15461	1917	9090	107
H(20I)	14956	1714	9704	107
H(38D)	19099	4448	5161	99
H(38E)	18675	3435	5176	99
H(38F)	19808	3900	5593	99
H(39D)	19588	5115	6426	75
H(39E)	18266	5508	6599	75
H(39F)	18884	5676	6000	75

XX

H(40D)	17128	5051	5378	98
H(40E)	16426	4914	5963	98
H(40F)	16502	4095	5407	98

- **Crystallographic data recorded for 32 (DMF inclusion complex)**

Table 0.17: Atomic coordinates ($*10^4$) and equivalent isotropic displacement parameters ($\text{Å}^2 * 10^3$) for **32 (DMF inclusion complex)**. U(eq) is defined as one third of the trace of the orthogonalised Uij tensor.

Atom	x	y	z	U(eq)
O(1)	8022(1)	566(1)	2337(1)	35(1)
O(2)	9169(1)	1900(1)	2217(1)	38(1)
O(3)	8346(1)	3884(1)	2273(1)	36(1)
O(4)	7133(1)	2540(1)	2249(1)	44(1)
O(5)	8831(1)	878(1)	3147(1)	43(1)
O(6)	7408(1)	4550(1)	2934(1)	44(1)
O(7)	11813(1)	2056(1)	2086(1)	55(1)
O(8A)	5406(3)	6257(4)	1431(2)	64(2)
O(9)	7225(1)	2388(2)	−56(1)	81(1)
O(8)	5167(3)	6312(4)	1482(2)	66(2)
N(1)	10927(1)	2273(1)	3262(1)	43(1)
N(2)	11391(1)	2192(1)	2906(1)	43(1)
N(3)	5170(1)	4685(2)	2550(1)	52(1)
N(4)	5046(1)	5139(2)	2133(1)	55(1)
N(5)	7866(1)	1982(1)	594(1)	36(1)
C(1)	7804(1)	168(2)	1922(1)	31(1)
C(2)	8384(1)	−203(2)	1679(1)	31(1)
C(3)	8155(1)	−620(2)	1272(1)	33(1)
C(4)	7371(1)	−673(2)	1108(1)	33(1)
C(5)	6819(1)	−239(2)	1360(1)	35(1)
C(6)	7016(1)	204(2)	1764(1)	33(1)
C(7)	7098(1)	−1182(2)	673(1)	38(1)
C(8)	7788(2)	−1608(2)	447(1)	54(1)
C(9)	6671(2)	−422(2)	365(1)	58(1)
C(10)	6541(2)	−2038(2)	759(1)	53(1)
C(11)	9250(1)	−126(2)	1838(1)	34(1)
C(12)	9586(1)	1726(2)	1864(1)	32(1)
C(13)	9655(1)	793(2)	1671(1)	31(1)
C(14)	10108(1)	714(2)	1313(1)	33(1)
C(15)	10500(1)	1519(2)	1147(1)	35(1)
C(16)	10422(1)	2429(2)	1356(1)	35(1)
C(17)	9969(1)	2560(2)	1705(1)	32(1)
C(18)	11018(1)	1434(2)	763(1)	41(1)
C(19)	10945(2)	397(2)	544(1)	58(1)
C(20)	10771(2)	2201(2)	416(1)	53(1)
C(21)	11871(2)	1587(3)	928(1)	54(1)
C(22)	9842(1)	3585(2)	1894(1)	35(1)
C(23)	8408(1)	4155(2)	1838(1)	34(1)
C(24)	9124(1)	4072(2)	1655(1)	34(1)
C(25)	9158(1)	4377(2)	1223(1)	38(1)
C(26)	8508(1)	4726(2)	965(1)	39(1)
C(27)	7797(1)	4743(2)	1156(1)	40(1)
C(28)	7731(1)	4459(2)	1588(1)	37(1)
C(29)	8599(2)	5072(2)	496(1)	45(1)

C(30)	9184(2)	5938(2)	515(1)	59(1)
C(31)	8921(2)	4222(2)	228(1)	62(1)
C(32)	7825(2)	5425(2)	262(1)	64(1)
C(33)	6933(1)	4441(2)	1769(1)	42(1)
C(34)	6474(1)	3491(2)	1653(1)	38(1)
C(35)	5926(1)	3482(2)	1286(1)	43(1)
C(36)	5510(1)	2623(2)	1151(1)	43(1)
C(37)	5655(1)	1774(2)	1404(1)	42(1)
C(38)	6200(1)	1735(2)	1765(1)	35(1)
C(39)	6608(1)	2615(2)	1890(1)	38(1)
C(40)	4918(2)	2590(2)	744(1)	52(1)
C(41)	5143(2)	1753(2)	433(1)	66(1)
C(42)	4103(2)	2357(2)	885(1)	68(1)
C(43)	4898(2)	3564(2)	486(1)	65(1)
C(44)	6401(1)	765(2)	1997(1)	38(1)
C(45)	8008(1)	−157(2)	2682(1)	41(1)
C(46)	8085(1)	397(2)	3104(1)	45(1)
C(47)	8973(1)	1507(2)	3500(1)	38(1)
C(48)	8456(1)	1610(2)	3825(1)	44(1)
C(49)	8646(2)	2236(2)	4176(1)	47(1)
C(50)	9331(2)	2764(2)	4205(1)	46(1)
C(51)	9841(2)	2671(2)	3883(1)	45(1)
C(52)	9677(1)	2036(2)	3522(1)	38(1)
C(53)	10230(1)	1947(2)	3186(1)	39(1)
C(54)	12124(1)	2343(2)	3022(1)	42(1)
C(55)	12725(1)	2326(2)	2717(1)	41(1)
C(56)	13512(2)	2483(2)	2874(1)	52(1)
C(57)	14100(2)	2479(2)	2596(1)	58(1)
C(58)	13924(2)	2320(2)	2155(1)	58(1)
C(59)	13156(2)	2180(2)	1990(1)	54(1)
C(60)	12556(1)	2183(2)	2267(1)	44(1)
C(61)	8563(1)	4665(2)	2581(1)	41(1)
C(62)	8238(1)	4424(2)	3005(1)	41(1)
C(63)	6941(1)	4323(2)	3259(1)	41(1)
C(64)	7216(2)	3974(2)	3670(1)	50(1)
C(65)	6687(2)	3747(2)	3973(1)	66(1)
C(66)	5893(2)	3857(2)	3867(1)	71(1)
C(67)	5620(2)	4187(2)	3460(1)	60(1)
C(68)	6134(1)	4442(2)	3149(1)	44(1)
C(69)	5866(2)	4831(2)	2719(1)	46(1)
C(70)	4362(4)	4751(6)	1948(3)	48(2)
C(71)	4225(3)	5330(4)	1465(2)	40(1)
C(72)	3530(3)	5026(4)	1237(2)	53(2)
C(73)	3300(3)	5365(5)	817(2)	55(1)
C(74)	3797(3)	6018(4)	622(2)	62(2)
C(75)	4516(4)	6313(5)	825(2)	67(2)
C(76)	4701(3)	5976(4)	1250(2)	40(1)
C(77)	7295(2)	2402(2)	345(1)	51(1)
C(78)	8484(2)	1451(2)	402(1)	67(1)
C(79)	7920(2)	2077(2)	1063(1)	52(1)
C(19A)	10533(11)	1239(15)	354(6)	57(5)
C(20A)	11502(11)	2514(13)	708(6)	55(5)
C(21A)	11658(9)	692(12)	870(5)	41(4)
C(70A)	4442(5)	4970(6)	1901(3)	46(2)
C(71A)	4099(3)	5088(4)	1521(2)	48(2)
C(72A)	3423(3)	4679(4)	1309(2)	49(2)
C(73A)	3139(3)	5006(4)	896(2)	55(2)
C(74A)	3526(3)	5774(4)	698(2)	50(1)
C(75A)	4212(3)	6197(4)	890(2)	53(2)
C(76A)	4469(4)	5841(4)	1304(2)	56(2)

XXII

Table 0.18: Bond lengths (Å) and angles (°) for **32 (DMF inclusion complex)**.

O(1)-C(1)	1.402(2)	C(26)-C(27)	1.394(3)
O(1)-C(45)	1.439(3)	C(26)-C(29)	1.532(3)
O(2)-C(12)	1.364(2)	C(27)-C(28)	1.392(3)
O(3)-C(23)	1.397(3)	C(28)-C(33)	1.517(3)
O(3)-C(61)	1.439(3)	C(29)-C(32)	1.529(4)
O(4)-C(39)	1.366(3)	C(29)-C(30)	1.533(3)
O(5)-C(47)	1.376(3)	C(29)-C(31)	1.534(4)
O(5)-C(46)	1.428(3)	C(33)-C(34)	1.525(3)
O(6)-C(63)	1.363(3)	C(34)-C(39)	1.392(3)
O(6)-C(62)	1.430(3)	C(34)-C(35)	1.403(3)
O(7)-C(60)	1.355(3)	C(35)-C(36)	1.400(3)
O(8A)-C(76)	1.340(8)	C(36)-C(37)	1.388(3)
O(9)-C(77)	1.225(3)	C(36)-C(40)	1.542(3)
O(8)-C(76A)	1.420(8)	C(37)-C(38)	1.391(3)
N(1)-C(53)	1.275(3)	C(38)-C(39)	1.409(3)
N(1)-N(2)	1.407(3)	C(38)-C(44)	1.510(3)
N(2)-C(54)	1.292(3)	C(40)-C(42)	1.527(4)
N(3)-C(69)	1.273(3)	C(40)-C(43)	1.529(4)
N(3)-N(4)	1.418(3)	C(40)-C(41)	1.543(4)
N(4)-C(70A)	1.226(8)	C(45)-C(46)	1.488(3)
N(4)-C(70)	1.360(8)	C(47)-C(48)	1.394(3)
N(5)-C(77)	1.316(3)	C(47)-C(52)	1.396(3)
N(5)-C(79)	1.441(3)	C(48)-C(49)	1.383(3)
N(5)-C(78)	1.442(3)	C(49)-C(50)	1.368(4)
C(1)-C(2)	1.383(3)	C(50)-C(51)	1.376(3)
C(1)-C(6)	1.396(3)	C(51)-C(52)	1.407(3)
C(2)-C(3)	1.396(3)	C(52)-C(53)	1.460(3)
C(2)-C(11)	1.524(3)	C(54)-C(55)	1.445(3)
C(3)-C(4)	1.394(3)	C(55)-C(60)	1.402(3)
C(4)-C(5)	1.397(3)	C(55)-C(56)	1.408(3)
C(4)-C(7)	1.535(3)	C(56)-C(57)	1.372(4)
C(5)-C(6)	1.389(3)	C(57)-C(58)	1.380(4)
C(6)-C(44)	1.522(3)	C(58)-C(59)	1.381(4)
C(7)-C(8)	1.530(3)	C(59)-C(60)	1.385(3)
C(7)-C(10)	1.530(3)	C(61)-C(62)	1.491(3)
C(7)-C(9)	1.534(3)	C(63)-C(64)	1.390(3)
C(11)-C(13)	1.524(3)	C(63)-C(68)	1.403(3)
C(12)-C(13)	1.394(3)	C(64)-C(65)	1.384(4)
C(12)-C(17)	1.405(3)	C(65)-C(66)	1.380(4)
C(13)-C(14)	1.398(3)	C(66)-C(67)	1.370(4)
C(14)-C(15)	1.392(3)	C(67)-C(68)	1.391(4)
C(15)-C(16)	1.390(3)	C(68)-C(69)	1.459(3)
C(15)-C(18)	1.537(3)	C(70)-C(71A)	1.426(10)
C(16)-C(17)	1.386(3)	C(71)-C(76)	1.3910(10)
C(17)-C(22)	1.515(3)	C(71)-C(72)	1.3913(10)
C(18)-C(19A)	1.468(18)	C(71)-C(70A)	1.442(9)
C(18)-C(21A)	1.498(15)	C(72)-C(73)	1.3912(10)
C(18)-C(20)	1.515(4)	C(73)-C(74)	1.3913(10)
C(18)-C(21)	1.520(4)	C(74)-C(75)	1.3907(10)
C(18)-C(19)	1.547(4)	C(75)-C(76)	1.3909(10)
C(18)-C(20A)	1.686(17)	C(71A)-C(72A)	1.3910(10)
C(22)-C(24)	1.525(3)	C(71A)-C(76A)	1.3914(10)
C(23)-C(24)	1.394(3)	C(72A)-C(73A)	1.3907(10)
C(23)-C(28)	1.395(3)	C(73A)-C(74A)	1.3917(10)
C(24)-C(25)	1.393(3)	C(74A)-C(75A)	1.3911(10)
C(25)-C(26)	1.391(3)	C(75A)-C(76A)	1.3917(10)
C(1)-O(1)-C(45)	113.03(16)	C(26)-C(29)-C(30)	108.1(2)
C(23)-O(3)-C(61)	113.71(16)	C(32)-C(29)-C(31)	108.4(2)

C(47)-O(5)-C(46)	116.67(17)	C(26)-C(29)-C(31)	110.20(19)
C(63)-O(6)-C(62)	119.93(18)	C(30)-C(29)-C(31)	108.8(2)
C(53)-N(1)-N(2)	114.3(2)	C(28)-C(33)-C(34)	112.97(18)
C(54)-N(2)-N(1)	111.9(2)	C(39)-C(34)-C(35)	118.8(2)
C(69)-N(3)-N(4)	111.5(2)	C(39)-C(34)-C(33)	121.7(2)
C(70A)-N(4)-C(70)	14.9(5)	C(35)-C(34)-C(33)	119.5(2)
C(70A)-N(4)-N(3)	120.0(4)	C(36)-C(35)-C(34)	122.3(2)
C(70)-N(4)-N(3)	105.7(4)	C(37)-C(36)-C(35)	116.6(2)
C(77)-N(5)-C(79)	121.8(2)	C(37)-C(36)-C(40)	120.2(2)
C(77)-N(5)-C(78)	120.6(2)	C(35)-C(36)-C(40)	123.2(2)
C(79)-N(5)-C(78)	117.6(2)	C(36)-C(37)-C(38)	123.6(2)
C(2)-C(1)-C(6)	122.7(2)	C(37)-C(38)-C(39)	118.0(2)
C(2)-C(1)-O(1)	118.56(19)	C(37)-C(38)-C(44)	121.3(2)
C(6)-C(1)-O(1)	118.65(19)	C(39)-C(38)-C(44)	120.5(2)
C(1)-C(2)-C(3)	117.7(2)	O(4)-C(39)-C(34)	123.6(2)
C(1)-C(2)-C(11)	121.66(19)	O(4)-C(39)-C(38)	115.8(2)
C(3)-C(2)-C(11)	120.57(19)	C(34)-C(39)-C(38)	120.6(2)
C(4)-C(3)-C(2)	122.3(2)	C(42)-C(40)-C(43)	109.9(2)
C(3)-C(4)-C(5)	116.9(2)	C(42)-C(40)-C(36)	109.4(2)
C(3)-C(4)-C(7)	123.39(19)	C(43)-C(40)-C(36)	112.4(2)
C(5)-C(4)-C(7)	119.67(19)	C(42)-C(40)-C(41)	107.8(2)
C(6)-C(5)-C(4)	123.2(2)	C(43)-C(40)-C(41)	107.4(2)
C(5)-C(6)-C(1)	116.9(2)	C(36)-C(40)-C(41)	109.9(2)
C(5)-C(6)-C(44)	120.3(2)	C(38)-C(44)-C(6)	110.09(18)
C(1)-C(6)-C(44)	122.68(19)	O(1)-C(45)-C(46)	107.29(19)
C(8)-C(7)-C(10)	108.2(2)	O(5)-C(46)-C(45)	108.71(18)
C(8)-C(7)-C(9)	108.4(2)	O(5)-C(47)-C(48)	122.9(2)
C(10)-C(7)-C(9)	109.4(2)	O(5)-C(47)-C(52)	116.5(2)
C(8)-C(7)-C(4)	111.65(19)	C(48)-C(47)-C(52)	120.7(2)
C(10)-C(7)-C(4)	109.57(19)	C(49)-C(48)-C(47)	119.8(2)
C(9)-C(7)-C(4)	109.57(18)	C(50)-C(49)-C(48)	120.6(2)
C(13)-C(11)-C(2)	113.83(17)	C(49)-C(50)-C(51)	119.9(2)
O(2)-C(12)-C(13)	123.98(19)	C(50)-C(51)-C(52)	121.5(2)
O(2)-C(12)-C(17)	115.27(19)	C(47)-C(52)-C(51)	117.5(2)
C(13)-C(12)-C(17)	120.73(19)	C(47)-C(52)-C(53)	122.1(2)
C(12)-C(13)-C(14)	118.24(19)	C(51)-C(52)-C(53)	120.4(2)
C(12)-C(13)-C(11)	121.83(19)	N(1)-C(53)-C(52)	119.6(2)
C(14)-C(13)-C(11)	119.93(19)	N(2)-C(54)-C(55)	123.2(2)
C(15)-C(14)-C(13)	122.9(2)	C(60)-C(55)-C(56)	118.1(2)
C(16)-C(15)-C(14)	116.6(2)	C(60)-C(55)-C(54)	122.6(2)
C(16)-C(15)-C(18)	120.10(19)	C(56)-C(55)-C(54)	119.3(2)
C(14)-C(15)-C(18)	123.3(2)	C(57)-C(56)-C(55)	121.2(3)
C(17)-C(16)-C(15)	123.3(2)	C(56)-C(57)-C(58)	119.9(3)
C(16)-C(17)-C(12)	118.26(19)	C(57)-C(58)-C(59)	120.3(3)
C(16)-C(17)-C(22)	121.21(19)	C(58)-C(59)-C(60)	120.4(3)
C(12)-C(17)-C(22)	120.41(19)	O(7)-C(60)-C(59)	117.9(2)
C(19A)-C(18)-C(21A)	114.9(10)	O(7)-C(60)-C(55)	122.0(2)
C(19A)-C(18)-C(20)	54.3(8)	C(59)-C(60)-C(55)	120.1(2)
C(21A)-C(18)-C(20)	139.8(6)	O(3)-C(61)-C(62)	108.62(18)
C(19A)-C(18)-C(21)	140.2(8)	O(6)-C(62)-C(61)	106.25(19)
C(21A)-C(18)-C(21)	49.5(6)	O(6)-C(63)-C(64)	124.2(2)
C(20)-C(18)-C(21)	110.3(2)	O(6)-C(63)-C(68)	115.1(2)
C(19A)-C(18)-C(15)	110.3(7)	C(64)-C(63)-C(68)	120.7(2)
C(21A)-C(18)-C(15)	109.8(6)	C(65)-C(64)-C(63)	119.4(3)
C(20)-C(18)-C(15)	110.1(2)	C(66)-C(65)-C(64)	120.3(3)
C(21)-C(18)-C(15)	109.5(2)	C(67)-C(66)-C(65)	120.3(3)
C(19A)-C(18)-C(19)	56.6(8)	C(66)-C(67)-C(68)	121.1(3)
C(21A)-C(18)-C(19)	61.8(7)	C(67)-C(68)-C(63)	118.2(2)
C(20)-C(18)-C(19)	107.4(2)	C(67)-C(68)-C(69)	122.6(2)
C(21)-C(18)-C(19)	107.9(2)	C(63)-C(68)-C(69)	119.2(2)
C(15)-C(18)-C(19)	111.7(2)	N(3)-C(69)-C(68)	121.8(2)

C(19A)-C(18)-C(20A)	108.5(10)	N(4)-C(70)-C(71A)	117.2(6)
C(21A)-C(18)-C(20A)	103.8(9)	C(76)-C(71)-C(72)	117.1(5)
C(20)-C(18)-C(20A)	57.1(7)	C(76)-C(71)-C(70A)	122.1(5)
C(21)-C(18)-C(20A)	56.6(7)	C(72)-C(71)-C(70A)	120.8(5)
C(15)-C(18)-C(20A)	109.3(6)	C(73)-C(72)-C(71)	122.3(5)
C(19)-C(18)-C(20A)	139.0(7)	C(72)-C(73)-C(74)	117.9(5)
C(17)-C(22)-C(24)	109.94(17)	C(75)-C(74)-C(73)	122.4(5)
C(24)-C(23)-C(28)	121.4(2)	C(74)-C(75)-C(76)	116.9(5)
C(24)-C(23)-O(3)	120.1(2)	O(8A)-C(76)-C(75)	115.1(5)
C(28)-C(23)-O(3)	118.48(19)	O(8A)-C(76)-C(71)	121.5(4)
C(25)-C(24)-C(23)	117.7(2)	C(75)-C(76)-C(71)	123.3(5)
C(25)-C(24)-C(22)	119.2(2)	O(9)-C(77)-N(5)	125.6(3)
C(23)-C(24)-C(22)	122.9(2)	N(4)-C(70A)-C(71)	128.0(6)
C(26)-C(25)-C(24)	123.2(2)	C(72A)-C(71A)-C(76A)	117.2(5)
C(25)-C(26)-C(27)	116.8(2)	C(72A)-C(71A)-C(70)	119.4(5)
C(25)-C(26)-C(29)	119.9(2)	C(76A)-C(71A)-C(70)	123.3(5)
C(27)-C(26)-C(29)	123.3(2)	C(73A)-C(72A)-C(71A)	121.0(5)
C(28)-C(27)-C(26)	122.5(2)	C(72A)-C(73A)-C(74A)	119.2(5)
C(27)-C(28)-C(23)	118.3(2)	C(75A)-C(74A)-C(73A)	122.2(5)
C(27)-C(28)-C(33)	119.9(2)	C(74A)-C(75A)-C(76A)	116.0(5)
C(23)-C(28)-C(33)	121.7(2)	C(71A)-C(76A)-C(75A)	124.3(6)
C(32)-C(29)-C(26)	112.5(2)	C(71A)-C(76A)-O(8)	122.8(4)
C(32)-C(29)-C(30)	108.7(2)	C(75A)-C(76A)-O(8)	113.0(5)

Table 0.19: Anisotropic displacement parameters ($\text{Å}^2 * 10^3$) for **32 (DMF inclusion complex)**. The anisotropic displacement factor exponent takes the form: $-2 g\pi^2 [h^2 a^{*2} U11 + ... + 2 h k a^* b^* U12]$

Atom	U11	U22	U33	U23	U13	U12
O(1)	37(1)	42(1)	26(1)	1(1)	2(1)	−6(1)
O(2)	41(1)	41(1)	33(1)	−2(1)	10(1)	−8(1)
O(3)	40(1)	39(1)	30(1)	−9(1)	3(1)	−5(1)
O(4)	43(1)	50(1)	39(1)	−6(1)	−6(1)	−10(1)
O(5)	38(1)	60(1)	31(1)	−4(1)	3(1)	−12(1)
O(6)	39(1)	58(1)	36(1)	3(1)	1(1)	4(1)
O(7)	44(1)	72(1)	47(1)	6(1)	−3(1)	−3(1)
O(9)	96(2)	98(2)	44(1)	6(1)	−15(1)	−1(1)
N(1)	39(1)	43(1)	49(1)	−5(1)	8(1)	−2(1)
N(2)	44(1)	39(1)	47(1)	−2(1)	5(1)	−2(1)
N(3)	46(1)	63(1)	46(1)	4(1)	1(1)	10(1)
N(4)	52(1)	68(2)	45(1)	−2(1)	1(1)	15(1)
N(5)	41(1)	38(1)	30(1)	1(1)	2(1)	3(1)
C(1)	35(1)	33(1)	24(1)	2(1)	1(1)	−5(1)
C(2)	32(1)	30(1)	32(1)	6(1)	2(1)	−1(1)
C(3)	35(1)	31(1)	34(1)	3(1)	4(1)	3(1)
C(4)	35(1)	33(1)	32(1)	−1(1)	3(1)	−3(1)
C(5)	29(1)	41(1)	34(1)	−1(1)	0(1)	−4(1)
C(6)	32(1)	36(1)	31(1)	1(1)	4(1)	−5(1)
C(7)	40(1)	39(1)	35(1)	−7(1)	2(1)	0(1)
C(8)	54(2)	64(2)	46(2)	−20(1)	6(1)	1(1)
C(9)	75(2)	56(2)	39(2)	−10(1)	−14(1)	6(1)
C(10)	57(2)	57(2)	46(2)	−14(1)	2(1)	−12(1)
C(11)	33(1)	34(1)	34(1)	3(1)	1(1)	0(1)
C(12)	25(1)	44(1)	27(1)	3(1)	0(1)	1(1)
C(13)	25(1)	36(1)	32(1)	3(1)	−3(1)	1(1)
C(14)	30(1)	35(1)	33(1)	−1(1)	−1(1)	4(1)
C(15)	31(1)	43(1)	32(1)	3(1)	2(1)	4(1)
C(16)	29(1)	41(1)	35(1)	7(1)	1(1)	−5(1)

C(17)	28(1)	38(1)	28(1)	0(1)	−3(1)	−3(1)
C(18)	40(1)	46(1)	39(1)	2(1)	12(1)	3(1)
C(19)	73(2)	51(2)	53(2)	−10(2)	27(2)	−4(2)
C(20)	56(2)	67(2)	40(2)	11(2)	19(2)	13(2)
C(21)	44(2)	68(2)	50(2)	1(2)	15(2)	3(2)
C(22)	33(1)	39(1)	33(1)	−1(1)	3(1)	−7(1)
C(23)	42(1)	29(1)	30(1)	−6(1)	0(1)	−3(1)
C(24)	37(1)	31(1)	34(1)	−7(1)	2(1)	−6(1)
C(25)	44(1)	34(1)	35(1)	−5(1)	5(1)	−4(1)
C(26)	53(2)	29(1)	34(1)	−6(1)	0(1)	−2(1)
C(27)	45(2)	32(1)	40(2)	−6(1)	−6(1)	3(1)
C(28)	41(1)	31(1)	38(1)	−10(1)	1(1)	1(1)
C(29)	64(2)	35(1)	36(1)	1(1)	−1(1)	−7(1)
C(30)	78(2)	45(2)	52(2)	8(1)	−3(2)	−13(1)
C(31)	97(2)	50(2)	40(2)	−2(1)	16(2)	−7(2)
C(32)	80(2)	63(2)	47(2)	9(1)	−13(2)	−7(2)
C(33)	42(1)	39(1)	44(2)	−12(1)	−1(1)	8(1)
C(34)	30(1)	47(1)	39(1)	−15(1)	1(1)	5(1)
C(35)	40(1)	44(1)	45(2)	−9(1)	1(1)	10(1)
C(36)	32(1)	53(2)	42(2)	−13(1)	−3(1)	7(1)
C(37)	30(1)	49(2)	48(2)	−14(1)	4(1)	−2(1)
C(38)	25(1)	48(1)	34(1)	−12(1)	6(1)	1(1)
C(39)	29(1)	50(2)	35(1)	−11(1)	4(1)	4(1)
C(40)	41(2)	58(2)	54(2)	−12(1)	−10(1)	8(1)
C(41)	56(2)	83(2)	56(2)	−25(2)	−14(1)	9(2)
C(42)	38(2)	96(2)	66(2)	−10(2)	−9(1)	5(2)
C(43)	62(2)	78(2)	51(2)	−7(2)	−13(2)	8(2)
C(44)	31(1)	50(1)	34(1)	−7(1)	7(1)	−10(1)
C(45)	42(1)	48(1)	32(1)	6(1)	3(1)	−11(1)
C(46)	44(2)	61(2)	31(1)	3(1)	7(1)	−14(1)
C(47)	44(1)	43(1)	28(1)	3(1)	−2(1)	−1(1)
C(48)	44(2)	54(2)	33(1)	2(1)	2(1)	−1(1)
C(49)	52(2)	54(2)	35(1)	3(1)	5(1)	11(1)
C(50)	58(2)	42(1)	39(2)	−3(1)	2(1)	7(1)
C(51)	49(2)	38(1)	46(2)	4(1)	−4(1)	0(1)
C(52)	42(1)	36(1)	35(1)	6(1)	−2(1)	1(1)
C(53)	44(2)	38(1)	36(1)	2(1)	0(1)	−3(1)
C(54)	44(2)	39(1)	43(2)	−6(1)	−1(1)	−1(1)
C(55)	42(1)	35(1)	45(2)	−4(1)	2(1)	0(1)
C(56)	45(2)	55(2)	55(2)	−8(1)	−3(1)	−4(1)
C(57)	40(2)	70(2)	64(2)	−1(2)	3(1)	−7(1)
C(58)	48(2)	71(2)	56(2)	4(2)	10(1)	−5(1)
C(59)	52(2)	66(2)	45(2)	4(1)	5(1)	−7(1)
C(60)	38(1)	44(1)	49(2)	3(1)	1(1)	−2(1)
C(61)	38(1)	48(1)	38(1)	−16(1)	3(1)	−8(1)
C(62)	34(1)	53(2)	36(1)	−10(1)	−4(1)	3(1)
C(63)	43(1)	41(1)	38(1)	−1(1)	4(1)	3(1)
C(64)	51(2)	56(2)	44(2)	5(1)	3(1)	6(1)
C(65)	67(2)	83(2)	48(2)	27(2)	9(2)	10(2)
C(66)	64(2)	90(2)	62(2)	33(2)	18(2)	9(2)
C(67)	45(2)	76(2)	59(2)	15(2)	8(1)	9(1)
C(68)	41(1)	48(2)	44(2)	4(1)	6(1)	8(1)
C(69)	42(2)	52(2)	43(2)	2(1)	5(1)	10(1)
C(77)	53(2)	55(2)	43(2)	−1(1)	−2(1)	1(1)
C(78)	67(2)	59(2)	78(2)	10(2)	33(2)	12(2)
C(79)	77(2)	42(2)	35(1)	2(1)	−3(1)	1(1)

XXVI

Table 0.20: Hydrogen coordinates (*10^4) and isotropic displacement parameters (Å^2 * 10^3) for **32 (DMF inclusion complex)**.

Atom	x	y	z	U(eq)
H(2)	8842	1440	2239	45
H(4)	7441	3027	2256	53
H(7)	11499	2097	2282	65
H(8)	5471	6037	1688	77
H(8A)	5303	6065	1728	79
H(3)	8546	−877	1100	40
H(5)	6284	−247	1250	42
H(8D)	8138	−1066	374	81
H(8B)	7591	−1952	178	81
H(8C)	8078	−2080	644	81
H(9A)	6204	−177	496	87
H(9B)	6514	−742	84	87
H(9C)	7022	137	318	87
H(10A)	6816	−2528	952	80
H(10B)	6361	−2356	481	80
H(10C)	6088	−1778	898	80
H(11A)	9299	−115	2162	41
H(11B)	9524	−728	1743	41
H(14)	10149	82	1178	39
H(16)	10693	2989	1253	42
H(19A)	10398	280	434	87
H(19B)	11111	−117	759	87
H(19C)	11279	370	299	87
H(20A)	11112	2151	175	80
H(20B)	10814	2869	544	80
H(20C)	10227	2077	304	80
H(21A)	12202	1525	683	80
H(21B)	12025	1083	1150	80
H(21C)	11937	2252	1057	80
H(22A)	10310	4004	1863	42
H(22B)	9766	3527	2210	42
H(25)	9647	4346	1099	45
H(27)	7339	4956	985	48
H(30A)	9252	6170	217	88
H(30B)	9690	5713	653	88
H(30C)	8985	6485	686	88
H(31A)	8539	3677	202	93
H(31B)	9414	3980	376	93
H(31C)	9015	4467	−64	93
H(32A)	7451	4870	239	96
H(32B)	7916	5663	−31	96
H(32C)	7610	5968	429	96
H(33A)	6625	5021	1653	50
H(33B)	7003	4507	2091	50
H(35)	5834	4079	1124	52
H(37)	5365	1189	1325	51
H(41A)	5673	1872	346	98
H(41B)	4771	1745	172	98
H(41C)	5128	1110	583	98
H(42A)	4113	1716	1038	102
H(42B)	3727	2325	626	102
H(42C)	3944	2882	1081	102
H(43A)	4739	4110	671	97
H(43B)	4522	3505	228	97
H(43C)	5421	3703	391	97
H(44A)	5922	351	2003	46

H(44B)	6602	901	2303	46
H(45A)	8447	−633	2669	49
H(45B)	7509	−534	2654	49
H(46A)	7661	898	3109	54
H(46B)	8039	−70	3351	54
H(48)	7976	1252	3806	53
H(49)	8296	2299	4400	56
H(50)	9455	3194	4447	56
H(51)	10314	3044	3905	54
H(53)	10070	1647	2912	47
H(54)	12276	2472	3321	50
H(56)	13637	2593	3178	62
H(57)	14628	2586	2708	70
H(58)	14332	2307	1963	70
H(59)	13038	2082	1685	65
H(61A)	8352	5310	2469	50
H(61B)	9141	4719	2624	50
H(62A)	8368	3729	3093	50
H(62B)	8458	4877	3238	50
H(64)	7763	3891	3742	60
H(65)	6872	3515	4256	79
H(66)	5533	3703	4077	85
H(67)	5071	4243	3389	72
H(69)	6219	5203	2560	55
H(70)	4073	4274	2098	57
H(72)	3200	4571	1372	63
H(73)	2818	5157	668	66
H(74)	3640	6272	339	74
H(75)	4864	6726	681	81
H(77)	6904	2745	488	61
H(78A)	8360	1402	85	100
H(78B)	8533	781	528	100
H(78C)	8980	1811	462	100
H(79A)	7465	2445	1152	77
H(79B)	8401	2437	1161	77
H(79C)	7932	1413	1197	77
H(19D)	10872	1135	116	85
H(19E)	10188	1809	285	85
H(19F)	10215	641	389	85
H(20D)	11876	2438	486	82
H(20E)	11784	2692	989	82
H(20F)	11126	3042	619	82
H(21D)	11428	35	914	61
H(21E)	11967	896	1139	61
H(21F)	11999	659	629	61
H(70A)	4071	4549	2024	56
H(72A)	3152	4169	1449	59
H(73A)	2686	4709	751	65
H(74A)	3315	6017	422	60
H(75A)	4489	6698	748	64

- **Crystallographic data recorded for 37**

Table 0.21: Atomic coordinates (*10^4) and equivalent isotropic displacement parameters (Å^2 * 10^3) for **37**. U(eq) is defined as one third of the trace of the orthogonalised Uij tensor.

Atom	x	y	z	U(eq)
O(1)	148(1)	9125(1)	−1975(1)	33(1)
O(2)	1690(1)	9997(1)	−2027(1)	33(1)
O(3)	1532(1)	8506(1)	−2000(1)	36(1)
O(4)	157(1)	7705(1)	−1533(1)	32(1)
O(5)	3062(1)	10567(1)	−764(1)	35(1)
O(6)	5(1)	8113(1)	−236(1)	37(1)
O(7)	3808(1)	6336(1)	1965(1)	41(1)
O(8)	2815(1)	4701(1)	1851(1)	36(1)
O(9)	2771(1)	3924(1)	548(1)	38(1)
O(10)	2018(1)	5773(1)	2007(1)	34(1)
O(11)	2813(1)	7143(1)	1626(1)	33(1)
O(12)	1599(1)	6769(1)	329(1)	34(1)
O(1S)	8445(1)	7266(1)	1982(1)	63(1)
O(2S)	9677(1)	8026(1)	2003(1)	56(1)
O(3S)	4683(3)	9697(3)	−3751(2)	147(2)
O(4S)	4626(2)	10271(2)	−2831(2)	86(1)
O(5S)	5141(3)	3068(2)	2128(2)	86(1)
O(6S)	4818(3)	3903(2)	2680(2)	75(1)
O(5T)	5833(7)	4552(6)	2833(5)	113(3)
O(6T)	4238(5)	2316(4)	2042(4)	77(2)
N(1)	4120(1)	9161(1)	−998(1)	39(1)
N(2)	4736(2)	8189(2)	−1423(2)	69(1)
N(3)	3208(2)	6664(2)	−1472(2)	72(1)
N(4)	2357(1)	8138(1)	−714(1)	44(1)
N(5)	−915(1)	9592(1)	230(1)	37(1)
N(6)	−1477(2)	10651(1)	558(1)	45(1)
N(7)	−3288(2)	10066(3)	−739(2)	107(2)
N(8)	−2477(2)	8566(2)	−1249(2)	63(1)
N(9)	5143(1)	5221(1)	868(1)	40(1)
N(10)	6809(2)	6136(1)	1443(1)	57(1)
N(11)	6682(2)	7713(2)	1523(1)	59(1)
N(12)	4237(2)	6447(1)	668(1)	47(1)
N(13)	−808(1)	5435(1)	−192(1)	33(1)
N(14)	−2424(1)	4460(1)	−576(1)	41(1)
N(15)	−2981(2)	4863(1)	794(1)	52(1)
N(16)	−605(2)	6350(1)	1379(1)	53(1)
C(1)	−567(1)	9083(1)	−2423(1)	29(1)
C(2)	−1312(1)	8556(1)	−2456(1)	31(1)
C(3)	−2068(2)	8518(1)	−2862(1)	36(1)
C(4)	−2107(2)	8963(1)	−3264(1)	37(1)
C(5)	−1347(2)	9456(1)	−3241(1)	34(1)
C(6)	−576(2)	9534(1)	−2826(1)	31(1)
C(7)	−2955(2)	8917(2)	−3692(2)	47(1)
C(8)	−2857(3)	9312(3)	−4230(3)	55(1)
C(9)	−3394(5)	9169(4)	−3266(4)	86(2)
C(10)	−3495(4)	8146(3)	−4099(3)	65(1)
C(11)	225(2)	10100(1)	−2815(1)	35(1)
C(12)	773(2)	9804(1)	−3112(1)	32(1)
C(13)	1475(1)	9751(1)	−2711(1)	31(1)
C(14)	1932(1)	9418(1)	−2975(1)	32(1)
C(15)	1697(2)	9174(1)	−3657(1)	33(1)
C(16)	1025(2)	9246(1)	−4083(1)	33(1)
C(17)	569(2)	9557(1)	−3790(1)	34(1)

C(18)	828(2)	9023(1)	−4834(1)	39(1)
C(19)	1301(3)	9647(2)	−5040(2)	82(1)
C(20)	1087(4)	8421(3)	−5048(2)	98(2)
C(21)	−98(2)	8787(3)	−5192(2)	79(1)
C(22)	2642(2)	9296(1)	−2531(1)	37(1)
C(23)	2434(2)	8517(1)	−2634(1)	36(1)
C(24)	1842(2)	8129(1)	−2380(1)	33(1)
C(25)	1583(2)	7401(1)	−2517(1)	35(1)
C(26)	1953(2)	7075(2)	−2892(1)	40(1)
C(27)	2558(2)	7438(2)	−3143(1)	45(1)
C(28)	2785(2)	8163(2)	−3005(1)	42(1)
C(29)	2920(2)	7056(2)	−3588(2)	59(1)
C(30)	2860(5)	6358(3)	−3460(4)	144(3)
C(31)	3812(3)	7508(3)	−3512(2)	98(2)
C(32)	2377(3)	6890(3)	−4298(2)	101(2)
C(33)	898(2)	6972(1)	−2278(1)	36(1)
C(34)	68(2)	7025(1)	−2582(1)	32(1)
C(35)	−272(1)	7393(1)	−2209(1)	30(1)
C(36)	−988(2)	7498(1)	−2496(1)	31(1)
C(37)	−1388(2)	7194(1)	−3171(1)	35(1)
C(38)	−1084(2)	6810(1)	−3568(1)	36(1)
C(39)	−346(2)	6745(1)	−3257(1)	35(1)
C(40)	−1497(2)	6537(2)	−4320(1)	47(1)
C(41)	−1046(3)	7090(2)	−4619(2)	90(1)
C(42)	−1423(2)	5848(2)	−4598(2)	65(1)
C(43)	−2429(2)	6400(2)	−4520(2)	79(1)
C(44)	−1287(2)	7991(1)	−2112(1)	33(1)
C(45)	2271(2)	10724(1)	−1767(1)	34(1)
C(46)	2528(2)	10903(1)	−1028(1)	33(1)
C(47)	3891(1)	10837(1)	−731(1)	33(1)
C(48)	4345(2)	11540(1)	−660(1)	42(1)
C(49)	5189(2)	11770(2)	−605(2)	47(1)
C(50)	5581(2)	11302(2)	−621(1)	45(1)
C(51)	5138(2)	10606(2)	−696(1)	39(1)
C(52)	4282(2)	10358(1)	−754(1)	34(1)
C(53)	3819(2)	9622(1)	−845(1)	35(1)
C(54)	3679(2)	8456(1)	−1073(1)	38(1)
C(55)	2930(2)	8238(1)	−895(1)	37(1)
C(56)	4003(2)	7990(2)	−1295(2)	47(1)
C(57)	3555(2)	7248(2)	−1397(2)	52(1)
C(58)	−103(2)	7235(1)	−1148(1)	35(1)
C(59)	353(2)	7614(1)	−432(1)	36(1)
C(60)	422(2)	8590(1)	370(1)	35(1)
C(61)	1120(2)	8585(2)	816(1)	49(1)
C(62)	1526(2)	9104(2)	1411(1)	54(1)
C(63)	1241(2)	9629(2)	1575(1)	51(1)
C(64)	548(2)	9629(2)	1137(1)	40(1)
C(65)	126(2)	9118(1)	530(1)	34(1)
C(66)	−627(2)	9121(1)	74(1)	36(1)
C(67)	−1634(2)	9590(2)	−189(1)	37(1)
C(68)	−2119(2)	9034(2)	−787(2)	45(1)
C(69)	−1892(2)	10114(2)	6(1)	42(1)
C(70)	−2668(2)	10095(2)	−409(2)	63(1)
C(71)	4643(1)	6691(1)	2328(1)	37(1)
C(72)	5081(2)	6277(2)	2508(1)	40(1)
C(73)	5928(2)	6606(2)	2868(1)	43(1)
C(74)	6354(2)	7332(2)	3063(1)	42(1)
C(75)	5892(2)	7726(2)	2878(1)	40(1)
C(76)	5040(2)	7423(1)	2512(1)	37(1)
C(77)	7281(2)	7699(2)	3501(1)	50(1)
C(78)	7753(2)	8316(2)	3273(2)	87(1)

XXX

C(79)	7301(2)	7947(3)	4203(2)	102(2)
C(80)	7738(2)	7203(2)	3476(2)	80(1)
C(81)	4567(2)	7876(2)	2321(1)	39(1)
C(82)	3896(1)	7842(1)	2651(1)	33(1)
C(83)	4117(2)	8171(1)	3320(1)	35(1)
C(84)	3523(2)	8137(1)	3641(1)	34(1)
C(85)	2686(2)	7726(1)	3273(1)	33(1)
C(86)	2433(1)	7378(1)	2607(1)	32(1)
C(87)	3047(1)	7463(1)	2300(1)	31(1)
C(88)	3763(2)	8561(1)	4360(1)	41(1)
C(89)	3252(2)	8143(2)	4732(2)	68(1)
C(90)	3575(3)	9219(2)	4352(2)	76(1)
C(91)	4686(2)	8777(2)	4739(2)	72(1)
C(92)	1522(1)	6887(1)	2239(1)	33(1)
C(93)	1270(1)	6286(1)	2543(1)	31(1)
C(94)	1568(1)	5755(1)	2443(1)	30(1)
C(95)	1393(1)	5221(1)	2756(1)	30(1)
C(96)	906(2)	5234(1)	3170(1)	34(1)
C(97)	578(2)	5744(1)	3270(1)	36(1)
C(98)	775(2)	6266(1)	2951(1)	35(1)
C(99)	−4(2)	5726(2)	3693(2)	48(1)
C(100)	−8(4)	5224(3)	4112(3)	65(1)
C(101)	−900(4)	5484(3)	3223(3)	70(2)
C(102)	235(4)	6456(3)	4137(3)	64(1)
C(103)	1730(2)	4652(1)	2647(1)	35(1)
C(104)	2679(2)	4951(1)	2934(1)	34(1)
C(105)	3192(2)	4985(1)	2535(1)	33(1)
C(106)	4054(2)	5350(1)	2793(1)	37(1)
C(107)	4414(2)	5655(1)	3473(1)	41(1)
C(108)	3927(2)	5623(1)	3893(1)	40(1)
C(109)	3058(2)	5271(1)	3611(1)	39(1)
C(110)	4330(2)	6032(2)	4624(2)	55(1)
C(111)	4208(5)	6732(3)	4691(3)	140(3)
C(112)	3895(3)	5667(3)	5056(2)	124(2)
C(113)	5251(3)	6195(4)	4880(2)	126(2)
C(114)	4606(2)	5492(2)	2356(1)	45(1)
C(115)	2687(2)	7617(1)	1249(1)	36(1)
C(116)	2452(2)	7256(1)	533(1)	35(1)
C(117)	1279(1)	6315(1)	−291(1)	30(1)
C(118)	1733(2)	6305(1)	−729(1)	34(1)
C(119)	1363(2)	5814(1)	−1341(1)	37(1)
C(120)	540(2)	5332(1)	−1526(1)	38(1)
C(121)	87(2)	5351(1)	−1096(1)	34(1)
C(122)	444(1)	5837(1)	−472(1)	30(1)
C(123)	−32(1)	5842(1)	−12(1)	31(1)
C(124)	−1270(1)	5427(1)	240(1)	32(1)
C(125)	−927(2)	5925(1)	882(1)	39(1)
C(126)	−2074(2)	4929(1)	20(1)	34(1)
C(127)	−2577(2)	4895(1)	454(1)	40(1)
C(128)	2619(2)	3960(1)	1637(1)	35(1)
C(129)	2196(2)	3711(1)	902(1)	35(1)
C(130)	3345(2)	3614(1)	561(1)	34(1)
C(131)	3147(2)	2907(1)	530(1)	42(1)
C(132)	3751(2)	2629(2)	516(2)	47(1)
C(133)	4540(2)	3045(2)	529(1)	45(1)
C(134)	4743(2)	3748(2)	571(1)	41(1)
C(135)	4149(2)	4047(1)	590(1)	35(1)
C(136)	4372(2)	4798(1)	669(1)	36(1)
C(137)	5367(2)	5941(1)	977(1)	39(1)
C(138)	4755(2)	6242(1)	816(1)	39(1)
C(139)	6197(2)	6365(1)	1266(1)	42(1)

C(140)	6451(2)	7114(2)	1405(1)	43(1)
C(200)	−689(9)	5008(7)	3529(7)	91(4)
C(201)	−396(9)	6264(7)	3689(7)	87(3)
C(202)	553(11)	5851(9)	4434(8)	114(5)
C(8A)	−3013(12)	8837(11)	−4368(9)	121(5)
C(9A)	−3110(6)	9573(5)	−3312(5)	52(2)
C(10A)	−3725(7)	8321(6)	−3648(6)	68(3)
C(1S)	8584(2)	7593(2)	998(2)	81(1)
C(2S)	8874(2)	7606(2)	1706(2)	54(1)
C(3S)	10028(2)	8032(2)	2679(2)	58(1)
C(4S)	10934(2)	8507(2)	2901(2)	69(1)
C(5S)	3673(2)	10243(2)	−3783(2)	85(1)
C(6S)	4351(3)	10023(2)	−3459(2)	80(1)
C(7S)	5543(6)	10256(4)	−2410(3)	152(3)
C(8S)	5168(4)	9579(5)	−2360(3)	168(4)
C(9S)	5948(4)	4378(3)	2269(3)	65(2)
C(10S)	5227(4)	3690(4)	2336(3)	77(2)
C(11S)	4171(4)	3310(3)	2799(3)	64(1)
C(12S)	3764(4)	3608(3)	3236(3)	62(1)
C(9T)	4596(7)	3760(6)	2172(6)	70(3)
C(10T)	6959(13)	5054(11)	2598(10)	140(6)
C(11T)	4727(12)	4048(11)	3270(10)	130(6)
C(12T)	3910(20)	2659(18)	2694(16)	209(12)

Table 0.22: Bond lengths (Å) and angles (°) for **37**.

O(1)-C(1)	1.373(3)	**O(2)-C(13)**	1.396(3)
O(2)-C(45)	1.446(3)	**O(3)-C(24)**	1.375(3)
O(4)-C(35)	1.401(3)	**O(4)-C(58)**	1.438(3)
O(5)-C(47)	1.378(3)	**O(5)-C(46)**	1.435(3)
O(6)-C(60)	1.365(3)	**O(6)-C(59)**	1.437(3)
O(7)-C(71)	1.377(3)	**O(8)-C(105)**	1.403(3)
O(8)-C(128)	1.436(3)	**O(9)-C(130)**	1.382(3)
O(9)-C(129)	1.428(3)	**O(10)-C(94)**	1.379(3)
O(11)-C(87)	1.396(3)	**O(11)-C(115)**	1.435(3)
O(12)-C(117)	1.368(3)	**O(12)-C(116)**	1.431(3)
O(1S)-C(2S)	1.211(4)	**O(2S)-C(2S)**	1.330(4)
O(2S)-C(3S)	1.448(4)	**O(3S)-C(6S)**	1.232(5)
O(4S)-C(6S)	1.279(5)	**O(4S)-C(7S)**	1.687(8)
O(5S)-C(10S)	1.248(7)	**O(6S)-C(10S)**	1.286(7)
O(6S)-C(11S)	1.501(7)	**O(6T)-C(12T)**	1.79(3)
N(1)-C(53)	1.286(3)	**N(1)-C(54)**	1.385(4)
N(2)-C(56)	1.348(4)	**N(3)-C(57)**	1.137(4)
N(4)-C(55)	1.151(3)	**N(5)-C(66)**	1.289(3)
N(5)-C(67)	1.383(3)	**N(6)-C(69)**	1.344(4)
N(7)-C(70)	1.142(4)	**N(8)-C(68)**	1.145(4)
N(9)-C(136)	1.281(3)	**N(9)-C(137)**	1.388(3)
N(10)-C(139)	1.336(4)	**N(11)-C(140)**	1.145(4)
N(12)-C(138)	1.146(4)	**N(13)-C(123)**	1.281(3)
N(13)-C(124)	1.389(3)	**N(14)-C(126)**	1.339(3)
N(15)-C(127)	1.144(3)	**N(16)-C(125)**	1.148(3)
C(1)-C(2)	1.397(3)	**C(1)-C(6)**	1.399(3)
C(2)-C(3)	1.392(3)	**C(2)-C(44)**	1.517(3)
C(3)-C(4)	1.394(4)	**C(4)-C(5)**	1.391(4)
C(4)-C(7)	1.538(3)	**C(5)-C(6)**	1.393(3)
C(6)-C(11)	1.518(3)	**C(7)-C(8A)**	1.424(18)
C(7)-C(9)	1.484(7)	**C(7)-C(10)**	1.544(6)
C(7)-C(8)	1.557(6)	**C(7)-C(10A)**	1.560(11)
C(7)-C(9A)	1.618(10)	**C(11)-C(12)**	1.524(3)

C(12)-C(17)	1.388(4)	C(12)-C(13)	1.395(3)
C(13)-C(14)	1.394(3)	C(14)-C(15)	1.390(3)
C(14)-C(22)	1.523(3)	C(15)-C(16)	1.397(3)
C(16)-C(17)	1.396(4)	C(16)-C(18)	1.535(3)
C(18)-C(19)	1.512(4)	C(18)-C(21)	1.513(4)
C(18)-C(20)	1.520(4)	C(22)-C(23)	1.514(4)
C(23)-C(28)	1.393(4)	C(23)-C(24)	1.398(3)
C(24)-C(25)	1.395(4)	C(25)-C(26)	1.387(4)
C(25)-C(33)	1.523(3)	C(26)-C(27)	1.388(4)
C(27)-C(28)	1.393(4)	C(27)-C(29)	1.541(4)
C(29)-C(31)	1.510(6)	C(29)-C(30)	1.513(6)
C(29)-C(32)	1.520(6)	C(33)-C(34)	1.521(3)
C(34)-C(39)	1.390(4)	C(34)-C(35)	1.396(3)
C(35)-C(36)	1.389(3)	C(36)-C(37)	1.393(3)
C(36)-C(44)	1.526(3)	C(37)-C(38)	1.398(4)
C(38)-C(39)	1.392(4)	C(38)-C(40)	1.536(4)
C(40)-C(41)	1.522(5)	C(40)-C(43)	1.527(5)
C(40)-C(42)	1.527(4)	C(45)-C(46)	1.500(3)
C(47)-C(48)	1.389(4)	C(47)-C(52)	1.402(3)
C(48)-C(49)	1.388(4)	C(49)-C(50)	1.383(4)
C(50)-C(51)	1.370(4)	C(51)-C(52)	1.408(3)
C(52)-C(53)	1.441(4)	C(54)-C(56)	1.367(4)
C(54)-C(55)	1.432(4)	C(56)-C(57)	1.444(5)
C(58)-C(59)	1.497(4)	C(60)-C(61)	1.389(4)
C(60)-C(65)	1.404(3)	C(61)-C(62)	1.385(4)
C(62)-C(63)	1.385(4)	C(63)-C(64)	1.369(4)
C(64)-C(65)	1.397(4)	C(65)-C(66)	1.469(3)
C(67)-C(69)	1.366(4)	C(67)-C(68)	1.436(4)
C(69)-C(70)	1.445(4)	C(71)-C(72)	1.395(4)
C(71)-C(76)	1.397(4)	C(72)-C(73)	1.388(4)
C(72)-C(114)	1.515(4)	C(73)-C(74)	1.391(4)
C(74)-C(75)	1.391(4)	C(74)-C(77)	1.543(4)
C(75)-C(76)	1.397(3)	C(76)-C(81)	1.513(4)
C(77)-C(79)	1.513(5)	C(77)-C(80)	1.522(5)
C(77)-C(78)	1.529(5)	C(81)-C(82)	1.526(3)
C(82)-C(83)	1.392(3)	C(82)-C(87)	1.396(3)
C(83)-C(84)	1.393(4)	C(84)-C(85)	1.395(3)
C(84)-C(88)	1.533(4)	C(85)-C(86)	1.389(3)
C(86)-C(87)	1.392(3)	C(86)-C(92)	1.525(3)
C(88)-C(89)	1.526(4)	C(88)-C(91)	1.525(4)
C(88)-C(90)	1.529(4)	C(92)-C(93)	1.513(3)
C(93)-C(98)	1.391(3)	C(93)-C(94)	1.393(3)
C(94)-C(95)	1.399(3)	C(95)-C(96)	1.395(3)
C(95)-C(103)	1.512(3)	C(96)-C(97)	1.390(4)
C(97)-C(98)	1.392(4)	C(97)-C(99)	1.539(4)
C(99)-C(100)	1.510(6)	C(99)-C(200)	1.510(14)
C(99)-C(201)	1.513(13)	C(99)-C(102)	1.521(6)
C(99)-C(101)	1.535(7)	C(99)-C(202)	1.603(17)
C(103)-C(104)	1.520(3)	C(104)-C(109)	1.396(4)
C(104)-C(105)	1.397(4)	C(105)-C(106)	1.387(3)
C(106)-C(107)	1.395(4)	C(106)-C(114)	1.521(4)
C(107)-C(108)	1.399(4)	C(108)-C(109)	1.398(4)
C(108)-C(110)	1.530(4)	C(110)-C(113)	1.500(5)
C(110)-C(112)	1.512(6)	C(110)-C(111)	1.544(6)
C(115)-C(116)	1.495(3)	C(117)-C(118)	1.390(3)
C(117)-C(122)	1.406(3)	C(118)-C(119)	1.385(4)
C(119)-C(120)	1.390(4)	C(120)-C(121)	1.377(4)
C(121)-C(122)	1.399(3)	C(122)-C(123)	1.459(3)
C(124)-C(126)	1.373(3)	C(124)-C(125)	1.438(4)
C(126)-C(127)	1.446(4)	C(128)-C(129)	1.505(4)
C(130)-C(131)	1.393(4)	C(130)-C(135)	1.401(3)

XXXIII

C(131)-C(132)	1.387(4)	C(132)-C(133)	1.381(4)
C(133)-C(134)	1.378(4)	C(134)-C(135)	1.406(4)
C(135)-C(136)	1.459(4)	C(137)-C(139)	1.366(4)
C(137)-C(138)	1.439(4)	C(139)-C(140)	1.437(4)
C(1S)-C(2S)	1.494(5)	C(3S)-C(4S)	1.494(4)
C(5S)-C(6S)	1.500(6)	C(7S)-C(8S)	1.393(8)
C(9S)-C(10S)	1.642(9)	C(11S)-C(12S)	1.498(7)

C(13)-O(2)-C(45)	112.91(17)	C(35)-O(4)-C(58)	111.76(18)
C(47)-O(5)-C(46)	118.67(18)	C(60)-O(6)-C(59)	117.27(18)
C(105)-O(8)-C(128)	112.93(18)	C(130)-O(9)-C(129)	117.17(19)
C(87)-O(11)-C(115)	110.88(18)	C(117)-O(12)-C(116)	117.30(18)
C(2S)-O(2S)-C(3S)	115.9(3)	C(6S)-O(4S)-C(7S)	118.8(3)
C(10S)-O(6S)-C(11S)	112.7(5)	C(53)-N(1)-C(54)	121.0(2)
C(66)-N(5)-C(67)	121.0(2)	C(136)-N(9)-C(137)	121.1(2)
C(123)-N(13)-C(124)	121.3(2)	O(1)-C(1)-C(2)	115.9(2)
O(1)-C(1)-C(6)	123.7(2)	C(2)-C(1)-C(6)	120.4(2)
C(3)-C(2)-C(1)	119.0(2)	C(3)-C(2)-C(44)	120.6(2)
C(1)-C(2)-C(44)	120.1(2)	C(2)-C(3)-C(4)	122.4(2)
C(5)-C(4)-C(3)	116.6(2)	C(5)-C(4)-C(7)	122.4(2)
C(3)-C(4)-C(7)	120.9(2)	C(4)-C(5)-C(6)	123.3(2)
C(5)-C(6)-C(1)	118.2(2)	C(5)-C(6)-C(11)	120.1(2)
C(1)-C(6)-C(11)	121.8(2)	C(8A)-C(7)-C(9)	134.7(8)
C(8A)-C(7)-C(4)	112.7(8)	C(9)-C(7)-C(4)	109.8(4)
C(8A)-C(7)-C(10)	69.9(8)	C(9)-C(7)-C(10)	109.8(4)
C(4)-C(7)-C(10)	109.2(3)	C(8A)-C(7)-C(8)	35.3(8)
C(9)-C(7)-C(8)	112.4(4)	C(4)-C(7)-C(8)	112.0(3)
C(10)-C(7)-C(8)	103.4(3)	C(8A)-C(7)-C(10A)	108.7(9)
C(9)-C(7)-C(10A)	66.0(5)	C(4)-C(7)-C(10A)	113.7(5)
C(10)-C(7)-C(10A)	45.3(4)	C(8)-C(7)-C(10A)	131.3(5)
C(8A)-C(7)-C(9A)	118.1(9)	C(9)-C(7)-C(9A)	32.2(4)
C(4)-C(7)-C(9A)	105.7(4)	C(10)-C(7)-C(9A)	136.7(5)
C(8)-C(7)-C(9A)	86.1(4)	C(10A)-C(7)-C(9A)	97.2(6)
C(6)-C(11)-C(12)	113.1(2)	C(17)-C(12)-C(13)	118.2(2)
C(17)-C(12)-C(11)	120.7(2)	C(13)-C(12)-C(11)	121.2(2)
C(14)-C(13)-O(2)	119.4(2)	C(14)-C(13)-C(12)	121.5(2)
O(2)-C(13)-C(12)	118.9(2)	C(15)-C(14)-C(13)	117.9(2)
C(15)-C(14)-C(22)	120.8(2)	C(13)-C(14)-C(22)	121.2(2)
C(14)-C(15)-C(16)	122.8(2)	C(17)-C(16)-C(15)	116.8(2)
C(17)-C(16)-C(18)	121.8(2)	C(15)-C(16)-C(18)	121.3(2)
C(12)-C(17)-C(16)	122.6(2)	C(19)-C(18)-C(21)	108.4(3)
C(19)-C(18)-C(20)	109.0(3)	C(21)-C(18)-C(20)	107.8(3)
C(19)-C(18)-C(16)	108.5(2)	C(21)-C(18)-C(16)	111.6(2)
C(20)-C(18)-C(16)	111.5(2)	C(23)-C(22)-C(14)	110.5(2)
C(28)-C(23)-C(24)	118.3(2)	C(28)-C(23)-C(22)	121.9(2)
C(24)-C(23)-C(22)	119.7(2)	O(3)-C(24)-C(25)	123.1(2)
O(3)-C(24)-C(23)	116.1(2)	C(25)-C(24)-C(23)	120.8(2)
C(26)-C(25)-C(24)	118.3(2)	C(26)-C(25)-C(33)	120.9(2)
C(24)-C(25)-C(33)	120.8(2)	C(25)-C(26)-C(27)	123.1(3)
C(26)-C(27)-C(28)	116.8(2)	C(26)-C(27)-C(29)	121.7(3)
C(28)-C(27)-C(29)	121.4(3)	C(27)-C(28)-C(23)	122.6(2)
C(31)-C(29)-C(30)	111.0(4)	C(31)-C(29)-C(32)	109.0(3)
C(30)-C(29)-C(32)	106.5(5)	C(31)-C(29)-C(27)	111.6(3)
C(30)-C(29)-C(27)	111.2(3)	C(32)-C(29)-C(27)	107.3(3)
C(34)-C(33)-C(25)	111.4(2)	C(39)-C(34)-C(35)	118.0(2)
C(39)-C(34)-C(33)	120.2(2)	C(35)-C(34)-C(33)	121.6(2)
C(36)-C(35)-C(34)	121.8(2)	C(36)-C(35)-O(4)	119.2(2)
C(34)-C(35)-O(4)	118.8(2)	C(35)-C(36)-C(37)	117.8(2)
C(35)-C(36)-C(44)	122.1(2)	C(37)-C(36)-C(44)	119.9(2)
C(36)-C(37)-C(38)	122.8(2)	C(39)-C(38)-C(37)	116.8(2)
C(39)-C(38)-C(40)	121.5(2)	C(37)-C(38)-C(40)	121.4(2)

C(34)-C(39)-C(38)	122.6(2)	C(41)-C(40)-C(43)	110.0(3)
C(41)-C(40)-C(42)	108.8(3)	C(43)-C(40)-C(42)	107.2(3)
C(41)-C(40)-C(38)	107.6(3)	C(43)-C(40)-C(38)	111.6(2)
C(42)-C(40)-C(38)	111.5(2)	C(2)-C(44)-C(36)	108.40(19)
O(2)-C(45)-C(46)	107.92(19)	O(5)-C(46)-C(45)	112.3(2)
O(5)-C(47)-C(48)	124.0(2)	O(5)-C(47)-C(52)	115.9(2)
C(48)-C(47)-C(52)	120.1(2)	C(49)-C(48)-C(47)	119.9(3)
C(50)-C(49)-C(48)	120.4(3)	C(51)-C(50)-C(49)	120.2(2)
C(50)-C(51)-C(52)	120.7(2)	C(47)-C(52)-C(51)	118.7(2)
C(47)-C(52)-C(53)	121.1(2)	C(51)-C(52)-C(53)	120.2(2)
N(1)-C(53)-C(52)	121.3(2)	C(56)-C(54)-N(1)	117.6(2)
C(56)-C(54)-C(55)	122.0(3)	N(1)-C(54)-C(55)	120.4(2)
N(4)-C(55)-C(54)	172.5(3)	N(2)-C(56)-C(54)	123.1(3)
N(2)-C(56)-C(57)	117.3(3)	C(54)-C(56)-C(57)	119.6(3)
N(3)-C(57)-C(56)	179.2(4)	O(4)-C(58)-C(59)	108.8(2)
O(6)-C(59)-C(58)	108.25(19)	O(6)-C(60)-C(61)	123.6(2)
O(6)-C(60)-C(65)	116.8(2)	C(61)-C(60)-C(65)	119.6(2)
C(62)-C(61)-C(60)	120.0(3)	C(63)-C(62)-C(61)	121.0(3)
C(64)-C(63)-C(62)	118.9(3)	C(63)-C(64)-C(65)	121.8(2)
C(64)-C(65)-C(60)	118.7(2)	C(64)-C(65)-C(66)	120.8(2)
C(60)-C(65)-C(66)	120.5(2)	N(5)-C(66)-C(65)	120.5(2)
C(69)-C(67)-N(5)	117.6(2)	C(69)-C(67)-C(68)	121.2(2)
N(5)-C(67)-C(68)	121.1(2)	N(8)-C(68)-C(67)	175.6(3)
N(6)-C(69)-C(67)	124.8(2)	N(6)-C(69)-C(70)	117.0(3)
C(67)-C(69)-C(70)	118.1(3)	N(7)-C(70)-C(69)	178.6(5)
O(7)-C(71)-C(72)	116.1(2)	O(7)-C(71)-C(76)	122.8(2)
C(72)-C(71)-C(76)	121.1(2)	C(73)-C(72)-C(71)	118.6(3)
C(73)-C(72)-C(114)	122.0(3)	C(71)-C(72)-C(114)	119.1(2)
C(72)-C(73)-C(74)	122.6(3)	C(75)-C(74)-C(73)	116.8(2)
C(75)-C(74)-C(77)	120.5(3)	C(73)-C(74)-C(77)	122.5(3)
C(74)-C(75)-C(76)	123.1(3)	C(71)-C(76)-C(75)	117.7(2)
C(71)-C(76)-C(81)	121.3(2)	C(75)-C(76)-C(81)	120.9(2)
C(79)-C(77)-C(80)	108.7(3)	C(79)-C(77)-C(78)	110.8(4)
C(80)-C(77)-C(78)	106.6(3)	C(79)-C(77)-C(74)	107.7(2)
C(80)-C(77)-C(74)	111.9(3)	C(78)-C(77)-C(74)	111.2(3)
C(76)-C(81)-C(82)	113.0(2)	C(83)-C(82)-C(87)	117.9(2)
C(83)-C(82)-C(81)	120.7(2)	C(87)-C(82)-C(81)	121.4(2)
C(82)-C(83)-C(84)	122.4(2)	C(83)-C(84)-C(85)	117.2(2)
C(83)-C(84)-C(88)	122.0(2)	C(85)-C(84)-C(88)	120.8(2)
C(86)-C(85)-C(84)	122.8(2)	C(85)-C(86)-C(87)	117.6(2)
C(85)-C(86)-C(92)	120.8(2)	C(87)-C(86)-C(92)	121.5(2)
C(86)-C(87)-O(11)	119.3(2)	C(86)-C(87)-C(82)	122.0(2)
O(11)-C(87)-C(82)	118.7(2)	C(89)-C(88)-C(91)	107.4(3)
C(89)-C(88)-C(90)	108.4(3)	C(91)-C(88)-C(90)	109.2(3)
C(89)-C(88)-C(84)	111.5(2)	C(91)-C(88)-C(84)	112.5(2)
C(90)-C(88)-C(84)	107.7(2)	C(93)-C(92)-C(86)	109.88(19)
C(98)-C(93)-C(94)	118.4(2)	C(98)-C(93)-C(92)	121.4(2)
C(94)-C(93)-C(92)	120.1(2)	O(10)-C(94)-C(93)	116.5(2)
O(10)-C(94)-C(95)	122.3(2)	C(93)-C(94)-C(95)	121.1(2)
C(96)-C(95)-C(94)	118.0(2)	C(96)-C(95)-C(103)	121.6(2)
C(94)-C(95)-C(103)	120.3(2)	C(97)-C(96)-C(95)	122.7(2)
C(96)-C(97)-C(98)	117.1(2)	C(96)-C(97)-C(99)	122.2(2)
C(98)-C(97)-C(99)	120.7(2)	C(93)-C(98)-C(97)	122.6(2)
C(100)-C(99)-C(200)	55.6(6)	C(100)-C(99)-C(201)	129.9(6)
C(200)-C(99)-C(201)	108.6(8)	C(100)-C(99)-C(102)	108.9(4)
C(200)-C(99)-C(102)	136.7(6)	C(201)-C(99)-C(102)	46.2(5)
C(100)-C(99)-C(101)	107.6(4)	C(200)-C(99)-C(101)	54.5(6)
C(201)-C(99)-C(101)	62.8(6)	C(102)-C(99)-C(101)	108.2(4)
C(100)-C(99)-C(97)	113.5(3)	C(200)-C(99)-C(97)	112.5(6)
C(201)-C(99)-C(97)	116.2(6)	C(102)-C(99)-C(97)	110.6(3)
C(101)-C(99)-C(97)	107.8(3)	C(100)-C(99)-C(202)	49.3(6)

C(200)-C(99)-C(202)	103.9(9)	C(201)-C(99)-C(202)	108.6(8)
C(102)-C(99)-C(202)	66.7(7)	C(101)-C(99)-C(202)	144.9(7)
C(97)-C(99)-C(202)	106.2(6)	C(95)-C(103)-C(104)	111.1(2)
C(109)-C(104)-C(105)	118.3(2)	C(109)-C(104)-C(103)	119.2(2)
C(105)-C(104)-C(103)	122.1(2)	C(106)-C(105)-C(104)	121.6(2)
C(106)-C(105)-O(8)	119.4(2)	C(104)-C(105)-O(8)	118.8(2)
C(105)-C(106)-C(107)	118.6(2)	C(105)-C(106)-C(114)	122.3(2)
C(107)-C(106)-C(114)	118.9(2)	C(106)-C(107)-C(108)	121.8(2)
C(109)-C(108)-C(107)	117.8(2)	C(109)-C(108)-C(110)	121.3(2)
C(107)-C(108)-C(110)	120.5(2)	C(104)-C(109)-C(108)	121.8(2)
C(113)-C(110)-C(112)	109.6(4)	C(113)-C(110)-C(108)	113.4(3)
C(112)-C(110)-C(108)	112.5(3)	C(113)-C(110)-C(111)	108.4(5)
C(112)-C(110)-C(111)	106.1(4)	C(108)-C(110)-C(111)	106.5(3)
C(72)-C(114)-C(106)	109.4(2)	O(11)-C(115)-C(116)	108.9(2)
O(12)-C(116)-C(115)	107.1(2)	O(12)-C(117)-C(118)	123.8(2)
O(12)-C(117)-C(122)	115.8(2)	C(118)-C(117)-C(122)	120.4(2)
C(119)-C(118)-C(117)	119.7(2)	C(118)-C(119)-C(120)	120.7(2)
C(121)-C(120)-C(119)	119.5(2)	C(120)-C(121)-C(122)	121.3(2)
C(121)-C(122)-C(117)	118.4(2)	C(121)-C(122)-C(123)	121.0(2)
C(117)-C(122)-C(123)	120.5(2)	N(13)-C(123)-C(122)	120.4(2)
C(126)-C(124)-N(13)	116.7(2)	C(126)-C(124)-C(125)	121.7(2)
N(13)-C(124)-C(125)	121.5(2)	N(16)-C(125)-C(124)	174.8(3)
N(14)-C(126)-C(124)	123.9(2)	N(14)-C(126)-C(127)	117.3(2)
C(124)-C(126)-C(127)	118.8(2)	N(15)-C(127)-C(126)	179.3(3)
O(8)-C(128)-C(129)	108.1(2)	O(9)-C(129)-C(128)	112.3(2)
O(9)-C(130)-C(131)	123.1(2)	O(9)-C(130)-C(135)	116.2(2)
C(131)-C(130)-C(135)	120.6(2)	C(132)-C(131)-C(130)	119.4(2)
C(133)-C(132)-C(131)	120.7(3)	C(134)-C(133)-C(132)	120.1(3)
C(133)-C(134)-C(135)	120.6(2)	C(130)-C(135)-C(134)	118.5(2)
C(130)-C(135)-C(136)	120.6(2)	C(134)-C(135)-C(136)	120.9(2)
N(9)-C(136)-C(135)	120.4(2)	C(139)-C(137)-N(9)	117.6(2)
C(139)-C(137)-C(138)	120.3(2)	N(9)-C(137)-C(138)	122.0(2)
N(12)-C(138)-C(137)	176.4(3)	N(10)-C(139)-C(137)	124.6(3)
N(10)-C(139)-C(140)	116.1(2)	C(137)-C(139)-C(140)	119.3(2)
N(11)-C(140)-C(139)	177.5(3)	O(1S)-C(2S)-O(2S)	122.9(3)
O(1S)-C(2S)-C(1S)	124.9(3)	O(2S)-C(2S)-C(1S)	112.1(3)
O(2S)-C(3S)-C(4S)	106.7(3)	O(3S)-C(6S)-O(4S)	121.4(5)
O(3S)-C(6S)-C(5S)	125.3(4)	O(4S)-C(6S)-C(5S)	113.0(4)
C(8S)-C(7S)-O(4S)	93.6(7)	O(5S)-C(10S)-O(6S)	126.1(7)
O(5S)-C(10S)-C(9S)	124.9(5)	O(6S)-C(10S)-C(9S)	108.7(5)
C(12S)-C(11S)-O(6S)	109.1(4)		

Table 0.23: Anisotropic displacement parameters ($\text{Å}^2 * 10^3$) for **37**. The anisotropic displacement factor exponent takes the form: $-2 g\pi^2 [h^2 a^{*2} U11 + ... + 2 h k a^* b^* U12]$.

Atom	U11	U22	U33	U23	U13	U12
O(1)	26(1)	37(1)	37(1)	14(1)	7(1)	12(1)
O(2)	30(1)	29(1)	34(1)	9(1)	8(1)	4(1)
O(3)	33(1)	35(1)	45(1)	14(1)	18(1)	16(1)
O(4)	32(1)	31(1)	34(1)	13(1)	10(1)	12(1)
O(5)	25(1)	38(1)	45(1)	17(1)	12(1)	12(1)
O(6)	39(1)	43(1)	35(1)	10(1)	11(1)	27(1)
O(7)	25(1)	43(1)	44(1)	1(1)	5(1)	8(1)
O(8)	37(1)	29(1)	39(1)	7(1)	8(1)	13(1)
O(9)	33(1)	40(1)	46(1)	16(1)	17(1)	14(1)
O(10)	31(1)	39(1)	40(1)	14(1)	15(1)	17(1)
O(11)	31(1)	33(1)	29(1)	10(1)	4(1)	10(1)
O(12)	25(1)	35(1)	32(1)	5(1)	4(1)	4(1)
O(1S)	42(1)	65(2)	73(2)	12(1)	21(1)	13(1)

O(2S)	42(1)	49(1)	68(1)	18(1)	11(1)	11(1)
O(3S)	216(5)	177(4)	71(2)	10(2)	29(3)	130(4)
O(4S)	84(2)	96(2)	79(2)	13(2)	29(2)	42(2)
O(5S)	118(4)	79(3)	91(3)	18(2)	43(3)	69(3)
O(6S)	111(3)	88(3)	69(3)	33(2)	43(2)	79(3)
N(1)	35(1)	47(1)	44(1)	19(1)	15(1)	22(1)
N(2)	65(2)	66(2)	112(3)	39(2)	56(2)	42(2)
N(3)	74(2)	58(2)	110(3)	35(2)	49(2)	37(2)
N(4)	40(1)	51(1)	48(1)	22(1)	17(1)	22(1)
N(5)	35(1)	44(1)	42(1)	17(1)	17(1)	21(1)
N(6)	47(1)	53(2)	50(1)	18(1)	21(1)	34(1)
N(7)	83(2)	212(5)	65(2)	32(2)	23(2)	110(3)
N(8)	47(2)	72(2)	59(2)	9(2)	16(1)	16(1)
N(9)	35(1)	39(1)	43(1)	8(1)	17(1)	10(1)
N(10)	34(1)	41(1)	84(2)	7(1)	13(1)	10(1)
N(11)	52(2)	44(2)	65(2)	18(1)	7(1)	6(1)
N(12)	37(1)	44(1)	56(2)	15(1)	16(1)	9(1)
N(13)	27(1)	33(1)	37(1)	11(1)	7(1)	12(1)
N(14)	27(1)	41(1)	42(1)	4(1)	8(1)	5(1)
N(15)	42(1)	54(2)	64(2)	11(1)	26(1)	20(1)
N(16)	44(1)	52(2)	53(2)	−4(1)	9(1)	18(1)
C(1)	28(1)	30(1)	30(1)	6(1)	7(1)	15(1)
C(2)	31(1)	31(1)	34(1)	7(1)	11(1)	16(1)
C(3)	29(1)	32(1)	41(1)	5(1)	7(1)	12(1)
C(4)	34(1)	32(1)	40(1)	3(1)	2(1)	17(1)
C(5)	39(1)	31(1)	33(1)	8(1)	7(1)	18(1)
C(6)	32(1)	27(1)	34(1)	5(1)	9(1)	15(1)
C(7)	33(1)	48(2)	51(2)	13(1)	−2(1)	16(1)
C(11)	35(1)	30(1)	39(1)	11(1)	10(1)	15(1)
C(12)	30(1)	26(1)	39(1)	12(1)	9(1)	10(1)
C(13)	28(1)	26(1)	33(1)	10(1)	8(1)	6(1)
C(14)	25(1)	31(1)	40(1)	15(1)	9(1)	9(1)
C(15)	29(1)	32(1)	40(1)	13(1)	12(1)	12(1)
C(16)	32(1)	28(1)	35(1)	12(1)	9(1)	8(1)
C(17)	31(1)	33(1)	38(1)	15(1)	6(1)	13(1)
C(18)	39(1)	40(1)	34(1)	10(1)	9(1)	14(1)
C(19)	100(3)	72(3)	43(2)	21(2)	17(2)	−5(2)
C(20)	164(5)	119(4)	41(2)	9(2)	22(2)	107(4)
C(21)	47(2)	118(3)	40(2)	−2(2)	2(1)	13(2)
C(22)	26(1)	43(2)	42(1)	18(1)	9(1)	12(1)
C(23)	30(1)	47(2)	38(1)	20(1)	11(1)	20(1)
C(24)	29(1)	42(1)	34(1)	15(1)	11(1)	20(1)
C(25)	36(1)	41(1)	37(1)	17(1)	13(1)	23(1)
C(26)	45(2)	47(2)	41(1)	17(1)	17(1)	28(1)
C(27)	50(2)	61(2)	47(2)	26(1)	26(1)	36(1)
C(28)	38(1)	60(2)	46(2)	29(1)	22(1)	29(1)
C(29)	78(2)	72(2)	66(2)	32(2)	48(2)	51(2)
C(30)	247(7)	130(5)	208(6)	105(5)	190(6)	150(5)
C(31)	69(3)	135(4)	104(3)	9(3)	46(2)	58(3)
C(32)	106(4)	133(4)	69(3)	1(3)	43(3)	55(3)
C(33)	38(1)	36(1)	42(1)	16(1)	16(1)	21(1)
C(34)	34(1)	28(1)	39(1)	16(1)	15(1)	14(1)
C(35)	32(1)	27(1)	33(1)	13(1)	11(1)	10(1)
C(36)	31(1)	27(1)	36(1)	12(1)	12(1)	11(1)
C(37)	31(1)	36(1)	38(1)	13(1)	9(1)	14(1)
C(38)	40(1)	31(1)	36(1)	13(1)	12(1)	13(1)
C(39)	44(1)	33(1)	38(1)	14(1)	20(1)	19(1)
C(40)	57(2)	48(2)	34(1)	11(1)	10(1)	23(1)
C(41)	126(4)	85(3)	46(2)	32(2)	22(2)	22(3)
C(42)	80(2)	71(2)	40(2)	1(2)	10(2)	37(2)
C(43)	68(2)	106(3)	47(2)	−8(2)	−4(2)	45(2)

C(44)	29(1)	34(1)	38(1)	11(1)	13(1)	15(1)
C(45)	29(1)	27(1)	39(1)	9(1)	8(1)	5(1)
C(46)	27(1)	34(1)	38(1)	10(1)	11(1)	13(1)
C(47)	26(1)	41(1)	29(1)	8(1)	7(1)	11(1)
C(48)	33(1)	38(2)	48(2)	7(1)	11(1)	11(1)
C(49)	36(1)	41(2)	52(2)	10(1)	10(1)	3(1)
C(50)	26(1)	55(2)	46(2)	13(1)	10(1)	10(1)
C(51)	29(1)	51(2)	40(1)	14(1)	11(1)	17(1)
C(52)	28(1)	41(1)	31(1)	10(1)	8(1)	12(1)
C(53)	30(1)	45(2)	37(1)	16(1)	13(1)	18(1)
C(54)	38(1)	45(2)	43(1)	20(1)	17(1)	24(1)
C(55)	39(1)	39(1)	39(1)	18(1)	11(1)	21(1)
C(56)	47(2)	53(2)	57(2)	25(1)	23(1)	30(1)
C(57)	54(2)	56(2)	68(2)	28(2)	30(2)	36(2)
C(58)	40(1)	35(1)	39(1)	18(1)	17(1)	18(1)
C(59)	45(1)	39(1)	37(1)	15(1)	17(1)	27(1)
C(60)	36(1)	44(2)	32(1)	13(1)	14(1)	20(1)
C(61)	59(2)	67(2)	37(2)	15(1)	13(1)	46(2)
C(62)	55(2)	79(2)	36(2)	11(2)	6(1)	44(2)
C(63)	51(2)	68(2)	34(1)	5(1)	10(1)	32(2)
C(64)	43(2)	47(2)	38(1)	11(1)	18(1)	25(1)
C(65)	36(1)	42(1)	34(1)	16(1)	16(1)	22(1)
C(66)	33(1)	40(1)	41(1)	15(1)	16(1)	18(1)
C(67)	33(1)	50(2)	39(1)	19(1)	17(1)	22(1)
C(68)	35(1)	61(2)	47(2)	20(2)	18(1)	22(1)
C(69)	38(1)	62(2)	45(2)	26(1)	23(1)	31(1)
C(70)	57(2)	106(3)	52(2)	22(2)	24(2)	58(2)
C(71)	22(1)	49(2)	33(1)	2(1)	10(1)	9(1)
C(72)	29(1)	47(2)	38(1)	0(1)	13(1)	13(1)
C(73)	32(1)	58(2)	39(1)	9(1)	13(1)	19(1)
C(74)	29(1)	58(2)	33(1)	9(1)	9(1)	12(1)
C(75)	28(1)	49(2)	34(1)	9(1)	8(1)	7(1)
C(76)	26(1)	48(2)	31(1)	9(1)	10(1)	9(1)
C(77)	27(1)	64(2)	43(2)	10(1)	3(1)	8(1)
C(78)	31(2)	94(3)	104(3)	43(3)	−6(2)	−1(2)
C(79)	43(2)	175(5)	45(2)	−5(2)	−2(2)	20(2)
C(80)	33(2)	91(3)	91(3)	7(2)	−5(2)	21(2)
C(81)	28(1)	47(2)	35(1)	13(1)	7(1)	5(1)
C(82)	27(1)	35(1)	33(1)	12(1)	5(1)	7(1)
C(83)	25(1)	34(1)	36(1)	10(1)	2(1)	4(1)
C(84)	32(1)	30(1)	35(1)	9(1)	5(1)	10(1)
C(85)	31(1)	31(1)	37(1)	10(1)	9(1)	12(1)
C(86)	26(1)	26(1)	39(1)	11(1)	4(1)	8(1)
C(87)	29(1)	27(1)	29(1)	8(1)	3(1)	9(1)
C(88)	42(1)	39(2)	33(1)	8(1)	6(1)	12(1)
C(89)	73(2)	77(2)	43(2)	10(2)	22(2)	16(2)
C(90)	111(3)	52(2)	57(2)	2(2)	11(2)	39(2)
C(91)	59(2)	99(3)	35(2)	−4(2)	−2(1)	25(2)
C(92)	26(1)	30(1)	39(1)	9(1)	5(1)	10(1)
C(93)	22(1)	30(1)	33(1)	5(1)	3(1)	8(1)
C(94)	22(1)	32(1)	29(1)	4(1)	5(1)	7(1)
C(95)	25(1)	29(1)	32(1)	5(1)	5(1)	9(1)
C(96)	31(1)	35(1)	34(1)	10(1)	10(1)	10(1)
C(97)	34(1)	35(1)	34(1)	3(1)	13(1)	9(1)
C(98)	29(1)	29(1)	41(1)	2(1)	8(1)	11(1)
C(99)	49(2)	50(2)	50(2)	7(1)	27(1)	19(1)
C(103)	34(1)	29(1)	42(1)	8(1)	13(1)	11(1)
C(104)	34(1)	27(1)	43(1)	9(1)	11(1)	15(1)
C(105)	33(1)	27(1)	40(1)	6(1)	9(1)	16(1)
C(106)	33(1)	32(1)	46(2)	3(1)	11(1)	17(1)
C(107)	38(1)	40(2)	45(2)	3(1)	11(1)	19(1)

C(108)	39(1)	37(1)	40(1)	1(1)	8(1)	18(1)
C(109)	41(1)	35(1)	44(2)	9(1)	13(1)	19(1)
C(110)	50(2)	59(2)	41(2)	−4(1)	8(1)	16(2)
C(111)	220(7)	78(3)	83(3)	−25(3)	5(4)	65(4)
C(112)	110(4)	142(5)	44(2)	−11(3)	24(2)	−23(3)
C(113)	74(3)	223(7)	48(2)	−6(3)	1(2)	54(4)
C(114)	34(1)	49(2)	49(2)	−2(1)	14(1)	20(1)
C(115)	33(1)	30(1)	35(1)	12(1)	1(1)	5(1)
C(116)	27(1)	32(1)	35(1)	11(1)	3(1)	2(1)
C(117)	29(1)	28(1)	28(1)	7(1)	2(1)	10(1)
C(118)	28(1)	34(1)	35(1)	11(1)	6(1)	8(1)
C(119)	37(1)	40(1)	33(1)	12(1)	11(1)	14(1)
C(120)	38(1)	36(1)	32(1)	5(1)	3(1)	13(1)
C(121)	28(1)	31(1)	35(1)	7(1)	4(1)	8(1)
C(122)	27(1)	27(1)	34(1)	10(1)	5(1)	10(1)
C(123)	28(1)	26(1)	34(1)	7(1)	4(1)	11(1)
C(124)	27(1)	31(1)	36(1)	8(1)	7(1)	12(1)
C(125)	29(1)	40(2)	48(2)	11(1)	13(1)	17(1)
C(126)	28(1)	35(1)	39(1)	10(1)	8(1)	15(1)
C(127)	29(1)	35(1)	50(2)	6(1)	9(1)	12(1)
C(128)	35(1)	29(1)	41(1)	7(1)	13(1)	12(1)
C(129)	28(1)	36(1)	39(1)	8(1)	13(1)	10(1)
C(130)	32(1)	37(1)	33(1)	9(1)	11(1)	13(1)
C(131)	38(1)	36(1)	49(2)	10(1)	18(1)	11(1)
C(132)	49(2)	37(2)	54(2)	8(1)	17(1)	18(1)
C(133)	42(2)	45(2)	47(2)	6(1)	15(1)	21(1)
C(134)	34(1)	45(2)	40(1)	5(1)	13(1)	13(1)
C(135)	35(1)	38(1)	31(1)	7(1)	12(1)	12(1)
C(136)	32(1)	38(1)	38(1)	11(1)	14(1)	10(1)
C(137)	34(1)	38(1)	40(1)	8(1)	15(1)	9(1)
C(138)	37(1)	36(1)	40(1)	11(1)	17(1)	5(1)
C(139)	36(1)	39(2)	47(2)	9(1)	17(1)	10(1)
C(140)	32(1)	44(2)	47(2)	13(1)	11(1)	9(1)
C(1S)	61(2)	96(3)	74(3)	35(2)	7(2)	18(2)
C(2S)	39(2)	52(2)	65(2)	13(2)	12(1)	15(1)
C(3S)	50(2)	54(2)	59(2)	6(2)	8(2)	20(2)
C(4S)	51(2)	57(2)	81(2)	−1(2)	4(2)	21(2)
C(5S)	56(2)	85(3)	80(3)	13(2)	21(2)	−7(2)
C(6S)	114(4)	74(3)	67(3)	25(2)	49(3)	40(3)
C(7S)	318(11)	119(5)	113(4)	69(4)	122(6)	144(7)
C(8S)	104(5)	216(9)	119(5)	−4(6)	40(4)	6(5)
C(9S)	85(4)	96(4)	59(3)	34(3)	38(3)	75(4)
C(10S)	87(4)	93(5)	66(4)	19(3)	22(3)	55(4)
C(11S)	67(3)	46(3)	89(4)	32(3)	31(3)	25(3)
C(12S)	70(3)	65(3)	61(3)	26(3)	22(3)	32(3)

Table 0.24: Hydrogen coordinates ($*10^4$) and isotropic displacement parameters ($\text{Å}^2 * 10^3$) for **37**.

Atom	x	y	z	U(eq)
H(1)	569	9409	−2030	40
H(3)	1178	8231	−1874	43
H(7)	3600	6625	1870	50
H(10)	2255	5489	2039	41
H(2A)	5029	8636	−1364	83
H(2B)	4922	7870	−1564	83
H(6A)	−1001	10683	824	54
H(6B)	−1680	10971	653	54
H(10D)	6689	5683	1374	68

H(10E)	7332	6438	1628	68
H(14A)	−2135	4460	−852	49
H(14B)	−2943	4152	−692	49
H(31)	−2576	8175	−2865	43
H(5)	−1354	9753	−3523	41
H(8C)	−2519	9160	−4471	82
H(8B)	−2579	9819	−4019	82
H(8A)	−3411	9205	−4537	82
H(9A)	−3044	9655	−3002	129
H(9B)	−3500	8870	−2972	129
H(9C)	−3928	9149	−3542	129
H(10A)	−4028	8117	−4384	97
H(10B)	−3604	7854	−3799	97
H(10C)	−3196	7978	−4370	97
H(11A)	549	10382	−2353	41
H(11B)	77	10417	−3064	41
H(15)	2006	8948	−3842	40
H(17)	101	9603	−4067	41
H(19A)	1903	9808	−4810	123
H(19B)	1113	10027	−4926	123
H(19C)	1195	9508	−5517	123
H(20A)	871	8241	−5531	147
H(20B)	856	8045	−4854	147
H(20C)	1699	8591	−4900	147
H(21A)	−274	9176	−5084	119
H(21B)	−416	8390	−5055	119
H(21C)	−204	8641	−5669	119
H(22A)	3165	9515	−2632	44
H(22B)	2735	9520	−2064	44
H(26)	1785	6580	−2980	48
H(28)	3196	8425	−3172	50
H(30A)	3127	6140	−3729	215
H(30B)	2269	6047	−3577	215
H(30C)	3144	6433	−2992	215
H(31A)	4168	7611	−3058	146
H(31B)	3832	7948	−3614	146
H(31C)	4014	7257	−3816	146
H(32A)	2569	6619	−4594	152
H(32B)	2419	7330	−4411	152
H(32C)	1792	6615	−4346	152
H(33A)	828	6473	−2394	43
H(33B)	1067	7144	−1791	43
H(37)	−1889	7250	−3371	42
H(39)	−116	6499	−3517	42
H(41A)	−1278	6919	−5101	135
H(41B)	−447	7182	−4481	135
H(41C)	−1123	7525	−4467	135
H(42A)	−1728	5671	−5072	98
H(42B)	−1663	5502	−4376	98
H(42C)	−832	5930	−4524	98
H(43A)	−2498	6844	−4399	119
H(43B)	−2705	6078	−4291	119
H(43C)	−2683	6188	−4997	119
H(44A)	−1852	7726	−2097	39
H(44B)	−899	8208	−1654	39
H(45A)	1999	11032	−1926	41
H(45B)	2768	10793	−1915	41
H(46A)	2827	11418	−843	39
H(46B)	2021	10757	−892	39
H(48)	4079	11864	−650	50
H(49)	5499	12251	−555	57

H(50)	6160	11463	−579	53
H(51)	5411	10287	−710	47
H(53)	3281	9475	−790	43
H(58A)	27	6816	−1270	42
H(58B)	−715	7077	−1233	42
H(59A)	288	7274	−165	43
H(59B)	958	7859	−362	43
H(61)	1319	8225	714	58
H(62)	2007	9100	1712	65
H(63)	1522	9983	1985	61
H(64)	349	9987	1249	48
H(66)	−904	8772	−339	43
H(73)	6228	6323	2986	52
H(75)	6168	8223	3006	48
H(78A)	7686	8153	2804	130
H(78B)	8350	8511	3531	130
H(78C)	7528	8681	3337	130
H(79A)	7014	8272	4227	153
H(79B)	7884	8189	4492	153
H(79C)	7017	7542	4346	153
H(80A)	7484	6817	3653	120
H(80B)	8330	7461	3741	120
H(80C)	7696	7013	3018	120
H(81A)	4299	7722	1836	47
H(81B)	4970	8370	2444	47
H(83)	4693	8428	3565	42
H(85)	2273	7683	3486	40
H(89A)	2663	8070	4549	102
H(89B)	3465	8405	5200	102
H(89C)	3301	7687	4687	102
H(90A)	3910	9500	4124	114
H(90B)	3718	9498	4806	114
H(90C)	2978	9082	4121	114
H(91A)	4816	8358	4725	108
H(91B)	4804	9028	5198	108
H(91C)	5033	9086	4536	108
H(92A)	1156	7150	2262	40
H(92B)	1452	6699	1769	40
H(96)	794	4879	3393	41
H(98)	561	6623	3013	42
H(10X)	−386	5239	4370	98
H(10Z)	560	5360	4412	98
H(10Y)	−200	4746	3827	98
H(10G)	−1064	5015	2930	105
H(10H)	−922	5814	2959	105
H(10I)	−1284	5468	3481	105
H(10J)	188	6777	3865	97
H(10K)	813	6628	4431	97
H(10L)	−143	6435	4400	97
H(10M)	1559	4426	2168	42
H(10N)	1486	4287	2857	42
H(11C)	4532	7015	4459	211
H(11D)	4401	6990	5158	211
H(11E)	3612	6636	4498	211
H(11F)	3318	5641	4943	186
H(11G)	4196	5931	5520	186
H(11H)	3887	5190	4987	186
H(11I)	5345	5759	4790	189
H(11J)	5461	6417	5356	189
H(11K)	5548	6516	4660	189
H(11L)	5006	5259	2437	54

H(11M)	4255	5297	1886	54
H(11N)	3207	8044	1382	44
H(11O)	2236	7759	1331	44
H(11P)	2511	7603	274	42
H(11Q)	2820	7005	464	42
H(118)	2294	6635	−608	41
H(119)	1675	5805	−1638	44
H(120)	292	4994	−1945	45
H(121)	−478	5026	−1226	41
H(123)	235	6149	423	37
H(12A)	2243	3705	1859	42
H(12B)	3139	3870	1749	42
H(12C)	1917	3192	763	42
H(12D)	1758	3902	788	42
H(131)	2605	2617	518	50
H(132)	3620	2148	498	56
H(133)	4944	2847	510	54
H(134)	5290	4033	587	50
H(136)	3944	4974	572	44
H(20D)	−1036	5021	3815	136
H(20E)	−438	4665	3598	136
H(20F)	−1038	4871	3067	136
H(20G)	−754	6184	3240	130
H(20H)	46	6737	3838	130
H(20I)	−734	6219	3986	130
H(20J)	231	5903	4733	170
H(20K)	1063	6278	4560	170
H(20L)	707	5447	4463	170
H(8D)	−3553	8829	−4616	182
H(8E)	−2965	8395	−4549	182
H(8F)	−2558	9231	−4406	182
H(9D)	−2669	10014	−3287	78
H(9E)	−3097	9543	−2865	78
H(9F)	−3657	9559	−3553	78
H(10F)	−4240	8306	−3948	102
H(10G)	−3743	8414	−3195	102
H(10H)	−3674	7869	−3772	102
H(1S1)	8021	7227	780	122
H(1S2)	8970	7494	779	122
H(1S3)	8572	8051	970	122
H(3S1)	9966	7552	2704	69
H(3S2)	9738	8208	2961	69
H(4S1)	11198	8527	3358	103
H(4S2)	10986	8980	2873	103
H(4S3)	11212	8327	2617	103
H(5S1)	3926	10720	−3819	127
H(5S2)	3299	10232	−3518	127
H(5S3)	3353	9919	−4225	127
H(7S1)	5936	10291	−2668	183
H(7S2)	5821	10614	−1977	183
H(8S1)	5599	9440	−2119	252
H(8S2)	4878	9251	−2802	252
H(8S3)	4764	9570	−2122	252
H(9S1)	6336	4229	2089	97
H(9S2)	6257	4716	2705	97
H(9S3)	5681	4599	1973	97
H(11R)	3744	3002	2374	77
H(11S)	4440	3026	3012	77
H(12E)	3341	3224	3317	93
H(12F)	3494	3885	3021	93
H(12G)	4189	3910	3657	93

- **Crystallographic data recorded for 46**

Table 0.25: Atomic coordinates (*10^4) and equivalent isotropic displacement parameters (Å^2 * 10^3) for **46**. U(eq) is defined as one third of the trace of the orthogonalised Uij tensor.

Atom	x	y	z	U(eq)
O(1)	414(1)	8847(1)	1430(1)	20(1)
C(1)	557(1)	7531(1)	1622(1)	17(1)
C(2)	−97(1)	6539(1)	988(1)	21(1)
C(3)	38(1)	5141(1)	1155(1)	21(1)
C(4)	853(1)	4668(1)	1952(1)	19(1)
N(1)	999(1)	3204(1)	2143(1)	23(1)
O(2)	427(1)	2385(1)	1543(1)	34(1)
O(3)	1691(1)	2812(1)	2901(1)	30(1)
C(5)	1502(1)	5593(1)	2600(1)	18(1)
C(6)	1361(1)	7010(1)	2471(1)	17(1)
C(7)	2024(1)	7900(1)	3313(1)	17(1)
O(4)	2750(1)	7420(1)	3982(1)	23(1)
N(2)	1776(1)	9227(1)	3355(1)	19(1)
C(8)	2303(1)	10131(1)	4227(1)	19(1)
C(9)	1681(1)	10854(1)	4691(1)	19(1)
N(3)	1183(1)	9842(1)	5107(1)	18(1)

Table 0.26: Bond lengths (Å) and angles (°) for **46**.

O(1)-C(1)	1.3003(16)	N(1)-O(2)	1.2393(16)
C(1)-C(2)	1.4259(19)	C(5)-C(6)	1.3869(18)
C(1)-C(6)	1.4365(17)	C(6)-C(7)	1.4919(18)
C(2)-C(3)	1.3720(19)	C(7)-O(4)	1.2422(15)
C(3)-C(4)	1.3976(19)	C(7)-N(2)	1.3467(17)
C(4)-C(5)	1.3858(19)	N(2)-C(8)	1.4537(17)
C(4)-N(1)	1.4403(17)	C(8)-C(9)	1.5195(19)
N(1)-O(3)	1.2361(16)	C(9)-N(3)	1.4906(17)
O(1)-C(1)-C(2)	120.49(12)	C(4)-C(5)-C(6)	120.93(12)
O(1)-C(1)-C(6)	122.34(12)	C(5)-C(6)-C(1)	119.68(12)
C(2)-C(1)-C(6)	117.16(12)	C(5)-C(6)-C(7)	116.25(11)
C(3)-C(2)-C(1)	122.11(12)	C(1)-C(6)-C(7)	123.77(12)
C(2)-C(3)-C(4)	119.20(13)	O(4)-C(7)-N(2)	121.25(12)
C(5)-C(4)-C(3)	120.76(12)	O(4)-C(7)-C(6)	121.42(12)
C(5)-C(4)-N(1)	119.39(12)	N(2)-C(7)-C(6)	117.21(11)
C(3)-C(4)-N(1)	119.77(12)	C(7)-N(2)-C(8)	121.73(11)
O(3)-N(1)-O(2)	122.41(13)	N(2)-C(8)-C(9)	111.75(11)
O(3)-N(1)-C(4)	118.70(12)	N(3)-C(9)-C(8)	111.63(11)
O(2)-N(1)-C(4)	118.88(12)		

Table 0.27: Anisotropic displacement parameters (Å^2 * 10^3) for **46**. The anisotropic displacement factor exponent takes the form: $-2 g\pi^2$ [h^2 a*^{2} U11 + ... + 2 h k a* b* U12].

Atom	U11	U22	U33	U23	U13	U12
O(1)	21(1)	16(1)	18(1)	2(1)	4(1)	3(1)
C(1)	18(1)	18(1)	16(1)	2(1)	7(1)	3(1)
C(2)	19(1)	21(1)	19(1)	0(1)	4(1)	2(1)
C(3)	18(1)	22(1)	21(1)	−1(1)	7(1)	−1(1)
C(4)	21(1)	16(1)	20(1)	2(1)	9(1)	1(1)

N(1)	26(1)	20(1)	26(1)	3(1)	12(1)	0(1)
O(2)	31(1)	20(1)	47(1)	−2(1)	10(1)	−7(1)
O(3)	37(1)	22(1)	28(1)	8(1)	9(1)	6(1)
C(5)	18(1)	20(1)	17(1)	2(1)	6(1)	2(1)
C(6)	16(1)	18(1)	16(1)	1(1)	6(1)	1(1)
C(7)	17(1)	19(1)	15(1)	2(1)	6(1)	1(1)
O(4)	19(1)	21(1)	22(1)	1(1)	1(1)	4(1)
N(2)	18(1)	18(1)	17(1)	0(1)	2(1)	4(1)
C(8)	18(1)	19(1)	18(1)	0(1)	3(1)	1(1)
C(9)	20(1)	15(1)	20(1)	1(1)	6(1)	1(1)
N(3)	17(1)	17(1)	18(1)	0(1)	4(1)	1(1)

Table 0.28: Hydrogen coordinates ($*10^4$) and isotropic displacement parameters ($\text{Å}^2 * 10^3$) for **46**.

Atom	x	y	z	U(eq)
H(2)	−643	6856	432	25
H(3)	−416	4503	733	25
H(5)	2050	5251	3138	22
H(2N)	1295(14)	9500(20)	2842(16)	29
H(8A)	2632	10834	3975	23
H(8B)	2776	9578	4784	23
H(9A)	2062	11473	5270	23
H(9B)	1221	11430	4140	23
H(3A)	818	10306	5379	27
H(3B)	1605	9321	5623	27
H(3C)	824	9281	4574	27

- **Crystallographic data recorded for 47**

Table 0.29: Atomic coordinates ($*10^4$) and equivalent isotropic displacement parameters ($\text{Å}^2 * 10^3$) for **47**. U(eq) is defined as one third of the trace of the orthogonalised Uij tensor.

Atom	x	y	z	U(eq)
O(1)	4025(2)	9103(2)	1392(1)	30(1)
C(1)	2189(3)	8406(2)	705(1)	21(1)
C(2)	2131(3)	8541(2)	−451(2)	24(1)
C(3)	328(3)	7855(2)	−1216(1)	22(1)
C(4)	−1439(3)	7006(2)	−817(1)	18(1)
N(1)	−3294(2)	6186(2)	−1643(1)	22(1)
O(2)	−3354(2)	6363(2)	−2640(1)	30(1)
O(3)	−4733(2)	5313(2)	−1305(1)	35(1)
C(5)	−1442(3)	6856(2)	319(1)	19(1)
C(6)	379(3)	7560(2)	1110(1)	18(1)
C(7)	550(3)	7396(2)	2342(1)	19(1)
O(4)	2210(2)	8058(2)	3011(1)	27(1)
N(2)	−1084(2)	6471(2)	2677(1)	20(1)
C(8)	−966(3)	5982(2)	3776(1)	21(1)
C(9)	−2941(3)	6623(2)	4557(1)	21(1)
N(3)	−2633(2)	8455(2)	5188(1)	22(1)
Cl(1)	2493(1)	8898(1)	6321(1)	23(1)

Table 0.30: Bond lengths (Å) and angles (°) for **47**.

O(1)-C(1)	1.3392(19)	N(1)-O(3)	1.2332(18)
C(1)-C(2)	1.399(2)	C(5)-C(6)	1.395(2)
C(1)-C(6)	1.414(2)	C(6)-C(7)	1.497(2)
C(2)-C(3)	1.368(2)	C(7)-O(4)	1.2440(19)
C(3)-C(4)	1.393(2)	C(7)-N(2)	1.338(2)
C(4)-C(5)	1.381(2)	N(2)-C(8)	1.457(2)
C(4)-N(1)	1.454(2)	C(8)-C(9)	1.518(2)
N(1)-O(2)	1.2246(18)	C(9)-N(3)	1.486(2)
O(1)-C(1)-C(2)	116.85(14)	C(4)-C(5)-C(6)	119.80(14)
O(1)-C(1)-C(6)	122.46(14)	C(5)-C(6)-C(1)	118.00(14)
C(2)-C(1)-C(6)	120.70(15)	C(5)-C(6)-C(7)	123.12(14)
C(3)-C(2)-C(1)	120.75(15)	C(1)-C(6)-C(7)	118.83(14)
C(2)-C(3)-C(4)	118.37(15)	O(4)-C(7)-N(2)	121.66(15)
C(5)-C(4)-C(3)	122.38(15)	O(4)-C(7)-C(6)	120.40(14)
C(5)-C(4)-N(1)	118.83(13)	N(2)-C(7)-C(6)	117.89(14)
C(3)-C(4)-N(1)	118.73(14)	C(7)-N(2)-C(8)	124.03(14)
O(2)-N(1)-O(3)	122.73(14)	N(2)-C(8)-C(9)	113.19(14)
O(2)-N(1)-C(4)	119.35(13)	N(3)-C(9)-C(8)	112.35(13)
O(3)-N(1)-C(4)	117.90(13)		

Table 0.31: Anisotropic displacement parameters (Å^2 * 10^3) for **47**. The anisotropic displacement factor exponent takes the form: $-2\,g\pi^2$ [h^2 a*^{2} U11 + ... + 2 h k a* b* U12].

Atom	U11	U22	U33	U23	U13	U12
O(1)	25(1)	42(1)	24(1)	10(1)	−2(1)	−18(1)
C(1)	20(1)	23(1)	20(1)	5(1)	2(1)	−5(1)
C(2)	25(1)	25(1)	24(1)	9(1)	6(1)	−8(1)
C(3)	27(1)	22(1)	18(1)	7(1)	5(1)	−2(1)
C(4)	19(1)	19(1)	17(1)	5(1)	0(1)	−3(1)
N(1)	22(1)	24(1)	19(1)	6(1)	0(1)	−2(1)
O(2)	34(1)	41(1)	17(1)	11(1)	−4(1)	−6(1)
O(3)	29(1)	48(1)	28(1)	15(1)	−5(1)	−21(1)
C(5)	17(1)	21(1)	20(1)	7(1)	4(1)	−3(1)
C(6)	19(1)	18(1)	17(1)	5(1)	3(1)	−1(1)
C(7)	20(1)	19(1)	18(1)	5(1)	3(1)	0(1)
O(4)	24(1)	34(1)	21(1)	8(1)	−4(1)	−9(1)
N(2)	21(1)	24(1)	16(1)	7(1)	−1(1)	−5(1)
C(8)	25(1)	22(1)	17(1)	8(1)	3(1)	0(1)
C(9)	22(1)	25(1)	18(1)	8(1)	2(1)	−7(1)
N(3)	19(1)	26(1)	21(1)	9(1)	2(1)	−1(1)
Cl(1)	19(1)	32(1)	22(1)	12(1)	2(1)	−3(1)

Table 0.32: Hydrogen coordinates (*10^4) and isotropic displacement parameters (Å^2 * 10^3) for **47**.

Atom	x	y	z	U(eq)
H(1O)	3860(40)	8890(30)	2110(20)	36
H(2)	3359	9117	−708	29
H(3)	281	7954	−1999	26
H(5)	−2681	6274	562	23
H(1N)	−2150(30)	6060(30)	2232(17)	24
H(8A)	497	6433	4210	25
H(8B)	−965	4725	3598	25

H(9A)	−4388	6448	4069	26
H(9B)	−3071	5951	5138	26
H(3A)	−3855	8789	5640	32
H(3B)	−2533	9080	4656	32
H(3C)	−1324	8619	5652	32

- **Crystallographic data recorded for 48**

Table 0.33: Atomic coordinates (*10^4) and equivalent isotropic displacement parameters (Å^2 * 10^3) for **48**. U(eq) is defined as one third of the trace of the orthogonalised Uij tensor.

Atom	**x**	**y**	**z**	**U(eq)**
Cu(1)	5000	5924(1)	2500	19(1)
O(1)	5957(1)	6859(1)	3004(1)	21(1)
C(1)	6879(2)	6776(1)	3523(1)	18(1)
C(2)	7480(2)	7575(1)	3787(1)	20(1)
C(3)	8463(2)	7571(1)	4328(1)	20(1)
C(4)	8872(2)	6747(1)	4621(1)	20(1)
N(1)	9865(2)	6728(1)	5215(1)	22(1)
O(2)	10472(1)	7426(1)	5357(1)	30(1)
O(3)	10050(1)	6032(1)	5565(1)	27(1)
C(5)	8314(2)	5952(1)	4390(1)	19(1)
C(6)	7304(2)	5946(1)	3840(1)	18(1)
C(7)	6713(2)	5086(1)	3596(1)	18(1)
O(4)	5949(1)	5008(1)	3036(1)	23(1)
N(2)	7017(2)	4347(1)	3974(1)	20(1)
C(8)	6439(2)	3487(1)	3771(1)	23(1)
C(9)	6974(2)	3095(1)	3076(1)	25(1)
N(3)	8412(2)	2983(1)	3143(1)	25(1)
O(1W)	10000	4361(2)	2500	47(1)
Cl(1)	2424(2)	5613(1)	3789(1)	30(1)
O(11)	1417(4)	5724(2)	3238(2)	63(1)
O(12)	2790(4)	4685(2)	3870(3)	57(1)
O(13)	3439(14)	6106(9)	3512(8)	55(3)
O(14)	2018(9)	5940(8)	4477(4)	39(2)
Cl(1')	7192(3)	5435(2)	1095(2)	34(1)
O(11')	6179(7)	4963(5)	673(3)	90(2)
O(12')	7809(7)	4782(4)	1536(4)	74(2)
O(13')	6440(20)	6102(13)	1421(11)	43(4)
O(14')	8003(17)	5848(13)	592(8)	58(4)

Table 0.34: Bond lengths (Å) and angles (°) for **48**.

Cu(1)-O(1)	1.9140(13)	**C(5)-C(6)**	1.403(2)
Cu(1)-O(1)#1	1.9140(12)	**C(6)-C(7)**	1.482(2)
Cu(1)-O(4)#1	1.9175(13)	**C(7)-O(4)**	1.259(2)
Cu(1)-O(4)	1.9175(13)	**C(7)-N(2)**	1.329(2)
Cu(1)-O(13)	2.515(13)	**N(2)-C(8)**	1.457(2)
Cu(1)-O(13')	2.528(19)	**C(8)-C(9)**	1.519(3)
O(1)-C(1)	1.309(2)	**C(9)-N(3)**	1.487(2)
C(1)-C(2)	1.418(2)	**Cl(1)-O(13)**	1.393(8)
C(1)-C(6)	1.427(2)	**Cl(1)-O(11)**	1.412(4)
C(2)-C(3)	1.372(2)	**Cl(1)-O(14)**	1.424(7)

C(3)-C(4)	1.398(3)	Cl(1)-O(12)	1.443(3)
C(4)-C(5)	1.376(2)	Cl(1')-O(12')	1.395(6)
C(4)-N(1)	1.447(2)	Cl(1')-O(14')	1.409(10)
N(1)-O(3)	1.229(2)	Cl(1')-O(13')	1.410(10)
N(1)-O(2)	1.236(2)	Cl(1')-O(11')	1.445(6)

O(1)-Cu(1)-O(1)#1	86.24(8)	O(2)-N(1)-C(4)	117.94(15)
O(1)-Cu(1)-O(4)#1	178.06(5)	C(4)-C(5)-C(6)	120.27(16)
O(1)#1-Cu(1)-O(4)#1	92.49(6)	C(5)-C(6)-C(1)	118.84(16)
O(1)-Cu(1)-O(4)	92.49(6)	C(5)-C(6)-C(7)	119.72(15)
O(1)#1-Cu(1)-O(4)	178.06(5)	C(1)-C(6)-C(7)	121.44(16)
O(4)#1-Cu(1)-O(4)	88.81(8)	O(4)-C(7)-N(2)	117.51(16)
O(1)-Cu(1)-O(13)	84.5(3)	O(4)-C(7)-C(6)	123.49(16)
O(1)#1-Cu(1)-O(13)	86.4(4)	N(2)-C(7)-C(6)	118.98(15)
O(4)#1-Cu(1)-O(13)	96.9(3)	C(7)-O(4)-Cu(1)	128.63(12)
O(4)-Cu(1)-O(13)	92.0(4)	C(7)-N(2)-C(8)	121.32(15)
O(1)-Cu(1)-O(13')	89.2(6)	N(2)-C(8)-C(9)	113.01(16)
O(1)#1-Cu(1)-O(13')	82.0(3)	N(3)-C(9)-C(8)	112.13(15)
O(4)#1-Cu(1)-O(13')	89.2(6)	O(13)-Cl(1)-O(11)	102.6(7)
O(4)-Cu(1)-O(13')	99.5(3)	O(13)-Cl(1)-O(14)	113.2(7)
O(13)-Cu(1)-O(13')	167.2(2)	O(11)-Cl(1)-O(14)	110.1(4)
C(1)-O(1)-Cu(1)	127.66(12)	O(13)-Cl(1)-O(12)	110.4(7)
O(1)-C(1)-C(2)	116.86(15)	O(11)-Cl(1)-O(12)	111.3(3)
O(1)-C(1)-C(6)	124.68(16)	O(14)-Cl(1)-O(12)	109.1(5)
C(2)-C(1)-C(6)	118.45(16)	Cl(1)-O(13)-Cu(1)	136.4(8)
C(3)-C(2)-C(1)	122.11(16)	O(12')-Cl(1')-O(14')	114.3(9)
C(2)-C(3)-C(4)	118.14(16)	O(12')-Cl(1')-O(13')	119.7(9)
C(5)-C(4)-C(3)	122.18(16)	O(14')-Cl(1')-O(13')	108.5(12)
C(5)-C(4)-N(1)	118.50(16)	O(12')-Cl(1')-O(11')	104.9(5)
C(3)-C(4)-N(1)	119.24(16)	O(14')-Cl(1')-O(11')	107.8(7)
O(3)-N(1)-O(2)	122.90(15)	O(13')-Cl(1')-O(11')	99.9(11)
O(3)-N(1)-C(4)	119.14(15)	Cl(1')-O(13')-Cu(1)	127.3(13)

Table 0.35: Anisotropic displacement parameters ($\text{Å}^2 * 10^3$) for **48**. The anisotropic displacement factor exponent takes the form: $-2 g\pi^2 [h^2 a^{*2} U11 + ... + 2 h k a^* b^* U12]$.

Atom	U11	U12	U33	U23	U13	U12
Cu(1)	20(1)	16(1)	21(1)	0	−10(1)	0
O(1)	22(1)	17(1)	21(1)	1(1)	−9(1)	−1(1)
C(1)	17(1)	20(1)	16(1)	1(1)	−3(1)	0(1)
C(2)	21(1)	18(1)	19(1)	1(1)	−3(1)	0(1)
C(3)	20(1)	20(1)	19(1)	−2(1)	−2(1)	−3(1)
C(4)	17(1)	23(1)	18(1)	−1(1)	−6(1)	0(1)
N(1)	19(1)	26(1)	19(1)	−2(1)	−5(1)	1(1)
O(2)	31(1)	27(1)	29(1)	−1(1)	−14(1)	−7(1)
O(3)	26(1)	27(1)	26(1)	3(1)	−10(1)	2(1)
C(5)	19(1)	19(1)	19(1)	0(1)	−4(1)	2(1)
C(6)	18(1)	18(1)	18(1)	−1(1)	−4(1)	1(1)
C(7)	16(1)	19(1)	20(1)	−1(1)	−2(1)	1(1)
O(4)	25(1)	17(1)	25(1)	0(1)	−13(1)	0(1)
N(2)	24(1)	18(1)	18(1)	−1(1)	−7(1)	0(1)
C(8)	26(1)	17(1)	26(1)	1(1)	−4(1)	−2(1)
C(9)	26(1)	21(1)	27(1)	−4(1)	−10(1)	2(1)
N(3)	28(1)	22(1)	23(1)	−5(1)	−8(1)	3(1)
O(1W)	59(2)	27(1)	53(2)	0	−19(1)	0
Cl(1)	39(1)	18(1)	33(1)	2(1)	5(1)	−4(1)
O(11)	78(3)	55(2)	52(2)	−4(2)	−33(2)	−19(2)
O(12)	59(2)	19(2)	95(3)	8(2)	14(2)	−2(2)

O(13)	77(7)	25(5)	67(6)	4(4)	45(5)	−4(3)
O(14)	37(3)	57(4)	21(2)	4(2)	4(2)	17(3)
Cl(1')	41(1)	26(1)	35(1)	0(1)	14(1)	1(1)
O(11')	104(5)	101(5)	66(4)	−28(3)	12(4)	−55(4)
O(12')	73(5)	50(4)	99(5)	30(4)	14(4)	27(3)
O(13')	51(6)	33(8)	46(5)	15(5)	18(4)	21(5)
O(14')	64(7)	58(6)	53(7)	2(5)	26(5)	4(5)

Table 0.36: Hydrogen coordinates (*10^4) and isotropic displacement parameters ($Å^2$ * 10^3) for **48**.

Atom	x	y	z	U(eg)
H(2)	7193	8131	3584	23
H(3)	8855	8114	4498	24
H(5)	8613	5405	4604	23
H(2N)	7437	4380	4407	24
H(8A)	5485	3561	3694	28
H(8B)	6601	3061	4183	28
H(9A)	6564	2506	2975	30
H(9B)	6744	3493	2653	30
H(3A)	8694	2747	2717	37
H(3B)	8627	2609	3525	37
H(3C)	8795	3525	3226	37
H(1WA)	10407	4726	2824	56

- **Crystallographic data recorded for 49**

Table 0.37: Atomic coordinates (*10^4) and equivalent isotropic displacement parameters ($Å^2$ * 10^3) for **49**. U(eq) is defined as one third of the trace of the orthogonalised Uij tensor.

Atom	x	y	z	U(eq)
Cu(1)	884(1)	6624(1)	2062(1)	15(1)
O(1)	819(1)	4875(1)	1744(1)	18(1)
C(1)	1058(2)	4388(2)	961(1)	14(1)
C(2)	1133(2)	3023(2)	914(2)	18(1)
C(3)	1364(2)	2399(2)	130(2)	18(1)
C(4)	1549(2)	3129(2)	−643(1)	16(1)
N(1)	1819(1)	2511(2)	−1472(1)	20(1)
O(2)	1774(1)	1320(2)	−1512(1)	28(1)
O(3)	2106(2)	3160(2)	−2122(1)	28(1)
C(5)	1498(2)	4461(2)	−626(1)	15(1)
C(6)	1250(1)	5113(2)	163(1)	14(1)
C(7)	1199(2)	6545(2)	101(1)	14(1)
O(4)	1268(1)	7051(1)	−675(1)	17(1)
N(2)	1118(1)	7214(2)	857(1)	15(1)
C(8)	1123(2)	8614(2)	794(1)	18(1)
C(9)	1413(2)	9149(2)	1711(2)	19(1)
N(3)	848(1)	8459(2)	2418(1)	19(1)
O(1W)	692(1)	6031(2)	3336(1)	19(1)

Table 0.38: Bond lengths (Å) and angles (°) for **49**.

Cu(1)-O(1)	1.8854(15)	C(4)-N(1)	1.433(3)
Cu(1)-N(2)	1.9106(17)	N(1)-O(3)	1.238(3)
Cu(1)-N(3)	1.9849(17)	N(1)-O(2)	1.245(2)
Cu(1)-O(1W)	2.0005(15)	C(5)-C(6)	1.390(3)
O(1)-C(1)	1.304(2)	C(6)-C(7)	1.498(3)
C(1)-C(6)	1.425(3)	C(7)-O(4)	1.266(2)
C(1)-C(2)	1.429(3)	C(7)-N(2)	1.322(3)
C(2)-C(3)	1.366(3)	N(2)-C(8)	1.463(3)
C(3)-C(4)	1.396(3)	C(8)-C(9)	1.518(3)
C(4)-C(5)	1.391(3)	C(9)-N(3)	1.482(3)
O(1)-Cu(1)-N(2)	94.98(7)	C(3)-C(4)-N(1)	120.06(18)
O(1)-Cu(1)-N(3)	175.82(8)	O(3)-N(1)-O(2)	121.66(19)
N(2)-Cu(1)-N(3)	86.61(8)	O(3)-N(1)-C(4)	119.87(18)
O(1)-Cu(1)-O(1W)	85.98(7)	O(2)-N(1)-C(4)	118.45(18)
N(2)-Cu(1)-O(1W)	177.75(7)	C(6)-C(5)-C(4)	121.06(19)
N(3)-Cu(1)-O(1W)	92.57(7)	C(5)-C(6)-C(1)	118.62(17)
C(1)-O(1)-Cu(1)	125.85(13)	C(5)-C(6)-C(7)	116.58(18)
O(1)-C(1)-C(6)	125.01(18)	C(1)-C(6)-C(7)	124.80(18)
O(1)-C(1)-C(2)	116.63(18)	O(4)-C(7)-N(2)	123.57(18)
C(6)-C(1)-C(2)	118.36(18)	O(4)-C(7)-C(6)	117.83(18)
C(3)-C(2)-C(1)	122.13(19)	N(2)-C(7)-C(6)	118.56(17)
C(2)-C(3)-C(4)	118.48(18)	C(7)-N(2)-C(8)	118.18(17)
C(5)-C(4)-C(3)	121.33(19)	C(7)-N(2)-Cu(1)	129.22(14)
C(5)-C(4)-N(1)	118.59(19)	C(8)-N(2)-Cu(1)	112.40(13)

Table 0.39: Anisotropic displacement parameters (Å^2 * 10^3) for **49**. The anisotropic displacement factor exponent takes the form: $-2 g\pi^2$ [h^2 a^{*2} U11 + ... + 2 h k a* b* U12].

Atom	U11	U22	U33	U23	U13	U12
Cu(1)	21(1)	13(1)	12(1)	0(1)	2(1)	0(1)
O(1)	29(1)	12(1)	14(1)	0(1)	4(1)	−3(1)
C(1)	16(1)	12(1)	15(1)	−1(1)	−2(1)	−1(1)
C(2)	20(1)	14(1)	19(1)	3(1)	1(1)	−2(1)
C(3)	20(1)	11(1)	23(1)	0(1)	−3(1)	0(1)
C(4)	18(1)	13(1)	16(1)	−4(1)	−2(1)	1(1)
N(1)	24(1)	16(1)	19(1)	−5(1)	−6(1)	3(1)
O(2)	38(1)	14(1)	33(1)	−10(1)	−4(1)	−1(1)
O(3)	45(1)	24(1)	16(1)	−2(1)	2(1)	8(1)
C(5)	18(1)	13(1)	15(1)	0(1)	−2(1)	0(1)
C(6)	14(1)	12(1)	15(1)	1(1)	−2(1)	1(1)
C(7)	14(1)	14(1)	13(1)	1(1)	0(1)	0(1)
O(4)	25(1)	14(1)	11(1)	1(1)	2(1)	2(1)
N(2)	23(1)	11(1)	12(1)	−1(1)	1(1)	0(1)
C(8)	27(1)	11(1)	14(1)	−2(1)	1(1)	1(1)
C(9)	24(1)	17(1)	17(1)	−4(1)	2(1)	−1(1)
N(3)	27(1)	15(1)	14(1)	−1(1)	0(1)	4(1)
O(1W)	31(1)	14(1)	14(1)	0(1)	2(1)	0(1)

Table 0.40: Hydrogen coordinates (*10^4) and isotropic displacement parameters ($\mathring{A}^2 * 10^3$) for **49**.

Atom	x	y	z	U(eq)
H(2)	1018	2533	1445	21
H(3)	1399	1490	111	21
H(5)	1635	4933	−1161	18
H(8A)	459	8929	623	21
H(8B)	1600	8896	328	21
H(9A)	2130	9031	1811	23
H(9B)	1265	10078	1738	23
H(3A)	208	8751	2441	22
H(3B)	1134	8572	2976	22
H(1WA)	950(20)	5344(18)	3440(20)	29
H(1WB)	880(20)	6540(20)	3750(18)	29

- **Crystallographic data recorded for 64**

Table 0.41: Atomic coordinates (*10^4) and equivalent isotropic displacement parameters ($\mathring{A}^2 * 10^3$) for **64**. U(eq) is defined as one third of the trace of the orthogonalised Uij tensor.

Atom	x	y	z	U(eq)
O(1A)	2756(1)	2648(1)	367(1)	32(1)
C(1A)	2180(1)	2676(2)	170(1)	34(1)
C(2A)	1892(1)	2661(2)	−450(2)	37(1)
C(3A)	1320(1)	2713(2)	−637(2)	45(1)
C(4A)	1038(1)	2783(2)	−227(2)	49(1)
C(5A)	406(1)	2878(3)	−444(2)	68(1)
C(6A)	246(4)	3863(10)	−807(6)	83(4)
C(7A)	149(3)	1986(7)	−774(6)	80(3)
C(8A)	208(3)	3105(12)	135(4)	107(5)
C(5X)	406(1)	2878(3)	−444(2)	68(1)
C(6X)	164(3)	2678(10)	−1220(6)	106(4)
C(7X)	162(3)	1953(7)	−245(6)	74(3)
C(8X)	238(4)	3877(7)	−374(9)	114(7)
C(9A)	1344(1)	2757(2)	386(2)	47(1)
C(10A)	1915(1)	2687(2)	605(2)	39(1)
C(11A)	2220(1)	2562(2)	1278(2)	43(1)
C(12A)	3003(1)	3657(2)	459(2)	38(1)
C(13A)	3598(1)	3585(3)	849(2)	40(1)
O(2A)	3894(1)	4343(2)	878(1)	58(1)
N(1A)	3773(1)	2716(2)	1153(1)	42(1)
C(14A)	4346(1)	2652(3)	1564(2)	55(1)
C(15A)	4467(2)	1690(3)	1910(2)	62(1)
N(2A)	4129(1)	1574(3)	2313(1)	58(1)
C(16A)	3975(2)	662(3)	2427(2)	53(1)
O(3A)	4120(1)	−155(2)	2256(1)	73(1)
C(17A)	3556(1)	626(3)	2760(2)	51(1)
C(18A)	3429(1)	−347(3)	2905(2)	54(1)
C(19A)	3026(2)	−476(3)	3169(2)	57(1)
N(3A)	2870(2)	−1521(4)	3273(2)	76(1)
O(4A)	3166(2)	−2245(3)	3224(2)	105(1)
O(5A)	2446(2)	−1635(3)	3396(2)	98(1)
C(20A)	2752(2)	355(4)	3298(2)	65(1)

C(21A)	2870(2)	1327(4)	3163(2)	63(1)
C(22A)	3272(2)	1476(3)	2892(2)	55(1)
O(6A)	3394(1)	2425(2)	2744(1)	69(1)
C(23A)	3124(2)	3302(4)	2885(2)	87(2)
O(1B)	2896(1)	901(2)	1225(1)	40(1)
C(1B)	2466(1)	664(2)	1426(1)	36(1)
C(2B)	2135(1)	1488(2)	1484(1)	39(1)
C(3B)	1710(1)	1277(3)	1711(2)	43(1)
C(4B)	1589(1)	293(3)	1861(1)	43(1)
C(5B)	1097(1)	119(3)	2090(2)	53(1)
C(6B)	567(2)	445(4)	1590(2)	71(1)
C(7B)	1048(2)	−1007(3)	2256(2)	75(1)
C(8B)	1167(2)	781(4)	2657(2)	74(1)
C(9B)	1925(1)	−508(3)	1792(1)	40(1)
C(10B)	2359(1)	−344(2)	1573(1)	37(1)
C(11B)	2709(1)	−1249(2)	1503(1)	39(1)
O(1C)	3296(1)	−665(1)	701(1)	33(1)
C(1C)	2832(1)	−1306(2)	460(1)	32(1)
C(2C)	2556(1)	−1633(2)	846(1)	35(1)
C(3C)	2120(1)	−2322(2)	615(1)	37(1)
C(4C)	1958(1)	−2676(2)	20(2)	37(1)
C(5C)	1514(1)	−3505(2)	−229(2)	46(1)
C(6C)	1758(2)	−4405(3)	−475(3)	84(2)
C(7C)	1028(2)	−3073(4)	−734(2)	78(1)
C(8C)	1315(2)	−3932(4)	278(2)	88(2)
C(9C)	2223(1)	−2261(2)	−360(2)	37(1)
C(10C)	2659(1)	−1569(2)	−156(1)	33(1)
C(11C)	2910(1)	−1124(2)	−605(1)	35(1)
C(12C)	3813(1)	−1205(2)	873(2)	37(1)
C(13C)	4243(1)	−560(2)	732(1)	37(1)
O(2C)	4727(1)	−845(2)	915(1)	46(1)
N(1C)	4062(1)	296(2)	413(1)	39(1)
C(14C)	4394(1)	1034(3)	225(2)	45(1)
C(15C)	4190(1)	1174(2)	−464(2)	42(1)
N(2C)	4345(1)	2185(2)	−624(1)	41(1)
C(16C)	4064(1)	3028(2)	−567(1)	37(1)
O(3C)	3649(1)	2958(2)	−418(1)	50(1)
C(17C)	4271(1)	4077(2)	−666(1)	33(1)
C(18C)	4037(1)	4914(2)	−472(1)	38(1)
C(19C)	4214(1)	5904(2)	−521(1)	38(1)
N(3C)	3971(1)	6773(2)	−297(1)	52(1)
O(4C)	3574(1)	6613(2)	−141(2)	75(1)
O(5C)	4179(1)	7636(2)	−277(1)	67(1)
C(20C)	4623(1)	6098(2)	−766(2)	40(1)
C(21C)	4857(1)	5286(2)	−967(2)	40(1)
C(22C)	4686(1)	4278(2)	−921(1)	33(1)
O(6C)	4906(1)	3449(2)	−1114(1)	41(1)
C(23C)	5320(1)	3623(3)	−1392(2)	45(1)
O(1D)	2904(1)	921(2)	−219(1)	35(1)
C(1D)	2544(1)	712(2)	−789(1)	34(1)
C(2D)	2545(1)	−297(2)	−1003(1)	37(1)
C(3D)	2182(2)	−540(3)	−1579(1)	45(1)
C(4D)	1819(2)	172(3)	−1949(2)	51(1)
C(5D)	1410(2)	−146(3)	−2573(2)	77(1)
C(6D)	1055(5)	−982(7)	−2464(4)	93(4)
C(7D)	1780(5)	−607(9)	−2945(4)	108(4)
C(8D)	1090(5)	737(8)	−2928(6)	99(5)
C(5Y)	1410(2)	−146(3)	−2573(2)	77(1)
C(6Y)	1508(10)	−1252(11)	−2773(7)	149(10)
C(7Y)	1428(9)	605(17)	−3040(8)	137(11)
C(8Y)	822(7)	−140(20)	−2514(8)	172(12)

C(9D)	1837(2)	1169(3)	−1720(2)	48(1)
C(10D)	2189(1)	1464(2)	−1147(1)	38(1)
C(11D)	2185(1)	2559(2)	−920(1)	38(1)
C(1S)	1382(2)	−26(3)	−141(2)	62(1)
Cl(1)	1085(1)	−125(1)	−916(1)	80(1)
Cl(2)	954(1)	−446(2)	246(1)	115(1)
O(1W)	5099(2)	−969(5)	2151(3)	68(2)
O(2W)	3747(3)	6964(4)	2090(4)	91(2)
O(3W)	5842(3)	521(9)	2395(4)	125(3)
O(4W)	2833(3)	5583(6)	1684(4)	92(2)
O(5W)	3178(3)	4919(5)	1748(3)	86(2)
O(6W)	5466(5)	−1318(8)	2038(4)	136(3)
O(7W)	3180(6)	6021(8)	1432(5)	153(5)
O(8W)	5869(4)	1014(10)	1824(7)	101(4)
O(9W)	5629(7)	−164(18)	2139(13)	165(14)

Table 0.42: Bond lengths (Å) and angles (°) for **64**.

O(1A)-C(1A)	1.401(3)	**O(1C)-C(1C)**	1.409(3)
O(1A)-C(12A)	1.435(3)	**O(1C)-C(12C)**	1.438(3)
C(1A)-C(2A)	1.385(4)	**C(1C)-C(2C)**	1.388(4)
C(1A)-C(10A)	1.400(4)	**C(1C)-C(10C)**	1.392(4)
C(2A)-C(3A)	1.394(4)	**C(2C)-C(3C)**	1.397(4)
C(2A)-C(11D)	1.529(5)	**C(3C)-C(4C)**	1.383(4)
C(3A)-C(4A)	1.385(5)	**C(4C)-C(9C)**	1.394(4)
C(4A)-C(9A)	1.380(5)	**C(4C)-C(5C)**	1.533(4)
C(4A)-C(5A)	1.542(4)	**C(5C)-C(7C)**	1.510(6)
C(5A)-C(7A)	1.421(9)	**C(5C)-C(6C)**	1.522(5)
C(5A)-C(6A)	1.508(12)	**C(5C)-C(8C)**	1.539(6)
C(5A)-C(8A)	1.620(10)	**C(9C)-C(10C)**	1.390(4)
C(9A)-C(10A)	1.392(4)	**C(10C)-C(11C)**	1.516(4)
C(10A)-C(11A)	1.507(5)	**C(11C)-C(2D)**	1.517(4)
C(11A)-C(2B)	1.509(5)	**C(12C)-C(13C)**	1.511(4)
C(12A)-C(13A)	1.504(4)	**C(13C)-O(2C)**	1.234(3)
C(13A)-O(2A)	1.230(4)	**C(13C)-N(1C)**	1.327(4)
C(13A)-N(1A)	1.325(4)	**N(1C)-C(14C)**	1.445(4)
N(1A)-C(14A)	1.469(4)	**C(14C)-C(15C)**	1.521(5)
C(14A)-C(15A)	1.458(6)	**C(15C)-N(2C)**	1.451(4)
C(15A)-N(2A)	1.487(5)	**N(2C)-C(16C)**	1.340(4)
N(2A)-C(16A)	1.299(5)	**C(16C)-O(3C)**	1.234(4)
C(16A)-O(3A)	1.230(5)	**C(16C)-C(17C)**	1.503(4)
C(16A)-C(17A)	1.531(5)	**C(17C)-C(18C)**	1.387(4)
C(17A)-C(18A)	1.369(6)	**C(17C)-C(22C)**	1.411(4)
C(17A)-C(22A)	1.410(5)	**C(18C)-C(19C)**	1.375(4)
C(18A)-C(19A)	1.383(5)	**C(19C)-C(20C)**	1.380(4)
C(19A)-C(20A)	1.374(6)	**C(19C)-N(3C)**	1.466(4)
C(19A)-N(3A)	1.453(6)	**N(3C)-O(4C)**	1.214(4)
N(3A)-O(5A)	1.230(5)	**N(3C)-O(5C)**	1.232(4)
N(3A)-O(4A)	1.237(5)	**C(20C)-C(21C)**	1.369(4)
C(20A)-C(21A)	1.355(6)	**C(21C)-C(22C)**	1.390(4)
C(21A)-C(22A)	1.397(5)	**C(22C)-O(6C)**	1.358(4)
C(22A)-O(6A)	1.339(5)	**O(6C)-C(23C)**	1.441(4)
O(6A)-C(23A)	1.425(6)	**O(1D)-C(1D)**	1.368(3)
O(1B)-C(1B)	1.375(3)	**C(1D)-C(2D)**	1.395(4)
C(1B)-C(10B)	1.398(4)	**C(1D)-C(10D)**	1.403(4)
C(1B)-C(2B)	1.401(4)	**C(2D)-C(3D)**	1.391(4)
C(2B)-C(3B)	1.394(4)	**C(3D)-C(4D)**	1.388(5)
C(3B)-C(4B)	1.383(5)	**C(4D)-C(9D)**	1.389(5)
C(4B)-C(9B)	1.394(5)	**C(4D)-C(5D)**	1.539(5)

C(4B)-C(5B)	1.549(4)	C(5D)-C(8D)	1.486(12)
C(5B)-C(7B)	1.521(6)	C(5D)-C(6D)	1.492(10)
C(5B)-C(6B)	1.528(6)	C(5D)-C(7D)	1.605(11)
C(5B)-C(8B)	1.534(5)	C(9D)-C(10D)	1.392(4)
C(9B)-C(10B)	1.393(4)	C(10D)-C(11D)	1.513(4)
C(10B)-C(11B)	1.520(4)	C(1S)-Cl(1)	1.711(4)
C(11B)-C(2C)	1.528(4)	C(1S)-Cl(2)	1.731(5)

C(1A)-O(1A)-C(12A)	113.3(2)	C(2C)-C(1C)-C(10C)	122.3(3)
C(2A)-C(1A)-C(10A)	122.1(3)	C(2C)-C(1C)-O(1C)	118.3(3)
C(2A)-C(1A)-O(1A)	118.8(3)	C(10C)-C(1C)-O(1C)	119.4(2)
C(10A)-C(1A)-O(1A)	119.1(3)	C(1C)-C(2C)-C(3C)	117.9(3)
C(1A)-C(2A)-C(3A)	117.9(3)	C(1C)-C(2C)-C(11B)	122.2(3)
C(1A)-C(2A)-C(11D)	121.6(3)	C(3C)-C(2C)-C(11B)	119.9(3)
C(3A)-C(2A)-C(11D)	120.4(3)	C(4C)-C(3C)-C(2C)	122.1(3)
C(4A)-C(3A)-C(2A)	122.3(3)	C(3C)-C(4C)-C(9C)	117.4(3)
C(9A)-C(4A)-C(3A)	117.4(3)	C(3C)-C(4C)-C(5C)	123.1(3)
C(9A)-C(4A)-C(5A)	121.1(4)	C(9C)-C(4C)-C(5C)	119.5(3)
C(3A)-C(4A)-C(5A)	121.5(4)	C(7C)-C(5C)-C(6C)	109.3(4)
C(7A)-C(5A)-C(6A)	113.1(8)	C(7C)-C(5C)-C(4C)	110.9(3)
C(7A)-C(5A)-C(4A)	111.3(4)	C(6C)-C(5C)-C(4C)	109.0(3)
C(6A)-C(5A)-C(4A)	108.2(5)	C(7C)-C(5C)-C(8C)	109.0(4)
C(7A)-C(5A)-C(8A)	112.1(8)	C(6C)-C(5C)-C(8C)	107.5(4)
C(6A)-C(5A)-C(8A)	102.2(7)	C(4C)-C(5C)-C(8C)	111.1(3)
C(4A)-C(5A)-C(8A)	109.6(4)	C(10C)-C(9C)-C(4C)	122.9(3)
C(4A)-C(9A)-C(10A)	123.3(3)	C(9C)-C(10C)-C(1C)	117.0(3)
C(9A)-C(10A)-C(1A)	116.8(3)	C(9C)-C(10C)-C(11C)	119.5(3)
C(9A)-C(10A)-C(11A)	120.6(3)	C(1C)-C(10C)-C(11C)	123.5(3)
C(1A)-C(10A)-C(11A)	122.5(3)	C(10C)-C(11C)-C(2D)	111.5(2)
C(10A)-C(11A)-C(2B)	110.4(2)	O(1C)-C(12C)-C(13C)	110.6(2)
O(1A)-C(12A)-C(13A)	110.4(2)	O(2C)-C(13C)-N(1C)	124.6(3)
O(2A)-C(13A)-N(1A)	123.6(3)	O(2C)-C(13C)-C(12C)	119.6(3)
O(2A)-C(13A)-C(12A)	118.3(3)	N(1C)-C(13C)-C(12C)	115.7(2)
N(1A)-C(13A)-C(12A)	118.1(3)	C(13C)-N(1C)-C(14C)	125.9(3)
C(13A)-N(1A)-C(14A)	118.9(3)	N(1C)-C(14C)-C(15C)	111.5(3)
C(15A)-C(14A)-N(1A)	113.0(3)	N(2C)-C(15C)-C(14C)	110.5(3)
C(14A)-C(15A)-N(2A)	111.9(3)	C(16C)-N(2C)-C(15C)	120.2(3)
C(16A)-N(2A)-C(15A)	120.2(4)	O(3C)-C(16C)-N(2C)	121.1(3)
O(3A)-C(16A)-N(2A)	124.5(4)	O(3C)-C(16C)-C(17C)	119.8(3)
O(3A)-C(16A)-C(17A)	118.7(4)	N(2C)-C(16C)-C(17C)	119.1(2)
N(2A)-C(16A)-C(17A)	116.6(4)	C(18C)-C(17C)-C(22C)	117.8(3)
C(18A)-C(17A)-C(22A)	118.5(3)	C(18C)-C(17C)-C(16C)	116.0(3)
C(18A)-C(17A)-C(16A)	114.9(3)	C(22C)-C(17C)-C(16C)	126.2(3)
C(22A)-C(17A)-C(16A)	126.4(4)	C(19C)-C(18C)-C(17C)	120.4(3)
C(17A)-C(18A)-C(19A)	119.8(4)	C(18C)-C(19C)-C(20C)	121.7(3)
C(20A)-C(19A)-C(18A)	121.5(4)	C(18C)-C(19C)-N(3C)	119.3(3)
C(20A)-C(19A)-N(3A)	119.9(4)	C(20C)-C(19C)-N(3C)	119.1(3)
C(18A)-C(19A)-N(3A)	118.6(4)	O(4C)-N(3C)-O(5C)	123.0(3)
O(5A)-N(3A)-O(4A)	123.8(4)	O(4C)-N(3C)-C(19C)	118.8(3)
O(5A)-N(3A)-C(19A)	118.0(4)	O(5C)-N(3C)-C(19C)	118.2(3)
O(4A)-N(3A)-C(19A)	118.3(4)	C(21C)-C(20C)-C(19C)	119.1(3)
C(21A)-C(20A)-C(19A)	120.1(4)	C(20C)-C(21C)-C(22C)	120.3(3)
C(20A)-C(21A)-C(22A)	119.4(4)	O(6C)-C(22C)-C(21C)	122.3(3)
O(6A)-C(22A)-C(21A)	121.0(4)	O(6C)-C(22C)-C(17C)	117.0(3)
O(6A)-C(22A)-C(17A)	118.3(3)	C(21C)-C(22C)-C(17C)	120.7(3)
C(21A)-C(22A)-C(17A)	120.6(4)	C(22C)-O(6C)-C(23C)	118.7(2)
C(22A)-O(6A)-C(23A)	119.7(4)	O(1D)-C(1D)-C(2D)	116.6(3)
O(1B)-C(1B)-C(10B)	122.7(3)	O(1D)-C(1D)-C(10D)	122.4(3)
O(1B)-C(1B)-C(2B)	116.8(3)	C(2D)-C(1D)-C(10D)	121.0(3)
C(10B)-C(1B)-C(2B)	120.5(3)	C(3D)-C(2D)-C(1D)	118.3(3)
C(3B)-C(2B)-C(1B)	118.1(3)	C(3D)-C(2D)-C(11C)	120.6(3)

C(3B)-C(2B)-C(11A)	121.1(3)	C(1D)-C(2D)-C(11C)	121.0(3)
C(1B)-C(2B)-C(11A)	120.7(3)	C(4D)-C(3D)-C(2D)	123.0(3)
C(4B)-C(3B)-C(2B)	123.3(3)	C(3D)-C(4D)-C(9D)	116.7(3)
C(3B)-C(4B)-C(9B)	116.8(3)	C(3D)-C(4D)-C(5D)	121.0(3)
C(3B)-C(4B)-C(5B)	120.1(3)	C(9D)-C(4D)-C(5D)	122.3(3)
C(9B)-C(4B)-C(5B)	123.1(3)	C(8D)-C(5D)-C(6D)	113.1(7)
C(7B)-C(5B)-C(6B)	109.1(3)	C(8D)-C(5D)-C(4D)	113.4(5)
C(7B)-C(5B)-C(8B)	108.1(3)	C(6D)-C(5D)-C(4D)	107.5(4)
C(6B)-C(5B)-C(8B)	108.5(4)	C(8D)-C(5D)-C(7D)	107.7(7)
C(7B)-C(5B)-C(4B)	112.0(3)	C(6D)-C(5D)-C(7D)	109.5(7)
C(6B)-C(5B)-C(4B)	109.1(3)	C(4D)-C(5D)-C(7D)	105.3(5)
C(8B)-C(5B)-C(4B)	110.0(3)	C(4D)-C(9D)-C(10D)	123.2(3)
C(10B)-C(9B)-C(4B)	122.5(3)	C(9D)-C(10D)-C(1D)	117.8(3)
C(9B)-C(10B)-C(1B)	118.7(3)	C(9D)-C(10D)-C(11D)	120.8(3)
C(9B)-C(10B)-C(11B)	120.2(3)	C(1D)-C(10D)-C(11D)	121.4(3)
C(1B)-C(10B)-C(11B)	121.1(3)	C(10D)-C(11D)-C(2A)	113.3(2)
C(10B)-C(11B)-C(2C)	113.1(2)	Cl(1)-C(1S)-Cl(2)	112.7(2)
C(1C)-O(1C)-C(12C)	114.2(2)		

Table 0.43: Anisotropic displacement parameters ($\text{Å}^2 * 10^3$) for **64**. The anisotropic displacement factor exponent takes the form: $-2\,g\pi^2\,[\,h^2\,a^{*2}\,U11 + ... + 2\,h\,k\,a^*\,b^*\,U12]$.

Atom	U11	U22	U33	U23	U13	U12
O(1A)	20(1)	29(1)	47(1)	−3(1)	11(1)	−6(1)
C(1A)	20(1)	26(1)	53(2)	−3(1)	10(1)	−2(1)
C(2A)	28(1)	26(1)	53(2)	3(1)	8(1)	−4(1)
C(3A)	30(2)	30(2)	66(2)	6(1)	2(2)	−3(1)
C(4A)	23(2)	33(2)	90(3)	6(2)	17(2)	−2(1)
C(5A)	20(2)	49(2)	125(4)	13(2)	14(2)	2(1)
C(6A)	21(4)	94(8)	120(10)	20(8)	7(5)	17(4)
C(7A)	26(4)	61(5)	138(10)	−25(6)	7(5)	−17(3)
C(8A)	24(4)	224(15)	78(6)	10(8)	22(4)	35(6)
C(5X)	20(2)	49(2)	125(4)	13(2)	14(2)	2(1)
C(6X)	28(4)	108(9)	160(12)	26(8)	2(6)	3(5)
C(7X)	27(4)	59(5)	132(9)	−2(6)	23(5)	−9(3)
C(8X)	30(5)	37(5)	280(20)	−26(9)	59(10)	2(4)
C(9A)	32(2)	35(2)	81(3)	−5(2)	28(2)	−1(1)
C(10A)	31(2)	28(1)	62(2)	−8(1)	19(1)	−5(1)
C(11A)	41(2)	38(2)	57(2)	−17(2)	26(2)	−9(1)
C(12A)	26(1)	32(2)	57(2)	−5(1)	14(1)	−10(1)
C(13A)	29(2)	45(2)	47(2)	−7(1)	14(1)	−10(1)
O(2A)	34(1)	54(2)	80(2)	0(1)	13(1)	−21(1)
N(1A)	25(1)	55(2)	44(2)	2(1)	9(1)	−9(1)
C(14A)	32(2)	81(3)	46(2)	8(2)	6(2)	−8(2)
C(15A)	45(2)	84(3)	59(2)	5(2)	22(2)	1(2)
N(2A)	43(2)	76(2)	53(2)	−1(2)	14(1)	0(2)
C(16A)	56(2)	61(2)	39(2)	2(2)	11(2)	−2(2)
O(3A)	72(2)	77(2)	84(2)	−6(2)	45(2)	3(2)
C(17A)	35(2)	81(3)	33(2)	−2(2)	7(1)	4(2)
C(18A)	42(2)	84(3)	33(2)	6(2)	8(2)	6(2)
C(19A)	46(2)	87(3)	35(2)	11(2)	11(2)	7(2)
N(3A)	75(2)	97(3)	61(2)	25(2)	27(2)	6(2)
O(4A)	123(3)	91(3)	125(3)	15(2)	75(3)	20(2)
O(5A)	83(2)	118(3)	110(3)	44(2)	56(2)	7(2)
C(20A)	51(2)	103(3)	45(2)	14(2)	21(2)	8(2)
C(21A)	56(2)	92(3)	44(2)	5(2)	22(2)	11(2)
C(22A)	51(2)	79(3)	30(2)	1(2)	10(2)	−7(2)
O(6A)	75(2)	73(2)	65(2)	−7(2)	29(2)	3(2)

C(23A)	113(4)	82(3)	71(3)	−1(2)	36(3)	2(3)
O(1B)	34(1)	40(1)	51(1)	−4(1)	21(1)	−5(1)
C(1B)	29(1)	46(2)	35(2)	−7(1)	12(1)	−10(1)
C(2B)	34(2)	44(2)	41(2)	−14(1)	16(1)	−11(1)
C(3B)	35(2)	51(2)	48(2)	−17(2)	20(1)	−9(1)
C(4B)	35(2)	58(2)	39(2)	−12(2)	16(1)	−14(2)
C(5B)	44(2)	65(2)	59(2)	−16(2)	32(2)	−18(2)
C(6B)	42(2)	101(3)	78(3)	−8(2)	29(2)	−10(2)
C(7B)	70(3)	77(3)	96(3)	−9(2)	54(3)	−22(2)
C(8B)	67(3)	100(3)	73(3)	−32(2)	46(2)	−27(2)
C(9B)	40(2)	47(2)	35(2)	−4(1)	14(1)	−14(1)
C(10B)	34(2)	44(2)	31(2)	−5(1)	10(1)	−5(1)
C(11B)	35(2)	46(2)	37(2)	6(1)	13(1)	−5(1)
O(1C)	26(1)	32(1)	43(1)	1(1)	13(1)	1(1)
C(1C)	29(1)	26(1)	42(2)	1(1)	13(1)	−1(1)
C(2C)	33(2)	33(2)	40(2)	4(1)	15(1)	1(1)
C(3C)	37(2)	34(2)	45(2)	5(1)	20(1)	−4(1)
C(4C)	35(2)	31(2)	48(2)	2(1)	16(1)	−1(1)
C(5C)	46(2)	36(2)	57(2)	−7(2)	20(2)	−10(1)
C(6C)	82(3)	42(2)	135(5)	−22(2)	45(3)	−13(2)
C(7C)	55(2)	66(3)	98(3)	0(2)	5(2)	−18(2)
C(8C)	84(3)	97(4)	87(3)	−9(3)	35(3)	−55(3)
C(9C)	41(2)	27(1)	44(2)	−3(1)	18(1)	1(1)
C(10C)	33(2)	25(1)	45(2)	−1(1)	19(1)	4(1)
C(11C)	40(2)	31(2)	40(2)	−3(1)	19(1)	−2(1)
C(12C)	31(2)	36(2)	46(2)	8(1)	16(1)	6(1)
C(13C)	31(2)	37(2)	43(2)	4(1)	13(1)	4(1)
O(2C)	29(1)	53(1)	58(1)	14(1)	16(1)	7(1)
N(1C)	27(1)	40(1)	51(2)	8(1)	15(1)	0(1)
C(14C)	32(2)	45(2)	57(2)	11(2)	13(2)	−5(1)
C(15C)	36(2)	40(2)	53(2)	5(1)	21(2)	−2(1)
N(2C)	36(1)	40(1)	54(2)	7(1)	24(1)	1(1)
C(16C)	26(1)	46(2)	38(2)	6(1)	11(1)	0(1)
O(3C)	34(1)	47(1)	75(2)	10(1)	27(1)	1(1)
C(17C)	22(1)	41(2)	33(2)	4(1)	6(1)	0(1)
C(18C)	29(2)	46(2)	38(2)	8(1)	10(1)	5(1)
C(19C)	31(2)	42(2)	38(2)	1(1)	7(1)	6(1)
N(3C)	47(2)	51(2)	59(2)	0(1)	18(1)	8(1)
O(4C)	76(2)	55(2)	116(3)	6(2)	63(2)	16(1)
O(5C)	64(2)	48(2)	92(2)	−18(1)	28(2)	−1(1)
C(20C)	30(2)	38(2)	48(2)	−1(1)	8(1)	−4(1)
C(21C)	28(2)	43(2)	50(2)	2(1)	13(1)	−4(1)
C(22C)	25(1)	41(2)	32(2)	2(1)	7(1)	0(1)
O(6C)	38(1)	38(1)	55(1)	0(1)	25(1)	−2(1)
C(23C)	36(2)	50(2)	58(2)	−3(2)	26(2)	−3(1)
O(1D)	29(1)	31(1)	40(1)	−3(1)	6(1)	2(1)
C(1D)	33(2)	35(2)	35(2)	0(1)	12(1)	−4(1)
C(2D)	43(2)	34(2)	37(2)	1(1)	19(1)	−4(1)
C(3D)	65(2)	36(2)	35(2)	−3(1)	19(2)	−11(2)
C(4D)	67(2)	47(2)	33(2)	0(1)	7(2)	−14(2)
C(5D)	111(4)	56(2)	41(2)	−1(2)	−6(2)	−27(2)
C(6D)	120(9)	65(5)	60(5)	−6(4)	−16(5)	−42(5)
C(7D)	178(11)	95(7)	37(4)	−18(5)	17(5)	−10(7)
C(8D)	111(9)	69(5)	67(7)	13(4)	−38(7)	−41(6)
C(5Y)	111(4)	56(2)	41(2)	−1(2)	−6(2)	−27(2)
C(6Y)	240(30)	63(9)	68(10)	−30(8)	−51(13)	12(12)
C(7Y)	170(20)	136(17)	45(8)	23(9)	−41(13)	−72(18)
C(8Y)	78(12)	320(40)	94(13)	−90(20)	4(9)	−82(18)
C(9D)	54(2)	41(2)	41(2)	9(1)	4(2)	−8(2)
C(10D)	36(2)	35(2)	40(2)	4(1)	10(1)	−3(1)
C(11D)	32(2)	33(2)	43(2)	7(1)	5(1)	−2(1)

C(1S)	45(2)	46(2)	84(3)	−7(2)	7(2)	1(2)
Cl(1)	89(1)	75(1)	81(1)	5(1)	37(1)	0(1)
Cl(2)	118(1)	158(2)	82(1)	20(1)	52(1)	43(1)
O(1W)	56(3)	100(5)	49(3)	16(3)	18(3)	38(3)
O(2W)	90(4)	45(3)	176(7)	27(4)	93(5)	23(3)
O(3W)	84(5)	181(9)	96(6)	−19(6)	12(5)	−28(6)
O(4W)	69(4)	93(5)	114(6)	0(4)	29(4)	17(4)
O(5W)	124(6)	65(4)	79(4)	−3(3)	46(4)	10(4)
O(6W)	169(10)	125(8)	83(6)	7(5)	2(6)	2(7)
O(7W)	243(13)	105(7)	125(8)	29(6)	81(8)	98(8)
O(8W)	54(6)	106(9)	144(12)	−10(8)	35(7)	−28(6)
O(9W)	60(10)	138(18)	220(30)	−140(20)	−59(13)	19(11)

Table 0.44: Hydrogen coordinates ($*10^4$) and isotropic displacement parameters ($Å^2 * 10^3$) for **64**.

Atom	x	y	z	U(eq)
H(3A)	1117	2701	−1061	54
H(6A1)	431	4452	−556	124
H(6A2)	−153	3957	−932	124
H(6A3)	357	3821	−1170	124
H(7A1)	−252	2064	−900	120
H(7A2)	261	1373	−513	120
H(7A3)	259	1905	−1135	120
H(8A1)	396	3722	351	161
H(8A2)	298	2510	412	161
H(8A3)	−190	3220	−7	161
H(6X1)	271	1986	−1311	159
H(6X2)	320	3199	−1420	159
H(6X3)	−238	2736	−1371	159
H(7X1)	335	1323	−330	111
H(7X2)	−234	1929	−468	111
H(7X3)	225	1998	194	111
H(8X1)	454	4373	−520	171
H(8X2)	296	4008	57	171
H(8X3)	−153	3956	−612	171
H(9A)	1155	2788	673	57
H(11A)	2087	3080	1509	52
H(11B)	2617	2684	1362	52
H(12A)	2806	4110	660	46
H(12B)	2972	3967	60	46
H(1A)	3550	2185	1111	50
H(14A)	4593	2713	1320	66
H(14B)	4422	3242	1851	66
H(15A)	4861	1677	2162	74
H(15B)	4396	1098	1625	74
H(2A)	4034	2126	2476	69
H(18A)	3617	−931	2825	65
H(20A)	2479	247	3483	78
H(21A)	2681	1903	3252	75
H(23A)	3260	3933	2750	131
H(23B)	3200	3335	3326	131
H(23C)	2727	3242	2675	131
H(1B)	3068	359	1205	60
H(3B)	1493	1838	1765	52
H(6B1)	597	1170	1482	107
H(6B2)	256	367	1739	107
H(6B3)	509	8	1230	107

H(7B1)	1003	−1445	1899	112
H(7B2)	728	−1088	2389	112
H(7B3)	1381	−1212	2587	112
H(8B1)	1196	1512	2559	111
H(8B2)	1501	570	2985	111
H(8B3)	848	686	2790	111
H(9B)	1856	−1191	1899	48
H(11C)	2669	−1826	1764	47
H(11D)	3101	−1036	1649	47
H(3C)	1927	−2556	874	44
H(6C1)	2074	−4687	−148	127
H(6C2)	1878	−4161	−809	127
H(6C3)	1479	−4946	−626	127
H(7C1)	868	−2498	−576	117
H(7C2)	752	−3617	−888	117
H(7C3)	1150	−2824	−1066	117
H(8C1)	1629	−4214	608	131
H(8C2)	1044	−4481	112	131
H(8C3)	1146	−3373	438	131
H(9C)	2101	−2460	−777	44
H(11E)	2967	−1686	−867	42
H(11F)	3274	−821	−378	42
H(12C)	3765	−1869	648	44
H(12D)	3936	−1362	1314	44
H(1C)	3707	425	305	47
H(14C)	4780	793	361	54
H(14D)	4384	1709	423	54
H(15C)	4350	629	−652	50
H(15D)	3785	1102	−624	50
H(2C)	4623	2244	−760	49
H(18C)	3753	4804	−304	46
H(20C)	4741	6787	−795	48
H(21C)	5137	5411	−1138	48
H(23D)	5437	2958	−1510	68
H(23E)	5637	3972	−1100	68
H(23F)	5168	4058	−1755	68
H(1D)	2874	1544	−133	52
H(3D)	2182	−1226	−1726	54
H(6D1)	1287	−1545	−2234	140
H(6D2)	812	−1247	−2857	140
H(6D3)	833	−702	−2232	140
H(7D1)	2000	−1186	−2718	162
H(7D2)	2026	−66	−3000	162
H(7D3)	1542	−850	−3345	162
H(8D1)	1344	1252	−2993	149
H(8D2)	872	1053	−2702	149
H(8D3)	845	487	−3323	149
H(6Y1)	1493	−1750	−2461	224
H(6Y2)	1869	−1285	−2823	224
H(6Y3)	1222	−1420	−3161	224
H(7Y1)	1168	395	−3437	205
H(7Y2)	1800	629	−3062	205
H(7Y3)	1327	1291	−2933	205
H(8Y1)	807	−647	−2208	257
H(8Y2)	547	−312	−2908	257
H(8Y3)	744	553	−2388	257
H(9D)	1596	1675	−1967	58
H(11G)	2001	3014	−1271	45
H(11H)	2568	2802	−735	45
H(1S1)	1482	706	−33	74
H(1S2)	1724	−440	−9	74

Fin.